Aerodynamic and Structural Analyses of the 5 MW Wind Turbine Using BEM and Lifting Line Theories

Vipul Gupta

Department of Mechanical Engineering - Sustainable Energy Technology

Eindhoven University of Technology

Thesis Report

TU Delft and ECN

December 2011 - August 2012

Abstract

Uncertainty in aerodynamic load prediction is an important parameter driving the price of wind energy and thus the wind turbine community is in need of more sophisticated tools for evaluating aerodynamic blade loading. Blade Element Momentum (BEM) theory is the current standard for estimating the wind forces in load case calculations. The predictive capability of BEM falls short for e.g. yawed flow and dynamic inflow cases and also has shortcomings in its assumptions. A physically more correct approach to model the rotor aerodynamics is presented by a lifting line method with a free vortex wake. This approach includes more physics, however the resulting computations are more time consuming. The thesis is attributed to find significant differences in prediction of aerodynamic performance and loads using BEM theory and lifting line theory. For this purpose ECN has modelled a state of art software, ECN AEROMODULE. The software has both BEM and lifting line (AWSM) modules. To underline the differences between BEM and lifting line (AWSM) implementation, two load cases are selected from the IEC standard and two test load cases are formulated. For all the load cases, both aerodynamic and structural analysis is done and the results are validated with FOCUS software results. FOCUS software is well developed software and is being used in wind energy industry for many years, it is based on BEM theory. Frequency analysis of the ART wind turbine is done at rated wind speed during normal operating condition to check whether the natural frequencies of blades and tower coincide with the important excitation frequencies. Aerodynamic phenomena like dynamic inflow and tower presence are studied for both the theories and the contributions of both phenomena on loading of wind turbine are also discussed.

Acknowledgements

I would like to express my profound gratitude to Prof.dr. G.J.W. van Bussel and Dr.ir. W.A.A.M. Bierbooms for being my supervisor during the course of the study at Delft University of Technology. I had been very fortunate to have both of them as my supervisors.

I would also like to especially thank Peter Eecen for giving me the opportunity to do the thesis at the Energy research Centre of the Netherlands. My sincere thanks to Francesco Grasso and Koen Boorsma for guiding me at every moment during the thesis work and improving my knowledge of aerodynamics. They were a great motivating factor during the thesis work, they taught me how to research and zoom in the simulation results to get more aerodynamic insight. My sincere thanks to Feike Savenije for helping me to overcome the problems in FOCUS software and for keeping me motivated and increasing my knowledge about wind turbine controllers. As well, I am equally thankful to Herman Snel, Koert Lindenburg, Ozlem Ceyhan, Jessica Holierhoek, Johan Peeringa and Gerard Schepers for their insight and discussions during the course of the thesis work. I am grateful to everyone for their time and support throughout the duration of my thesis work in ECN.

I would like to give my special thanks to my friend Ishleen Kaur for looking closely at the final version of the thesis for English style and grammar. Her constant support enabled me to complete the thesis work on time.

Finally I gratefully acknowledge the scholarship provided by the Eindhoven University of Technology for doing MSc. Without this scholarship it would not have been possible to do my studies in the Netherlands.

Nomenclature

English symbols

Symbol	Description	Unit
z	Height above the ground	m
c	Chord length of the airfoil	m
a	Axial Induction Factor	-
$a^{'}$	Tangential Induction Factor	-
r	Radial distance from hub	m
q	Yaw Rate	°/s
g	Acceleration due to gravity	m/s^2
dm	Mass of blade element	kg
$c_{gravity}$	Centre of gravity	-
$c_{\frac{1}{4}}$	Quarter chord point	-
P	Per revolution	-
L	Lift force	N
D	Drag force	N
C_l	2D-Lift Coefficient	-
C_d	2D-Drag Coefficient	-
C_m	2D-Moment Coefficient	-
A	Projected area of an airfoil (chord x span)	m^2
R	Blade Length	m
M	Pitching Moment	Nm
B	Number of blades	-
dT	Differential axial force	N
dQ	Differential torque	Nm
u_w	Wind velocity at far wake	m/s

Symbol	Description	Unit
u_d	Wind velocity at actuator disk	m/s
p_∞	Atmospheric pressure	N/m^2
p_d^+	Pressure just before actuator disk	N/m^2
p_d^-	Pressure just after actuator disk	N/m^2
dF_L	Incremental lift force	N
dF_D	Incremental drag force	N
dF_N	Incremental normal force to the plane of rotation	N
dF_T	Incremental force tangential to the circle swept by rotor	N
U_{rel}	Relative wind velocity	m/s
I_b	Mass moment of inertia	kgm^2
M_{yaw}	Moment on blade due to yaw motion	Nm
$F_{centrifugal}$	Differential centrifugal force on blade	N
F_c	Coriolis force	N
M_g	Moment due to gravity force	Nm
m_{blade}	Mass of blade	kg
Re	Reynold's number	-
F_g	Gravity force	N
V_{radial}	Radial velocity due to yawing and flapping action on blades	m/s
u_{ind}	Axial induced velocity on blade element	m/s
T	Tangential force distribution on blade element	N/m
N	Normal force distribution on blade element	N/m
c_l	Lift coefficient on blade element	-
U_{wind}	Axial wind velocity	m/s
$U_{i,rotor}$	Axial induced velocity on rotor	m/s
U_{tower}	Axial induced velocity on rotor due to tower	m/s
c_l	Lift coefficient on blade element, used in figures	-
u_{ind}	Axial induced velocity on blade element, used in figures	m/s
F_{ax}	Axial aerodynamic force on rotor, used in figures	N
U_{infty}	Free stream wind velocity	m/s
U_{wind}	Total wind velocity on rotor, used in figures	m/s
M_{flap}	Flapwise bending moment in the blade root, used in figures	Nm

Symbol	Description	Unit
M_{edge}	Edgewise bending moment in the blade root, used in figures	Nm
$M_{torsionblade}$	Torsional moment in the blade root, used in figures	Nm
M_{fore}	Fore-aft bending moment in the tower base, used in figures	Nm
M_{side}	Side-ways bending moment in the tower base, used in figures	Nm
$M_{torsiontower}$	Torsional moment in the tower top, used in figures	Nm
D_{flap}	Average flapwise displacement of blade tips, used in figures	m
$U_{inplane}$	Inplane wind speed, used in figures	m/s
U_{axial}	Axial wind speed, used in figures	m/s

Greek Symbols

Symbol	Description	Unit
ψ	Azimuth angle	$\circ$
α	Angle of Attack (AoA)	$\circ$
ρ	Density of air	kg/m^3
λ	Tip speed ratio	Nms/kg
Γ	Vortex strength	-
Δt	Time interval	$seconds$
Ω	Rotational speed	rpm
ω	Rotational speed of wake	rpm
Φ	Inflow angle of relative wind	rpm
ζ	Lag angle	$\circ$
θ_p	Section pitch angle	$\circ$
$\theta_{p,0}$	Blade pitch angle at tip	$\circ$
θ_T	Twist angle	$\circ$
λ	Tip speed ratio	-
λ_{opt}	Optimal tip speed ratio	-
β	Flapping angle	$\circ$
ϵ	Tilt angle	$\circ$
β_1	Lower blade cone angle when the rotor is tilted	$\circ$
β_2	Upper blade cone angle when the rotor is tilted	$\circ$
$\beta\cdot$	Flapping velocity	$\circ/s$

Abbreviations

Symbol	**Description**
$2D$	Two diminesional
$3D$	Three diminesional
ECN	Energy research Centre of the Netherlands
BEM	Blade Element Momentum
RPM	Revolutions per minute
AC	Alternating current
EWM	Extreme wind speed model
EOG	Extreme operating gust
NWP	Normal wind profile
NTM	Normal turbulence model
FFT	Fast fourier transform
AoA	Angle of attack
$NREL$	National Renewable Energy Laboratory
ART	5 MW Aerodynamic Reference Turbine
DLC	Design load case
$AWSM$	Aerodynamic Wind turbine Simulation Module
$PHATAS$	Program for Horizontal Axis wind Turbine Analysis and Simulation
$SWIFT$	Simulation of Wind Fields in Time
TWS	Turbulent wake state
TE	Trailing edge
MBS	Multi body simulation
MW	Megawatt
$UNFCCC$	United Nation Framework Convention on Climate Change
$HAWT$	Horizontal Axis Wind Turbines
$VAWT$	Vertical Axis Wind Turbines
CFD	Computational Fluid Dynamics
IEC	International Electrotechnical Commission

Contents

List of Figures

List of Tables

Chapter 1

Introduction

World is changing, energy and global warming are the most important problems in today's world. Fossil fuel prices are increasing day by day because of limited sources. Natural balance of earth is changing because of global warming. One of the main reasons of this change is burning excessive fossil fuel. Kyoto Protocol which is an agreement to reduce the emission of CO_2 and greenhouse gases by United Nation Framework Convention on Climate Change (UNFCCC) is ratified by many countries [33]. Therefore, alternative energy sources are needed. These are the reasons why wind energy becomes so important. Wind source is free and clean. Wind turbine technology is growing and wind is becoming one of the best alternative energy sources.

1.1 Wind Turbines

Wind turbine is a machine which converts wind power to electrical energy. There are several types of wind turbines. Generally, wind turbines are divided into two groups: Vertical Axis Wind Turbines (VAWT) and Horizontal Axis Wind Turbines (HAWT). In vertical axis wind turbines, blades are rotating on a vertical axis shaft. Their generator and gearboxes are placed on the ground which is easy to access and they don't need any yaw mechanism. The most common VAWT examples are Darrieus and Savonius type wind turbines, figure 1.1a depicts a Darrieus wind turbine. In horizontal axis wind turbines, turbine blades are connected to a shaft which is rotating on a horizontal axis. They are propeller type rotors which are located on the top of a tower with generators and gearboxes. HAWT are the most common wind turbine types, figure 1.1b shows the front view of a HAWT. Most of the electricity produced today is produced by HAWT. Although VAWT wind turbines have some advantages over HAWT by means of easy operations, still they cannot produce power as efficiently as HAWT. The advantages of HAWT design are [19]:

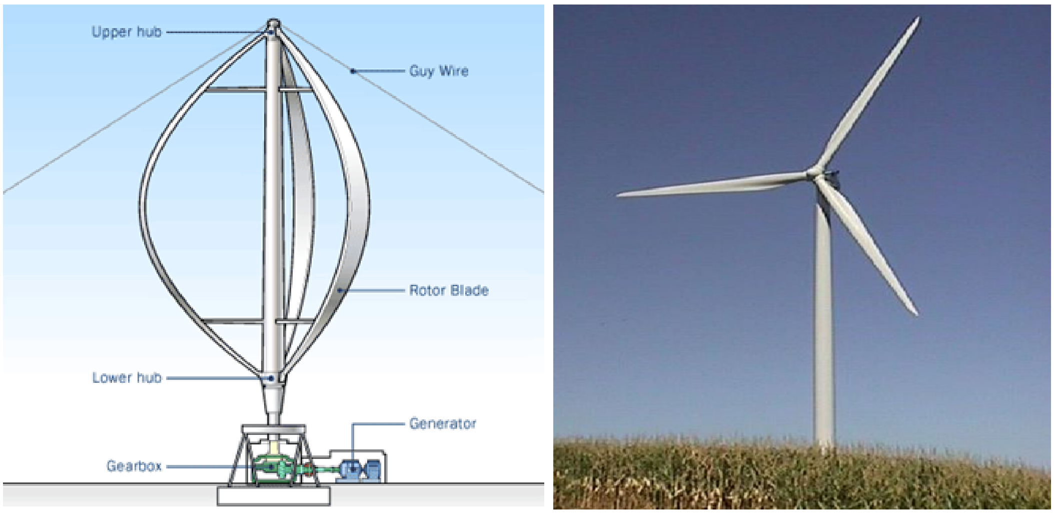

(a) (b)

Figure 1.1: Types of wind turbines. **a:** Darrieus wind turbine with the different components [30], **b:** Front view of a horizontal axis wind turbine (HAWT) [43].

- In propeller design, rotor speed and power output can be controlled by pitching the rotor blades about their longitudinal axis (blade pitch control). Moreover, rotor blade pitching is the most effective protection against over speed and extreme wind speeds, especially in large wind turbines.
- The rotor blade shape can be aerodynamically optimized and it has been proven that it will achieve its highest efficiency when aerodynamic lift is exploited to a maximum degree.
- No least, the technological lead in the development of the propeller design is a decisive factor.

Together, these advantages are the reason why almost all wind turbines for generating electricity built to date have horizontal axis rotors. In this thesis modern horizontal axis wind turbine is studied.

1.1.1 Horizontal Axis Wind Turbine (HAWT)

Horizontal axis wind turbines have some sub parts to convert wind power to electrical energy. These parts are shown in figure 1.2. Wind turbine rotor is the main part of the wind turbine. Generally, it consists of two or three blades which are connected to the rotor shaft by means of hub. In wind turbines with blade pitch control, the hub contains the blade pitch bearing and the blade pitch mechanism. Many smaller wind turbines are not fitted with a blade pitch control [8]. The rotor blades then have a fixed connection to the hub. The drive train of the wind turbine converts the rotor's mechanical rotational motion into electrical energy. In its narrow sense, the term drive train is only used for the mechanical components, excluding the electrical system. The rotor hub, the blade pitch mechanism, the rotor shaft (low speed shaft), the gearbox, the generator drive shaft and the rotor shaft (high speed shaft) are all part of the drive train. The drive train components are housed in the nacelle. The nacelle and rotor are turned into the wind direction by the yaw system or azimuth drive. The nacelle is mounted on top of tower. As rotor is the first element in the chain of functional elements of a wind turbine, its aerodynamic and dynamic properties, therefore, have a decisive influence on the entire system in many aspects. The capability of the rotor to convert maximum proportion of the wind energy largely determines the overall efficiency of the energy conversion of the energy collector. This is of prime importance with regard to the overall economies of the system [28]. Aerodynamic and dynamic properties of the rotor are important with respect to its capability to convert the fluctuating power input provided by the wind into uniform torque. While at the same time keeping the unavoidable dynamic loads on the system as low as possible. The magnitude of the load problems imposed on the downstream mechanical and electrical elements will depend on how well the above requirements are met by the rotor.

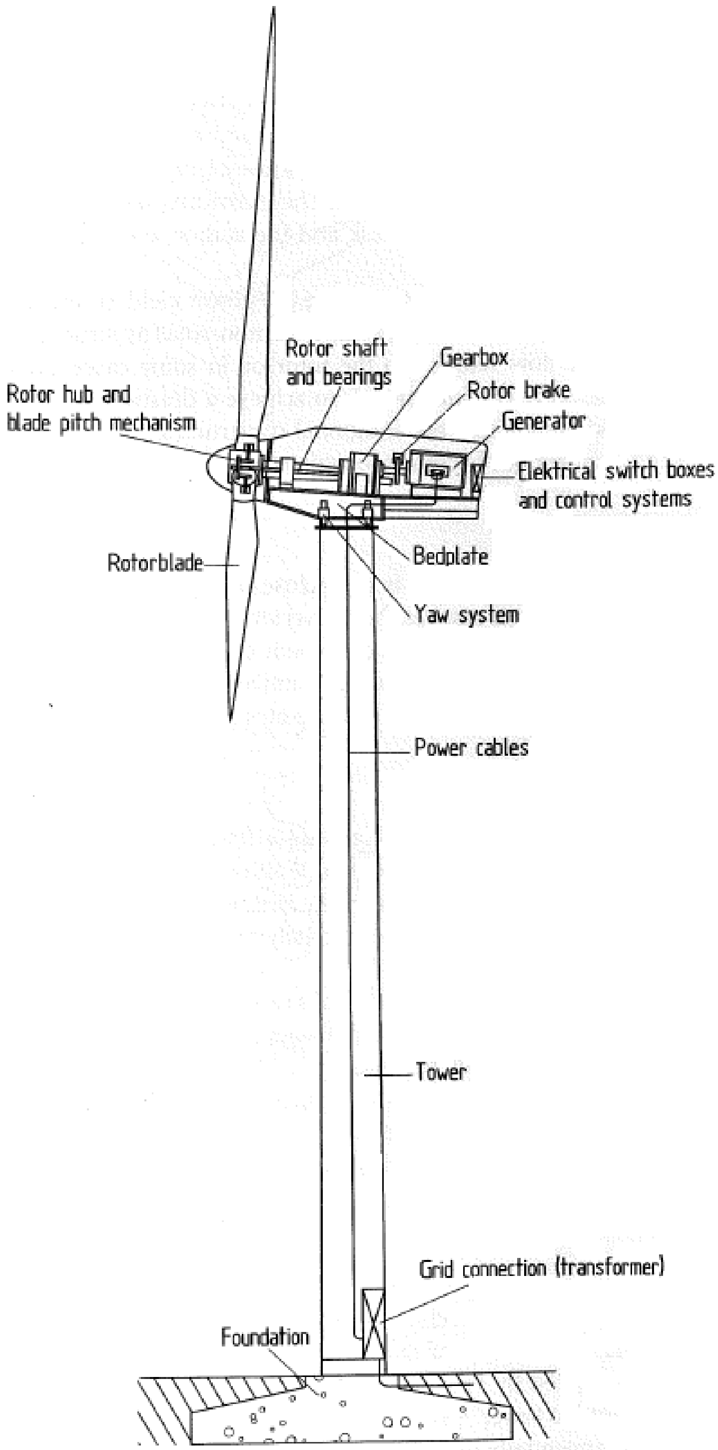

Figure 1.2: Components of a horizontal axis wind turbine [19].

1.1.2 Methods to predict the performance of a rotor

To predict the performance of a rotor of a HAWT several methods are used in the wind industry, some of these methods can list out as follows [22]:

1.1.2.1 Blade Element Momentum (BEM) Method

Most wind turbine design codes are based on Blade Element Momentum (BEM) method. The BEM method assumes that the blade can be analysed as a number of independent element in spanwise direction [45]. The induced velocity at each element is determined by performing the momentum balance for an annular control volume containing the blade element. The aerodynamic forces on the element are calculated using the lift and drag coefficient from the airfoil data at the geometric angle of attack (AOA) of the blade element relative to the local flow velocity. BEM methods have aspects of a reasonable tool, but are not suitable for accurate estimation of the effect of wake, the complex flow such as three-dimensional flow or dynamic stall because of their assumptions. The predictive capability of the current practice of BEM modelling fall short for e.g. yawed flow and dynamic inflow cases [28]. In addition to that, the variety in the several engineering extensions (for e.g. different dynamic stall models) used between different BEM implementations is large. BEM theory is explained in detail in appendix A.

1.1.2.2 Vortex Wake Method

Vortex wake method directly calculates the induced velocity from the bound vortices of blades and the trailing vortex in wake which are represented by lifting line [2] or lifting surface model [38]. The treatment of wake geometry can be classified roughly into two types, as a prescribed wake model [2] and a free wake model [38]. In the former model, the wake is represented by a line vortex or spiral vortices with fixed pitch. In the latter one, a fractional step scheme is adopted and the configurations of the wake are calculated at every time step using a local velocity including the components induced by wake and bound vortices. The free wake model is generally tackled with vortex lattice method which can fit on arbitrary blade shape with camber, taper and twist. Vortex wake methods are of accurate treatment of the wake effect such as yawed inflow or dynamic inflow, but they were not a common tool for design of turbines because of their computation burden. However, their use is increasing with increase of computer power.

1.1.2.3 CFD

Computational Fluid Dynamics (CFD) is a more accurate tool which overcomes all the disadvantages of the BEM theory but it takes a lot of computation time, therefore it is used only for analysis of specific problems which have high uncertainties for BEM methods [5] [37].

From the above three methods it can be said that the lifting line method with a free vortex wake is a better tool because it is more accurate though it takes more computation time than the most used method i.e. BEM method. Computation time in lifting line method with a free vortex wake is less than in CFD.

1.2 Research Questions

The main research question of this thesis work is to find out whether,

Are there significant differences in prediction of aerodynamic performance and loads using an aerodynamic module based upon BEM theory compared to a lifting line implementation?

The main research question can be divided into two sub questions, viz.

1. How do the differences in the aerodynamic model represent physical phenomena like dynamic inflow and tower presence?
2. Are there differences in loads calculated by different aero modules during physical phenomena like dynamic inflow and tower presence, if yes, on which parts of wind turbine the loads are important?

Secondary research questions which are formulated for the thesis work are:

1. Are the BEM code and lifting line (AWSM) implementation in AEROMODULE sufficiently validated?

2. Does the BEM implementation of AEROMODULE have same implementation as the well known BEM code of FOCUS? Beside the implementation differences are there any differences in both BEM modules?

3. Can AWSM be used in all conditions for which the BEM code of FOCUS is currently used?

4. Are there load cases that cannot yet be analysed using AWSM, if yes, then what load cases should be selected and do these selected load cases represent the full spectrum of load cases?

5. Is there a need of coupling a structural dynamic tool with an aerodynamic model like AEROMODULE, if yes, then what are the incompatibilities faced when coupling a structural dynamic tool with AEROMODULE?

1.3 Report structure

The thesis report can be outlined as follows:

- In chapter 2, aero modules based on Blade Element Momentum (BEM) and lifting line implementation (AWSM) are presented, viz. AEROMODULE(BEM), AEROMODULE(AWSM) and FOCUS(BEM). A structural tool (SIMPACK) is also presented because AEROMODULE needs to be coupled with SIMPACK in order to observe the dynamic behaviour of wind turbine.

- In chapter 3, the ART wind turbine is introduced and the complete load set calculation of the ART wind turbine according to the IEC standard in FOCUS software is shown. Some load cases are selected from the complete set which are also simulated in both the modules of AEROMODULE, so as to validate AEROMODULE by FOCUS. Some test load cases are also formulated and the simulation is done in all the three modules. Test load case-1 is presented in this chapter and other load cases with results of all the three modules are given appendices C and D. Both aerodynamic and structural analysis is done for load case-1. Frequency analysis is done for the ART wind turbine at rated wind speed during normal operating condition.

- In chapter 4, aerodynamic phenomena like tower presence and dynamic inflow are discussed. Modelling of both the aerodynamic phenomena in BEM and lifting line implementation (AWSM) are presented. The results obtained from both BEM and AWSM are also presented and discussed. The contribution of these phenomena on loading of wind turbine is shown for both the theories. Both phenomena are simulated for rigid and flexible ART wind turbines.

- In chapter 5 all the research questions mentioned in section 1.2 are answered based on the analysis done in chapters 2, 3 and 4. Some investigations which can be done in future are also discussed in this chapter.

Chapter 2

Wind Energy Softwares

Uncertainty in aerodynamic load prediction is an important parameter driving the price of wind energy and thus the wind turbine community is in need of more sophisticated tools for evaluating aerodynamic blade loading. Blade Element Momentum (BEM) theory is the current standard for estimating the wind forces in load case calculations. The predictive capability of BEM falls short for e.g. yawed flow and dynamic inflow cases and also has shortcomings in its assumptions. A physically more correct approach to model the rotor aerodynamics is presented by a lifting line method with a free vortex wake. This approach include more physics, however the resulting computations are more time consuming.

Energy research Centre of the Netherlands (ECN) has assembled the current state of the art of the above mentioned aerodynamic models in the ECN AEROMODULE. The package is to be coupled to arbitrary simulation software that solves the structural dynamics of a wind turbine. Blade position and velocity are given as input to the ECN AEROMODULE and forces and moments are then communicated back to the structural code. It is also possible to run the software stand alone for the purpose of aerodynamic calculations on a rigid turbine. Figure 2.1 shows the overview of ECN AEROMODULE software.

Two aerodynamic models are included in the ECN AEROMODULE, which are:

- Blade Element Momentum **(BEM)** method: This method is similar to the implementation in PHATAS [26].

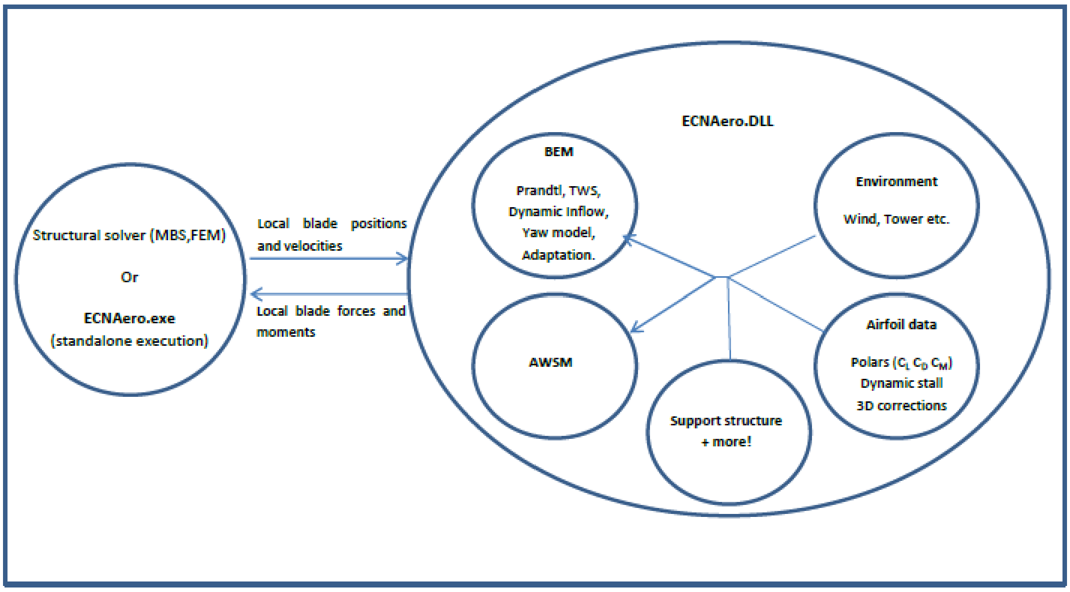

Figure 2.1: Overview of ECN AEROMODULE.

- Aerodynamic Wind turbine Simulation Module **(AWSM)**: This is in the form of free vortex code [11].

The ECN AEROMODULE is written using object oriented FORTRAN language and is divided into several modules. This modular program set-up allows for easy variation between aerodynamic models and maintains transparency. It is the aim of ECN to give the user maximum flexibility and offer a wide range of aerodynamic modelling options to choose from. Hence the trade-off between accuracy and computation is the responsibility of the user. In addition to that, this approach enables the use of the same models for tower effects, wind excitation (SWIFT or simple wind field) and airfoil data (including dynamic stall and rotational effects) for both the BEM and AWSM approach.

2.1 ECN AEROMODULE

In this section two models of ECN AEROMODULE are discussed.

2.1.1 BEM

Many different options exist for implementing BEM formulations, especially with regard to the various engineering extensions. Within the ECN AEROMODULE it is possible to switch off or vary many of these options, or the default settings. The most important BEM extensions relevant to the current work are briefly highlighted below.

1. **Oblique inflow** : To account for the variation of axial induction within each annulus , the model as defined by Schepers [35] [34] and implemented in PHATAS [26] is employed. A skew function is determined for each element as a function of effective yaw angle, azimuth angle and radial location. This skew function then relates the local induction at each element to the annulus averaged axial induction. The skew function from the yaw model [35] was originally developed from the correlation between annulus averaged and local induction velocities for an annulus by means of wind tunnel experiments. The Glauert correction for yaw [12], currently is the basis for most available BEM codes. The main difference with the present model lies in the refinement between inboard and outboard sections through inclusion of the effects of the root vortex.

2. **Prandtl correction** : To account for the finite number of blade, the Prandtl correction [32] (optional for both tip and root) is calculated for each element. In its implementation, axial wind speed, root or tip vortex location and annulus averaged axial and tangential induction at root or tip are necessary input for the evaluation of this function. The calculated Prandtl factor is incorporated in the iterative convergence procedure to relate the annulus averaged axial and tangential induction to local induction at each element.

3. **Dynamic inflow model** : The ECN dynamic inflow model [41] has been implemented. This model adds an extra term to the axial momentum equation to account for the aerodynamic rotor 'inertia' in the case of pitch action, rotational speed variation or wind speed variation.

4. **Turbulent wake state model** : For heavily loaded rotors, BEM theory predicts flow reversal in the wake, whilst in reality the wake transforms into a turbulent state by sucking in air from outside the stream tube. To account for this effect

the momentum equation is replaced by a turbulent wake state (TWS) equation if the annulus averaged axial induction coefficient exceeds a user specified value. The default value for this parameter is 0.35. The quadratic relationship between axial force and induction in the momentum equation is then replaced by a linear relationship tangent to the original quadratic line at the specified induction value.

2.1.2 Lifting Line Theory

The Aerodynamic Wind turbine Simulation Module (AWSM) has been developed at the Energy research Centre of the Netherlands (ECN) by *van Garrel* [11]. The main scope was to keep the advantages of BEM codes in terms of calculation time and ease to use, but to obtain a superior quality, especially concerning wake and time dependent wake related phenomena. The AWSM code [11] [14] [15] is based on generalized lifting line theory in combination with a free vortex wake method. The main assumption in this theory is that the extension of the geometry in spanwise direction is predominant compared to the ones in chord wise and thickness direction. Because of this, the real geometry is represented by a line passing through the quarter chord point of each cross section. Hence the total flow field in chord wise direction is concentrated in this point. Flow field model is depicted in figure 2.2.

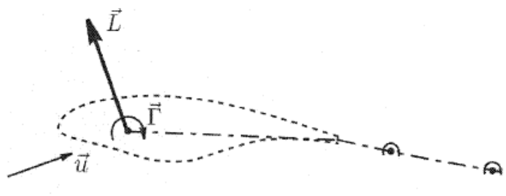

Figure 2.2: Flow field model.

In AWSM, the effects of viscosity are taken into account through the user supplied non-linear relationship between local flow direction and local lift, drag and pitching moment coefficients [11]. Along the lifting line, the generated elementary force can be determined by using the three dimensional form of the Kutta-Jukowsky theorem. The two dimensional aerodynamic characteristics of the sections are known, this means that the elementary force can be calculated also from the sectional properties. By matching these two formulations, the lift along the blade can be obtained.

2.1.2.1 Vortex wake

As in the continuous flow field representation, the vortices are shed from the trailing edge of the configuration surface and convected downstream in the AWSM flow model as time advances. The blade geometry consists of one or more strips that carry a vortex ring whose bound vortices are located at the quarter chord position and at the trailing edge. The vortex strengths Γ of these vortex rings are to be determined. At each time step Δt new vortex rings with these strengths are shed from the trailing edge and joined with the older vortex rings. These vortex rings together will form a vortex lattice. A sketch of the wake geometry for three strips after four time steps is shown in figure 2.3. The position of the first shed free spanwise vortex behind the trailing edge (TE) lies at some fraction between the current TE position and the wind convected TE position from the previous time step. Upstream of this position, the vortex rings have strength equal to the corresponding vortex ring at the configuration. The position of the downstream part of the wake is determined at each time step by convection of the wake vortex lattice nodes.

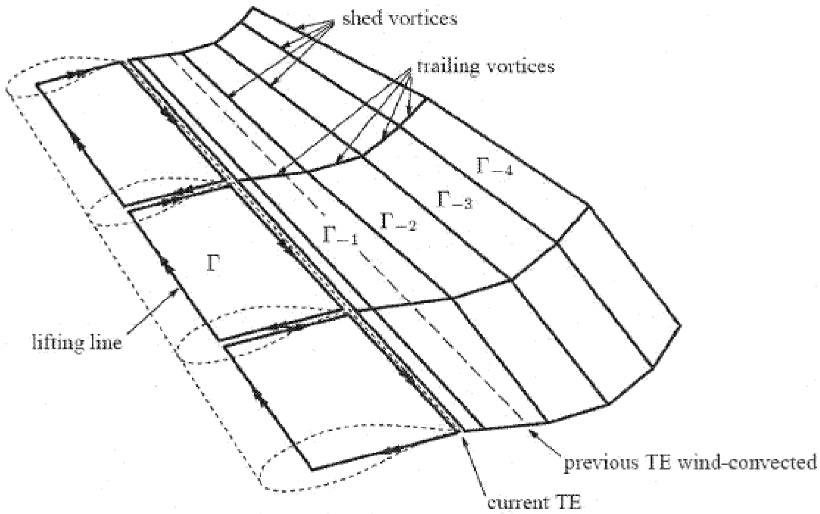

Figure 2.3: Wake geometry.

2.1.2.2 Tweaked version of AWSM

The position of the wake plays a crucial role in AWSM since the wake interacts with the blade inducing effects on it. For each time step, the wake is convected downstream.

The new position is function of the wind speed and the time interval and, of course, all the components (x,y,z) are updated. When the wake is free to roll-up, the positions of the wake points are different from the case where the wake is fixed and a geometrical helicoid is obtained. This is the main reason why the fixed wake case is not accurate like the free wake case; however, the fixed wake is much faster. In the tweaked version, the new position of the wake for fixed wake case is corrected by a scaling factor. In this way, the differences due to free/fixed wake are in part compensated (although the shape of the wake is not realistic like the free wake). Not all the components should be scaled in the same way but instead, the flow direction should be considered. In the actual implementation, due to time constraints, only the axial direction is affected. As a consequence, axial flow cases can be analysed, but not yawed cases.

2.2 FOCUS

There are numerous separate software tools available to design wind turbines. FOCUS software is the integrated modular tool to design wind turbines and wind turbine components like rotor blades and is developed by the Knowledge Centre WMC and ECN. For more than a decade, FOCUS is being used by the international wind turbine industry. The integrated modular tool FOCUS integrates various tools into one consistent user interface and provides consistent data.

- **FINSTRIP**: FINSTRIP is a design tool specially made to make a (relatively) quick local buckling analysis for cross sections of wind turbine rotor blades. FINSTRIP offers the possibility to analyse a complete cross-section, but is restricted to applications for long, slender beams.

- **SWIFT**: Swift stands for 'Simulation of Wind Fields in Time'. Swift is a computer program for numerical simulation of stochastic wind fields in the time domain. The resulting wind speed time series can be used as input to any wind turbine structural dynamics program based on BEM theory.

- **Bladmode**: Computer program Bladmode has been developed for the calculation of the eigen modes, frequencies, and damping of wind turbine rotor blades. The program is based on a description of a rotor blade following engineering bending theory of beams, in which torsional deformation and transverse shear flexibility as well as many aerodynamic and structural dynamic coupling terms for bending and torsion dynamics are included.

- **PHATAS**: The computer program PHATAS [26], 'Program for Horizontal Axis wind Turbine Analysis and Simulation', is developed for the time-domain calculation of the dynamic behaviour and the corresponding loads on a Horizontal Axis wind Turbine.

In the complete thesis work results from FOCUS are mentioned as FOCUS(BEM), in fact FOCUS results are calculated from PHATAS and PHATAS has BEM model in it.

2.3 SIMPACK

Wind turbines are anchored flexible complex machine which operate under highly dynamic stochastic loads. For onshore and offshore wind turbines, the request for high reliability requires comprehensive knowledge of dynamic behaviour already in the design phase [36]. This includes information about possible excitations and natural frequencies which can cause resonances in the operational speed range. Additionally, the displacements, deformations and resulting forces in the wind turbine, as well as the influence of wind turbine control under maximum loads during normal operation and emergency cases, has to be analysed. The multi-body method offers the ability to realistically model a wind turbine while considering all relevant components and degrees of freedom. This approach enables the required knowledge to be obtained in order to fully understand the dynamics of wind turbines.

SIMPACK [39] is a general purpose Multi Body Simulation (MBS) software which can be used for the dynamic analysis of any mechanical or mechatronic system. Recently SIMPACK also became popular amongst wind turbine manufacturers, for its calculation speed and extensive modelling freedom. The system can consist of both rigid bodies as well as flexible bodies with superimposed linear elastic deformation. It is up to the user to introduce flexibility by modal reduction and linearize around a specified state or to adopt a lumped mass or super element approach including non-linear effects.

2.4 AEROMODULE - SIMPACK couple

The AEROMODULE is an independent aerodynamic library consisting of a compilation of currently developed and future ECN models for simulation of rotor aerodynamics. For structural dynamics of a wind turbine, AEROMODULE is tailored for coupling to structural solvers such as SIMPACK. Blade position and velocity are given as input to the AEROMODULE and forces and moments are then communicated back to the structural code (SIMPACK). On coupling AEROMODULE with SIMPACK, an incompatibility in the controller interface was encountered. Same controller is used in FOCUS and for AEROMODULE-SIMPACK couple. The controller response showed a lot of fluctuations in the pitch angle of blades for AEROMODULE-SIMPACK couple than for FOCUS software. Lot of fluctuations in pitch angle of blade suggests fluctuations in loads of wind turbine which will subsequently lead to more fatigue. Incompatibility in the controller interface was more pronounced for small pitch angle of blades i.e. during normal operating conditions, than at large pitch angle of blades i.e. during extreme operating conditions.

2.5 Conclusion

This chapter explains the BEM implementations of AEROMODULE and FOCUS, lifting line implementation (AWSM) of AEROMODULE is also explained. In this thesis instead of the original version of AEROMODULE(AWSM), a tweaked version is used. Tweaked version of AEROMODULE(AWSM) is not capable for simulating yawed flow cases. BEM model of AEROMODULE is similar to the implementation in FOCUS(BEM). SIMPACK is a structural solver which is coupled with AEROMODULE to analyze structural dynamics of a wind turbine. There are incompatibility issues regarding the controller interface on coupling AEROMODULE with SIMPACK.

Chapter 3

Load Cases of ART Wind Turbine

In this chapter the ART wind turbine is introduced and a complete load set calculation of the ART wind turbine in FOCUS software is shown. Both fatigue and extreme loads according to the IEC standard [21] are shown for the ART wind turbine. Based on these loads some load cases are selected to draw differences between AEROMODULE(AWSM), AEROMODULE(BEM) and FOCUS(BEM). FOCUS(BEM) is used as a validation tool in the comparison between all the modules. Along with these selected load cases some test load cases are also simulated for all the modules. In this chapter one of the test load case (Load case-1) is discussed here for all the three modules. Other load cases with simulation results of all the three modules are discussed in appendices C and D. For Load case-1, both aerodynamic and structural analysis has been done. For aerodynamic analysis, angle of attack (α), lift coefficient (c_l), axial induced velocity (u_{ind}), normal force distribution (N) and tangential force distribution (T) are discussed for two blade stations, 0.23R and 0.81R. Aerodynamic zooming is done at 100th time step to analyse, angle of attack (α) and lift coefficient (c_l), normal force distribution (N) and tangential force distribution (T) for the complete blade length. For structural analysis, blade and tower moments will be discussed for the complete time series and for further investigation time series is zoomed at particular time intervals. A frequency analysis also has been done for the ART wind turbine at rated wind speed during normal operating conditions based on FOCUS(BEM) results.

3.1 The ART Wind Turbine

ART stand for 5 MW Aerodynamic Reference wind Turbine. The ART is a variable speed pitch regulated wind turbine[1] and is an aerodynamically more efficient form of the 5 MW NREL wind turbine [23], specification of the 5 MW NREL wind turbine is shown in table 3.1.

Table 3.1: Specification of the 5 MW NREL wind turbine.

Parameter	Value or Description	Unit
Wind Regime	IEC Class 1B / Class 6 winds	-
Rotor Orientation	Clockwise rotation - Upwind	-
Control	Variable Speed and Collective Pitch	-
Cut in wind speed	4	m/s
Cut out wind speed	25	m/s
Rated power	5	MW
Number of blades	3	-
Rotor Diameter	126.0	m
Hub Diameter	3.0	m
Hub Height	90.0	m
Rated Rotor Speed	12.1	rpm
Rated Generator Speed	1,173.7	rpm
Gearbox Ratio	97.0	-
Maximum Tip Speed	80.0	m/s
Hub Overhang	5.0	m
Shaft Tilt Angle	5.0	°
Rotor Precone Angle	-2.5	°

[1]The generator power output of variable speed pitch regulated wind turbine is controlled with rotational speed and blade pitch changes [8]. More detail about variable speed pitch regulated wind turbine is given in section A.5 of appendix A.

ECN has modified the blades of the 5 MW NREL wind turbine by changing its chord, mass and stiffness distribution, details are given in table B-2 in appendix B. During the complete thesis work the ART wind turbine is used to find the differences between BEM and AWSM.

3.2 Selection of load cases of the ART wind turbine

In FOCUS software, complete load set calculation of the ART wind turbine was done according to the IEC standard [21]. Fatigue and extreme loads on blade and tower during 20 years of the ART wind turbine operation are shown in figures 3.1 and 3.2 respectively. Fatigue and extreme torsional loads in blade root and tower top during 20 years of the ART wind turbine operation are shown in figure 3.3.
After the complete load set calculation of the ART wind turbine, some load cases are selected for further analysis in AEROMODULE-SIMPACK couple. The selection is done to find out the differences between BEM and AWSM. The selection is made for both fatigue and extreme loads, red circles in figures 3.1, 3.2 and 3.3 indicate the selected load cases. Following criteria were made to select the load cases:

1. Large equivalent fatigue and extreme loads on blade root, tower base and tower top.

2. Every load case addresses a different aspect. Almost all external conditions should be considered (like NWP, NTM etc.). Effect of wind speed and yaw angle should also be addressed.

Table 3.2 shows the selected load cases of the ART wind turbine. Brief description of the selected load cases is given in appendix B.

Table 3.2: Selected load cases of the ART wind turbine.

Type	Design load case (DLC)
Fatigue	Load cases - 0120, 0121, 0122, 2452, 3100 and 4180
Extreme	Load cases - 2677, 2888, 3271, 3280, 6001, 6233, 9150 and 9242

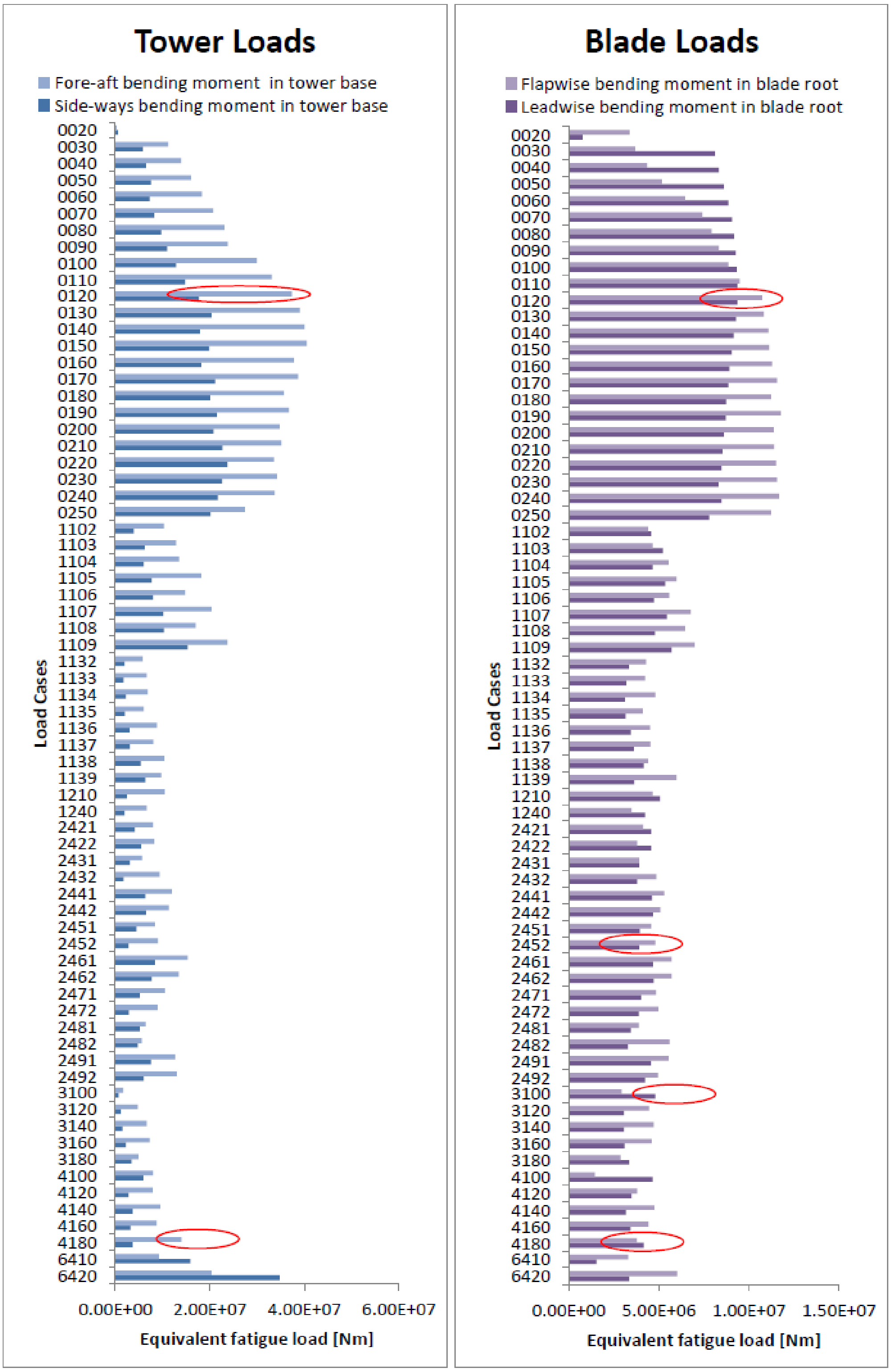

Figure 3.1: Left: Equivalent fatigue loads in tower base, Right: Equivalent fatigue loads in blade root.

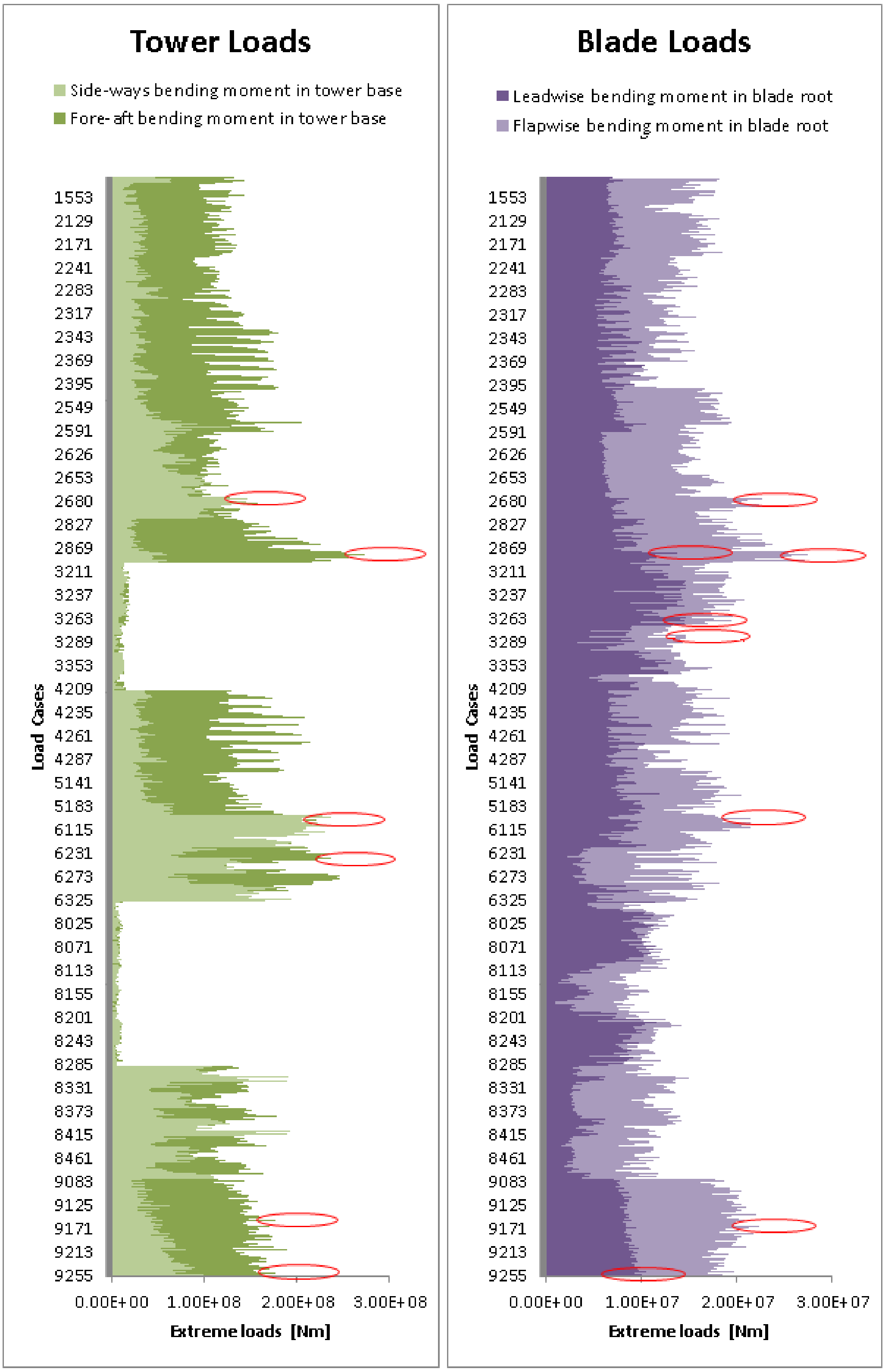

Figure 3.2: Left: Extreme loads in tower base, Right: Extreme loads in blade root.

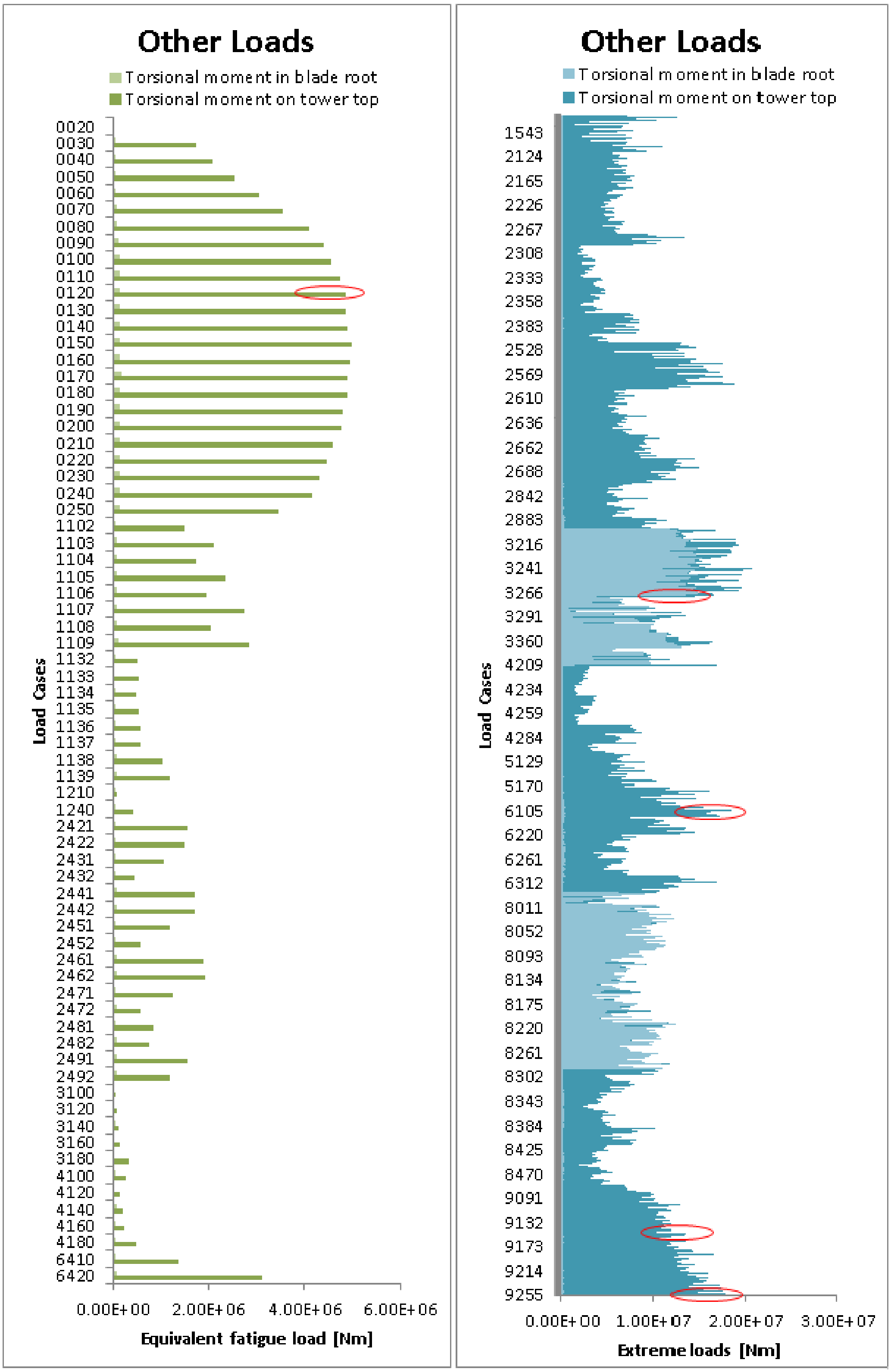

Figure 3.3: Left: Fatigue torsional loads in blade root and tower top, Right: Extreme torsional loads in blade root and tower top.

3.3 Differences between AEROMODULE and FOCUS(BEM)

Differences in AEROMODULE(BEM) and AEROMODULE(AWSM) as compared to FOCUS(BEM) can be listed as follow:

- AEROMODULE(BEM) has the same yaw model [34] as FOCUS(BEM), but the implementation is different.
- In AEROMODULE(AWSM) there is no dynamic stall model as compared to FOCUS(BEM).
- As compared to FOCUS(BEM), the tweaked version of AEROMODULE(AWSM) can simulate axial flow cases but not yawed flow cases.
- AEROMODULE(AWSM) calculates aerodynamic parameters at 1/4 chord point. On the other hand, AEROMODULE(BEM) and FOCUS(BEM) calculate aerodynamic parameters at 3/4 chord point. The significance of 3/4 chord point is given in the book by *Abbott* [1].

3.4 Validation of AEROMODULE with FOCUS

The BEM code and lifting line (AWSM) implementation in AEROMODULE are not sufficiently validated. Only for NASA Ames and MEXICO projects, AEROMODULE(BEM) and AEROMODULE(AWSM) were validated with experiment results [6]. Due to unavailability of experimental results of the ART wind turbine, FOCUS is used as validation tool for AEROMODULE(BEM) and AEROMODULE(AWSM). FOCUS is a well known tool used in wind industry, more description about FOCUS is given in section 2.2.

All the selected load cases are simulated in AEROMODULE(BEM)-SIMPACK couple and the results are compared with FOCUS(BEM). These results are presented in part-2 of this thesis report [17]. As the tweaked version of AWSM is used therefore only axial flow cases could be simulated, not yawed flow cases and out of the list there are only four axial flow cases i.e. load cases - 0122, 2888, 6001 and 9242. Load cases - 0122, 6001 and 9242 are simulated for 670 seconds and load case - 2888 is simulated for 130 seconds according to the IEC standard [21]. AEROMODULE(AWSM) takes lot of time to simulate than AEROMODULE(BEM) because of more physics involved in the former. For every load case in AEROMODULE(AWSM) a separate input file needs to be made with different blade stations because one input file for all load cases was not working without errors. Because of this reason and also due to large simulation time of 670 seconds, load cases - 0122, 6001 and 9242 were not simulated in AEROMODULE(AWSM). In order to make more comparison between BEM and AWSM, load case-3290 was simulated. Load case - 3280 without yaw misalignment is load case - 3290. So in total two load cases (load cases - 2888 and 3290) according to the IEC standard are simulated in AEROMODULE(AWSM) to draw comparison between AERMODULE(BEM), AEROMODULE(AWSM) and FOCUS(BEM). Apart from the selected load cases, seven test load cases are formulated and are simulated in AERMODULE(BEM) and FOCUS(BEM). Out of seven only two load cases are simulated in AERMODULE(AWSM) and they are discussed in this report. Other five test load cases with AERMODULE(BEM) and FOCUS(BEM) comparison are presented in part-2 of this thesis report [17].

Figure 3.4 shows the selected load cases which are simulated in both AEROMODULE(BEM) and AEROMODULE(AWSM) to make the comparison with FOCUS(BEM). This report discusses the load cases which are simulated in all the three modules, viz. AEROMODULE(BEM), AEROMODULE(AWSM) [7] and FOCUS(BEM).
For each load case a comparison is made between all the three modules while considering FOCUS(BEM) as a validation tool. As there are repetitions in all these cases, therefore load case-1 is discussed here and other load cases (load case-2888, load case-3290 and load case-2) are discussed in appendices C and D. A brief description of the load cases discussed in this report is given below:

- Load case-1: Step change in wind in a rigid ART wind turbine.
- Load case-2: Step change in wind in a flexible ART wind turbine.
- Load case-2888 (DLC2.2): Pitch controller failure in a flexible ART wind turbine.
- Load case-3290 (DLC3.2): Start up with extreme operating gust(EOG) in a flexible ART wind turbine.

Type	AEROMODULE(BEM)	AEROMODULE(AWSM)
Test load cases	Load case-1	Load case-1
	Load case-2	Load case-2
	Load case-3	-
	Load case-4	-
	Load case-5	-
	Load case-6	-
	Load case-7	-
Fatigue load cases	Load case-0120	-
	Load case-0121	-
	Load case-0122	-
	Load case-2452	-
	Load case-3100	-
	Load case-4180	-
Extreme load cases	Load case-2677	-
	Load case-2888	Load case-2888
	Load case-3271	-
	Load case-3280	-
	Load case-3290	Load case-3290
	Load case-6001	-
	Load case-6233	-
	Load case-9150	-
	Load case-9242	-

Figure 3.4: Load cases simulated in AEROMODULE(BEM) and AEROMODULE(AWSM).

For all these load cases both aerodynamic and structural analysis has been done. For aerodynamic analysis, angle of attack (α), lift coefficient (c_l), axial induced velocity (u_{ind}), normal force distribution (N) and tangential force distribution (T) are discussed for two blade stations, 0.23R and 0.81R. Aerodynamic zoomings are done at a certain time steps to analyze all the aerodynamic parameters for the complete blade length. For structural analysis, blade and tower moments will be discussed for the complete time series and for further investigation time series is zoomed at particular time intervals.

3.5 Load Case-1: Step change in wind speed in a rigid ART wind turbine

A step change in wind is considered from 12 m/s to 16 m/s at 70th second, and the wind is not turbulent. No surface roughness is considered therefore no wind shear. Figure 3.5 shows the step wind in load case-1. The wind turbine rotor is not taken with any

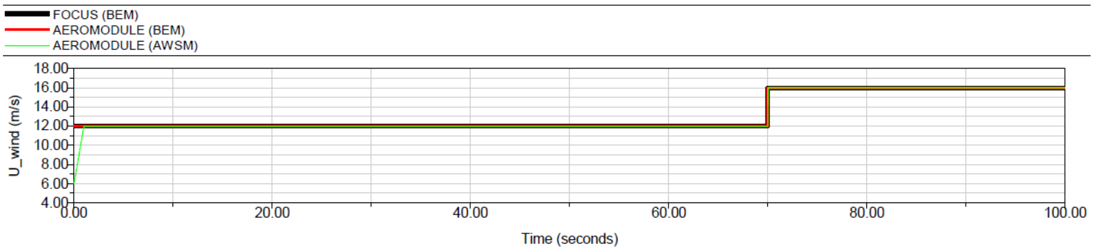

Figure 3.5: Case-1: Wind Speed at hub.

tilt and cone angle. The rotor of the ART wind turbine is not misaligned i.e. yaw angle is zero. The ART wind turbine structure is considered rigid i.e. both blades and tower are rigid. Controller operation is switched off, the pitch angle of all the blades and generator speed are maintained at a constant value of 4 degrees and 1,173.7 rpm respectively. All these parameters are given in all the three modules. As the pitch angle of all the blades and generator speed is constant, therefore the generator torque and generator power are also constant. The generator torque and generator power shows a sudden drop and this drop keeps on repeating again and again. Drops are because of the tower presence and it is explained in detail in section 4.1. Figures 3.6 and 3.7 shows generator torque and generator power respectively.

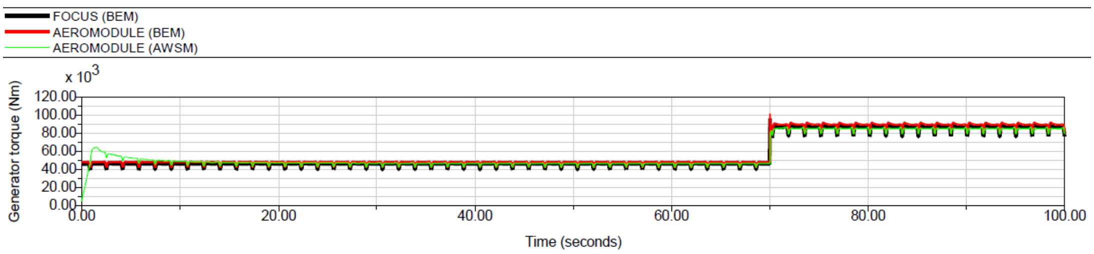

Figure 3.6: Case-1: Generator torque.

The axial aerodynamic force on the rotor is dependent on wind speed and it is given by:

$$F_{ax} \; \alpha \; U_{\infty}^{2} a(1-a), \tag{3.1}$$

As no controller is operating and the pitch angle is maintained at a constant value of 4 degrees, therefore the axial aerodynamic force on rotor also increases with the wind speed and this can be seen in figure 3.8. At the 70th second when the wind speed

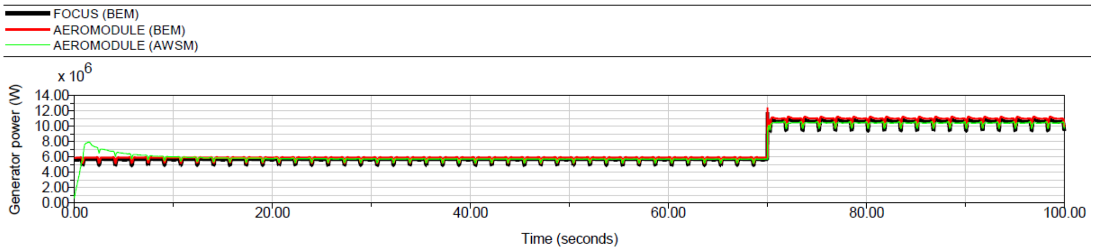

Figure 3.7: Case-1: Generator power.

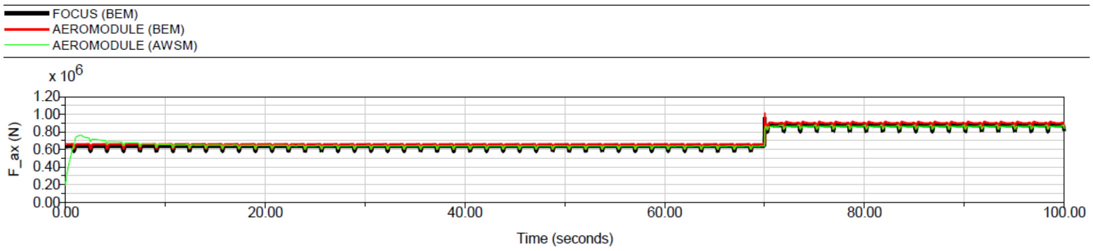

Figure 3.8: Case-1: Axial aerodynamic force on rotor.

changes in step fashion, there is a sudden rise in axial aerodynamic force on rotor, this is due to dynamic inflow, this can be seen by the purple circle in figure 3.9. Dynamic inflow is discussed in detail in section 4.2. The difference in axial aerodynamic force on

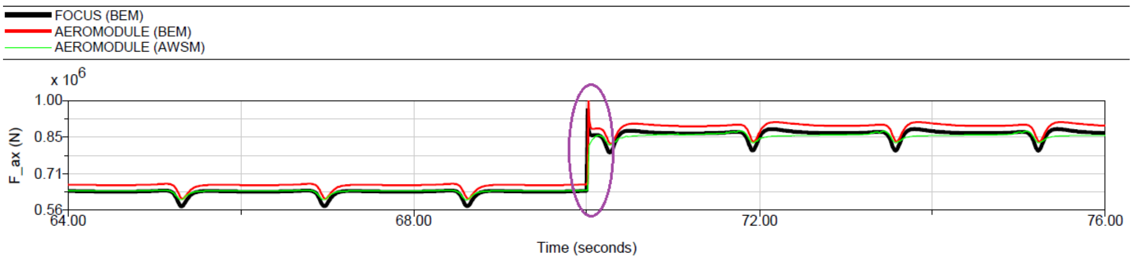

Figure 3.9: Case-1: Axial aerodynamic force on rotor during dynamic inflow.

rotor for all the modules is small. Difference is because when the wind speed increases the angle of attack α also increases and due to slightly different α, the axial aerodynamic force on rotor for all the modules differs slightly. AEROMODULE(AWSM) takes some time to stabilize because free wake (starting vortex) has to stabilize and this can be seen in figure 3.10. As the blades are rigid therefore there is no change in mean position of blade tip i.e. it is at a pre-bend of -2.05 m.

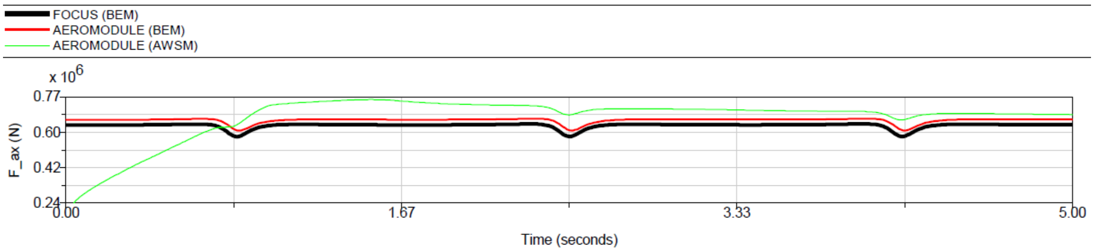

Figure 3.10: Case-1: Axial aerodynamic force on rotor for first 5 seconds.

3.5.1 Aerodynamic aspects

The angle of attack at which stall occurs for the airfoil (DU 35-A17) at 0.23R is 12.5 degrees and for airfoil (NACA 63418) at 0.81R is 14 degrees.

There is sharp drop in α and this is due to the tower presence and it is explained in section 4.1. We know,

$$\phi = \alpha + \theta_{pitch} + \theta_{twist} \tag{3.2}$$

Where ϕ is the inflow angle of relative wind, α is the angle of attack, θ_{twist} is the twist angle of the airfoil and θ_{pitch} is the pitch angle of the airfoil. As θ_{twist} and θ_{pitch} are constant for 0.81R and 0.23R, therefore ϕ is directly dependent on α. As the rotor speed is constant, therefore increase in wind speed cause increase in relative wind which in turn causes increase in ϕ . Therefore it can be seen that when the wind speed

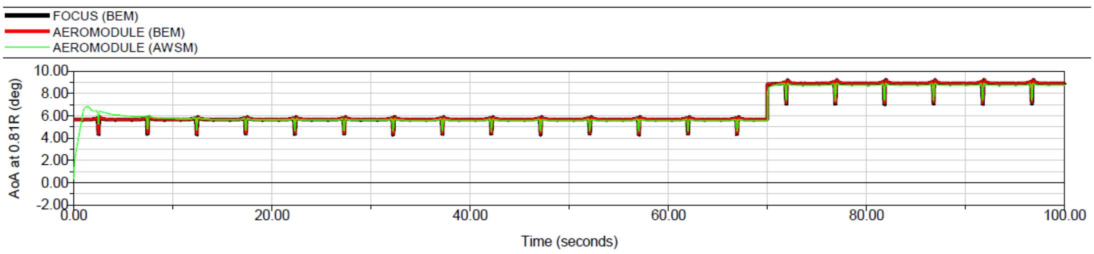

Figure 3.11: Case-1: Aerodynamic angle of attack at 0.81R blade station.

increases the angle of attack α also increases. At 0.81R, there is good match between all the modules for the angle of attack. As the angle of attack does not cross 14 degrees even on changing wind speed, therefore there is no stall at 0.81R. Figure 3.11 shows the aerodynamic angle of attack at 0.81R blade stations.

AEROMODULE(AWSM) takes some time for the free wake to stabilize, except the

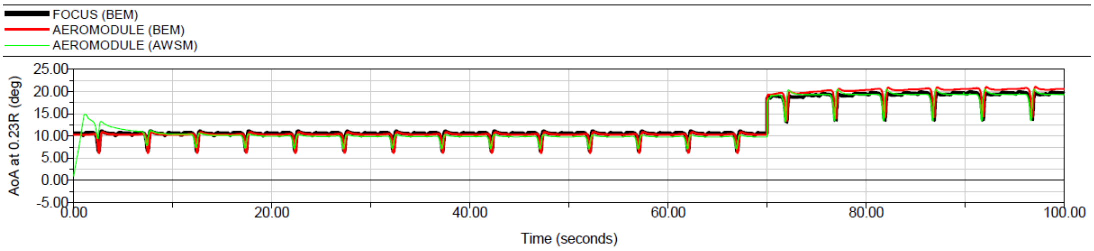

Figure 3.12: Case-1: Aerodynamic angle of attack at 0.23R blade station.

initial stabilization the angle of attack α at 0.23R is below 12.5 degrees when the wind speed is 12 m/s. This means the airfoil is not stalled, all the modules show similar results. On increasing the wind speed the angle of attack α crosses above 12.5 degrees and thus enter the stall region. Stall at 16 m/s of wind speed happens at 0.23R blade station because as there is no controller so the pitch angle is maintained at 4 degrees, pitch angle of 4 degrees is low at 16 m/s of wind speed to prevent the airfoil to get stalled. Figure 3.12 shows the aerodynamic angle of attack at 0.23R blade stations.

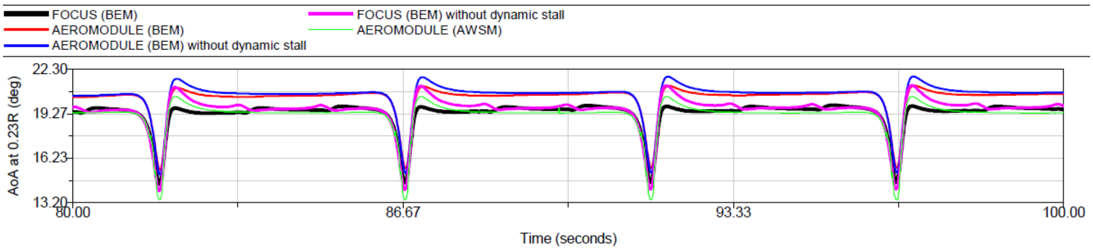

Figure 3.13: Case-1: Aerodynamic angle of attack at 0.23R blade station from 80th to 100th second.

The angle of attack α goes on increasing because of separation of flow at 0.23R airfoil at 16 m/s of wind speed. When the blade passes the tower the angle of attack α decreases because of reduction in relative wind speed. Figure 3.13 shows the aerodynamic angle of attack at 0.23R blade stations from 80th to 100th second. There is a small difference in α between all the modules at 0.23R when the wind speed is 16 m/s, AEROMODULE(BEM) and FOCUS(BEM) show rising trend but AEROMODULE(AWSM) doesn't show this is because of no dynamic stall model in it.

Lift coefficient c_l is directly proportional to the angle of attack α in the linear slope region, but after stall this relation is no more valid. As the airfoil at 0.81R does not cross 14 degrees of angle of attack therefore it does not reach stall and so therefore c_l has the same trend as the angle of attack α. Lift coefficient c_l at 0.81R shows the same trend for all the modules and this can be seen in figure 3.14. When the wind speed is

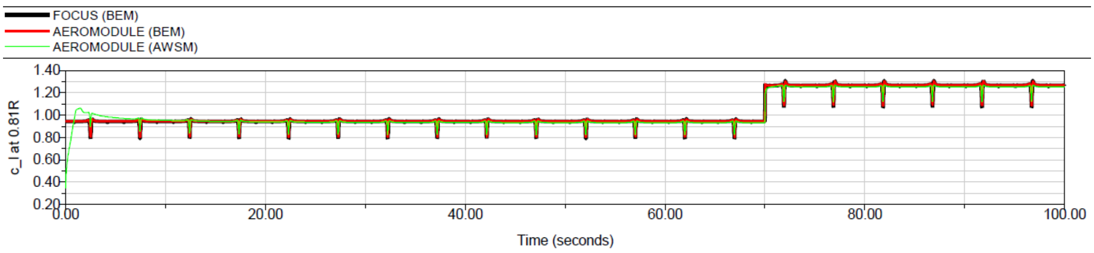

Figure 3.14: Case-1: Lift coefficient c_l at 0.81R blade station.

12 m/s, the airfoil at 0.23R does not cross 12.5 degrees of angle of attack and therefore it is not stalled so the trend of c_l is same as α. On increasing the wind speed, the angle of attack α for 0.23R airfoil increases above 19 degrees, and so the airfoil is stalled at 0.23R. Physics behind the dynamic stall is explained below. Figure 3.15 shows the lift coefficient c_l at 0.23R blade station. At 0.23R blade station, AEROMODULE(AWSM) shows better match with FOCUS(BEM) than AEROMODULE(BEM) for c_l when the wind speed is 12 m/s, opposite happens at 16 m/s of wind speed and this is because of difference in α.

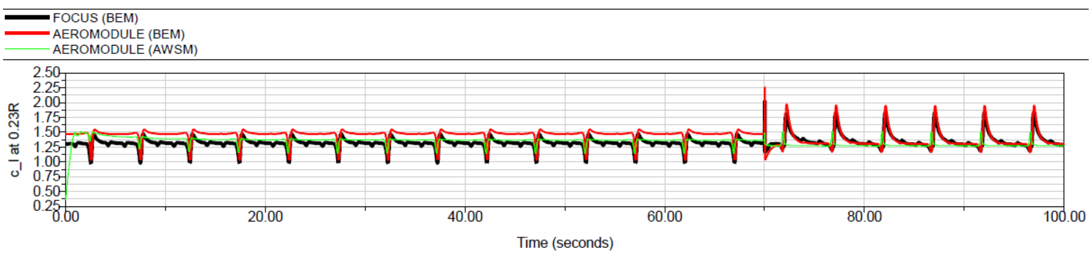

Figure 3.15: Case-1: Lift coefficient c_l at 0.23R blade station.

Dynamic stall

Dynamic stall is a non-linear unsteady aerodynamic effect that occurs when airfoils rapidly change the angle of attack. Rapid change in angle of attack can have increasing or decreasing slope. Figure 3.16 describes the flow physics for a 2D airfoil undergoing dynamic stall.

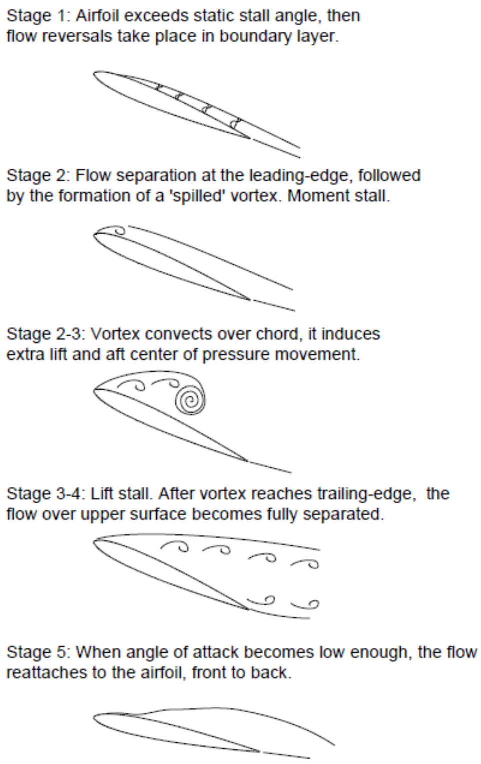

Figure 3.16: Case-1: Flow physics for a two-dimensional airfoil undergoing dynamic stall [25].

This rapid change causes a thin layer of reversed flow which develops at the bottom of the boundary layer. From the trailing edge of the stalling airfoil, this tongue of reversed flow starts at the rear of the airfoil and moves forward to the leading-edge region. The tongue of reversed flow i.e. vortex, develops and then moves back to the trailing edge at a speed somewhat less than $1/2\ U_\infty$ [29]. The vortex, containing high-velocity airflows, briefly increases the lift produced by the wing. As soon as it passes behind the trailing edge, the lift reduces dramatically, and the wing is in normal stall [8].

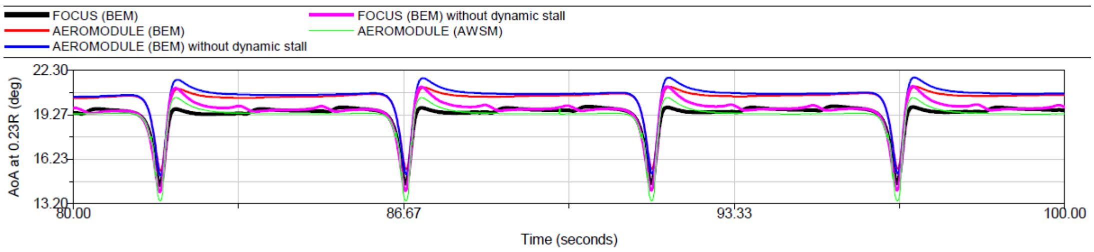

(a)

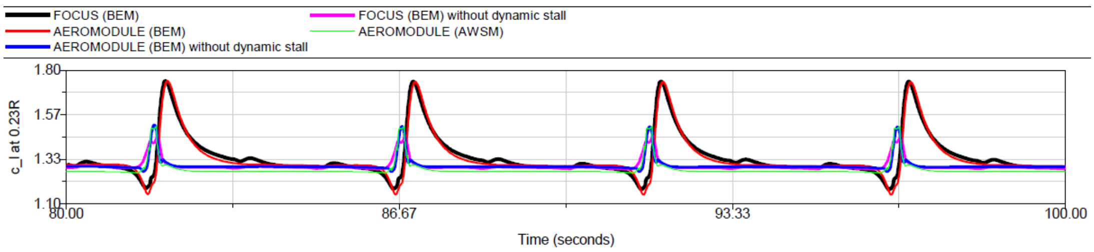

(b)

Figure 3.17: Case-1: Aerodynamic analysis at 0.23R blade station at 16 m/s wind speed from 80th to 100th second. **a:** Aerodynamic angle of attack (α), **b:** Lift coefficient (c_l).

From the figure 3.17a, it can be seen that α for 0.23R blade station (DU-35-A17) is above the stall angle of attack, whenever the blade passes the tower α decreases below 19 degrees and reaches approximately 13.2 degrees because of reduction in relative wind speed, this can be seen for all the modules. As α is above stall angle of attack i.e. it is not in the linear slope region, therefore c_l doesn't follow the trend of α. There is a small difference in α between all the modules at 0.23R when the wind speed is 16 m/s, AEROMODULE(BEM) and FOCUS(BEM) modules show rising trend but AEROMODULE(AWSM) doesn't show this is because of no dynamic stall model in it, and this is verified further by simulating the same case in AEROMODULE(BEM) and FOCUS(BEM) without dynamic stall. As both the BEM modules have dynamic stall model, they show c_l higher than the maximum 2D characteristic value. Because dynamic stall model defines a hysteresis loop for the c_l when α for the airfoil changes rapidly (above the stall α). Figure 3.17b also shows that due to presence of dynamic stall in both the BEM modules, the c_l trend shows a small dip when the blade is near the tower. There are very small peaks only in FOCUS(BEM) but not in other two modules and this needs more investigation. During the investigation it was found that these small peaks were also observed in the axial induced velocity, u_{ind}, at 0.23R blade station. For FOCUS(BEM), the upward peak is due to phenomenon of tower presence of one blade but the downward peaks are due to blade coupling. In BEM, the momentum equation includes all the three blades. As one blade passes the tower it causes a change in momentum and as no wake is produced in BEM therefore change in momentum due to one blade is also seen in other two blades. Therefore the upward peak A (blade-1 passing the tower) and downward peaks B and C (effect of blade-1 passing the tower on other two blades) in figure 3.18, can be given as,

$$\downarrow A = \uparrow B + \uparrow C \tag{3.3}$$

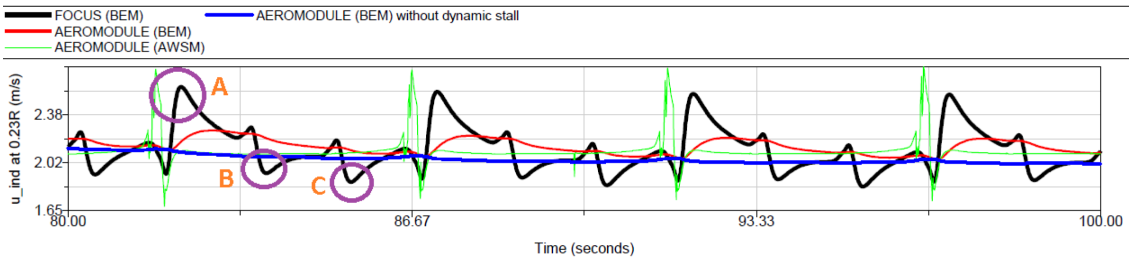

Figure 3.18: Case-1: Axial induced velocity at 0.23R blade station at 16 m/s wind speed from 80th to 100th second.

As wake is modelled in AEROMODULE(AWSM) therefore it includes the effect of blade coupling. AEROMODULE(BEM) is also based on BEM theory but it doesn't show the effect of blade coupling, this needs more investigation in future. The effect of blade coupling was also seen in FOCUS(BEM) at 0.23R blade station for 12 m/s of wind speed, figure 3.19c gives more insight about it. From figure 3.19, it can be seen that all the modules follow the same trend for c_l as their α because α is below the stall angle and thus lie in the linear slope region. AEROMODULE(BEM) shows the highest mean value for c_l and u_{ind} even though both the BEM modules have almost same mean values for α. Highest mean value of u_{ind} in AEROMODULE(BEM) is because u_{ind} is dependent on α and c_l.

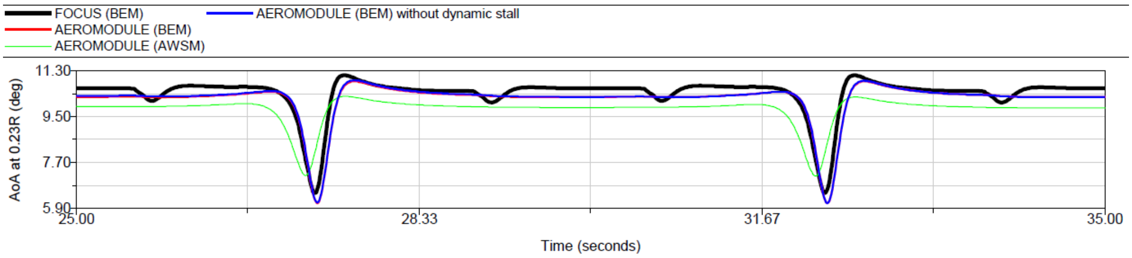

(a)

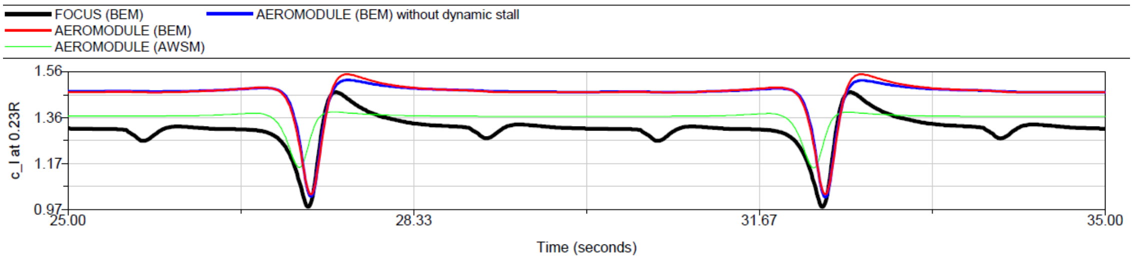

(b)

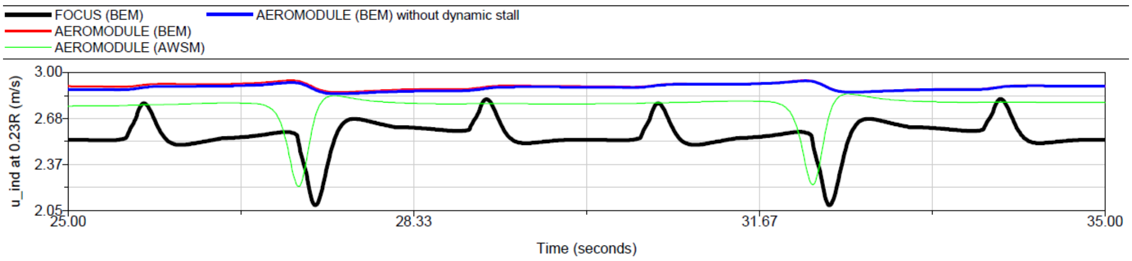

(c)

Figure 3.19: Case-1: Aerodynamic analysis at 0.23R blade station at 12 m/s wind speed.

Investigation was done to see if u_{ind} for AEROMODULE(BEM) is higher than other two modules for the complete length of blade. From figure 3.20, it can be seen that at 0.23R blade station, AEROMODULE(BEM) shows a peak which FOCUS(BEM) doesn't show. AEROMODULE(AWSM) also shows a high u_{ind} value because of fewer stations near 0.23R blade station. In AEROMODULE(AWSM) each blade station influences the other, so the missing stations near 0.23R blade station have an effect on neighbouring blade stations. At 0.81R blade station all the modules are close to each other because more blade stations are taken for all the modules near the tip.

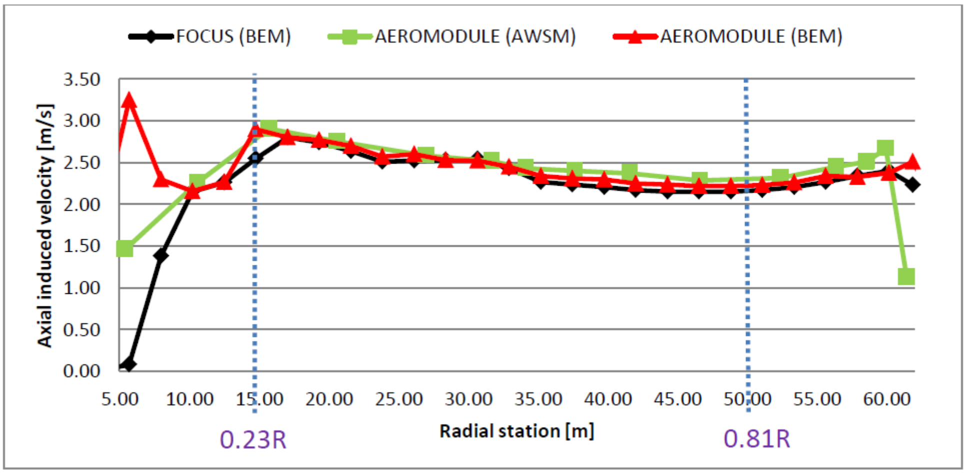

Figure 3.20: Case-1: Axial induced velocity along the complete length of blade at 30th second.

One more investigation is done to see if 3D correction is the cause of the strange behaviour in the mean value for c_l in AEROMODULE(BEM). In figure 3.21, it can be seen that there is no change even if 3D correction was not considered in AEROMODULE(BEM) as trends of AEROMODULE(BEM) without dynamic stall and AEROMODULE(BEM) without dynamic stall and 3D correction overlap each other. Hence more investigation in needed to study the strange behaviour of AEROMODULE(BEM) at 0.23R blade station.

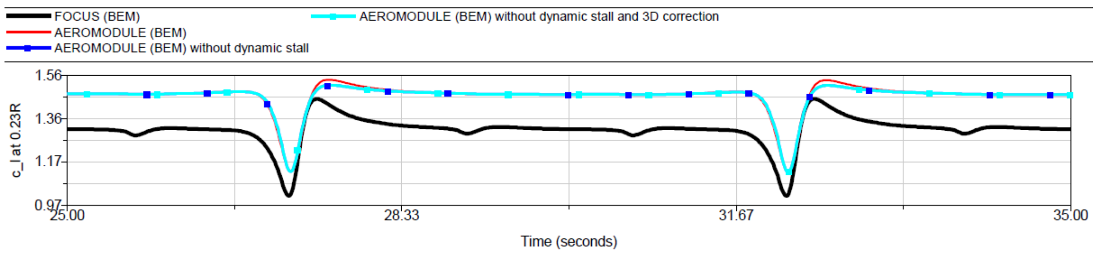

Figure 3.21: Case-1: Lift coefficient at 0.23R blade station at 12 m/s wind speed.

Figure 3.22 shows the variation of axial induced velocity along the length of the blade in FOCUS(BEM) and AEROMODULE(AWSM). Both AEROMODULE(BEM) and FOCUS(BEM) are based on BEM theory, so only FOCUS(BEM) is discussed here which in general represents the BEM theory. At the root and tip region the red circles shows

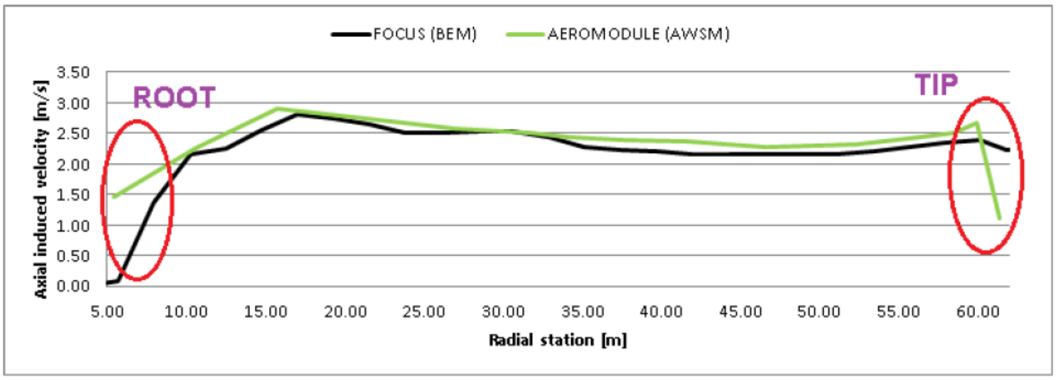

Figure 3.22: Case-1: Axial induced velocity along the span of the blade for BEM theory and lifting line (AWSM) implementation.

the difference between both the theories used in both modules. When the wind leaves the airfoils near the blade root it forms root vortex, root vortex have small rotational velocity as compared to the vortices shed from airfoils at tip. According to Fleming's right hand rule, the blade root vortex causes more tangential induced velocity than axial induced velocity. Therefore the contribution of root vortex to axial induced velocity is small near the root region. FOCUS(BEM) shows a smaller u_{ind} than AEROMODULE(AWSM) at root region because of root vortex. In FOCUS(BEM) there is no root vortex but in AEROMODULE(AWSM) it is, in BEM theory root vortex is modelled by Prandtl root loss factor. When the wind leaves the airfoils near the tip it forms tip vortex, tip vortex has large rotational velocity. According to Fleming's right hand rule, the blade tip vortex causes more axial induced velocity than tangential induced velocity. Near the tip section i.e. large 'r', AEROMODULE(AWSM) is below FOCUS(BEM), this deviation is because the axial induced velocity near tip region is mainly caused due to tip vortex. In FOCUS(BEM) there is no tip vortex but in AEROMODULE(AWSM) it is, in BEM theory tip vortex is modelled by Prandtl tip loss factor.

For airfoil at 0.81R the axial induced velocity for all the modules matches closely. For FOCUS(BEM), the downward peak is due to effect of tower presence of one blade but the upward peaks are due to blade coupling. Blade coupling is already explained above. When the step change is wind occurs the axial induced velocity also shoots up for all the modules. AEROMODULE(AWSM) shows the largest shoot up than both the BEM modules, more details about this are given in section 4.2. According to the figures 3.23a and 3.23b, the axial induced velocity at 0.23R is higher than 0.81R. All the modules show good similarity in trend for the axial induced velocity at 0.23R and 0.81R.

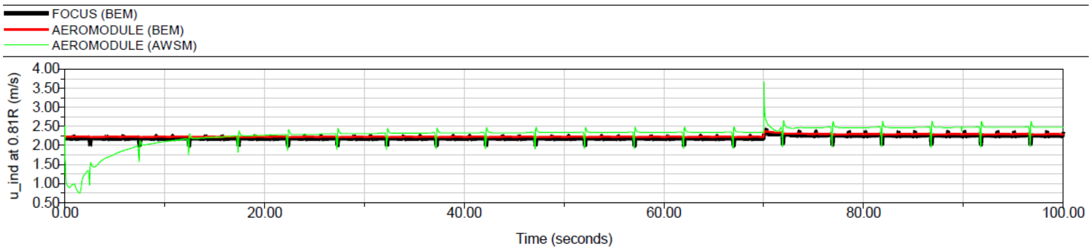

(a)

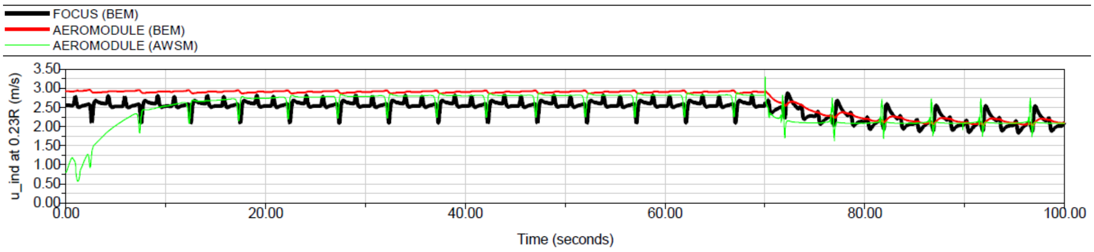

(b)

Figure 3.23: Case-1: Axial induced velocity at 0.81R and 0.23R blade station.

The normal force distribution is the distributed force normal to the chord, positive from airfoil pressure to suction side. All the modules show good match at 0.81R blade station. At 0.23R blade station difference in all the modules is because of different α, c_l and u_{ind}. Figures 3.24a and 3.24b show the normal force distributions at 0.81R and 0.23R blade stations respectively. Normal force distribution at 0.23R is less than at 0.81R because of smaller relative wind speed at 0.23R than at 0.81R blade station. All the modules show good match for tangential force distribution at 0.81R blade station. At 0.23R blade station difference in all modules is because of different α, c_l and u_{ind}. Tangential force distribution at 0.23R is less than at 0.81R because of smaller relative wind speed at 0.23R than at 0.81R blade station. Figures 3.24c and 3.24d show the tangential force distributions at 0.81R and 0.23R blade stations respectively.

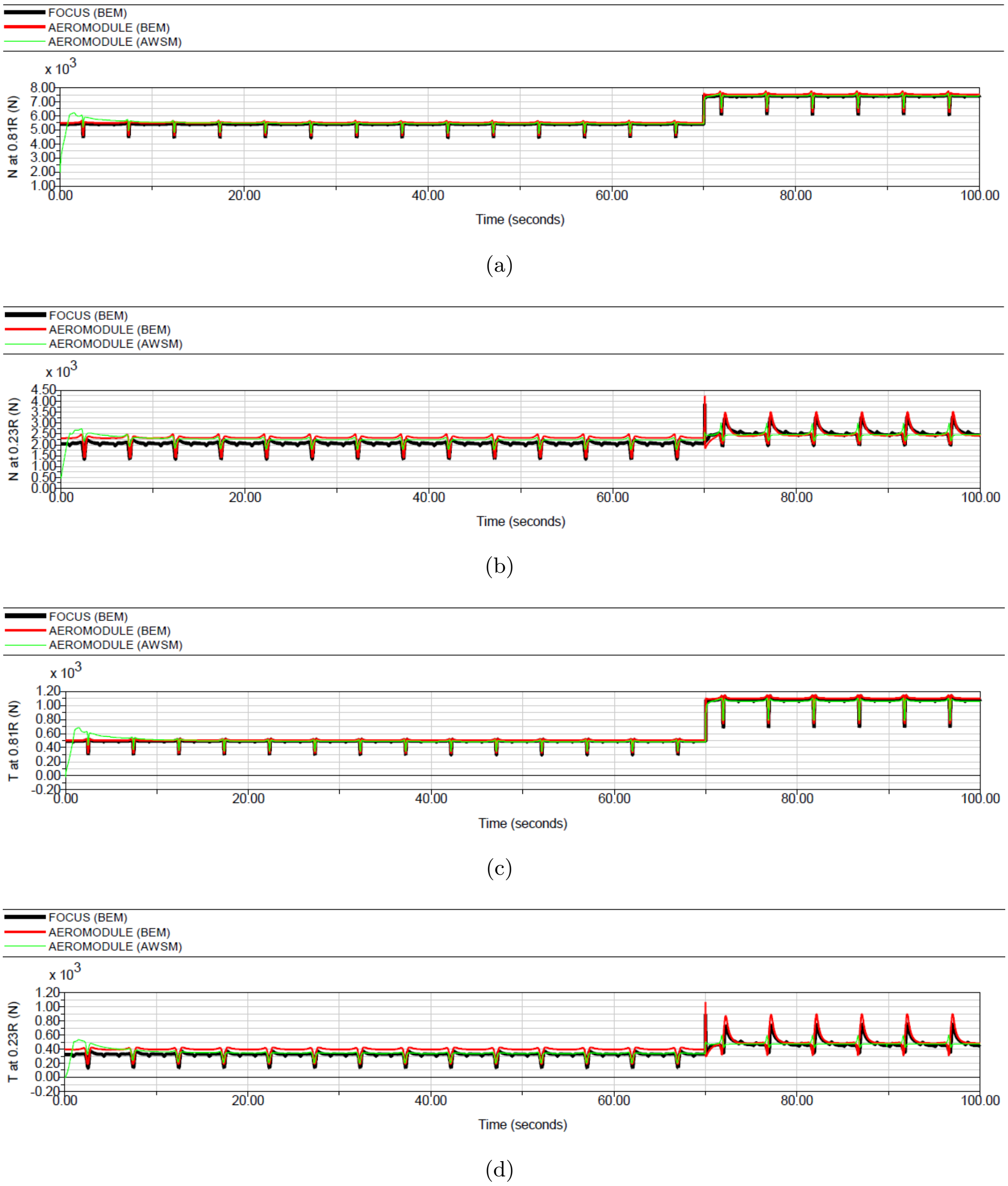

Figure 3.24: Case-1: Force distributions. **a:** Normal force distribution at 0.81R blade station, **b:** Normal force distribution at 0.23R blade station, **c:** Tangential force distribution at 0.81R blade station and **d:** Tangential force distribution at 0.23R blade station.

3.5.1.1 Aerodynamic aspects at 100th second

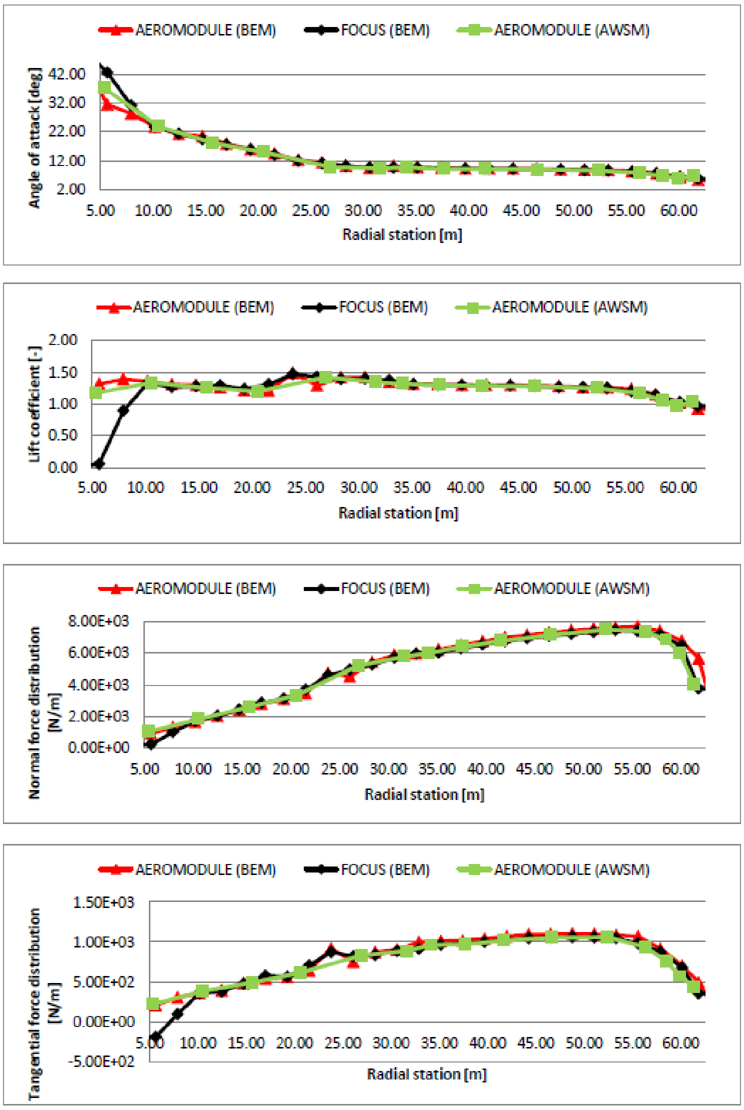

Figure 3.25: Case-1: Aerodynamic analysis at 100th second.

In this section aerodynamic analysis is done at 100th second along the complete length of blade. This analysis is done to observe the difference in the three modules when the flow completely stabilizes. From figure 3.25, it can be seen that all the three modules show a very good match in trend and coincide each other for α, c_l, N and T. In these figures, blade length starts from 5 m and ends at 62.5 m because blade stations before

5 m of length and after 62.5 m of length are not taken in AEROMODULE(AWSM) due to computation problems. There are small differences in all modules till blade length of 7 m, though both modules of AEROMODULE are close. FOCUS(BEM) shows the largest angle of attack, α, near root region therefore c_l is also smallest for it as the airfoils in this region are in stall. DU25-A17 airfoil is there at 24 m of blade length, AEROMODULE(AWSM) does not match with other two modules for c_l, and this is because of missing blade station there.

3.5.2 Structural aspects

In this section blade and tower loads are discussed. The theory behind blade and tower loads is explained in appendix A.

Blade loads

All the modules show good match for blade edgewise, flapwise and torsional bending moment in the blade root. The blade loads are explained only for one blade of the ART wind turbine.
As the blade is rigid and there is no tilt and cone angle in rotor, so the flap angle of blade is zero. Therefore the centrifugal force acts only in radial direction and has no component in flapwise direction. Due to no yaw misalignment the yaw rate is zero, so

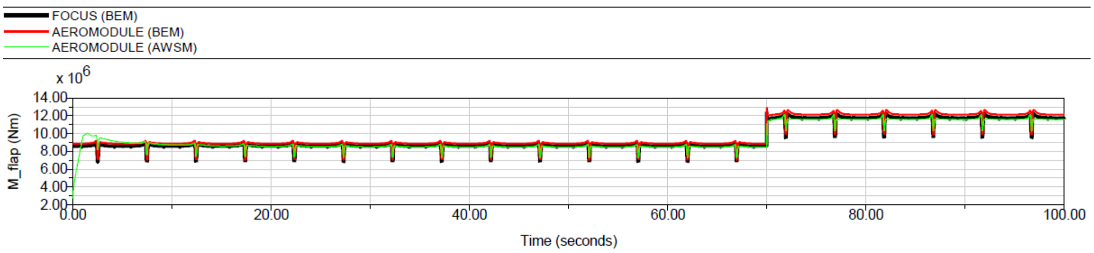

Figure 3.26: Case-1: Flapwise bending moment in the blade root.

the contribution of gyroscopic forces in flapwise direction of blade is also zero. Contribution due to gravity force is also zero because of zero flap angle as the blade is rigid. Axial aerodynamic force is the sole contributor of flapwise bending moment in the blade root. Axial aerodynamic force is dependent upon α, wind speed and u_{ind}.

Large dip in flapwise bending moment is due to blade passing the tower (tower presence). FOCUS(BEM) shows two small peaks also and this is because of blade coupling. Figure 3.26 shows the flapwise bending moment in the blade root.

Sudden increase in wind speed causes the rotor torque to increase which in turn increases the average value of edgewise moment. The amplitude of cyclic edgewise moment shows the contribution of gravity force of one blade. As the blade is rigid and there is no yaw misalignment therefore the flapping and yawing velocity is zero which makes the contribution of Coriolis force zero. It can be seen that the effect of tower

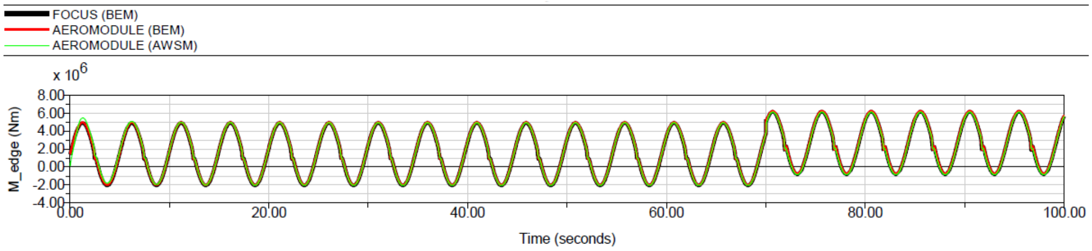

Figure 3.27: Case-1: Edgewise bending moment in the blade root.

presence is very small in edgewise bending moment in blade root, it only comes into picture when wind speed increases. This is because when the blade passes the tower there is fluctuation in the tangential speed of blades and the fluctuations become more pronounced when the wind speed is high. For all the modules there is really a good match. Figure 3.27 shows the edgewise bending moment in the blade root.

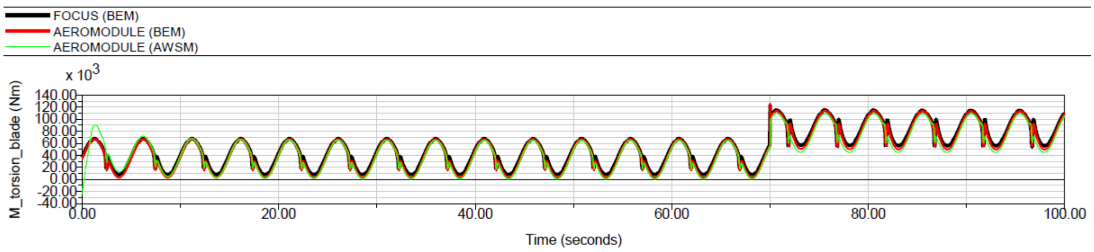

Figure 3.28: Case-1: Torsional moment in the blade root.

Figure 3.28 shows the torsional moment in the blade root. As there is no pitching action, torsion in blade root due to it is zero. As blades don't deform the torsional

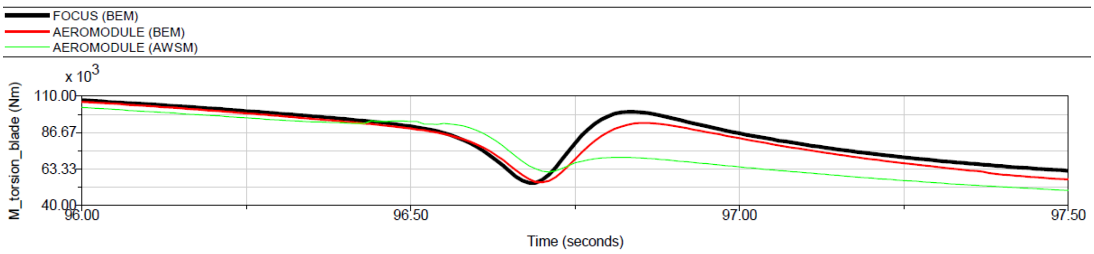

Figure 3.29: Case-1: Torsional moment in the blade root between 96th and 97.5th second.

moment due to centrifugal force is also zero. The offset between aerodynamic axis and elastic axis is very small, therefore the lift force which acts on $c_{1/4}$ point has a very small arm from the $c_{1/4}$ point to the elastic axis, and this causes a very small torsional moment in the blade root. As the blades are rigid therefore the blade lead-lag deflections are zero. So the blade flapwise bending moment along with blade lead-lag deflections does not cause torsional moment in the blade root. Due to blades flap pre bend and cyclic fluctuations in edgewise bending moment, blade root experiences torsional moment and this is the only contributor to it. All the modules show a good match except after 70th second. Figure 3.29 shows the torsional moment in the blade root between 96th and 97.5th second, it can be seen that both the BEM modules are close and have similar trend but AEROMODULE(AWSM) has slightly different trend and thus more investigation is needed here.

Tower loads

All the modules show good match for tower fore-aft and side-ways bending moment in the tower base and torsional moment in the tower top.

Fore-aft bending moment in the tower base is constant but when each blade passes the tower, the fore-aft bending moment shows a dip and this is due to the tower presence. The effect of tower presence on fore-aft bending moment is explained in section 4.1. The constant value is due to constant rotor thrust loading and drag loading due to wind. For all the modules there is really a good match. Figure 3.30 shows the fore-aft bending moment in the tower base.

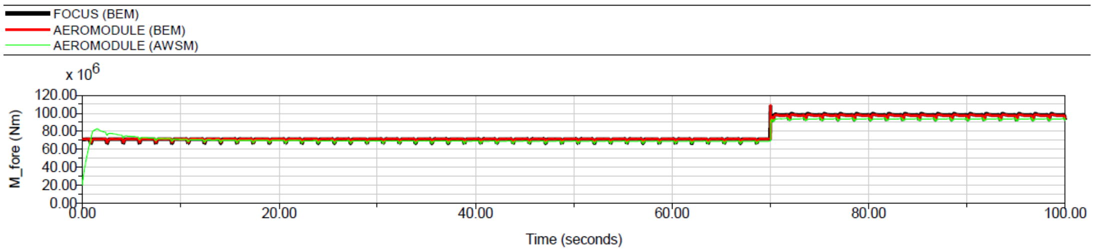

Figure 3.30: Case-1: Fore-aft bending moment in the tower base.

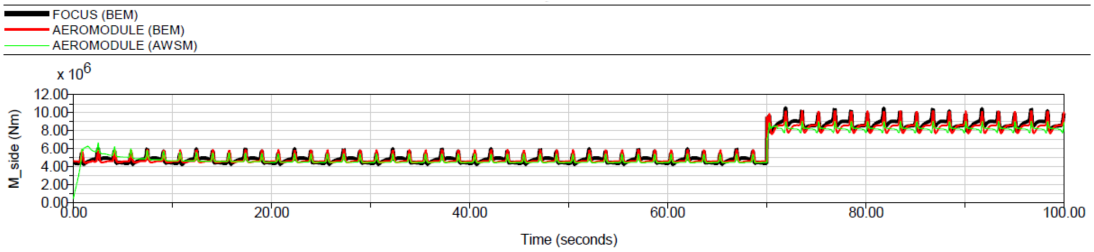

Figure 3.31: Case-1: Side-ways bending moment in the tower base.

Figure 3.31 shows the side-ways bending moment in the tower base. Side-ways tower bending moment is caused due to the edgewise forces in the blade. Rotor torque which acts on the tower top through gearbox/generator support also causes side-ways bending moment. This is the reason for its constant value. As no turbulence is taken into account in this case, therefore its contribution is zero. With zero yaw misalignment, gyroscopic force also doesn't cause side-ways bending moment. FOCUS(BEM) shows a sinusoidal curve while AEROMODULE(BEM) AND AEROMODULE(AWSM) do not, the reason is the mass imbalance in blades in FOCUS(BEM) and this can be seen in figure 3.32.

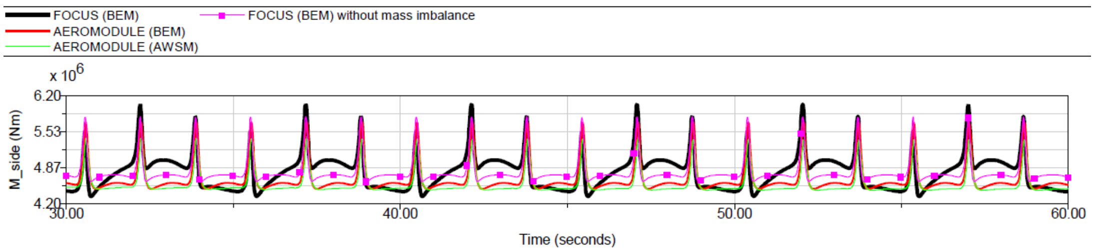

Figure 3.32: Case-1: Side-ways bending moment in the tower base after the 70th second.

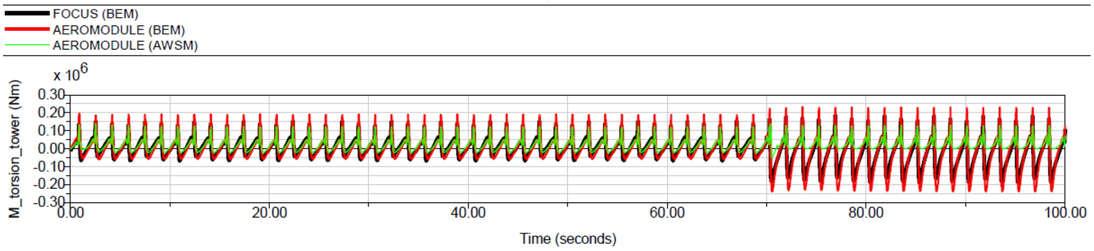

Figure 3.33: Case-1: Torsional moment in the tower top.

Figure 3.33 shows the torsional moment in the tower top. Torsional moment in the tower top is due to the rotor torque acting on it through gearbox/generator support when the rotor is tilted. As the yaw drive is working properly therefore its contribution is also zero. Because of zero yaw and tilt angle the mean value of fluctuation of torsional moment is zero. Peaks in torsional moment are due to tower presence. Tower presence causes sudden increase in edgewise forces in the blade root, this sudden increase along with pre-bend of rigid blade causes increase in torsional moment in the tower top. For all the modules there is really a good match but when the step change in wind speed takes place at the 70th second there is difference in the torsional moment in the tower top for all the three modules. Both the BEM modules have dynamic stall model but AEROMODULE(AWSM) does not take into consideration the effect of dynamic stall that is why the latter shows a different pattern as compared to former modules. Figure 3.34 shows the torsional moment in the tower top during step change in wind speed at 70th second.

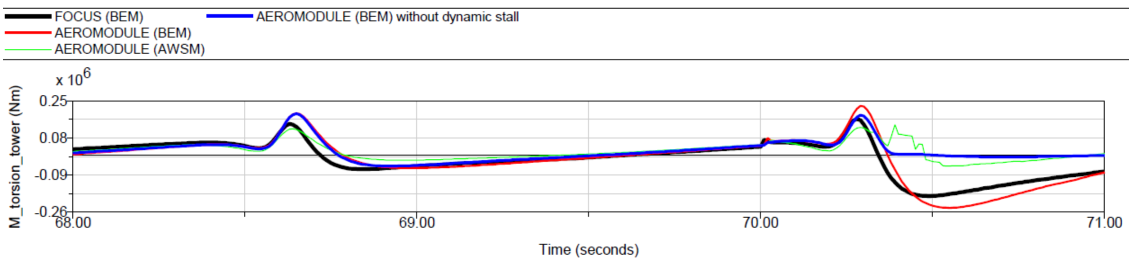

Figure 3.34: Case-1: Torsional moment in the tower top from 68th to 71st second.

3.6 Frequency Analysis of the ART wind turbine

In the frequency domain analysis a PSD function is used with a so called Fast Fourier Transform (FFT) of the measured time series. A peak in PSD plot represents a clear vibration at that frequency. These vibrations may be either response to excitations from the environment, or vibrations at the natural system frequencies. The PSD function thus helps in finding important contributors to fatigue loads. The phase information, which is present in the time signals is lost in the PSD.

The frequency analysis is done only at rated wind speed during normal operating condition based on FOCUS(BEM) results. All the excitation and natural frequencies can be seen in this operating condition. It is important for the dynamic behaviour of the wind turbine that natural system frequencies do not coincide with important excitation frequencies to avoid resonance. For frequency analysis *per revolution* (P)[1] representation is used and it is explained in equation 3.4.

Gravity load occurs once every revolution of rotor and hence is 1P in nature. Gravity load is discussed in section A.7.2. So it is necessary that natural frequencies of blade should not coincide with entire multiples of 1P. The average wind shear also gives an excitation at 1P and it is explained in section A.7.1. The fact is, wind shear fluctuates also in azimuth position, which results in the peak at 1P with a certain width. There are also peaks at nP (n = 2, 3, etc), which are results of smaller turbulent scales. The turbulence contains many structures that are smaller than the rotor size. When the blade passes through these structures, it feels excitations at entire multiples of 1P. This is known as the rotating sampling effect. The natural flapwise frequency of blade occurs in the range of 3P-4P and it will increase somewhat with rotational speed, due to centrifugal stiffening. Finally, for the normal operating condition, there is a clear peak at approximately 5.4P. This is a natural frequency (eigen frequency) of the system, the so called blade first edgewise mode. With respect to blade vibrations, also the phase difference between the vibrations of the individual blades is important. For instance, if the blades vibrate in phase in the edgewise sense (known as the collective rotor mode),

[1]A load which varies an integral number of times in relation to a complete revolution of the rotor is known as a 'Per rev' load and is given the symbol P.

$$1P = \frac{Frequency(Hz) \times 60}{\Omega} \tag{3.4}$$

there will be a reaction torque acting on the hub and the low speed shaft and hence in the drive train. This vibration can be damped actively in the generator and usually it is expected to be in 9P-11P range [15]. Figure 3.35a shows the collective edge mode on blades.

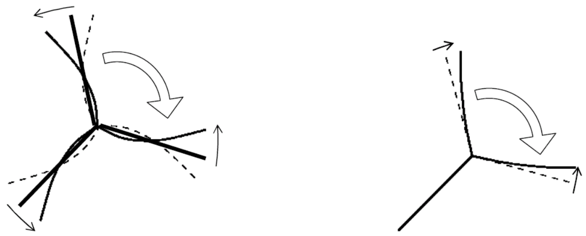

(a) (b)

Figure 3.35: a: Collective edge mode on blades, **b:** Reaction less mode on blades.

When the three blades vibrate at 120 degrees phase difference, the reaction torque is zero (reaction-less mode). Because of the nature of this mode, two components are present, one in backward direction and one in forward direction, the first one 1P lower than the natural blade frequency and the second one 1P higher than the natural blade frequency. In other terms, the rotor center of gravity moves at a frequency equal to the blade frequency plus or minus 1P, around the shaft center [27]. Due to this, the blade's vibration frequency f_{edge} translates to $f_{edge}\pm 1$P in the non-rotating frame. Figure 3.35b shows the reaction less mode on blades.
By looking at the fore-aft and side-ways tower bending moment curves, peaks at 1.45P represents the 1^{st} tower fore-aft and side-ways frequency respectively. Peak at 6.4P represents the effect of forward whirling mode on tower. The blade passing frequency can be seen in the fore-aft bending moment curve at 3P. The peak is at 3P because 3 blades are considered. Peak at 9.74P in the side-ways bending moment curve is because of the effect of collective edgewise frequency of blades. Figure 3.36 shows the natural and excitation frequencies on the ART wind turbine [23] [15]. From the figure 3.36 it can be seen that the natural frequencies of blades and tower did not coincide with the important excitation frequencies at rated wind speed during normal operating condition and thus there is no resonance.

Symbol	Description	Location
A	Self-weight of the blade	1P
B	Wind shear	1P
C	1st tower fore-aft frequency	1.45P
D	1st tower side-ways frequency	1.45P
E, F, I	Other turbulence	nP(n=2,3,4)
G	Blade passing frequency	3P
H	Natural flapwise frequency	3.2P
J	Backward whirling mode	1P lower than 'K'
K	Natural edgewise frequency	5.4P
L	Effect of forward whirling mode on tower	6.4P
M	Forward whirling mode	1P higher than 'K'
N	Collective edgewise frequency	9-11P
O	Effect of collective edgewise frequency on tower	9.74P

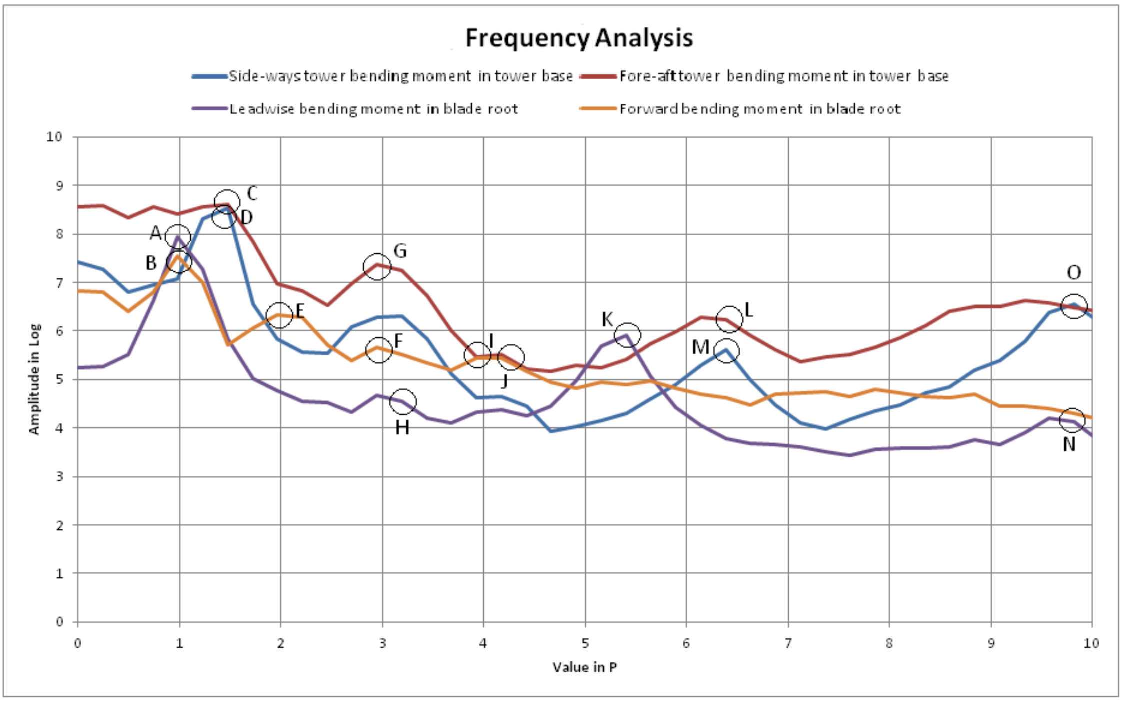

Figure 3.36: Frequency analysis of the ART wind turbine during normal operating condition at rated wind speed.

3.7 Conclusion

From the complete load set calculation of the ART wind turbine according to the IEC standard in FOCUS software, some load cases are selected which are also simulated in both the modules of AEROMODULE so as to validate AEROMODULE by FOCUS. Some test load cases are also formulated and simulation is done in all the modules. Test load case-1 is presented in this chapter and other load cases with results of all the three modules are given appendices C and D. Report [17] discusses the simulation results of all the other selected load cases and test load cases in both the BEM modules. From the aerodynamic analysis done for load case-1, it can be concluded that AEROMODULE(AWSM) doesn't have dynamic stall model but other two modules have it. Due to absence of dynamic stall model, at 0.23R blade station it shows 2D characteristics for c_l, while both the BEM modules show c_l higher than maximum 2D characteristic value because of dynamic stall model defined in them. At 70th second when dynamic inflow occurs, AEROMODULE(AWSM) shows a different trend as compared to both the BEM modules, this is because of wake modelling in AEROMODULE(AWSM) but not in other two modules. AEROMODULE(AWSM) initially takes more time to stabilize than both the BEM modules because the starting vortex shed from the rotor takes time to stabilize. More investigation is needed in AEROMODULE(BEM) as it doesn't take into account the effect of blade coupling while FOCUS(BEM) does. From both structural and aerodynamic analysis it was observed that there are repetitive peaks, these peaks are due to blade passing the tower i.e. tower presence. Structural aspects of load case-1 tells that as both tower and blades were rigid and there was zero yaw rate, therefore the contribution of Coriolis and gyroscopic force were zero respectively. Main contributing forces were gravity force, centrifugal, axial and tangential aerodynamic forces. From the frequency analysis it was found that the natural frequencies of blades and tower did not coincide with the important excitation frequencies at rated wind speed during normal operating condition and thus there is no resonance.

Chapter 4

Impact of Modelling in Physical Phenomena

In this chapter some aerodynamic phenomena are investigated in three modules viz. AEROMODULE(BEM), AEROMODULE(AWSM) and FOCUS(BEM). AEROMODULE is coupled with SIMPACK, in order to observe the structural behaviour of the ART wind turbine. For aerodynamic analysis, angle of attack (α), lift coefficient (c_l), axial induced velocity (u_{ind}), normal force distribution (N) and tangential force distribution (T) are discussed for all the modules.

4.1 Tower presence

4.1.1 Definition

In a HAWT, the wind starts bending away from the tower before it reaches the tower itself, even if the tower is round and smooth. Therefore, each time the rotor passes the tower, the power from the wind turbine drops slightly. Thus the reduction in power is caused due to the presence of tower.

4.1.2 Modelling in BEM and AWSM

In FOCUS(BEM) and AEROMODULE modules tower is modelled with a dipole. The flow around tower is shown in figure 4.1. The wind speed at the tower is zero because of stagnation, the wind slows down before it reaches this stagnation point. So when the blade passes the tower, the tower causes a small force in the upwind direction which

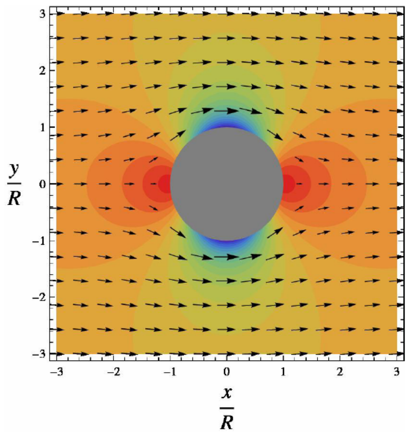

Figure 4.1: Flow around the tower (top view).

reduces the normal force on airfoil and thus reduces the effective axial wind velocity. The new effective axial wind velocity which the airfoil experiences is equal to,

$$U_{wind} - U_{i,rotor} - U_{tower}. \tag{4.1}$$

The dipole strength depends upon diameter of tower (d) and the local wind speed at the tower. In both the BEM modules local wind speed incident on the tower is given by,

$$U_{wind} - U_{i,rotor} * factor. \tag{4.2}$$

In both the BEM modules local wind speed is calculated at point 1 in figure 4.2, a factor is multiplied with $U_{i,rotor}$ and this factor is formulated by ECN [26]. The local wind velocity distribution implemented in both the BEM modules along the length of stream tube is shown in the figure 4.2. In the tweaked version of AEROMODULE(AWSM), the local wind speed incident on the tower is calculated at the same point as both the BEM modules. In AEROMODULE(AWSM), the wake of the rotor is modelled. As the wake moves downstream it breaks because of the tower presence. Because of the broken wake, the induction caused on the rotor is smaller as compared to unbroken wake. Due to the wake modelling, the local wind speed incident on the tower is smaller in AEROMODULE(AWSM) as compared to both the BEM modules. That means the dipole strength is smaller for AEROMODULE(AWSM) than both the BEM modules. More detail about the dipole model of tower is given in the PHATAS Manual [26].

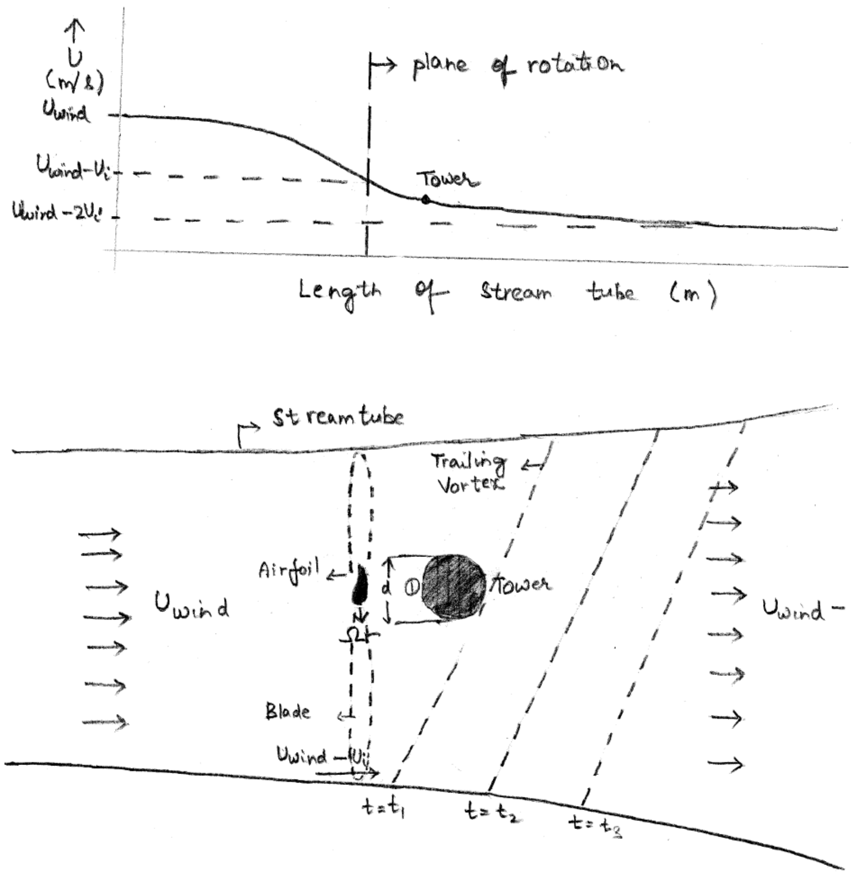

Figure 4.2: Sketch of the tower model in BEM and AWSM.

4.1.3 Comparison in BEM and AWSM

To investigate the effect of tower presence in all the three modules, wind speed of 12 m/s is considered. The pitch angle of blades is 4 degrees and are rotating with 12.1 rpm, blades are rigid. Below the tower presence is explained at 0.23R and 0.81R blade stations.

From figure 4.3, it can be seen that at 0.81R blade station, all the three modules almost follow the same trend for α, c_l, N and T. AEROMODULE(BEM) and FOCUS(BEM) show exactly the same trend because both of them are based on same theory. As α is not above 14 degrees therefore the airfoil at 0.81R blade station is not stalled and thus c_l follows the same trend as α for all the modules.

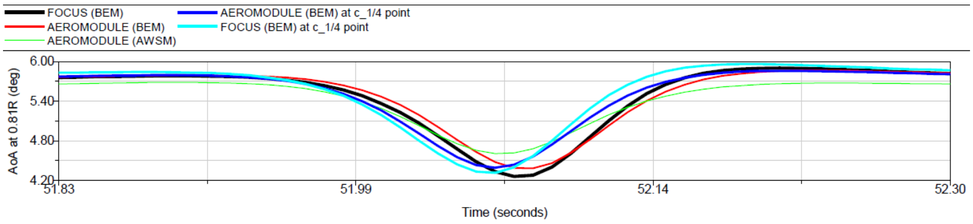

(a)

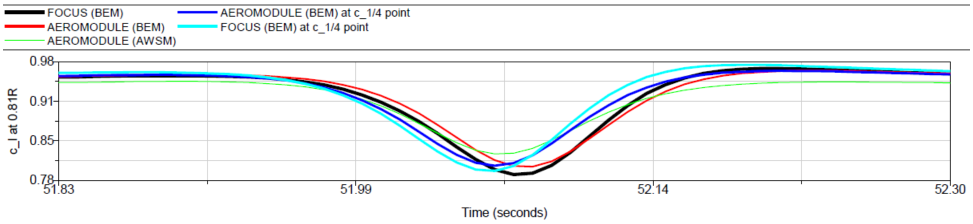

(b)

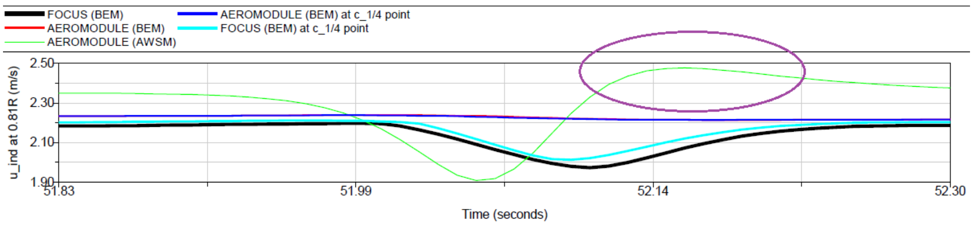

(c)

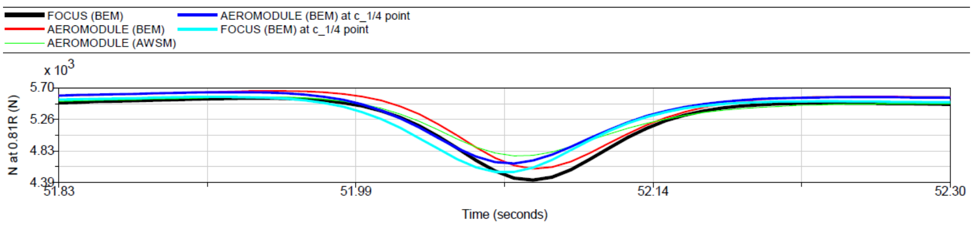

(d)

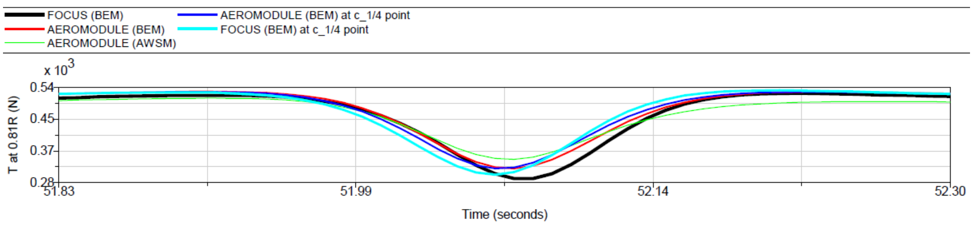

(e)

Figure 4.3: Aerodynamic analysis at 0.81R blade station from 51.83rd to 52.3rd second.

Tower is modelled by dipole in all the three modules, AEROMODULE(AWSM) slightly deviates in phase from both the BEM modules. This is because in AEROMODULE(AWSM), aerodynamic parameters are calculated at 1/4 chord point, whereas both the BEM modules calculate at 3/4 chord point. The 1/4 chord point of airfoil

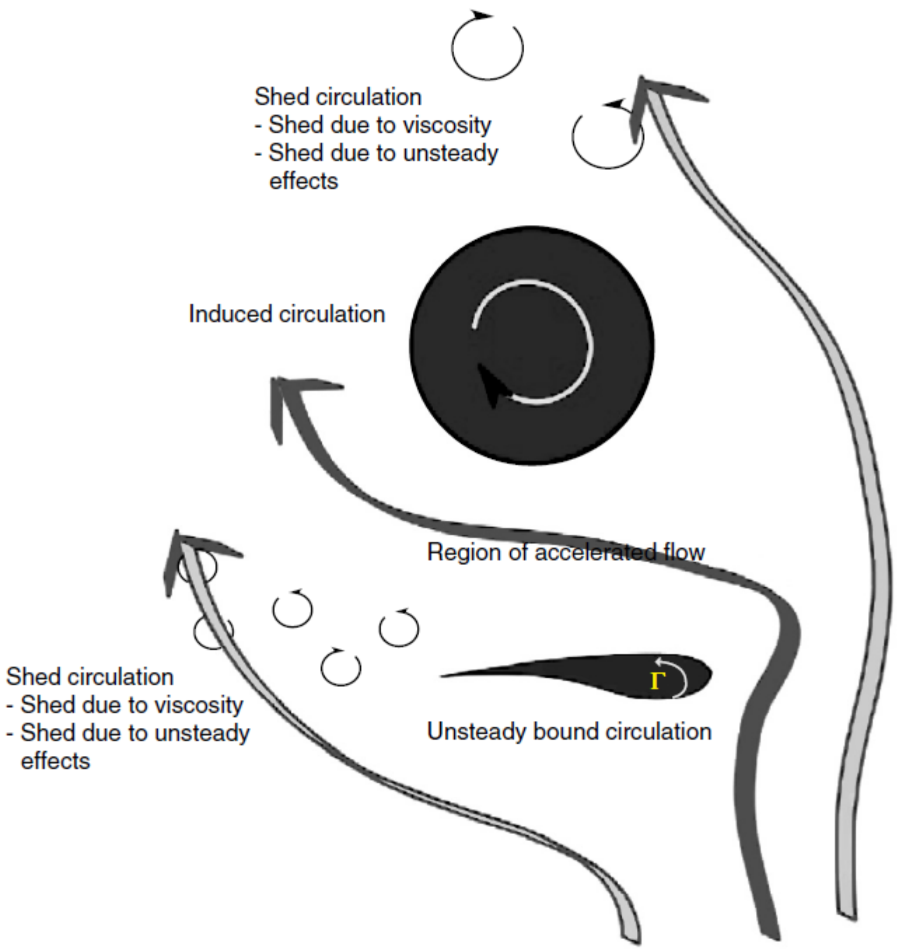

Figure 4.4: Phenomenon of tower presence in reality [13].

experiences the tower before than the 3/4 chord point. Due to different dipole strength in BEM and AWSM, there is difference in dip due to the tower presence in both the theories. u_{ind} for AEROMODULE(AWSM) shows larger dip than FOCUS(BEM) and also a different trend when the airfoil leaves the tower. In FOCUS(BEM), the rotor wake is not modelled while in AEROMODULE(AWSM) it is. As discussed in section

4.1.2, the wake of the rotor breaks because of the tower presence. Broken wake causes smaller induction as compared to unbroken wake. Because of the breaking of wake, AEROMODULE(AWSM) shows a larger dip for u_{ind} as compared to FOCUS(BEM), this can be seen in figure 4.3c. When the airfoil passes the tower, the shed vortex from the airfoil is deflected from its actual path because of the dipole strength, this can also be seen in figure 4.4. This may be the reason for a different trend (shown by purple circle) in AEROMODULE(AWSM). u_{ind} for AEROMODULE(AWSM) has slightly different phase than both the BEM modules (even when for both the BEM modules u_{ind} is calculated at 1/4 chord point), this may be due to the influence of the wake of the rotor blades, but more investigation is needed to prove this. AEROMODULE(BEM) does not show a dip for u_{ind} and thus needs to be investigated further. N and T are dependent on α and c_l and this can be seen in the trends of all the modules.

From figure 4.5, it can be seen that at 0.23R blade station, both the BEM modules are almost in the same phase but AEROMODULE(AWSM) is slightly deviated. Reason for this phase difference between BEM and AWSM is already explained above. All the modules have similar trend for α, c_l, N and T. As α is below 12.5 degrees therefore the airfoil at 0.23R blade station is not stalled and thus c_l follows the same trend as α for all the modules. As explained above, u_{ind} at 0.23R blade station also have a different phase and dip in AEROMODULE(AWSM) and FOCUS(BEM). AEROMODULE(BEM) doesn't show the dip and this is due to sudden increase in u_{ind} near 15 m of radial length, this can be seen in figures 4.6 and 4.7. At 0.23R blade station also N and T for all the modules show same trend as α and c_l. From the figure 4.5, it can be seen that AEROMODULE(AWSM) has a wider dip than both the BEM modules and this is because of the calculation of aerodynamic parameters at different chord wise point. But when aerodynamic parameters are calculated at 1/4 chord point for both the BEM modules, then there is hardly any difference in width of the dip.

Figures 4.6 and 4.7 give more aerodynamic insight about the tower presence. In these figures, blade length starts from 5 m and ends at 62.5 m because blade stations. Before 5 m of length and after 62.5 m of length, blade stations are not taken in AEROMODULE(AWSM) due to computation problems. At 51.92nd second, blade is near the tower and at 52.06th second it is in front of the tower. AEROMODULE(AWSM) calculates

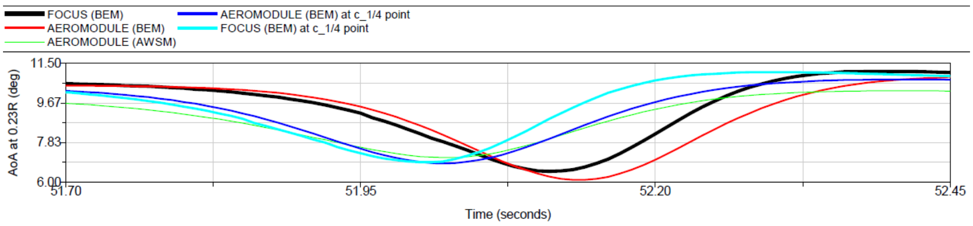

(a)

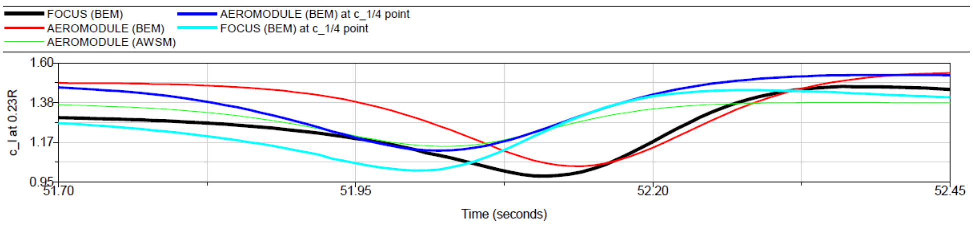

(b)

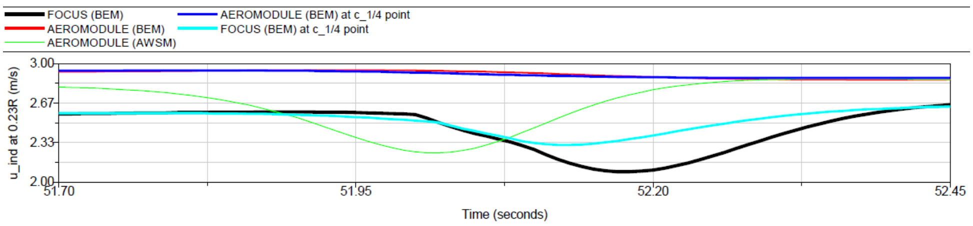

(c)

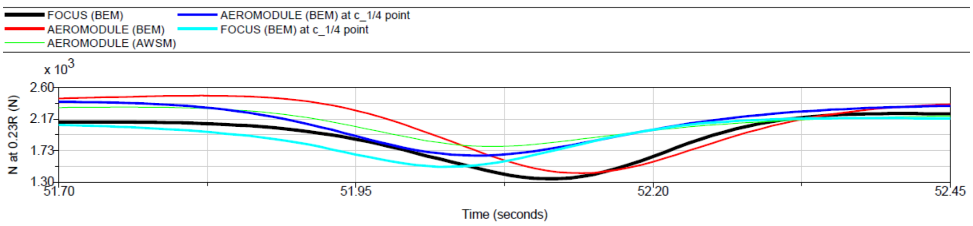

(d)

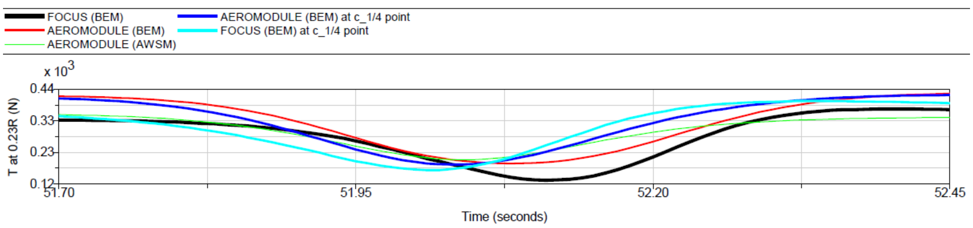

(e)

Figure 4.5: Aerodynamic analysis at 0.23R blade station from 51.7th to 52.45th second.

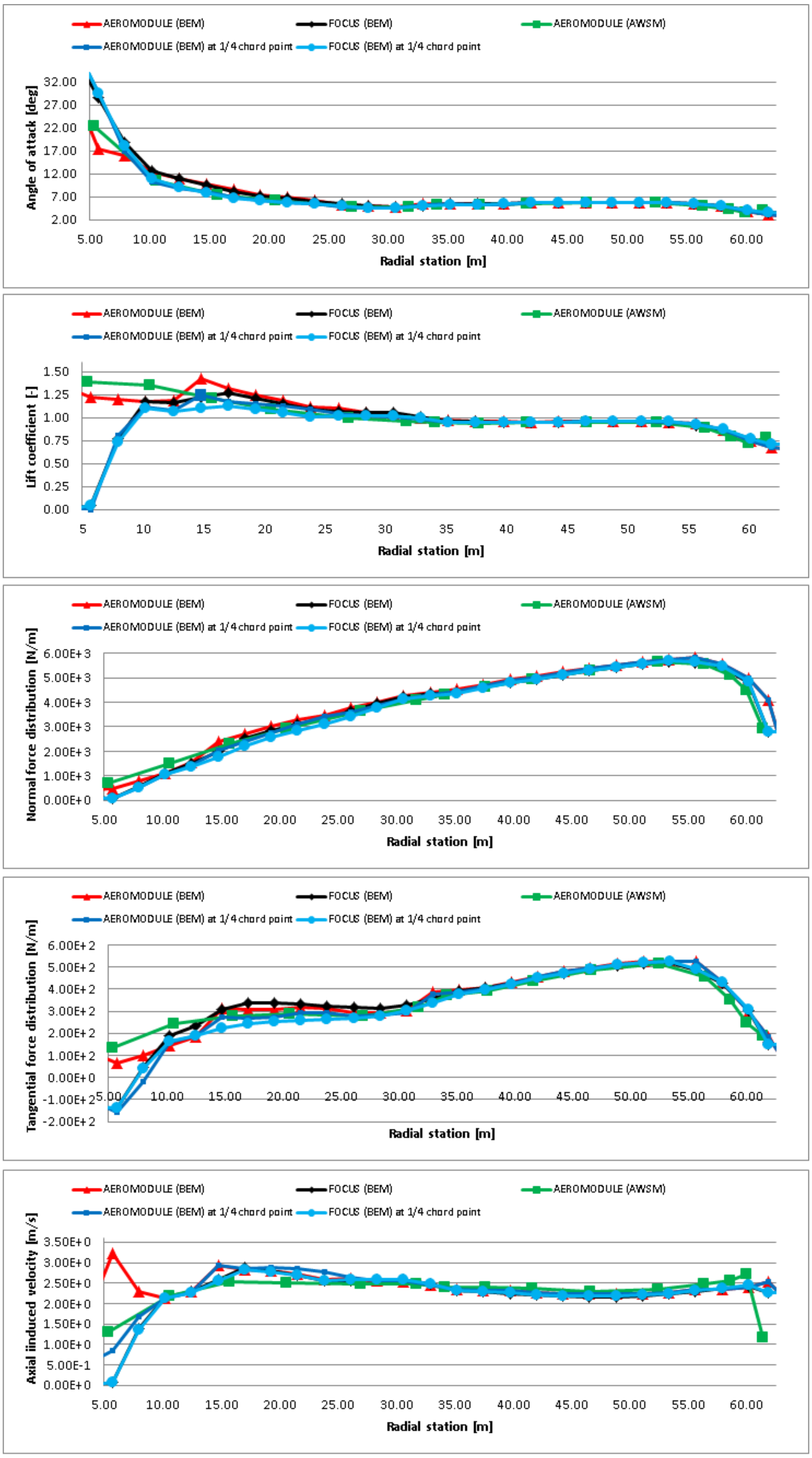

Figure 4.6: Aerodynamic insight at 51.92nd second.

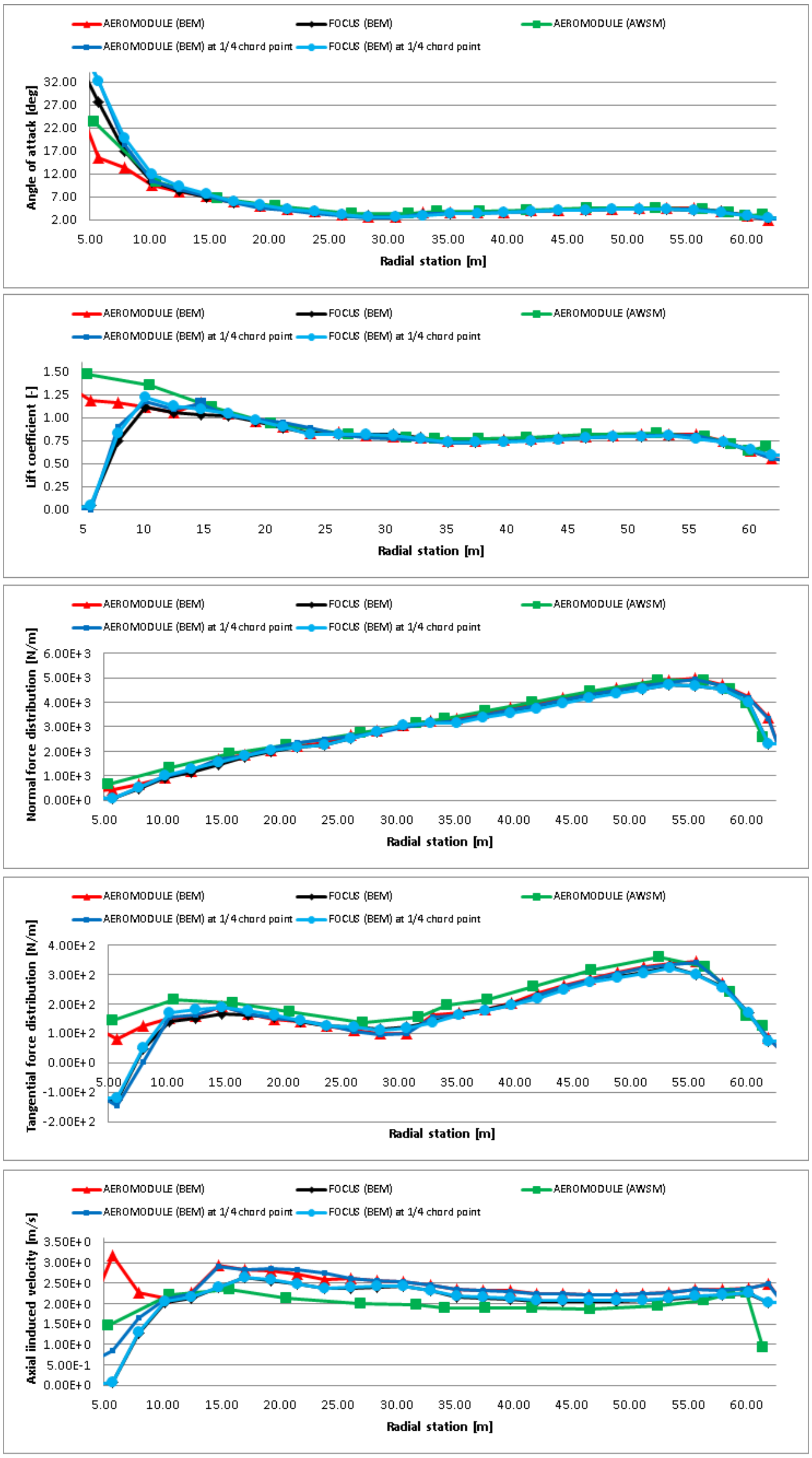

Figure 4.7: Aerodynamic insight at 52.06th second.

aerodynamic parameters at 1/4 chord point, whereas both the BEM modules calculate at 3/4 chord point. For more insight, aerodynamic parameters in both the BEM modules are also simulated at 1/4 chord point. There is a good match between all the modules at 51.92nd and 52.06th seconds, all the modules show similar trend because the tower is modelled as a dipole in all the modules.

From figures 4.6 and 4.7, it can be observed that when the blade is in front of tower the α distribution along the length of blade reduces because of the induction of the tower. Reduction in α distribution leads to decrease in c_l distribution because all the airfoils are below stall angle. Only at 5 m of radial length, α and c_l for AEROMODULE(AWSM) increases slightly. N and T are dependent upon α and c_l, and thus due to reduction in both of them it also causes reduction in N and T, this is observed in all the modules. Axial induced velocity u_{ind}, for FOCUS(BEM) and AEROMODULE(AWSM) decreases but not for AEROMODULE(BEM). Hence there is a need to do more investigation for AEROMODULE(BEM). As AEROMODULE(AWSM) doesn't have a dynamic stall model therefore it shows a higher c_l than FOCUS(BEM) near the root region in figures 4.6 and 4.7. AEROMODULE(BEM) also shows higher c_l than FOCUS(BEM) near the root region because of lower α. More investigation is needed to find out the cause of different α in both the BEM modules. When aerodynamic parameters are calculated at 1/4 chord point for AEROMODULE(BEM), there is good match with FOCUS(BEM) and FOCUS(BEM) at 1/4 chord point for α. AEROMODULE(BEM) shows a different trend near the root region for 1/4 and 3/4 chord points, this may be due to the contribution of unsteady aerodynamic loading at 1/4 chord point. More detail about the importance of 3/4 chord point in aerodynamics is given in the book by *Abbott* [1]. Due to lower α and higher c_l, AEROMODULE(BEM) shows a higher u_{ind} in the root region. At 15 m blade length, AEROMODULE(BEM) shows a peak for u_{ind} and this also needs to be further investigated.

4.1.4 Contribution of tower presence on loading of wind turbine

As discussed above, the effective wind velocity reduces on the blade when the blade passes the tower therefore the blades experience force in upwind direction, so the flapwise bending moment decreases, this can be seen in figure 4.8a.

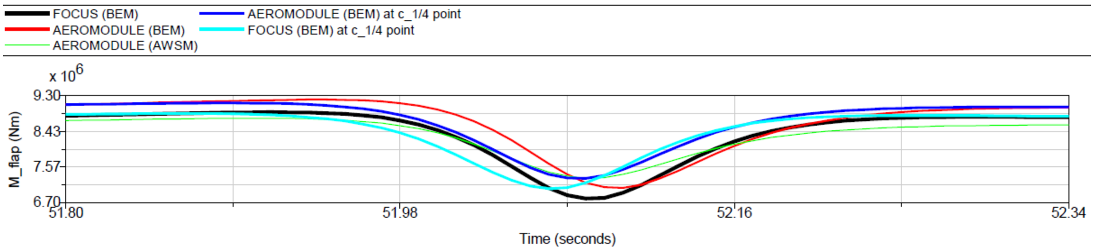

(a)

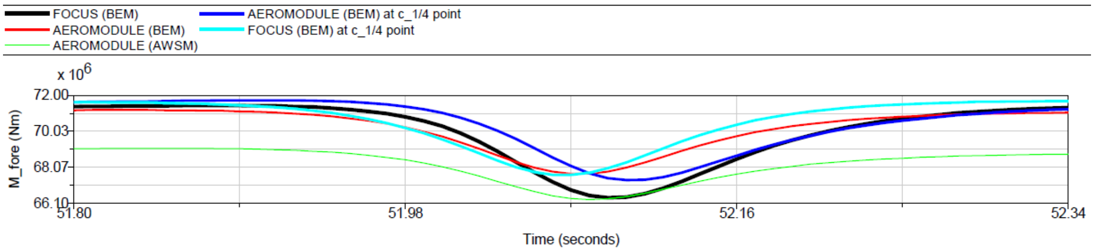

(b)

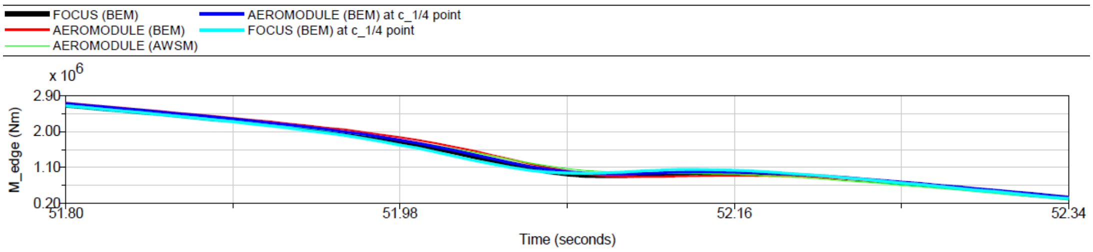

(c)

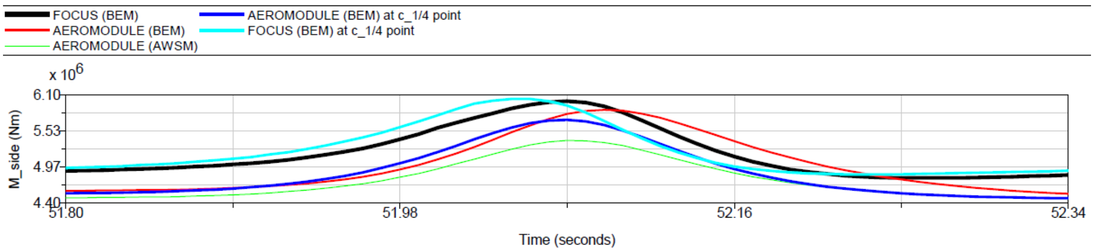

(d)

Figure 4.8: Contribution of tower presence on loading of wind turbine. **a:** Flapwise bending moment in the blade root, **b:** Fore-aft bending moment in the tower base, **c:** Edgewise bending moment in the blade root, **d:** Side-ways bending moment in the tower base.

Decrease in flapwise bending moment in the blade root causes decrement in fore-aft bending moment in the tower base because of dynamic interaction between rotor and tower. This can be seen in figures 4.9a and 4.8b. Both upwind direction of blade and fore direction of tower are considered in the $-X$ axis of the inertial reference system. Each time the rotor passes the tower, the power from the wind turbine drops slightly because the wind starts bending away from the tower before it reaches the tower itself. Drop in power means drop in torque (tangential force). Drop in tangential force has an effect on the edgewise bending moment in the blade root, and this can be seen in figure 4.8c. Due to different mean value of tangential force at different blades (blades near and away from the tower), the moment in the tower base changes. Figure 4.9b depicts the effect of tower presence on tower side-ways bending moment in the tower base. This change in moment in the tower base is in the positive direction of Y axis of inertia reference system. Figure 4.8d shows the increase in tower side-ways bending moment.

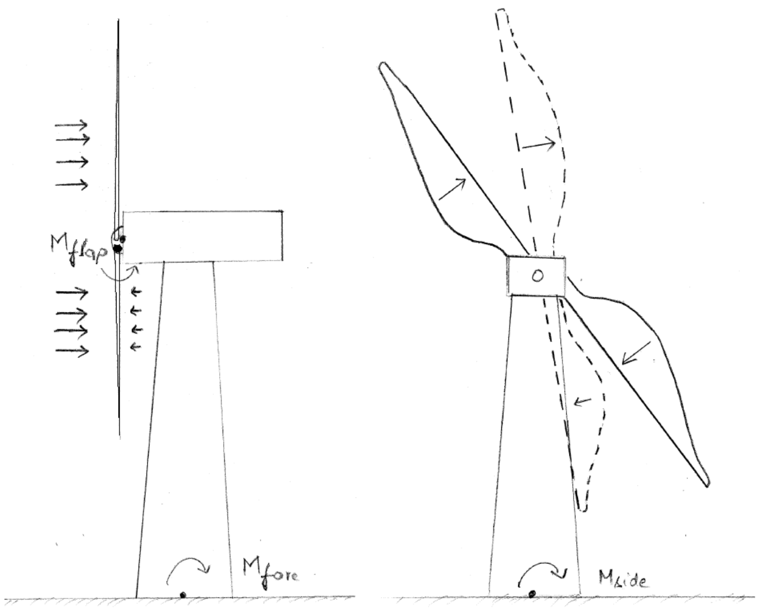

(a) (b)

Figure 4.9: a: Sketch for effect of tower presence in flapwise bending moment in the blade root and fore-aft bending moment in the tower base, **b:** Sketch for effect of tower presence in side-ways bending moment in the tower base.

4.1.5 Tower presence in rigid and flexible ART wind turbine

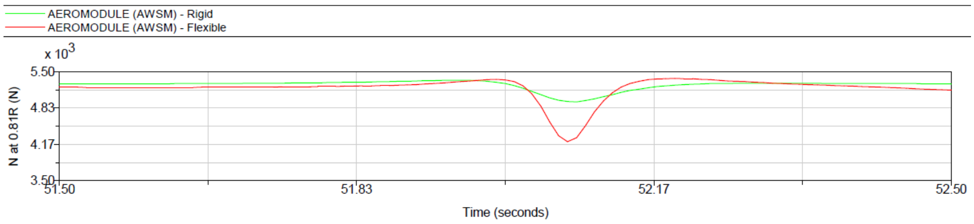

(a)

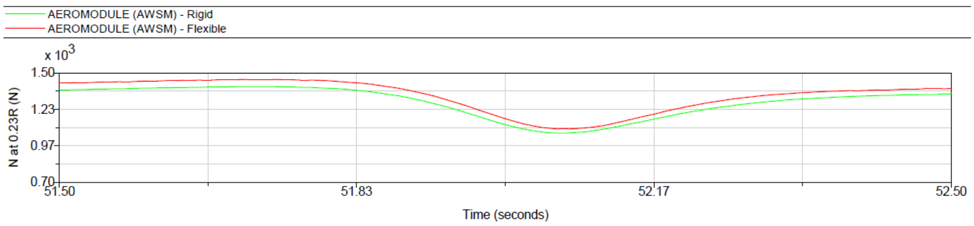

(b)

Figure 4.10: Tower presence in rigid and flexible ART wind turbine, **a:** At 0.81R blade station, **b:** At 0.23R blade station.

To study the phenomenon of tower presence in AEROMODULE(AWSM) for rigid and flexible ART wind turbine, following conditions are considered:

- Wind speed of 8 m/s is considered.
- The pitch angle of blades is 0 degree and the generator speed is constant at 1,173.7 rpm.
- The wind is not turbulent. No surface roughness is considered therefore no wind shear.
- The wind turbine rotor is not taken with any tilt and cone angle.
- The rotor of the ART wind turbine is not misaligned i.e. yaw angle is zero.

The tower causes an induction, whenever a blade passes in front of it. The net normal force on the blade decreases due to this induction. For flexible blade, dip in normal force distribution N is deeper compared to rigid blade because the former can deform while the latter can't. Flexibility in blade causes it to flap more in upwind direction which further reduces the net normal force on the blade station. Figure 4.10a shows the normal force distribution N for rigid and flexible blades at 0.81R blade station. There is hardly any difference in the dip of N at 0.23R blade station (near the root region) for rigid and flexible blades, this can be seen in figure 4.10b. Near root region airfoils are designed to be structurally more sound than aerodynamically, in order to support the complete blade. On comparing the figure 4.10a with figure 4.10b it can be concluded that at 0.81R blade station the dip due to tower presence is deeper than at 0.23R blade station because former has more flexibility than latter.

4.2 Dynamic inflow

4.2.1 Definition

Dynamic inflow [41] refers to the response of the larger flow field (downstream flow) to turbulence and changes in rotor operation. During rapid changes in flow and in rotor operation the larger flow field takes time to reach a steady state. Dynamic inflow happens when there is a sudden change in pitch angle of blade or a coherent gust strikes the rotor etc. So dynamic inflow is used to indicate the dynamic response of the inflow velocities in the rotor plane, to changes in the load conditions on the rotor [42].

4.2.2 Modelling in BEM and AWSM

To investigate dynamic inflow in all the three modules, a step change in wind speed is considered at 70th second from 12 to 16 m/s. The pitch angle of blades is 4 degrees and are rotating with 12.1 rpm, blades are rigid.
BEM theory gives two different equilibrium values of the induced velocity pertaining to the two wind speeds, viz. $u_{ind,12}$ and $u_{ind,16}$. As the step change in wind speed is considered at 70th second in 0.01 seconds, it can be said that according to BEM theory the inflow velocity will essentially change from 12 - $u_{ind,12}$ m/s to 16 - $u_{ind,16}$ m/s in 0.01 seconds at 70th second. But in reality this doesn't happen, more time is needed for the air to accelerate from 12 - $u_{ind,12}$ m/s to 16 - $u_{ind,16}$ m/s. This means that when change in wind speed is fast the inflow velocity will essentially still be equal to 12 - $u_{ind,12}$ m/s and only gradually change to the new equilibrium value of 16 - $u_{ind,16}$ m/s. AEROMODULE(BEM) and FOCUS(BEM) is based on this theory for

dynamic inflow model. In AEROMODULE(AWSM) whenever there is a step change in wind speed, the near wake behind the rotor changes because of changes in shed and trailing vortices, this changed near wake causes new induction in the rotor. The effect of dynamic inflow is smaller when there is a step change in wind speed than a step change in pitch angle [41] [40].

4.2.3 Comparison in BEM and AWSM

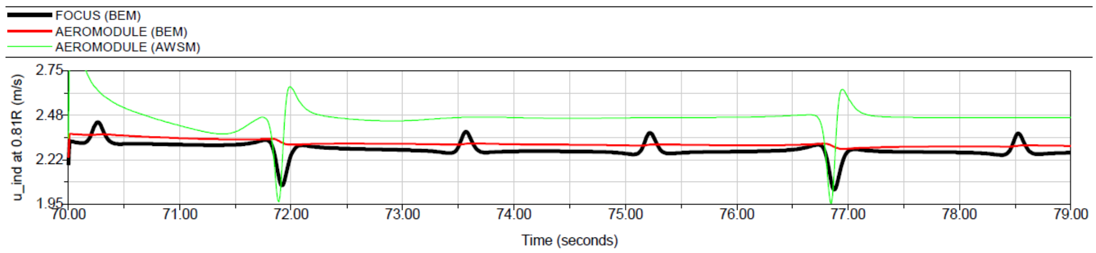

Figure 4.11: Axial induced velocity at 0.81R blade station from 70th to 79th second.

The time scale of dynamic inflow is directly proportional to D/U [41], where D is diameter of rotor and U is axial wind speed. Diameter of rotor is 128.4 m and U is 16 m/s, therefore time scale of dynamic inflow is around 8 seconds. From the figure 4.11, it can be seen clearly that the time taken by u_{ind} to become constant when the wind speed changes from 12 m/s to 16 m/s for all the modules are 3 seconds and it is in the same order of magnitude as calculated above. In this section the effect of dynamic inflow is explained at 0.23R and 0.81R blade stations.

From figure 4.12, it can be seen that at 0.81R blade station, all the three modules almost follow the same trend for α, c_l, N and T. AEROMODULE(BEM) and FOCUS(BEM) show exactly the same trend because both of them use the same principle for the dynamic inflow. AEROMODULE(AWSM) deviates from both the BEM modules because of different physics involved in dynamic inflow. Both the BEM modules hardly take any time for the flow to stabilize whereas, AEROMODULE(AWSM) takes more time to converge to the same trend than both the BEM modules. Whenever there is a change in wind speed the wake trailing behind the rotor takes some time to stabilize. The dynamic inflow peak in AEROMODULE(AWSM) is the smallest for α, c_l, N

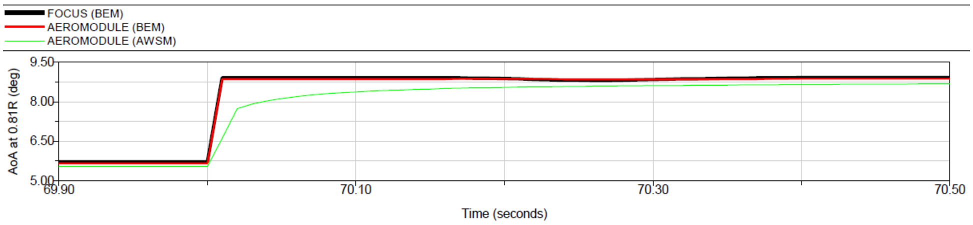

(a)

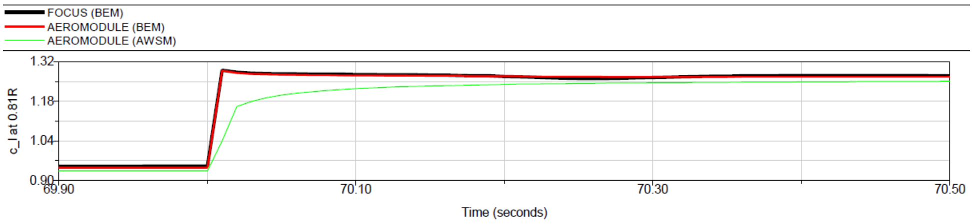

(b)

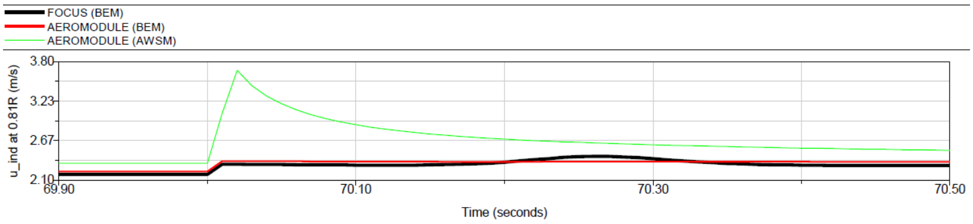

(c)

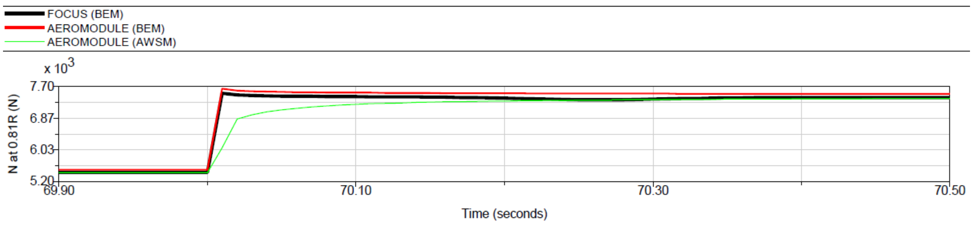

(d)

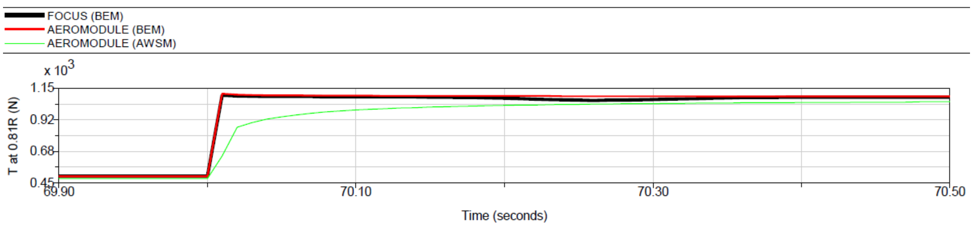

(e)

Figure 4.12: Aerodynamic analysis at 0.81R blade station from 69.9th to 70.5th second.

and T. Peak in AEROMODULE(AWSM) for axial induced velocity is due to dynamic inflow, and there is a sudden jump because the wake is disturbed due to increase in wind speed. Disturbed wake causes large axial induction on the rotor, it takes time for this disturbed wake to move away from the rotor and thus there is an exponential decrease in axial induced velocity for AEROMODULE(AWSM), this clearly shows how long it takes for the near wake to stabilize.

In BEM theory there are no vortices, in figure 4.13, bound vortex is considered for BEM in order to physically define the axial induction which is calculated at each airfoil. From the figure 4.13, it can be seen that in BEM there is no vortex from trailing

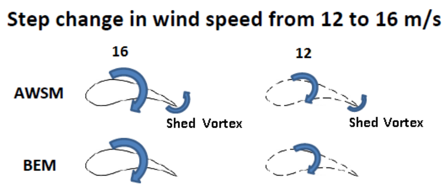

Figure 4.13: Difference between BEM and AWSM.

edge i.e. the shed vortex, while in AWSM it is taken into account. Now when the wind speed changes from 12 m/s to 16 m/s, the strength of bound vortex increases in both BEM and AWSM. In AWSM due to increase in wind speed the strength of shed vortex also increases and this has an effect on the axial induced velocity at every blade station. From the figure 4.12, it can be seen that AEROMODULE(AWSM) shows a smaller peak and a gradual change in α, c_l, N and T for the dynamic inflow effect while both the BEM modules show a larger peak and steep change. The differences in AEROMODULE(AWSM) and both the BEM modules may be because of inclusion of shed vortex in AEROMODULE(AWSM) but not in both the BEM modules. From figure 4.14, it can be seen that AEROMODULE(BEM) and FOCUS(BEM) trends are close to each other but AEROMODULE(AWSM) is far away at 0.23R blade station. Due to change in wind speed at 70th second, the airfoil at 0.23R blade station is in stall. At inboard region all the modules are trying to converge and both the BEM modules show large peaks as compared to AEROMODULE(AWSM), this is because both the BEM modules have dynamic stall model whereas AEROMODULE(AWSM) doesn't.

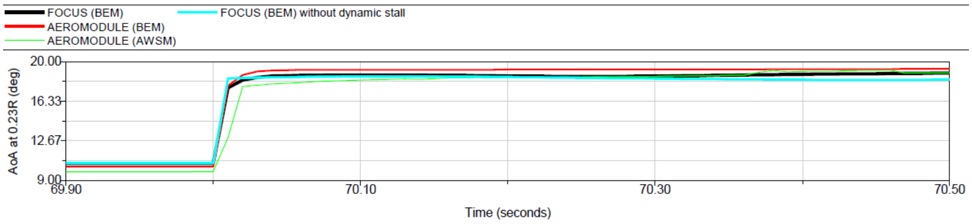

(a)

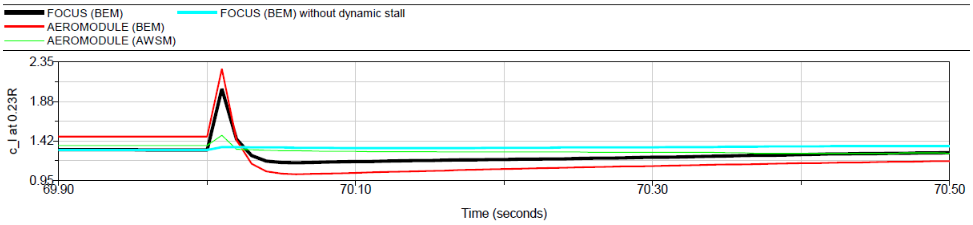

(b)

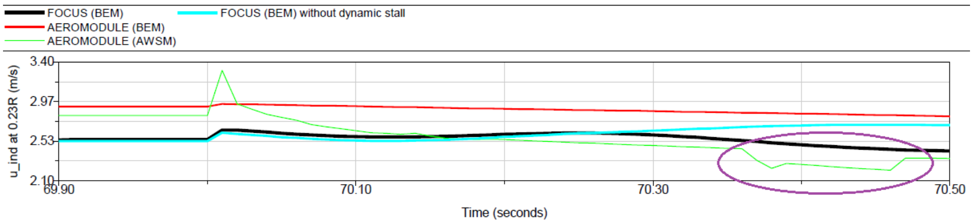

(c)

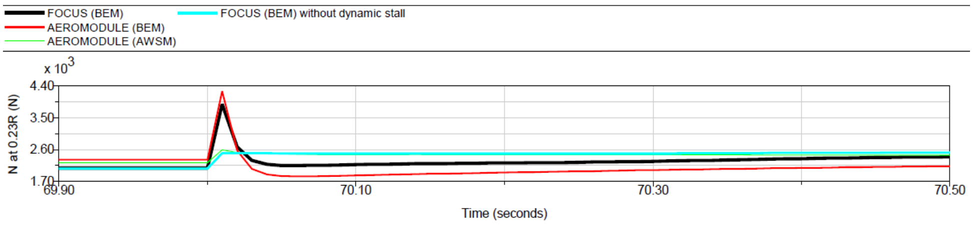

(d)

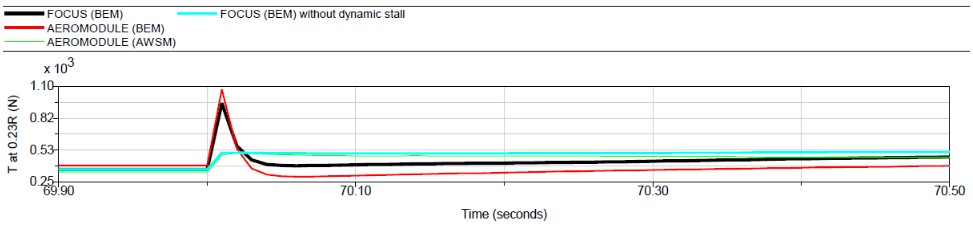

(e)

Figure 4.14: Aerodynamic analysis at 0.23R blade station from 69.9th to 70.5th second.

c_l, N and T for AEROMODULE(AWSM) converges faster than both the BEM modules because of absence of dynamic stall model. The axial induced velocity shows a higher peak for AEROMODULE(AWSM) than both the BEM modules, because of modelling of shed vortex in former and not in latter. There are some disturbances in u_{ind} and α and for AEROMODULE(AWSM) between 70.25 and 70.5 second, this is because the airfoil at 0.23R is in stall region. The time series is zoomed at 70th and 70.04th second to get more aerodynamic insight about dynamic inflow.

Figures 4.15 and 4.16 give the aerodynamic insight at 70th (before dynamic inflow) and 70.04th second (during dynamic inflow) respectively. In these figures, blade length starts from 5 m and ends at 62.5 m because blade stations before 5 m of length and after 62.5 m of length are not taken in AEROMODULE(AWSM) due to computation problems. It can be observed from the figures 4.15 and 4.16, that due to increase in wind speed in all the modules, α increases which leads to increase in c_l in mid-board and out-board region. Decrease in c_l at in-board region is only for FOCUS(BEM), because at in-board region airfoils are stalled, whereas in rest part of the blade they are not stalled. Due to increase in wind speed and c_l, N and T also increase. From axial induced velocity graphs in the figures 4.15 and 4.16, it can be seen that in both the BEM modules u_{ind} almost remains the same but for AEROMODULE(AWSM) it increases significantly from the radial distance of 20 m. From the axial induced velocity graphs it can be said that for AEROMODULE(AWSM) near the root region there is hardly any effect of dynamic inflow but at mid-board and out-board there is a significant increase. From aerodynamics theory it is known that dynamic inflow phenomena depends mainly on the trailing (tip) vortices and the shed near wake being accounted for through unsteady profile aerodynamics [40]. As AEROMODULE(AWSM) takes into consideration the tip and shed vortices therefore the change in axial induced velocity from 70th to 70.04th second may be because of them.

So it can be concluded that at 0.81R blade station, the dynamic inflow effect may be due to small contribution of shed vortex and large contribution of tip vortex. At 0.23R blade station, the influence of tip vortex is very small and thus the change in u_{ind} is also small for AEROMODULE(AWSM). Shed vortex also contributes a bit to the u_{ind} at 0.23R blade station. Still more investigation is needed to prove this conclusion.

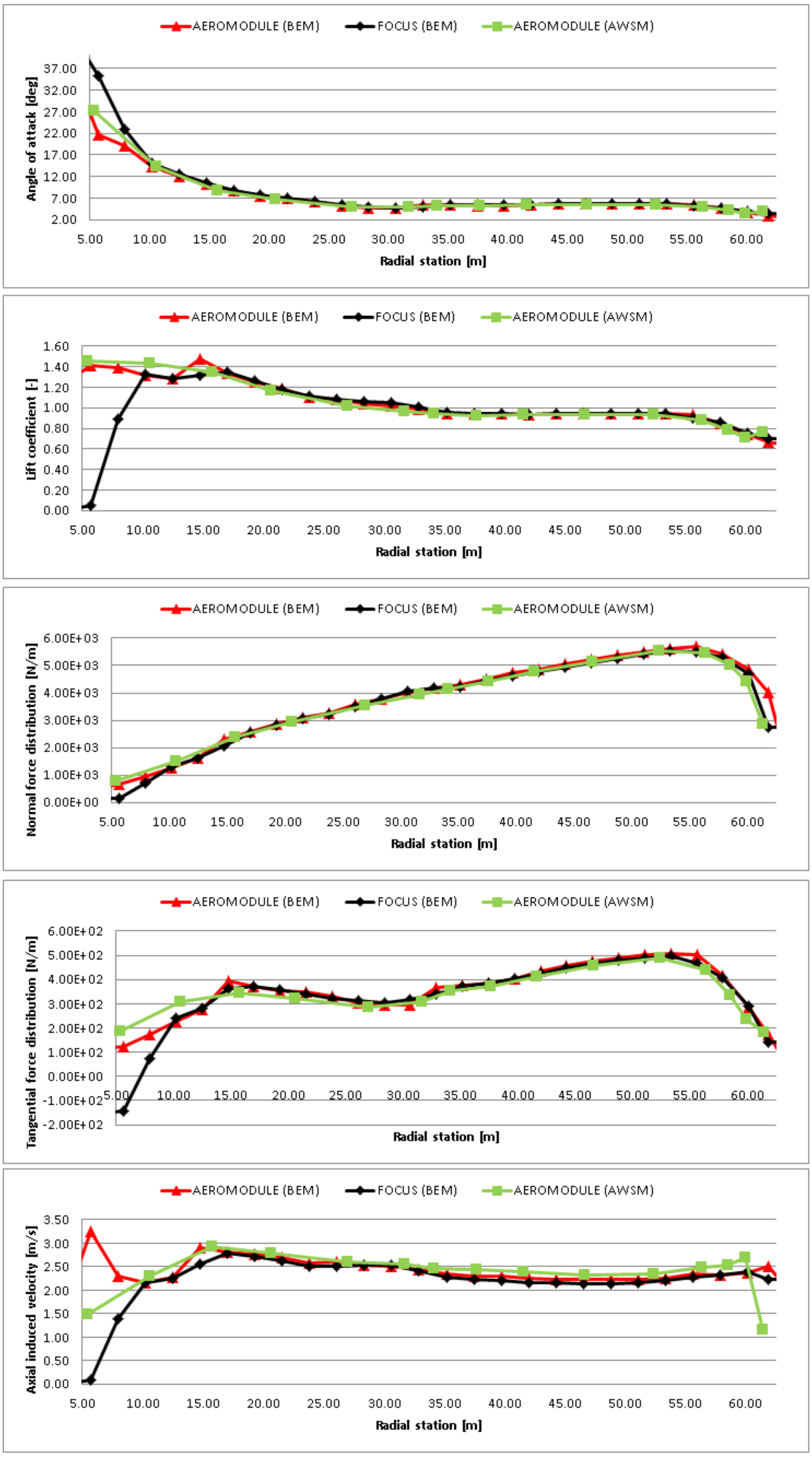

Figure 4.15: Aerodynamic insight at 70th second.

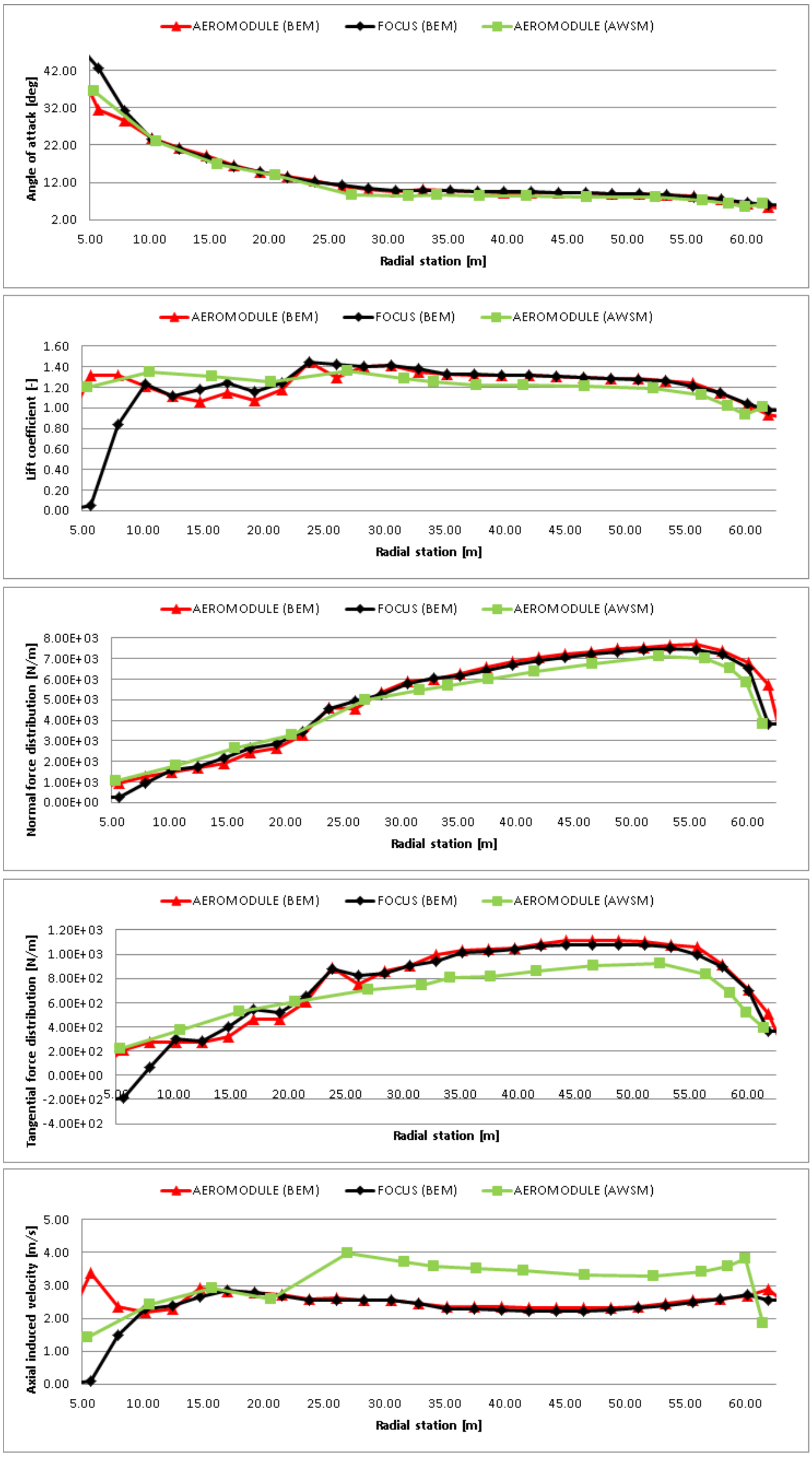

Figure 4.16: Aerodynamic insight at 70.04th second.

4.2.4 Contribution of dynamic inflow on loading of wind turbine

At the 70th second when the wind speed changes in step fashion, there is a sudden rise in axial aerodynamic force on rotor, this is due to dynamic inflow, this can be seen by the purple circle in figure 5.4a. When the wind speed increases the angle of attack

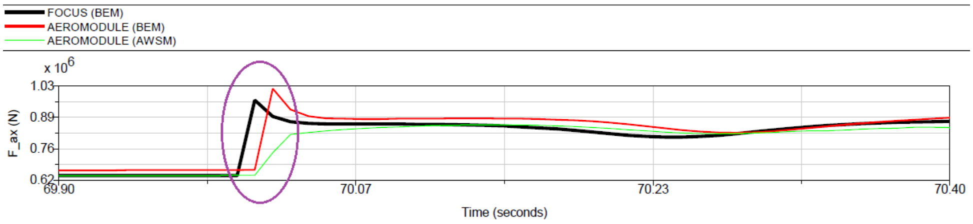

(a)

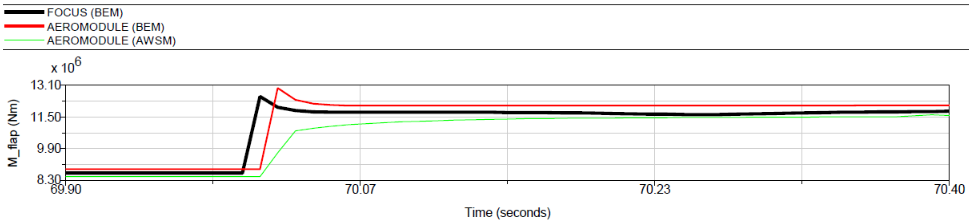

(b)

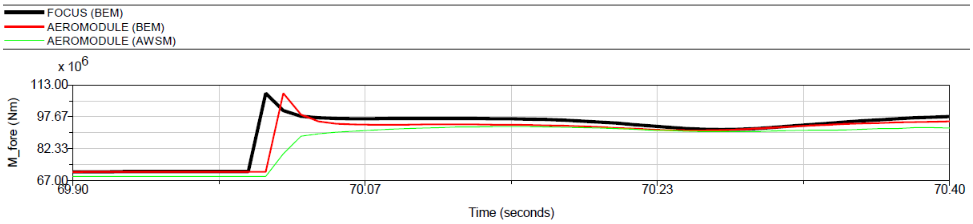

(c)

Figure 4.17: Effect of dynamic inflow on loading of wind turbine.

(α) also increases and due to slightly different α, the axial aerodynamic force on rotor for all the modules differs slightly. As axial aerodynamic force on rotor is the main contributor for blade flapwise and tower fore-aft bending moments, therefore similar effect of dynamic inflow can also be seen in blade and tower moments and this can be seen in figures 5.4b and 5.4c.

4.2.5 Dynamic inflow in rigid and flexible ART wind turbine

To study the phenomenon of dynamic inflow in AEROMODULE(AWSM) for rigid and flexible ART wind turbine, following conditions are considered:

- Step change in wind speed from 8 to 11 m/s is considered.
- The pitch angle of blades is 0 degree and the generator speed is constant at 1,173.7 rpm.
- The wind is not turbulent. No surface roughness is considered therefore no wind shear.
- The wind turbine rotor is not taken with any tilt and cone angle.
- The rotor of the ART wind turbine is not misaligned i.e. yaw angle is zero.

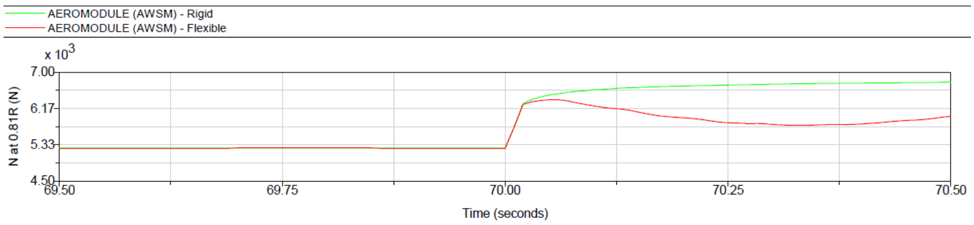

(a)

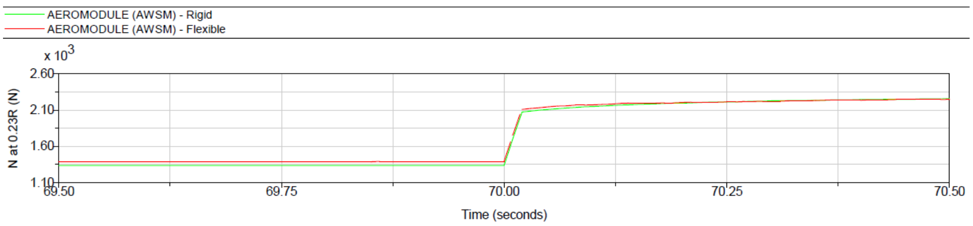

(b)

Figure 4.18: Dynamic inflow due to step change in wind speed from 8 to 11 m/s in rigid and flexible ART wind turbine, **a:** At 0.81R blade station, **b:** At 0.23R blade station.

From figure 4.18a, it can be seen that N at 0.81R blade station for flexible blade reduces after increasing (increase in N is due to increase in wind speed) but not in rigid blade. This is because the induction of the near wake causes the flexible blade to flap in upwind direction, while rigid blade can't flap. At 0.23R blade station, the airfoil is structurally more sound than aerodynamically. Therefore, both rigid and flexible blade show same results in figure 4.18b.

4.3 Conclusion

From the aerodynamic phenomena, it was found that AEROMODULE(AWSM) predicts tower presence and dynamic inflow in a different way than both the BEM modules. The dip due to tower presence is smaller in AEROMODULE(AWSM) than both the BEM modules because of different dipole strength. There is also a difference in phase in BEM and AWSM because of calculation of aerodynamic parameters at different chord wise points. Flexible blade has deeper dip than rigid blade near the tip region for the phenomenon of tower presence in AEROMODULE(AWSM). Effect of dynamic inflow due to increase in wind speed is small, both the BEM modules show a sudden peak which AEROMODULE(AWSM) does not show because of modelling of wake in latter. The phenomena of dynamic inflow is better predicted by AWSM because it considers trailing and shed vortices which BEM doesn't consider. Flexible blade shows a different trend for dynamic inflow as compared to rigid blade for AEROMODULE(AWSM).

Chapter 5

Results and Conclusions

Uncertainty in aerodynamic load prediction is an important parameter driving the price of wind energy and thus the wind turbine community is in need of more sophisticated tools for evaluating aerodynamic blade loading. This report presents tools which are based on two theories viz. Blade Element Momentum (BEM) and lifting line theory (AWSM). Both the theories were used in predicting the aerodynamic phenomena and loads on the ART wind turbine, difference between both the theories were observed and jotted down. Conclusions that can be drawn from this report are in line with the research questions which were formulated in the chapter 1.

5.1 Main Research Question

The main research question of the thesis was,

Are there significant differences in prediction of aerodynamic performance and loads using an aerodynamic module based upon BEM theory compared to a lifting line implementation?

From the thesis report it was found that there are significant differences in prediction of aerodynamic performance and loads using an aerodynamic module based upon BEM theory compared to a lifting line (AWSM) implementation. The differences in both the theories can be answered on the basis of the two sub questions of the main research question.

5.1.1 Sub Questions

In this section two sub questions of the main research question are discussed.

- ***Q1. How do the differences in the aerodynamic model represent physical phenomena like dynamic inflow and tower presence?***

For the aerodynamic performance, two physical phenomena were simulated for both the theories (BEM and AWSM) viz. dynamic inflow and tower presence. Results for both these physical phenomena are discussed below.

Dynamic inflow

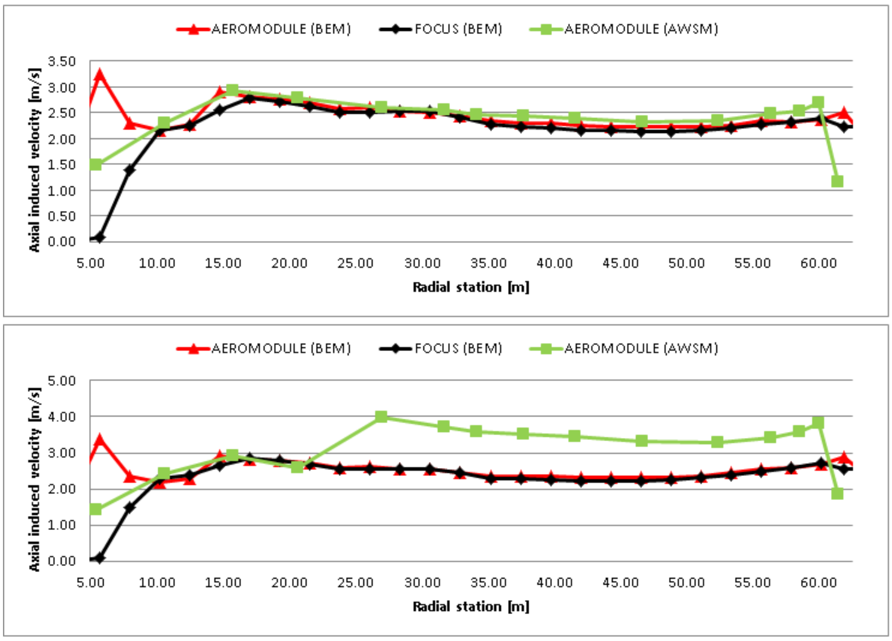

Figure 5.1: Axial induced velocities at 70th and 70.04th second.

Figure 5.1 shows the difference in axial induced velocity from 70th to 70.04th second, this time interval describes the dynamic inflow effect. For AEROMODULE(AWSM) there is a considerable change in axial induced velocity from 70th to 70.04th second at the mid-board and out-board parts of the blade, while for both the BEM modules there is not much change. This difference may be due to the contribution of shed vortex and influence of trailing vortex near the tip region. Near the root region, all the modules show almost similar trend for both 70th and 70.04th second. It can be observed that along the complete length of blade, it is near the tip and mid-board region where most effect of dynamic inflow can be seen for AEROMODULE(AWSM) but for both the BEM modules it is not much. From aerodynamic theory it is known that dynamic inflow phenomenon depends mainly on the trailing vortices and the shed near wake being accounted for through unsteady profile aerodynamics [40]. So from this statement it may be concluded that AEROMODULE(AWSM) predicts dynamic inflow in a more correct manner as compared to both the BEM modules, because it takes into consideration the trailing and shed vortices which both the BEM modules don't. Figure 5.2 gives more insight about the difference in AEROMODULE(AWSM) theory and BEM theory in general.

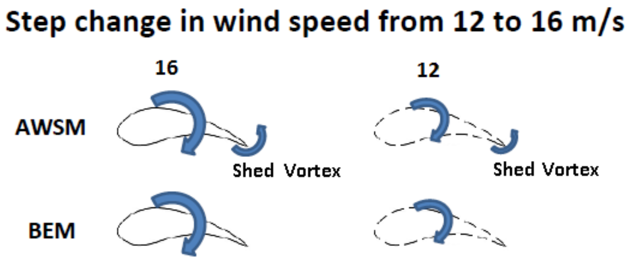

Figure 5.2: Dynamic inflow effect in both the BEM and AWSM on step change in wind.

Tower Presence

Figure 5.3a shows the angle of attack at 0.81R blade station from 51.83rd to 52.3rd second. It can be concluded from this figure that AEROMODULE(AWSM) shows tower presence differently than both the BEM modules even though all the modules have same dipole model for tower. AEROMODULE(AWSM) slightly deviates in phase from both the BEM modules. This is because in AEROMODULE(AWSM), aerodynamic parameters are calculated at 1/4 chord point, whereas both the BEM modules calculate at 3/4 chord point. The 1/4 chord point of airfoil experiences the tower before than the 3/4 chord point. Due to wake modelling in AEROMODULE(AWSM), the dipole strength for it is smaller than both the BEM modules. Due to different dipole strength

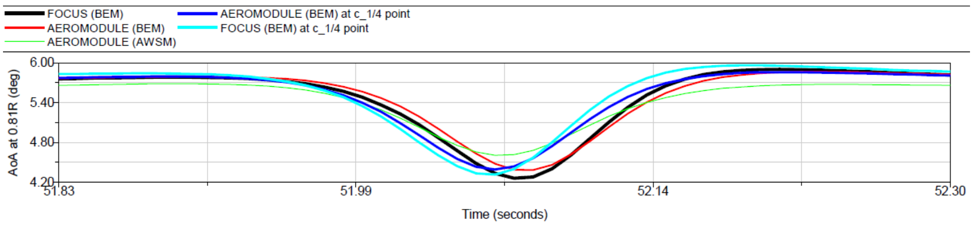

(a)

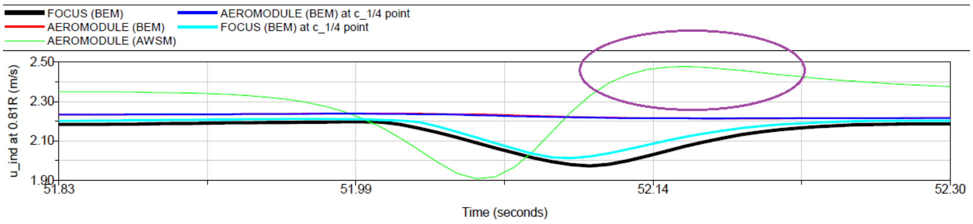

(b)

Figure 5.3: Aerodynamic analysis at 0.81R blade station from 51.83th to 52.3th second.

in BEM and AWSM, there is difference in dip due to tower presence in both the theories. u_{ind} for AEROMODULE(AWSM) shows larger dip than FOCUS(BEM) and also a different trend when the airfoil leaves the tower. In AEROMODULE(AWSM) the wake of the rotor breaks because of the tower presence. Broken wake causes smaller induction as compared to unbroken wake. Because of the breaking of wake, AEROMODULE(AWSM) shows a larger dip for u_{ind} as compared to FOCUS(BEM), this can be seen in figure 5.3b. When the airfoil passes the tower (shown by purple circle), the shed vortex from the airfoil is deflected from its actual path because of the dipole strength and that may be reason for a different trend in AEROMODULE(AWSM). u_{ind} for AEROMODULE(AWSM) has slightly different phase than both the BEM modules (even when for both the BEM modules u_{ind} is calculated at 1/4 chord point), this may be due to the influence of the wake of the rotor blades, but more investigation is needed to prove this. AEROMODULE(BEM) does not show a dip for u_{ind} and thus also needs to be investigated further.

- ***Q2. Are there differences in loads calculated by different aero modules during physical phenomena like dynamic inflow and tower presence, if yes, on which parts of wind turbine the loads are important?***

Contribution of dynamic inflow on loading of wind turbine

At the 70th second when the wind speed changes in step fashion, there is a sudden rise in axial aerodynamic force on rotor, this is due to dynamic inflow, this can be seen

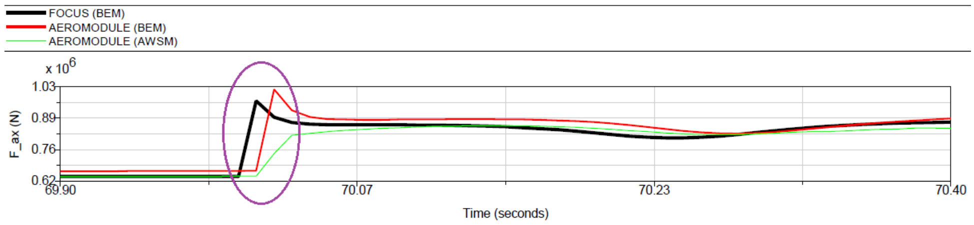

(a)

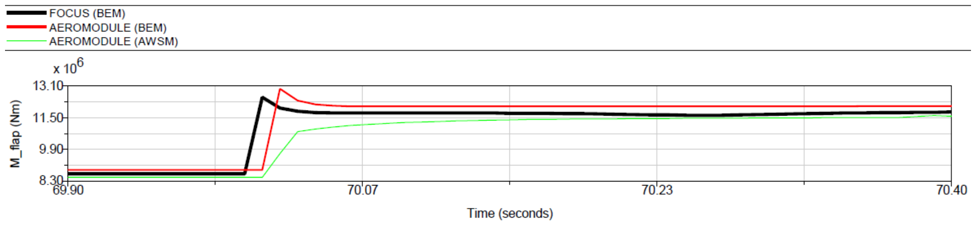

(b)

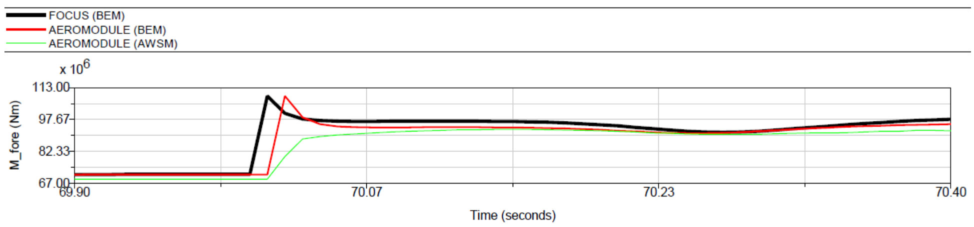

(c)

Figure 5.4: Effect of dynamic inflow on loading of wind turbine, **a:** Axial aerodynamic force on rotor, **b:** Flapwise bending moment in blade root, **c:** Fore-aft bending moment in the tower base

by the purple circle in figure 5.4a. When the wind speed increases the angle of attack (α) also increases and due to slightly different α, the axial aerodynamic force on rotor for all the modules differs slightly. As axial aerodynamic force on rotor is the main contributor for blade flapwise and tower fore-aft bending moments, therefore similar effect of dynamic inflow can also be seen in blade and tower moments in figure 5.4.

Contribution of tower presence on loading of wind turbine

The effective wind velocity reduces on the blade when the blade passes the tower

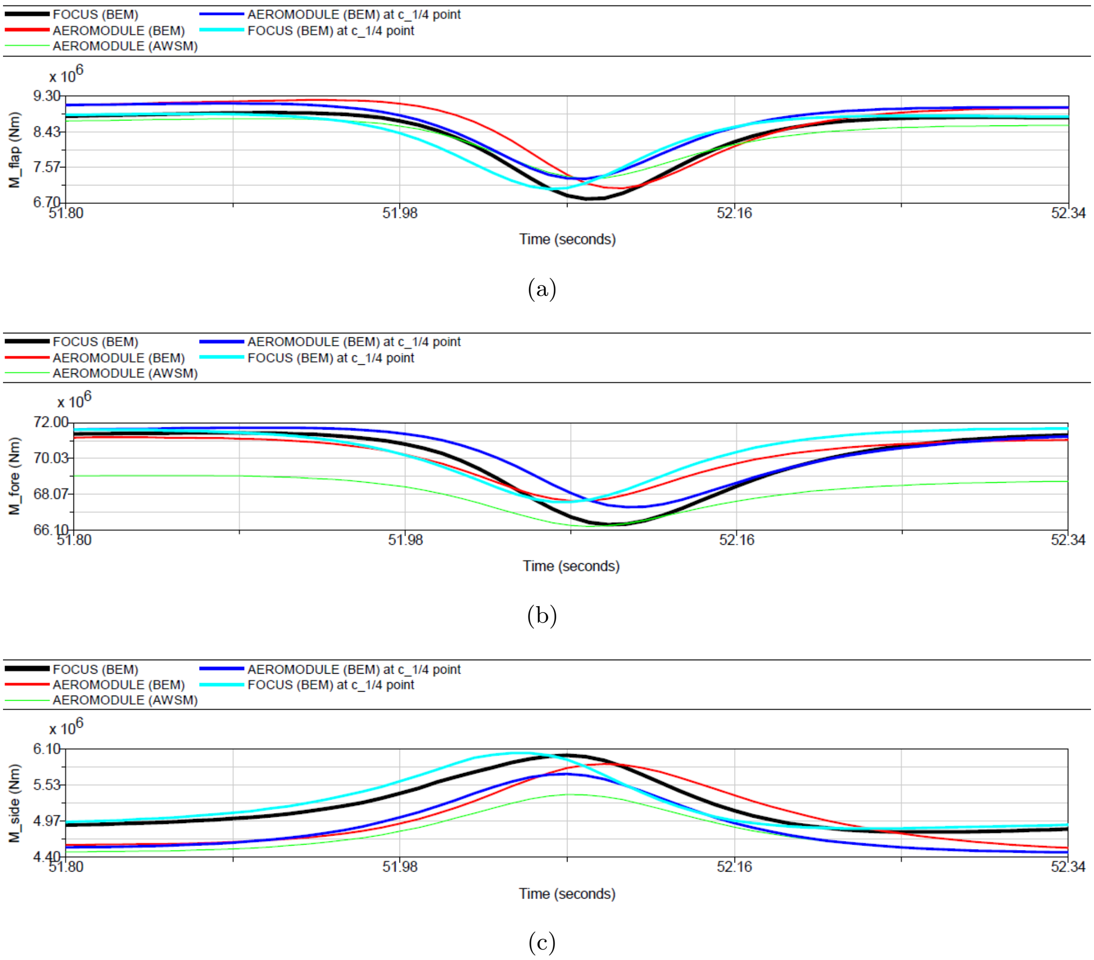

Figure 5.5: Contribution of tower presence on loading of wind turbine. **a:** Flapwise bending moment in the blade root, **b:** Fore-aft bending moment in the tower base, **c:** Side-ways bending moment in the tower base

therefore the blades experience force in upwind direction, so the flapwise bending moment decreases, this can be seen in figure 5.5a. Decrease in flapwise bending moment in the blade root causes decrement in fore-aft bending moment in the tower base because of dynamic interaction between rotor and tower. This can be seen in figure 5.5b. Both upwind direction of blade and fore direction of tower are considered in the $-X$ axis of the inertial reference system.

Each time the rotor passes the tower, the power from the wind turbine drops slightly because the wind starts bending away from the tower before it reaches the tower itself. Drop in power means drop in torque (tangential force). Due to different mean value of tangential force at different blades (blades near and away from the tower), the moment in the tower base changes. This change in moment in the tower base is in the positive direction of Y axis of inertia reference system. Figure 5.5c shows the increase in tower side-ways bending moment.

5.2 Secondary Research Questions

In this section secondary research questions are discussed. Secondary research questions which were formulated for the thesis work are:

- ***Q1. Are the BEM code and lifting line (AWSM) implementation in AEROMODULE sufficiently validated?***

The BEM code and lifting line (AWSM) implementation in AEROMODULE are not sufficiently validated. Only for NASA Ames and MEXICO projects, AEROMODULE(BEM) and AEROMODULE(AWSM) were validated with experiment results [6]. Due to unavailability of experimental results of the ART wind turbine, FOCUS(BEM) is used as validation tool for AEROMODULE(BEM) and AEROMODULE(AWSM). For the validation of both AEROMODULE(BEM) and AEROMODULE(AWSM) with FOCUS(BEM), following load cases were simulated for the ART wind turbine.

1. Load case-1 : Step change in wind speed in a rigid ART wind turbine with no controller and yaw misalignment.
2. Load case-2 : Step change in wind speed in a flexible ART wind turbine with no controller and yaw misalignment.

3. Load case-2888 (DLC2.2) : Pitch controller failure in a flexible ART wind turbine with no yaw misalignment.
4. Load case-3290 (DLC3.2) : Start up with extreme operating gust(EOG) in a flexible ART wind turbine with no yaw misalignment.

The first two load cases are the test load cases, and the last two load cases are from the IEC standard [21].

- ***Q2. Does the BEM implementation of AEROMODULE have same implementation as the well known BEM code of FOCUS? Beside the implementation differences are there any differences in both the BEM modules?***

The BEM implementations of AEROMODULE have similar implementations as the well known BEM code of FOCUS. There is a difference in the implementation of yaw model [34] in both of them though both of them use same yaw model. There were two other differences which were observed from the simulation results. Both the differences are explained below:

Blade coupling

From the simulation results of load case-1, small peaks were observed in the axial induced velocity, u_{ind}, at 0.23R blade station. For FOCUS(BEM), the upward peak is due to the phenomenon of tower presence of one blade but the downward peaks are due to blade coupling. In BEM, the momentum equation includes all the three blades. As one blade passes the tower it causes a change in momentum and as no wake is produced in BEM therefore change in momentum due to one blade is also seen in other two blades. Therefore the upward peak A (blade-1 passing the tower) and downward peaks B and C (effect of blade-1 passing the tower on other two blades) in the figure 5.6 can be given as,

$$\downarrow A = \uparrow B + \uparrow C \tag{5.1}$$

AEROMODULE(BEM) is also based on BEM theory as FOCUS(BEM) still it doesn't show the effect of blade coupling. This needs further investigation in future.

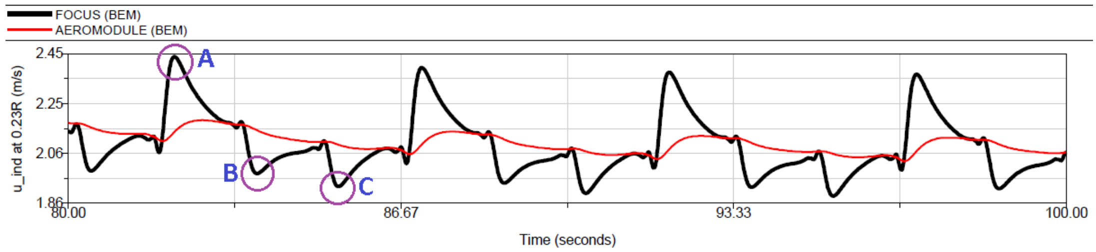

Figure 5.6: Axial induced velocity at 0.23R blade station at 16 m/s wind speed from 80th to 100th second.

Indifferent behaviour of AEROMODULE(BEM)

From simulation results it was found that at 0.23R blade station i.e. near the blade root region, AEROMODULE(BEM) shows a strange behaviour for the lift coefficient (c_l) even though both the BEM modules have same angle of attack (α). Figure 5.7 shows the strange peak for AEROMODULE(BEM) at 0.23R blade station. Further in-

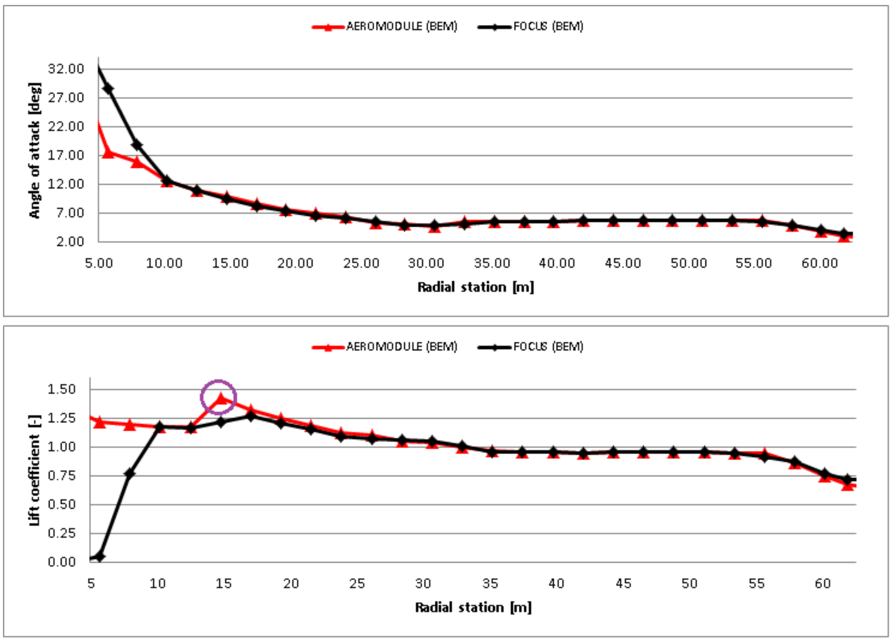

Figure 5.7: Aerodynamic insight at 51.92nd second.

vestigation was done to see whether dynamic stall model and 3D correction is the cause of the strange peaks and it was found that they were not the cause of this strange peak. Figure 5.8 gives more insight about it. So there is a need to do further investigation at 0.23R blade station for AEROMODULE(BEM).

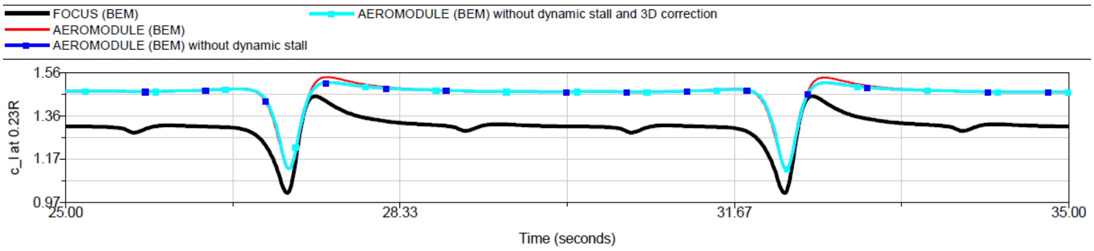

Figure 5.8: Lift coefficient at 0.23R blade station at 12 m/s wind speed.

- ***Q3. Can AWSM be used in all conditions for which the BEM code of FOCUS is currently used?***

Instead of the original AEROMODULE(AWSM), tweaked version of it was used to simulate the aerodynamic performance and loads on the ART wind turbine in order to save some computational time. Below a short description about the original and tweaked version of AEROMODULE(AWSM) is given:

Original AEROMODULE(AWSM)

The position of the wake plays a crucial role in AWSM since the wake interacts with the blade inducing effects on it. For each time step, the wake is convected downstream. The new position is function of the wind speed and the time interval and, of course, all the components (x,y,z) are updated. When the wake is free to roll-up, the positions of the wake points are different from the case where the wake is fixed and a geometrical helicoid is obtained. This is the main reason why the fixed wake case is not accurate like the free wake case, however the fixed wake is much faster.

Tweaked AEROMODULE(AWSM)

In the tweaked version, the new position of the wake for fixed wake case is corrected by a scaling factor. In this way, the differences due to free/fixed wake are in part compensated (although the shape of the wake is not realistic like the free wake). Not all the components should be scaled in the same way but instead, the flow direction should be considered. In the actual implementation, due to time constraints, only the axial direction is affected.

Dynamic stall

During the simulation results it was observed that due to no dynamic stall model in AEROMODULE(AWSM), it always showed 2D characteristics for lift coefficient (c_l)

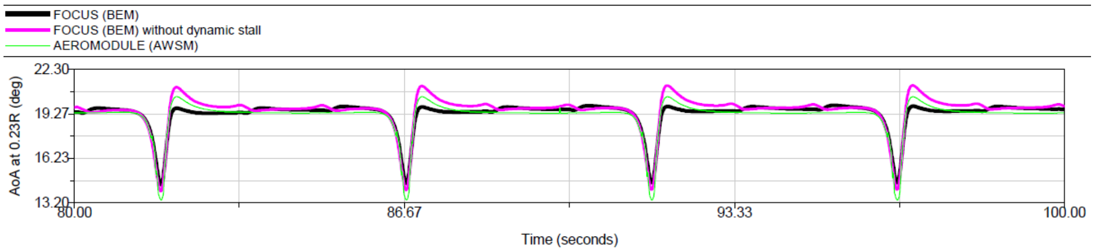

(a)

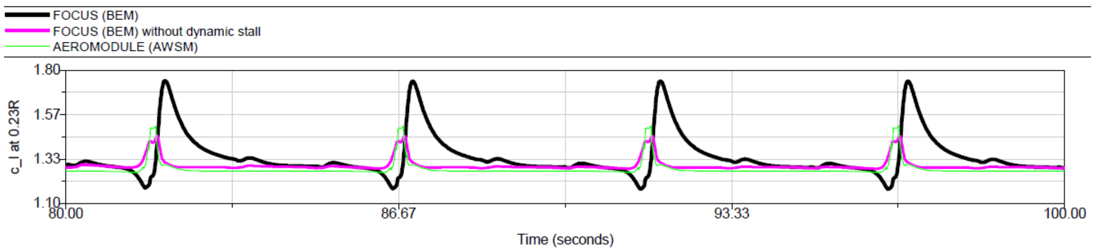

(b)

Figure 5.9: Aerodynamic analysis at 0.23R blade station from 80th to 100th second. **a:** Aerodynamic angle of attack(α), **b:** Lift coefficient c_l.

From the figure 5.9, it can be seen that α for 0.23R blade station(DU-35-A17) is above the stall angle of attack, whenever the blade passes the tower, α decreases below 19 degrees and reaches approximately 13.2 degrees because of reduction in relative wind speed, this can be seen for all the modules. As α is above stall angle of attack i.e. it is not in the linear slope region, therefore c_l doesn't follow the trend of α. There is a small difference in α between both the modules at 0.23R when the wind speed is 16 m/s, FOCUS(BEM) shows a rising trend but AEROMODULE(AWSM) doesn't, this is because of no dynamic stall model in it, and this is verified further by simulating the same case in FOCUS(BEM) without dynamic stall. As FOCUS(BEM) has dynamic stall model, it shows c_l higher than the maximum 2D characteristic value. Because dynamic stall model defines a hysteresis loop for the c_l when α for the airfoil changes rapidly (above stall α).

- ***Q4. Are there load cases that cannot yet be analysed using AWSM, if yes, then what load cases should be selected and do these selected load cases represent the full spectrum of load cases?***

A selection of load cases were done which could be simulated in both the BEM modules and AEROMODULE(AWSM), so that the differences between them could be observed, table 5.1 shows the selected load cases.

Table 5.1: Selected load cases of the ART wind turbine based on FOCUS(BEM) results.

Type	Design load case (DLC)
Fatigue	Load cases - 0120, 0121, 0122, 2452, 3100 and 4180
Extreme	Load cases - 2677, 2888, 3271, 3280, 6001, 6233, 9150 and 9242

Instead of original AEROMODULE(AWSM), tweaked version of AWSM is used therefore only axial flow cases could be simulated, not yawed flow cases and out of the list there are only four axial flow cases i.e. load cases - 0122, 2888, 6001 and 9242. Load cases - 0122, 6001 and 9242 are to be simulated for 670 seconds and load case - 2888 is to be simulated for 130 seconds according to IEC standard [21]. Tweaked version of AEROMODULE(AWSM) takes lot of time to simulate than AEROMODULE(BEM) because of more physics involved in the former. For every load case in AEROMODULE(AWSM) a separate input file needs to be made with different blade stations because one input file for all load cases was not working without errors. Because of this reason and also due to large simulation time of 670 seconds, load cases - 0122, 6001 and 9242 were not simulated in AEROMODULE(AWSM). In order to make more comparison between BEM and AWSM, load case - 3290 was simulated.

Load case - 3280 without yaw misalignment is load case - 3290. So in total two load cases (load cases - 2888 and 3290) according to IEC standard are simulated in AEROMODULE(AWSM) to draw comparison between AERMODULE(BEM), AEROMODULE(AWSM) and FOCUS(BEM). These two selected load cases don't represent the full spectrum of load cases according to the IEC standard [21].

- ***Q5. Is there a need of coupling a structural dynamic tool with an aerodynamic model like AEROMODULE, if yes, then what are the incompatibilities faced when coupling a structural dynamic tool with AEROMODULE?***

The AEROMODULE is an independent aerodynamic library consisting of a compilation of currently developed and future ECN models for simulation of rotor aerodynamics. For structural dynamics of a wind turbine, AEROMODULE is tailored for coupling to structural solvers such as SIMPACK. Blade position and velocity are given as input to the AEROMODULE and forces and moments are then communicated back to the structural code (SIMPACK). On coupling AEROMODULE with SIMPACK, an incompatibility in the controller interface was encountered. Same controller is used in FOCUS and for AEROMODULE-SIMPACK couple. The controller response showed a lot of fluctuations in the pitch angle of blades for AEROMODULE-SIMPACK couple than for FOCUS software. Lot of fluctuations in pitch angle of blade suggests fluctuations in loads of wind turbine which will subsequently lead to more fatigue. Incompatibility in the controller interface was more pronounced for small pitch angle of blades i.e. during normal operating conditions, than at large pitch angle of blades i.e. during extreme operating conditions.

5.3 Future work

There is still a need for further investigation in the thesis work, the future work can be enumerated as:

- To investigate the strange behaviour of AEROMODULE(BEM) near the root region.
- To observe the effect of dynamic stall model in AEROMODULE(AWSM).

- To do the complete load set calculation in original version of AEROMODULE(AWSM) and compare the results with FOCUS(BEM). Find the differences between BEM and AWSM in prediction of aerodynamic performance and loads on a wind turbine for the complete load set.
- To study other physical phenomena like yawed flow.
- To solve the incompatibility issue in AEROMODULE-SIMPACK couple controller interface.

References

[1] Ira H. Abbott and Albert E. von Doenhoff. *Theory of wing sections*. Dower publications, Inc., U.S.A, 1958.

[2] A. A. Afjeh and Jr. T. G. Keith. A vortex lifting line method for the analysis of horizontal axis wind turbines. *Journal of Solar Energy Engineering, Vol.108, pp.303-309*, 1986.

[3] J. D. Anderson. *Fundamentals of Aerodynamics*. McGraw Hill, California, 2006.

[4] James Arvo. *Fast random rotation matrices*. Academic Press Professional, San Diego, 1992.

[5] S. Benjanirat. Computational studies of horizontal axis wind turbines in high wind speed condition using advanced turbulence models. *Doctor of Philosophy Thesis, Georgia Institute of Technology*, December 2006.

[6] K. Boorsma and F. Grasso. Ecn aero-module, users manual. Technical report, Energy research Centre of the Netherlands, ECN, The Netherlands, 2010.

[7] K. Boorsma, F. Grasso, and J.G. Holierhoek. Enhanced approach for simulation of rotor aerodynamic loads. Technical report, ECN-M12-003, ECN, presented at EWEA Offshore 2011, Amsterdam, The Netherlands, 29 November 2011 - 1 December 2011.

[8] Tony Burton, David Sharpe, Nick Jenkins, and Ervin Bossanyi. *Wind Energy Handbook*. John Wiley & Sons Ltd, England, 2001.

[9] Ozlem Ceyhan. Aerodynamic design and optimization of horizontal axis wind turbine by using bem theory and genetic algorithm. Technical report, Middle East Technical University, 2008.

[10] David M. Eggleston and Forest S. Stoddard. *Wind Turbine Engineering Design*. Van Nostrand Reinhold Company Inc., U.S.A, 1987.

[11] A. Van Garrel. Development of a wind turbine aerodynamics simulation module. Technical report, ECN, The Netherlands, 2003.

[12] H. Glauert. A general theory of autogyro. *nr 1111*, 1926.

[13] Alejandro Gmez and Joerg R. Seume. Load pulses on wind turbine structures caused by tower interference. *WIND ENGINEERING VOLUME 33, NO. 6, pp 555570*, 2009.

[14] F. Grasso. Awsm external field calculations. Technical report, ECN, The Netherlands, 2009.

[15] F. Grasso. Awsm ground and wind shear effects in aerodynamic calculations. Technical report, ECN, The Netherlands, 2010.

[16] V. Gupta. Post processing and analyses of load cases of multi megawatt wind turbines. Technical report, TU Delft and ECN, The Netherlands, 2011.

[17] V. Gupta. Aerodynamic and structural analyses of the 5 mw wind turbine using bem and lifting line theories. Technical report, Thesis Report, Department of Mechanical Engineering - Sustainable Energy Technology, Delft University of Technology, The Netherlands, December 2011 - August 2012.

[18] Martin O.L. Hansen. *Aerodynamics of Wind Turbines.* James & James (Science Publishers) Ltd, England, 2008.

[19] E. Hau. *Wind Turbines: Fundamental, Technologies, Application and Economics.* Springer-Verlag Berlin Heidelberg, Germany, 2006.

[20] Stephens Ralph I. and Fuchs Henry O. *Metal Fatigue in Engineering.* John Wiley & Sons, England, 2001.

[21] IEC. Iec 61400-1. Technical report, International Standard, 2005-2008.

[22] Hiroshi Imamura. Aerodynamics of wind turbines. *79-5 Tokiwadai, Hodogaya-ku, Yokohama 240-8501, Japan*, 2001.

[23] J. Jonkman, S. Butterfield, W. Musial, and G. Scott. Definition of a 5-mw reference wind turbine for offshore system development. Technical report, National Renewable Energy Laboratory, U.S.A, 2009.

[24] Vadim Komkov. *Optimal control theory for the damping of vibrations of simple elastic systems. Lecture Notes in Mathematics.* Springer-Verlag, USA, 1972.

[25] J. Gordon Leishman. Challenges in modeling the unsteady aerodynamics of wind turbines. *Paper 2002-0037, Presented at the 21st ASME Wind Energy Symposium and the 40th AIAA Aerospace Sciences Meeting, Reno, NV,*, Jan. 1417, 2002.

[26] C. Lindenburg and J.G. Schepers. Phatas-iv aeroelastic modelling, release "dec-1999" and "nov-2000". Technical report, ECN, The Netherlands, 2000.

[27] Koert Lindenburg. Forward and backward whirl (why should a blade be 6p?). Technical report, Energy research Centre of the Netherlands, The Netherlands, 2009.

[28] J.F. Manwell, J.G. McGowan, and A.L. Rogers. *Wind Energy Explained: Theory, Design and Applications*. John Wiley and Sons Ltd, England, 2002.

[29] W. J. McCroskey. The phenomenon of dynamic stall. *NASA-TM-81264*, 9-13 March 1981.

[30] NTNU. Vertical axis wind turbine (vawt), June 2009. URL `http://www.ivt.ntnu.no`.

[31] Evangelos Politis and Vasilis Riziotis. The importance of nonlinear effects identified by aerodynamic and aero-elastic simulations of the 5 mw reference wind turbine. Technical report, National Technical University of Athens, Greece, 2007.

[32] L. Prandtl and A. Betz. Vier abhandlungen zur hydrodynamik und aerodynamik. *36-65*, 1927.

[33] Kyoto Protocol. Kyoto protocol website, August 2008. URL `http://unfccc.int/kyoto-protocol`.

[34] G. Schepers. An engineering model for yawed conditions, developed on basis of wind tunnel measurements. Technical report, AIAA, USA, 1999.

[35] J.G. Schepers and L.J. Vermeer. Een engineering model voor scheefstand op basis van windtunnelmetingen. Technical report, ECN, The Netherlands, 1998.

[36] Berthold Schlecht and Thomas Rosenlcher. Determining reliable load assumptions in wind turbines using simpack. Technical report, Institute of Machine Elements and Machine Design, Chair of Machine Elements, Dresden University of Technology, Dresden, Germany, September 2010.

[37] S. Schreck. Turbine aerodynamics and modelling uncertainties. *Sandia National Laboratories*, 2004 Wind Turbine Blade Workshop.

[38] F. J. Simoes and J. M. R. Graham. A free vortex model of the wake of a horizontal axis wind turbine. *pp.161-165*, 1990.

[39] Simpack. Multi-body simulation software, February 2012. URL `http://www.simpack.com`.

[40] H. Snel and J.G. Schepers. Engineering models for dynamic inflow phenomena. Technical report, The European wind energy conference 1, The Netherlands, 1991.

[41] H. Snel and J.G. Schepers. Joule1: Joint investigation of dynamic inflow effects and implementation of an engineering model. Technical report, ECN, The Netherlands, 1994.

[42] H. Snel and J.G. Schepers. Investigation and modelling of dynamic inflow effects. Technical report, Netherlands Energy Research Foundation, ECN, The Netherlands, 8-12 March, 1993.

[43] Carleton University. The history of carleton's first wind turbine, September 2004. URL `http://apps.carleton.edu`.

[44] Gijs van Kuik and Wim Bierbooms. Introduction to wind turbine design. *DUWIND, Delft University Wind Energy Research Institute*, 2002.

[45] R.E. Wilson and P.B.S. Lissaman. Applied aerodynamics of wind power machines. *NTIS PB 238594*, 1974.

Appendices

Appendices have been divided as A, B, C, and D. Appendix A describes the airfoil theory, blade element momentum theory, power curve of a variable speed pitch regulated wind turbine and mechanical loads on a wind turbine. Appendix B shows the chord, mass and stiffness distribution of the ART wind turbine and describes briefly some load cases of the ART wind turbine according to the IEC standard. Appendix C describes the DLC 2.2 load case-2888 and DLC3.2 load case-3290, in this section both aerodynamic and structural aspects of the ART wind turbine are discussed for these load cases and comparison is between all the modules. Appendix D describes a test load case which compares all the three modules, both aerodynamic and structural aspects are discussed for this load case.

A Basic wind turbine theory

This appendix explains airfoil theory, blade element momentum theory, power curve of a variable speed pitch regulated wind turbine [16]. Mechanical loads on a wind turbine are also discussed in this appendix.

A.1 Airfoil

Cross-sections of wind turbine blade have a shape of an airfoil. Different airfoils are used along the span of blade. This section focuses on airfoil terminology and its behaviour.

A.1.1 Airfoil Terminology

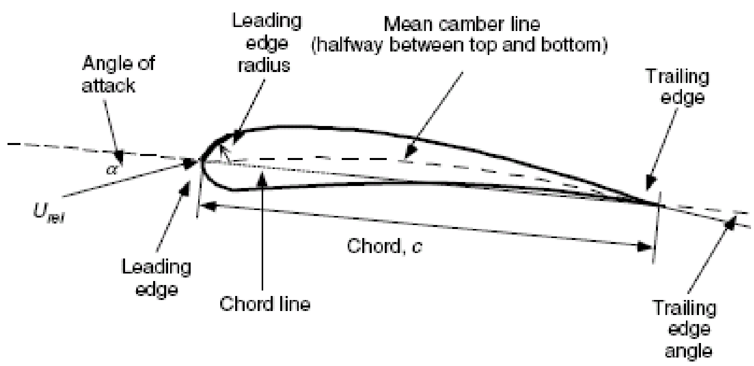

Figure A-1: Nomenclature of an airfoil [28].

Airfoils are characterized by different terms [3].

- The forward edge and rearward edge are called leading and trailing edges, respectively.
- The locus of points halfway between the upper and lower surfaces of the airfoil is defined as camber line.
- Straight line connecting the leading and trailing edges is chord line and the length of this line is called chord, c, of the airfoil.
- Distance between chord and camber line, measured perpendicular to the chord line is the camber of the airfoil.
- Angle between the chord line and the relative wind is defined as angle of attack (AoA).
- Angle between the chord line and trailing edge is called trailing edge angle.

A.1.2 Airfoil Parameters

Upper surface of the airfoil experiences low pressure, hence it is called suction side. Lower surface of the airfoil experiences high pressure, hence it is called the pressure side. Airflow over the airfoil produces distribution of forces and these forces can be categorized as pressure force and friction force [18]. Pressure forces are caused by unequal pressure distribution of forces on pressure and suction side. Friction forces are caused due to viscosity of air. Resultant of these forces can be resolved into two forces i.e. lift and drag. The resultant of the lift and drag force causes a moment about the pitch axis.

- **Lift force** is perpendicular to the direction of relative wind and is caused due to the pressure difference on the suction and pressure side.
- **Drag force** is parallel to the direction of relative wind and is caused due to the viscous forces and unequal pressure forces on the airfoil surface facing toward and away from direction of relative wind.
- **Pitching moment** is defined about an axis perpendicular to the airfoil cross-section.

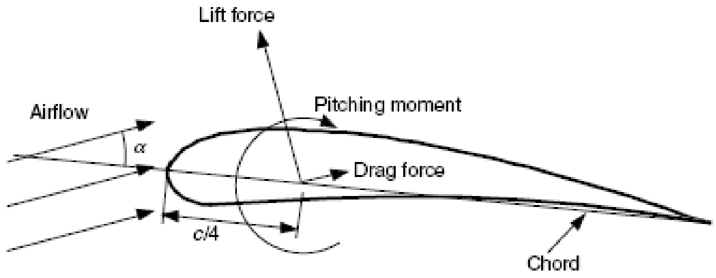

Figure A-2: Drag and lift forces on stationary airfoil, α, angle of attack; c, chord [28].

There is a practice of using non-dimensional parameters for airfoils. Lift force, drag force and pitching moment are non-dimensionalized by dynamic pressure force and dynamic pressure moment respectively.

Lift coefficient

$$C_l = \frac{L}{\frac{1}{2}\rho U_\infty^2 A}, \tag{A-1}$$

Drag coefficient

$$C_d = \frac{D}{\frac{1}{2}\rho U_\infty^2 A}, \tag{A-2}$$

Moment coefficient

$$C_m = \frac{M}{\frac{1}{2}\rho U_\infty^2 Ac}, \tag{A-3}$$

Where, ρ is the density of air, U_∞ is free stream velocity, L is the lift force, D is the drag force, M is the pitching moment, A is the projected area (chord $\times$ span) of airfoil and c is the chord length of airfoil.

A.1.3 Airfoil Behaviour

In order to understand the forces on wind turbine blades it is necessary to understand the behaviour of airfoils. Variation of lift, drag and pitching moment coefficient is drawn with AoA. Horizontal axis wind turbines have airfoils which are often designed to have high efficiency by working at maximum (C_l/C_d) and this is the reason why wind turbine airfoils operate in the constant slope region of C_l, α curve.

Figure A-3 shows the airfoil coefficients of DU-97-W-300 airfoil. C_l increases linearly with α with an approximation of 2π/rad, up to certain value of α where a maximum

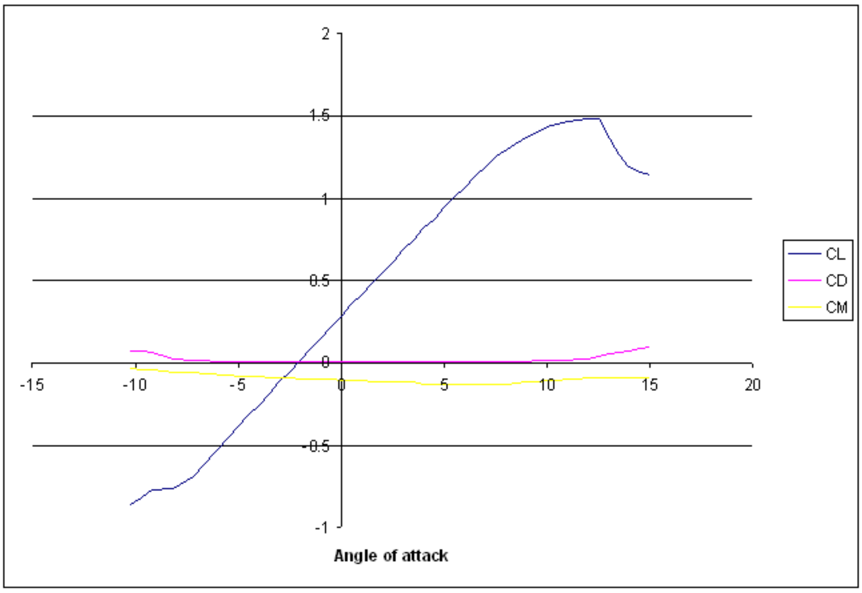

Figure A-3: Lift, drag and moment coefficients for the DU-97-W-300 airfoil at Reynolds number of 7×10^6.

value of C_l is reached. Hereafter the airfoil is said to be stall and C_l decreases in a very geometry-dependent manner. There are two regimes in the airfoil behaviour, namely: attached and stall regime [18].

A.1.4 Attached flow regime

When the airfoil is almost aligned with the flow, the boundary layer stays attached and the associated drag is mainly caused by friction with the air. In this regime the slope of the C_l curve is constant and positive whereas the C_d is relatively low.

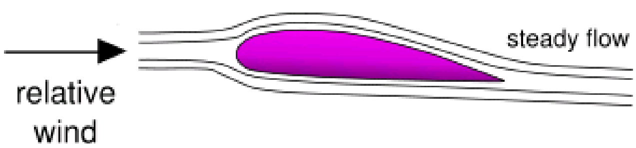

Figure A-4: Illustration of attached flow over an airfoil.

A.1.5 Stall regime

When the air flow starts to separate from the upper surface of the airfoil it causes the separation of boundary layer. The separated boundary layer formed above the airfoil reduces the lift and increases drag and causes the airfoil to stall.

The way an airfoil stalls is very dependent on the geometry. Thin airfoils with sharp

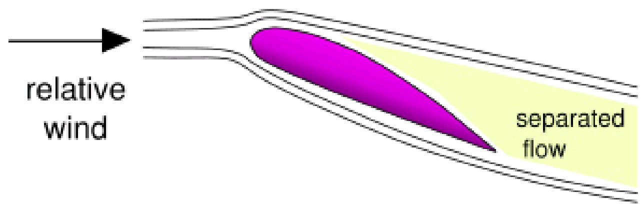

Figure A-5: Illustration of separated flow over an airfoil.

nose i.e. high curvature around the leading edge, tends to stall more abruptly than thick airfoils. Along the span of the blade, thickness of airfoil decreases from blade root to blade tip.

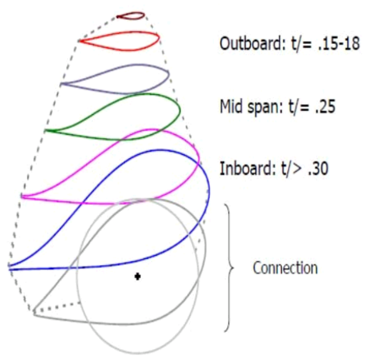

Figure A-6: Thickness variation of different parts of blade in spanwise direction.

For a stall regulated wind turbine, the stall progresses from inboard to outboard part, along the span of the blade causing decreased lift and increased drag. For a pitch regulated wind turbine stall may occur near blade root (cylindrical airfoil) but never occurs over the complete blade because the blade is pitched which changes the AoA and thus the airfoils along the blade operate in the constant slope region of C_l, α curve. Airfoils of outboard part of the blade are chosen to focus more on aerodynamic performance and inboard part of the blade is for structural support.

A.2 Momentum Theory

In this theory control volume analysis of forces at the blade based on conservation of linear and angular momentum is done. It assumes a control volume with its boundaries as a surface of stream tube and two cross-sections of the stream tube, figure A-7 shows a stream tube of a wind turbine. The wind turbine rotor is assumed as an actuator disk. Flow is only across the two cross-sections not from any other side of the stream tube. Cross-sectional area upstream of the rotor disk is smaller than that of the disk and at downstream of the disk the cross-sectional area is larger than the disk. This expansion of the stream tube is due to the conservation of mass flow rate. Momentum theory is based on some assumptions, namely:

- Homogeneous, incompressible, inviscid, uniform and steady state fluid flow.
- Uniform thrust over the rotor area.
- An infinite number of blades.
- No frictional drag.
- The static pressure far upstream and far downstream of the rotor is equal to the undisturbed ambient static pressure.
- Non-rotating wake behind the rotor.

From linear momentum theory axial or normal force on the wind turbine is calculated as,

$$dT = \rho U_\infty^2 .4a(1-a)\pi r dr \tag{A-4}$$

Axial induction factor, **a**, is defined as the fractional decrease in wind velocity between the free stream and the rotor plane.
From angular momentum theory torque on the wind turbine is calculated as,

$$dQ = \rho U_\infty .4a^{'}(1-a)\pi r^3 \Omega dr \tag{A-5}$$

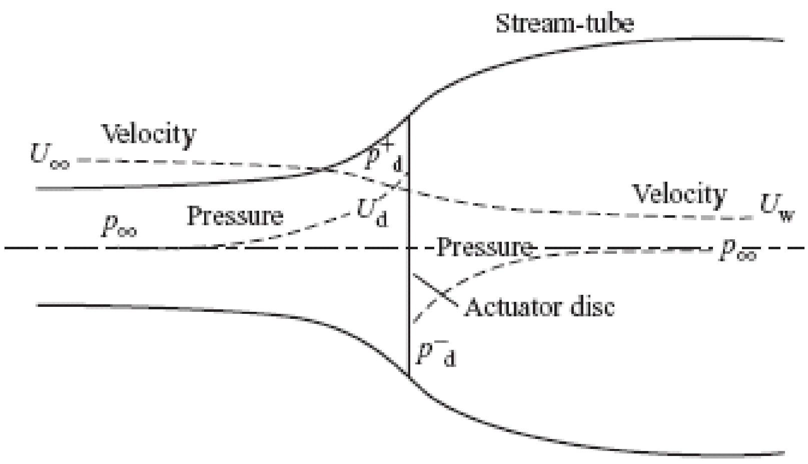

Figure A-7: Stream tube of a horizontal axis wind turbine [8].

Due to the rotation there is also loss in the rotational speed and it is called tangential induction and is represented by $a^{'}$.

$$a^{'} = \frac{\omega}{2.\Omega}, \tag{A-6}$$

Where, U_∞ is free stream velocity, ρ is density of air, r is the radial distance from hub, Ω is the rotational speed and ω is the rotational speed of wake.

A.3 Blade Element Theory

The forces on the blades of a wind turbine can also be expressed as a function of lift and drag coefficients and the angle of attack. Lift force is perpendicular and drag is parallel to the relative wind direction. Relative wind velocity is the vector sum of wind velocity at rotor and the wind velocity due to rotation of the blade. The blade is assumed to be divided into N sections which are also called as blade elements [44]. Blade element theory is based on some assumptions, namely:

- Uniform, incompressible, stationary flow
- No aerodynamic interaction between blade elements (no radial flow).
- The forces on the blades are determined solely by the lift and drag characteristics of the airfoil shape of the blades.

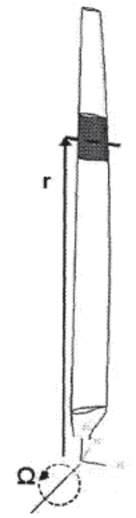

Figure A-8: Section of the blade [9].

- Finite number of blades.
- Tower is neglected.

Blade element theory gives the normal force and torque as dF_N and dQ respectively. Normal force or thrust can be written as,

$$dF_N = B\frac{1}{2}\rho U_{rel}^2(C_l \cos\phi + C_d \sin\phi)cdr \tag{A-7}$$

Tangential aerodynamic force is given as

$$dF_T = B\frac{1}{2}\rho U_{rel}^2(C_l \sin\phi - C_d \cos\phi)cdr \tag{A-8}$$

Torque due to tangential force is defined as

$$dQ = BrdF_T, \tag{A-9}$$

where B is the number of blades.

A.4 Blade Element Momentum (BEM) Theory

The BEM theory is the combination of momentum and blade element theory. The normal force and torque relations from both momentum and blade element theory are used in order to calculate axial induction and tangential induction factors, these factors are the losses in the axial and tangential velocities. After calculating the induction factors, the forces and torque values are calculated by using blade element theory [9].

A.5 Power Curve

Power production of a wind turbine varies with wind speeds. The power curve gives the electrical power produced as a function of the wind speed at hub height. Three key points on the velocity scale relate the performance of wind turbine generator.

- Cut-in speed: It is the minimum speed at which the wind turbine starts giving power output.
- Rated wind speed: It is the wind speed at which the rated power is achieved. It is the maximum power that the generator can produce.
- Cut-out speed: It is the maximum wind speed at which the wind turbine is allowed to deliver power. This is done for safety reasons.

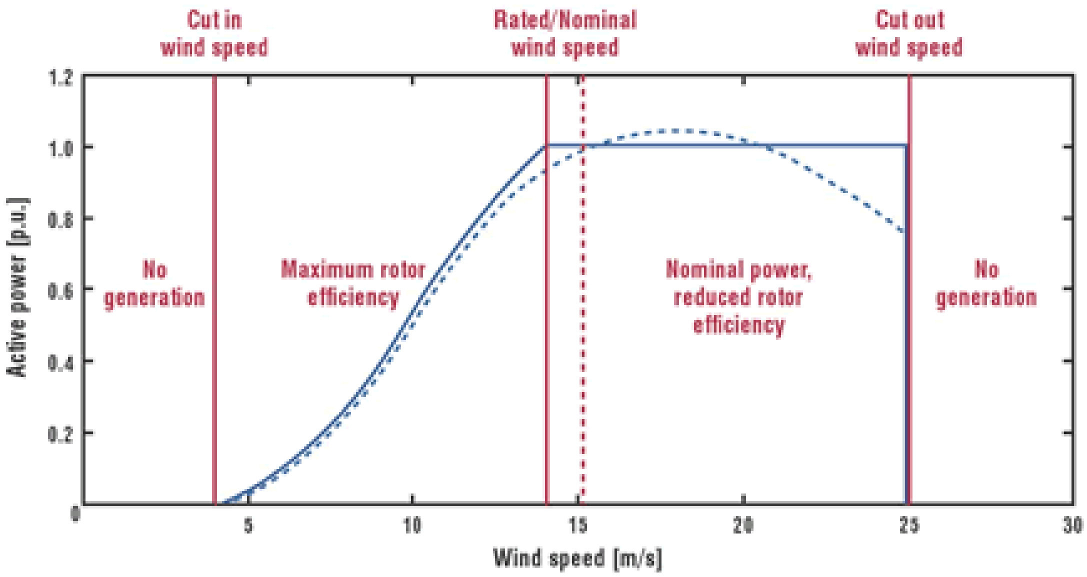

Figure A-9: Typical power curves and areas of operation of a stall limited (dashed line) and pitch controlled (solid line) wind turbine.

In this section, power curve of only variable speed pitch regulated wind turbine will be discussed [16]. Variable speed pitch regulated wind turbine has two methods for controlling the wind turbine operation:

- Rotational speed change
- Blade pitch change

At low wind speeds wind turbines are partly loaded, so they operate at constant pitch with a variable rotational speed. This is done so as to operate at optimal tip speed ratio.

$$\lambda = \frac{\Omega R}{U_\infty}, \tag{A-10}$$

Where, λ is the tip speed ratio, Ω is the rotational speed of rotor, R is the blade length and U_∞ is the free stream velocity.
As wind speed increases and reaches rated condition, the generator torque is used to control the generator power output and pitch control is used to maintain the rotational speed within the acceptable limits of generator specifications. If the wind speed drops then it leads to a drop in aerodynamic torque which subsequently decelerates the rotor but the generator power is kept constant. If there is a gust and wind speed does not cross the cut-out speed, the aerodynamic torque will increase but the generator power is maintained at a constant level. The increased energy is stored in the form of kinetic energy of the rotor. If the wind speed remains high, the blades will be pitched and this will reduce the aerodynamic torque and rotational speed. The generator power output of variable speed pitch regulated wind turbine is controlled with rotational speed and blade pitch changes [8].

A.6 Nature of Mechanical Loads

Mechanical loads are the forces which cause deformations and displacements in structures. Nature of the mechanical loads is of two types, namely:

- **Fatigue load**: Fatigue [20] occurs on a material when it is subjected to cyclic loading. If the cyclic load is above a threshold, microscopic cracks will begin to form at the surface. Eventually a crack will reach a critical size, and the structure will suddenly fracture.

- **Ultimate load**: Ultimate load is the amount of load applied to a component beyond which the component will fail. The chances of occurrence of this load is very small.

A wind turbine experiences various types of mechanical loads throughout its lifetime, which can lead to damage of the different parts. The three important parts of the wind turbine are blades, nacelle and tower.

A.7 Sources of Mechanical Loads

Loads on a wind turbine are caused by different sources, the nature of these loads are discussed below.

A.7.1 Aerodynamic Loads

Aerodynamic loads are caused by the wind and it is of particular concern in the structural design. When the wind turbine rotor is rotating, it is the lift force which creates the aerodynamic loading of concern while when the turbine is steady or quasi steady, drag forces are of primary concern [18]. Nature of winds can be steady and stochastic. Steady blowing wind can induce static loads on the various parts of a stationary wind turbine. When wind is stochastic it means it is turbulent in nature. Stochastic winds have different turbulent scales, wind shear has the highest turbulent scale. From figure A-10, variation of wind speed at different azimuth angle[1] can be seen when a vertical wind shear occurs. This variation suggests that the wind shear is a cosine function of azimuth. Hence in one complete revolution of rotor, wind shear completes one complete cosine cycle, so it is 1P[2]. Smaller turbulence scales will take more than one revolution to complete their cycles so they are nP (where n=2, 3.........).

[1]Azimuth angle is zero when the tip of the blade is down and it increases in the direction of rotation. It is represented by ψ.

[2]A load which varies an integral number of times in relation to a complete revolution of the rotor is known as a 'Per rev' load and is given the symbol P.

$$1P = \frac{Frequency(Hz) \times 60}{\Omega} \tag{A-11}$$

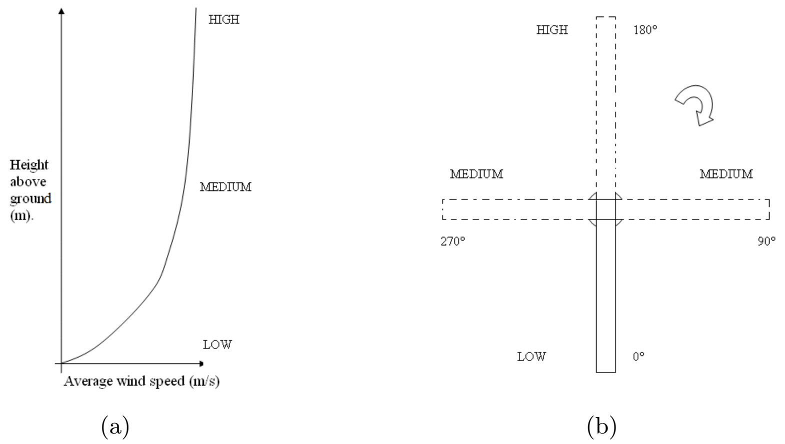

Figure A-10: (a) Vertical wind shear profile, (b) Variation of wind speed at different azimuths.

A.7.2 Gravity Loads

Gravity is an important source of load on large wind turbine though its magnitude is small for smaller wind turbines. Gravity loads are also cyclic in nature. From figure A-11, it can be seen that as the blade rotates, the lower part of the blade moves up when the azimuth angle changes from 90 to 270 degrees. At 0 and 180 degrees the blade is vertical. Similarly the gravity force follows the same cycle i.e. it is the lowest at 0 and 180 degrees and at 90 and 270 degrees it is the maximum but changes direction. So this suggests that the gravity force is sine in nature and same as wind shear it also completes its one cycle in one revolution of the rotor. So gravity force is 1P in nature. Mass center of blades usually lies at 30% of the blade length from the blade root.

A.7.3 Dynamic Interactions

Motion induced by aerodynamic and gravitational forces induces loads in other parts of the machine [28]. When wind direction changes, the wind turbine has to align itself in the direction of wind i.e. yawing. Yawing motion along with the rotation of rotor induces gyroscopic forces which can be substantial at high yaw rate.

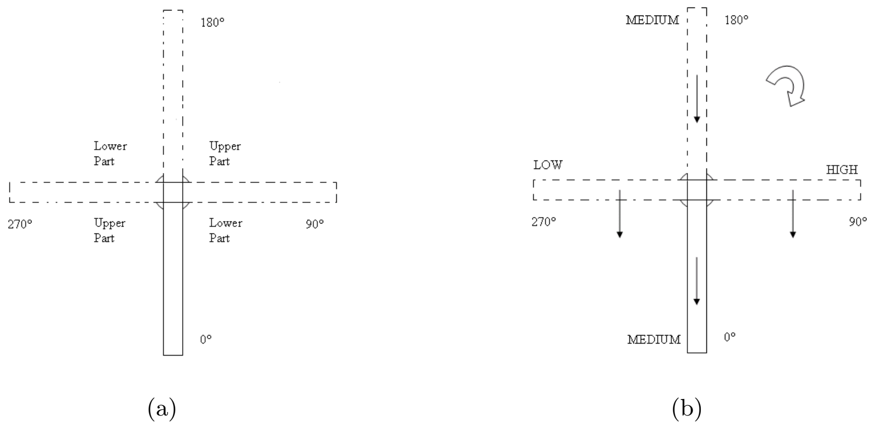

Figure A-11: a: Change in position of a blade, **b:** Variation of loads on wind turbine blades at different azimuths due to gravity.

A.7.4 Mechanical Control

When the wind turbine starts it uses an induction generator and when it stops, brakes are to be applied. During idling condition, the loads are disconnected from the wind turbine. These sudden actions generate substantial loads throughout the structure.

The above discussed sources of loads act on different parts of the wind turbine. Loads on the blades and tower are explained below.

A.8 Loads on Blade

Usually wind turbines blades experience forces and moments in four directions, namely: out of plane, in plane, spanwise and torsion. These forces and moments cause motions in these four directions [10]. Blade loads are analyzed at the blade root in first three directions.

A.8.1 Out of plane

Out of plane motion refers to the motion parallel to the axis of rotation of the rotor. When a wind turbine is aligned in the direction of wind then flapping will be in the direction of wind or opposite to it, figure A-12 shows the flapping motion on blades.

Out of plane motion is also called flapwise motion. Flapwise motion is associated with

Figure A-12: Flapping action on blades in the inertial reference system.

a flap angle[1]. Flapwise forces act on the complete length of the blades, the maximum flapwise moment occurs at the blade root. Factors causing flapwise forces and moments are discussed below.

- **Aerodynamic forces**: Axial aerodynamic force on the wind turbine causes the blades to move out of the rotor plane and it is dependent on the relative wind speed and axial induction factor, the relation can be seen in equation A-12.

$$dF_N = B\frac{1}{2}\rho U_{rel}^2(C_l \cos\phi + C_d \sin\phi)cdr \tag{A-12}$$

- **Gravity force**: Gravity force is one of the important forces that act on the blade root. Gravity force is cyclic in nature and it can either increase or decrease the flap angle depending upon the initial state of the rotor. Wind turbine blades can have a cone angle and the rotor/drive train can also have a tilt angle. Three cases can be made depending upon the initial state of the rotor blades, namely:

  1. **Case 1:** In this case, rotor blades are only considered to be coned i.e. there is no tilt angle. The gravity force has component in the direction perpendicular to blades. Figure A-13a describes the case 1. $F_g \sin\beta$ component of gravity force on lower blade causes the flap angle 'β' to decrease whereas on the upper blade it causes the flap angle to increase. With the rotation of the rotor blades, the lower blade moves up and the upper blade moves down. So the gravity force component '$F_g \sin\beta$' causes cyclic flapwise loads on blades.

[1]Flap angle is the angle that the deformed blade makes with the plane of rotation and it is represented with β.

2. **Case 2:** In this case, rotor blades are only considered to be tilted i.e. there is no cone angle. Tilt angle is represented by ϵ. Figure A-13b describes the case 2. In this case the component of gravity force '$F_g \sin\epsilon$' increases the tilt angle for upper blade and decreases the tilt angle for lower blade. With rotation of rotor, each blade experiences increasing and decreasing tilt angle. So the gravity force component '$F_g \sin\epsilon$' causes increasing and decreasing flapwise loads on each blade.

3. **Case 3:** In this case, rotor blades have both cone and tilt. This case is similar to case 1, but with a smaller flap angle for upper blade and larger flap angle for lower blade. Figure A-13c describes the case 3.

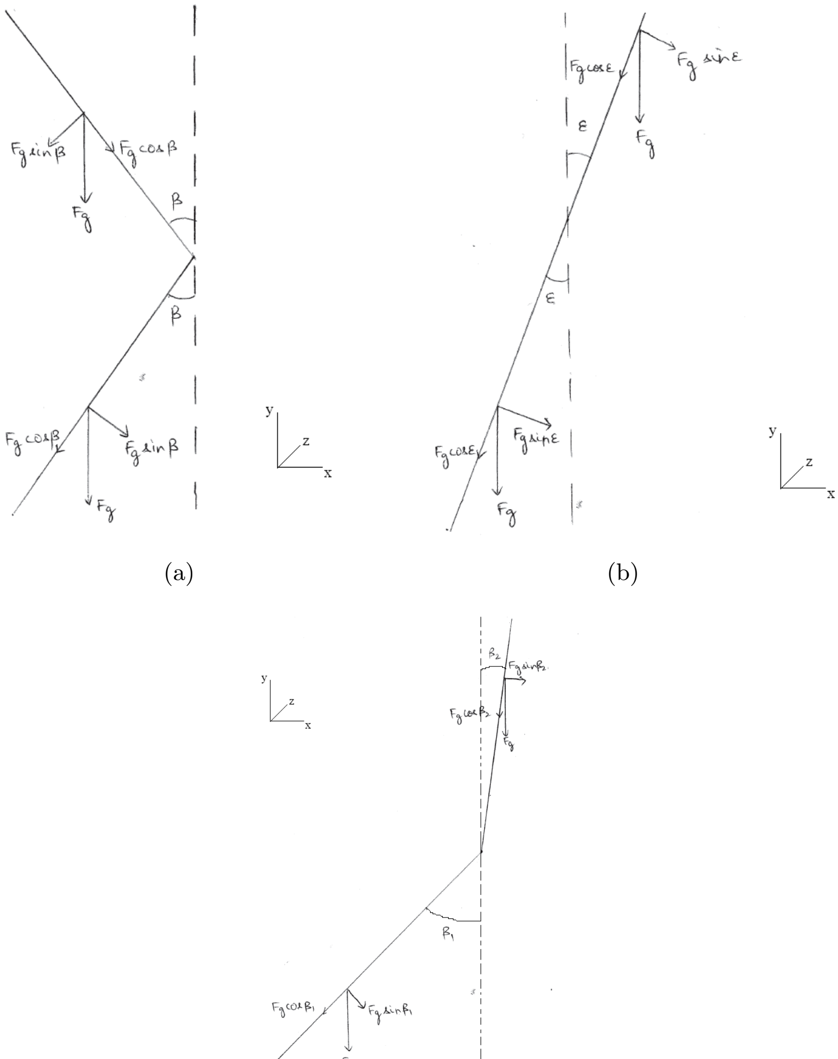

Figure A-13: Three cases of gravity loads on blades in flapwise direction. The figure only shows two blades of a 3 bladed wind turbine. Dashed line is the rotor axis and solid line is the rotor blades, **a:** Gravity loads on a coned rotor, **b:** Gravity loads on a tilted rotor and **c:** Gravity loads on a coned and tilted rotor.

- **Centrifugal force**: Centrifugal force causes a stiffening action on the blade root and is therefore also called centrifugal stiffening. Centrifugal force depends on the square of the rotation speed and distance to the axis of rotation and is shown in figure A-14. It acts on the center of mass of the blade and is perpendicular to rotor's axis of rotation. The magnitude of centrifugal force is given as,

$$F_{centrifugal} = r\Omega^2 dm \tag{A-13}$$

In flapwise direction, sine component of centrifugal force i.e. $F_{centrifugal} \sin\beta$ decreases the flap angle.

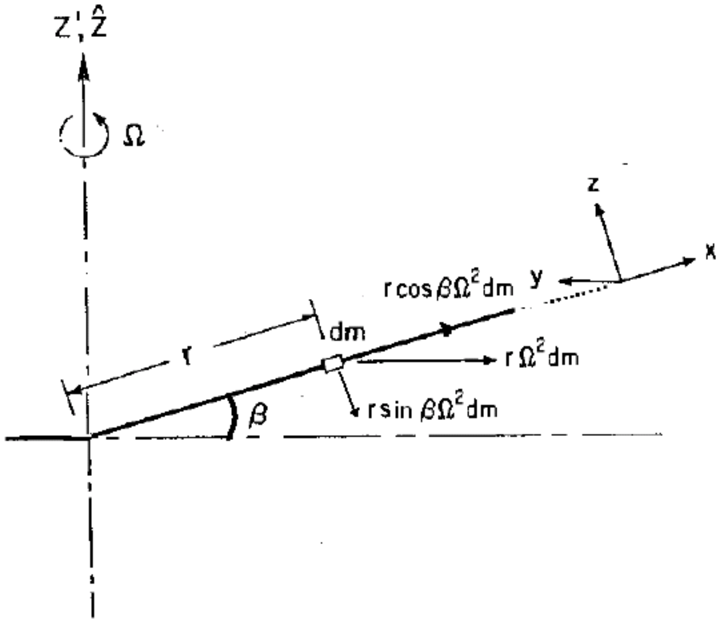

Figure A-14: Centrifugal force on blades in the blade reference system [10].

- **Yaw motion**: When the direction of wind changes, the rotating wind turbine rotor has to align itself in the direction of wind so as to extract the maximum power out of the wind. This motion of the rotor and nacelle together about the tower top is called yaw motion, and this motion results in gyroscopic moments which act on the rotor blades. Gyroscopic moment is dependent upon the yaw rate, rotational speed and the azimuth angle. Its magnitude in the out of plane direction is given as:

$$M_{yaw} = -2q\Omega \cos\psi I_b \cos\epsilon \tag{A-14}$$

Where, Ω is the rotational speed of the rotor, I_b is the mass moment of inertia of blade, ψ is the azimuth angle, ϵ is the tilt angle of rotor and q is the yaw rate.

A.8.2 In-plane

In-plane motion lies in the plane of rotation of rotor. In-plane moment is also called lead-lag or edgewise moment and is shown in figure A-15a. In leading motion blade will move faster than the overall rotational speed, and in lagging motion it will move slower.

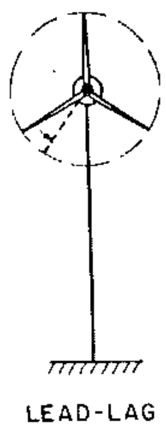

(a)

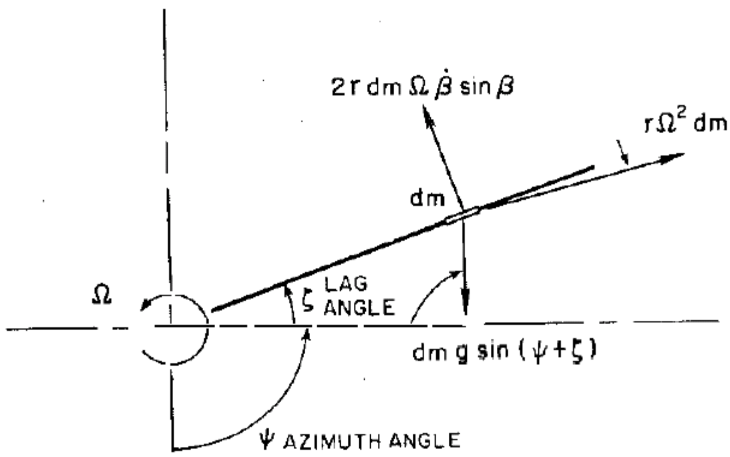

(b)

Figure A-15: a: Lead-lag action on blades in the inertial reference system, **b:** Edgewise loads on blade in the blade reference system [10].

Lead-lag forces cause fluctuations in torque in the main shaft and power in the generator. There are three lead-lag forces which cause edgewise moment and are shown in figure A-15b. Three lead-lag forces are discussed below.

- **Gravity force** is the most important contributor of lead-lag motion and is discussed in section A.7.2. Moment due to gravity force on blade is given as,

$$M_g = m_{blade} g c_{gravity} R \sin\psi. \tag{A-15}$$

For the ART wind turbine, m_{blade} is 17,740 kg, center of gravity i.e. $c_{gravity}$ is 30% from the blade root, length of the blade 'R' is 63 m. From equation A-15, moment due to gravity force on the blade 'M_g' is calculated to be 3.5 kNm. 3.5 kNm will be the maximum value of the moment due to gravity force at 90° and 270° azimuth.

- Lead-lag motion is also caused by the action of **Coriolis force**[1]. Coriolis force is given as

$$F_c = 2dm\Omega \times V_{radial}, \tag{A-16}$$

where, dm is the mass of blade element, Ω is the rotational speed of rotor and V_{radial} velocity in radial direction. Coriolis force, F_c, is perpendicular to both Ω and V_{radial}. V_{radial} occurs when there is yawing action and also when the blade is deformed due to flapping action.

- **Tangential wind force** is another force which causes edgewise moments. Equation A-17 shows the relation of tangential aerodynamic force with the relative wind speed.

$$dF_T = B\frac{1}{2}\rho U_{rel}^2(C_l \sin\phi - C_d \cos\phi)cdr \tag{A-17}$$

- **Braking** of wind turbine also causes edgewise moment on the blades.

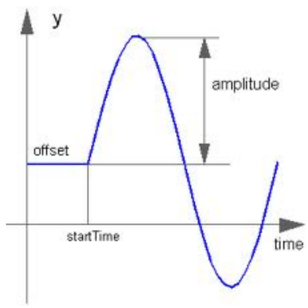

Figure A-16: Edgewise moment on blade root. Amplitude is the magnitude of gravity force and the offset value is the torque.

The absolute average value of edgewise moment variation with time gives the torque and the amplitude gives the gravity force and is shown in figureA-16.

[1]Bodies moving on the plane of rotation appear to experience a force, leftward if the rotation of the reference frame is clockwise, rightward if counter clockwise. Such motion gives rise to the Coriolis effect.

A.8.3 Torsion

In general in a blade, there are four non-coincident axes: the mass axis, the control axis, the aerodynamic axis and elastic axis. Blade spanwise axes are shown in figure A-17.

- The **mass axis** is the spanwise locus of section mass centers.
- The **elastic axis** is the spanwise locus of points about which no section torsional deflection is incurred with bending deflection.
- The **control axis** is simply the axis of mechanical feathering. It is completely determined by the blade retention and pitching mechanism.
- The aerodynamic axis for a conventional airfoil shape within the linear performance limits (C_l,α slope is constant) is at the blade section quarter chord (25% chord).

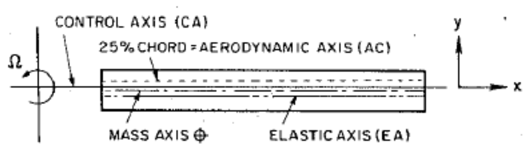

Figure A-17: Blade spanwise axes.

Torsion on the blade is caused when:

- The flapwise forces act on the blade, and the blade is deflected in in-plane direction.
- The edgewise forces act on the blade, and the blade is deflected in out of plane direction.
- There is distance between the $c_{\frac{1}{4}}$ point and elastic axis, then the lift force which acts on $c_{\frac{1}{4}}$ has an arm from the $c_{\frac{1}{4}}$ point to the elastic axis, this causes a torsional moment.
- Aerodynamic moment, described by $c_m(\alpha)$.

- The pitch mechanism starts operating at rated wind speed.
- Moment by centrifugal force. [31]

A.9 Loads on Tower

Usually tubular towers are used for wind turbines. Tubular towers are conical in shape i.e. their diameter increases towards the base. Loads on tower top differ from loads at tower base. Tower experiences loads in fore-aft, side-ways and torsion directions. Figure A-18 shows the fore-aft and side-ways tower motion. Tower loads are analyzed at tower base and top.

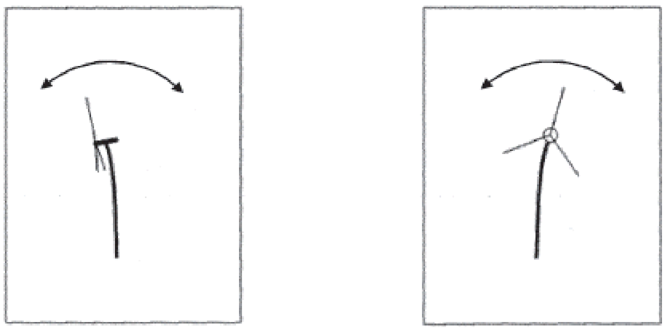

(a) (b)

Figure A-18: (a) I^{st} order fore-aft motion of tower, (b) I^{st} order side-ways motion of tower.

A.9.1 Fore-aft Bending Moment

Tower fore-aft bending moment results from rotor thrust loading. Wind also causes drag force on the tower which results in a small fore-aft bending moment about the tower base. Magnitude of drag load is low as compared to rotor loading.

A.9.2 Side-ways Bending Moment

Side-ways motion refers to the motion in lateral direction. Side-ways bending moment is caused when:

- The wind changes direction and the yaw drive is not working properly.

- Edgewise loads due to differential gravity loadings on different blades and torque fluctuations caused due to longitudinal turbulence can result in tower side-ways bending moments.
- Rotor torque acts on the tower top through gearbox/generator support.

Rotor provides some damping in the fore-aft direction, but in side-ways direction the aerodynamic damping is negligible and the only damping present is the structural damping. Fore-aft tower bending moment is usually higher in magnitude than side-ways tower bending moment. Lack of damping for side-ways bending can lead to fatigue.

A.9.3 Torsional moment

The nacelle is connected to the top of the tower by yaw bearing. Whenever the direction of wind changes, wind turbine aligns itself to the direction of wind. Yaw moment of the nacelle and rotor causes a torsional moment on the tower top. When the rotor is tilted, then there is a component of rotor torque acting in the tower axis at tower top. Torsional moment causes torsional deformation and this deformation is of more significance at tower top than at tower base.

B The ART Wind Turbine

Table B-2: Chord, mass and stiffness distributions of the ART wind turbine

Radial station	Chord[m]	Blade mass[Kg]	Flat-stiffness[Nm^2]	Edge-stiffness[Nm^2]
0	3.5	697.97	1.76E+10	1.76E+10
1.2	3.5	797.76	1.88E+10	1.90E+10
2.2	3.614	761.78	1.45E+10	1.96E+10
3.2	3.728	760.9	6.70E+09	1.00E+10
5.2	3.957	467.83	5.09E+09	7.79E+09
8.2	4.34	396.19	4.65E+09	6.65E+09
10.2	4.586	440.1	4.37E+09	6.93E+09
12.2	4.692	419.64	3.04E+09	6.81E+09
14.2	4.661	363.12	2.37E+09	4.80E+09
18.2	4.4883	348.9	2.20E+09	4.71E+09
24.2	4.05	322.33	1.67E+09	4.04E+09
26.2	3.9	302.82	1.24E+09	3.58E+09
34.2	3.26	246.39	6.31E+08	2.63E+09
40.2	2.784	183.54	3.82E+08	2.24E+09
42.2	2.6	169.04	2.97E+08	1.74E+09
48.2	2.23	133.04	1.68E+08	1.25E+09
50.2	2.1	109.24	1.21E+08	1.12E+09
54.2	1.88	92.044	7.41E+07	6.68E+08
56.2	1.84	74.612	6.00E+07	4.98E+08
57.7	1.74	67.877	2.33E+07	2.52E+08
58.2	1.75	60.849	1.92E+07	1.51E+08
60.7	1.55	42.646	4.50E+06	6.20E+07
61.2	1.2	12.348	1.87E+05	5.06E+06
62.6	0.4	6.4244	1.21E+05	4.43E+06

B.1 Description of the selected load cases of ART wind turbine

- **Load case - 012i** : This is a normal production load case with normal turbulence model (NTM) as the external condition. The first digit '0' suggests normal production load case. 2nd and 3rd digit represents the average wind velocity. The last digit 'i' can be either 0, 1, 2, 3 ,4 or 5. '0' and '3' represents normal production with negative misalignment, '1' and '4' represents normal production with positive misalignment and '2' and'5' represents normal production without misalignment.

- **Load case - 2452** : This load case belongs to DLC 2.1 according to the IEC standard. DLC 2.4 addresses control and protection system faults. Load case 2452 is about failed speed controller at rated wind speed at hub with normal turbulence model (NTM) as the external condition. In this load case the wind turbine is maintained at -8 degrees yaw angle i.e. there is yaw error of -8 degrees throughout the simulation time of 120 seconds.

- **Load case - 2677** : This load case belongs to DLC 2.1 according to the IEC standards. DLC 2.1 addresses control and protection system faults. Load case - 2677 is about negative yaw runaway and it happens at a wind speed of 25 m/s with normal turbulence model (NTM) as the external condition. Initially the nacelle is at -8 degree of yaw angle. Due to failure of yaw controller the yaw angle decreases to -72 degrees and thus the wind turbine is disoriented. This eventually leads to decrease in rotor speed.

- **Load Case - 3100** : This load case belongs to DLC 3.1 according to the IEC standard. Load case 3100 addresses the normal start up at cut-in wind speed at hub. In this load case the wind speed is maintained to 3 m/s with normal wind profile (NWP) as the external condition. In this load case the wind turbine is maintained at -8 degrees yaw angle .i.e. there is yaw error of -8 degrees throughout the simulation time of 120 seconds.

- **Load case - 3271** : This load case belongs to DLC 3.2 according to the IEC standard. Load case 3271 addresses start procedures with occurrence of 1-year extreme operating gust at 25 m/s wind speed at hub with extreme operating gust (EOG) as the external condition. The yaw angle is maintained at -8 degrees throughout the simulation.

- **Load case - 3280** : This load case belongs to DLC 3.2 according to the IEC standard. Load case 3280 addresses start procedures with occurrence of 1-year extreme operating gust at 25 m/s wind speed at hub with extreme operating gust (EOG) as the external condition. The yaw angle is maintained at 8 degrees throughout the simulation.

- **Load Case - 4180** : This load case belongs to DLC 4.1 according to the IEC standard. This load case addresses normal stop at 25m/s wind speed at hub with normal wind profile (NWP) as the external condition. The stop is activated by mechanical brake and pitch action. Yaw angle is maintained at -8 degrees and therefore the wind turbine rotor is always misaligned by 8 degrees.

- **Load case - 6001** : This load case belongs to DLC 6.0 according to the IEC standard. This load case addresses idling condition at 50-year extreme wind (i.e. 50 m/s) at hub with extreme wind model (EWM) as the external condition. Extreme wind is turbulent in nature. Yaw angle is maintained at 0 degree and therefore the wind turbine rotor is never misaligned.

- **Load case - 6233** : This load case belongs to DLC 6.2 according to the IEC standard. This load case addresses a parked rotor with failed yaw mechanism which implies that the rotor is idling and the wind comes from any direction. In this load case the wind turbine experiences 50-year extreme wind. Due to failure of yaw mechanism, the yaw angle is maintained at 109 degrees and therefore the wind turbine rotor is always misaligned to the wind direction.

- **Load Case - 9150** : This load case belongs to DLC 1.3 according to the IEC standard. This load cases addresses extreme turbulence model at an average wind speed of 15 m/s at hub. During the simulation the yaw angle is maintained at -8 degrees.

- **Load cases - 9242** : This load case belongs to DLC 1.3 according to the IEC standard. This load cases addresses extreme turbulence model at an average wind speed of 24 m/s at hub. During the simulation the yaw angle is maintained at 0 degree, hence no yaw misalignment.

C ART wind turbine load cases

C.1 Load case-2888: Pitch controller failure

This load case belongs to DLC 2.2 of the IEC standard and addresses faults that are considered rare events. Load case 2888 is about failed pitch controller at cut-out wind speed at hub with normal turbulence model (NTM) as the external condition. In this load case the wind turbine is not misaligned, hence zero yaw angle.

For the first 90 seconds the ART wind turbine operates in the normal operating state at cut-out wind. As the wind speed goes above rated wind speed then the pitch controller takes the charge and tries to reduce loads and maintain the power output to the design limit. Figure C-1 shows the wind speed at hub. As soon as the pitch controller fails,

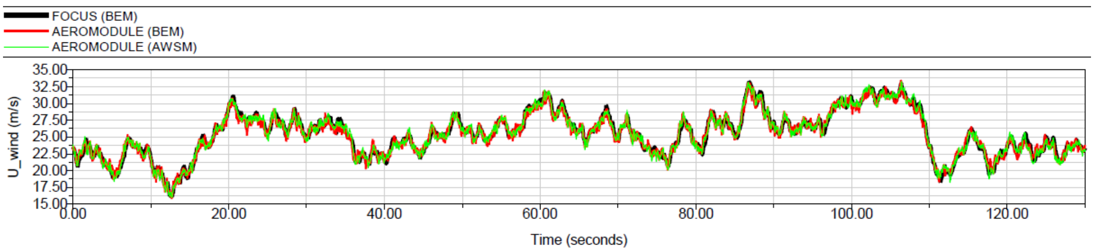

Figure C-1: Case-2888: Wind speed at hub.

the pitch angle of the blades starts to decrease i.e. blades pitch to work with maximum pitch rate of 6 degrees/s. While decreasing the pitch angle, the rotor speed increases and reaches above the over speed value. As soon as the rotor speed is above the over speed value then the supervisory controller comes into action and increases the pitch angle to 90 degrees i.e. the blades are pitched to vane with maximum pitch rate of 6 degrees/s. Increase in pitch angle causes the aerodynamic torque to decrease sharply. Now it is the responsibility of the supervisory controller to regulate the generator power. Figures C-2 and C-3 show the variation in pitch angle of one blade and rotor speed respectively. Even when supervisory controller takes the charge, the rotor speed increases because the pitch angle is small. At 95th second when the pitch angle is 20 degrees the generator speed reaches a peak and then starts reducing and the generator torque also reduces. Reduction in generator torque along with reduction in generator speed causes the generator power to decrease. Reduction in generator speed

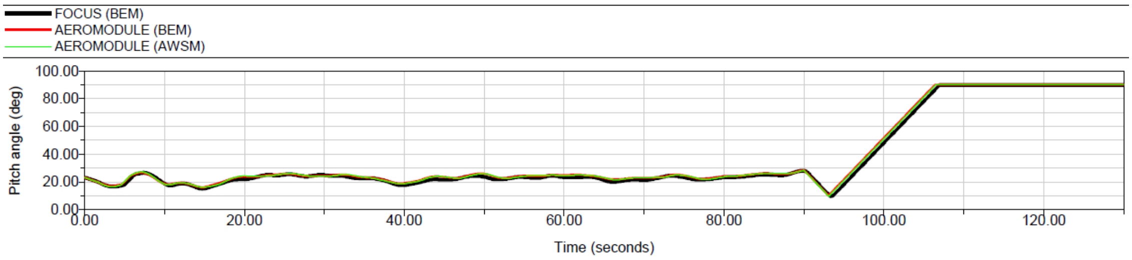

Figure C-2: Case-2888: Pitch angle of one blade.

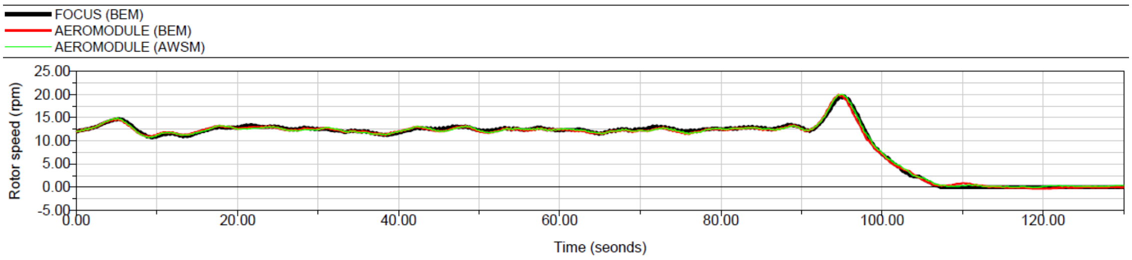

Figure C-3: Case-2888: Rotor speed.

causes reduction in rotor speed. Figures C-4 and C-5 shows the generator power and generator torque of the ART wind turbine respectively. In order to stop the reduction in generator power, the generator torque increases and thus the aerodynamic torque increases too and this can be clearly seen that from 97th second the slope of generator power changes. The axial aerodynamic force on rotor is dependent upon the pitch angle of the blades.

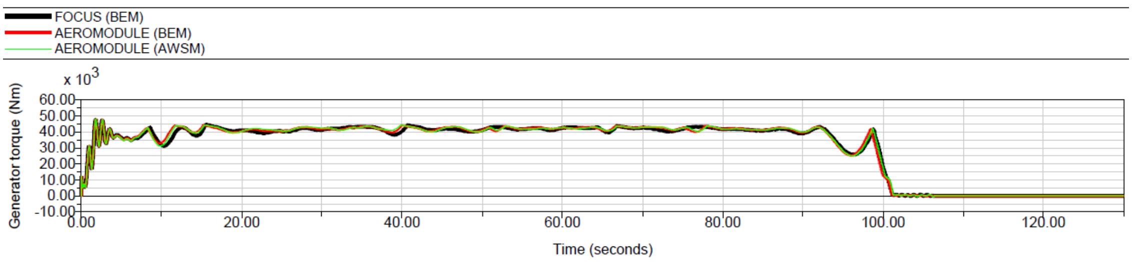

Figure C-4: Case-2888: Generator torque.

Figures C-6 and C-39 shows the axial aerodynamic force on rotor and average flapwise displacement of blade tips respectively. After the pitch controller failure the axial

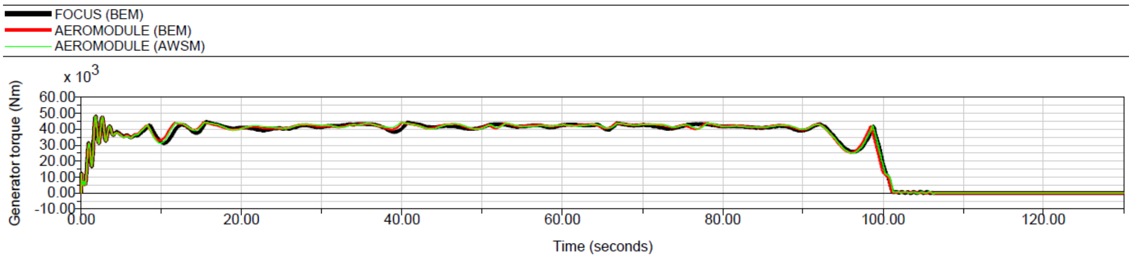

Figure C-5: Case-2888: Generator power.

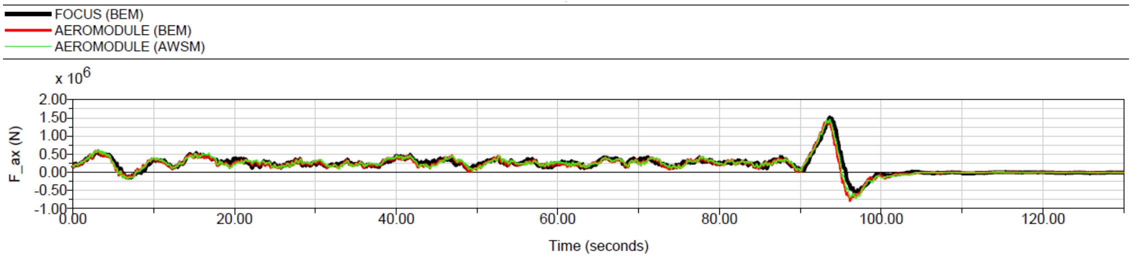

Figure C-6: Case-2888: Axial aerodynamic force on rotor.

aerodynamic force shows a peak because of reduction in pitch angle which in turn increases the exposed surface area of blade and this can be seen in figure C-7. When

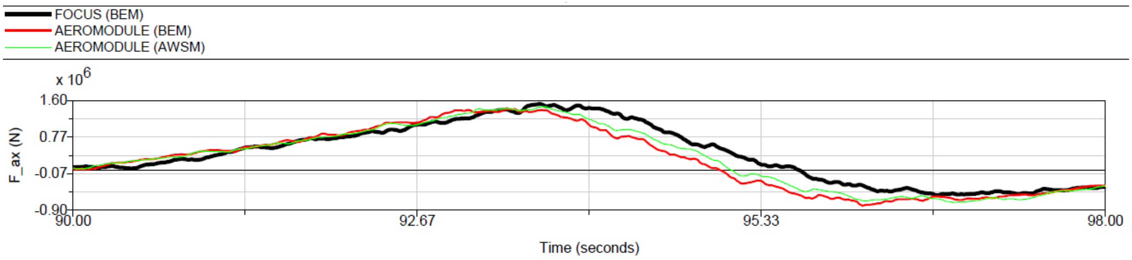

Figure C-7: Case-2888: Axial aerodynamic force on rotor from 90th to 98th second.

the pitch angle increases the exposed area of blade to wind decreases and this causes decrease in axial aerodynamic force on rotor. From 97th second when the pitch angle is 20 degrees the axial aerodynamic force increases because now the inertia of blades is greater than the wind thrust.

The average flapwise displacement of blade tips follows the same trend as axial aerodynamic force on rotor and increases from its initial pre bend (-2.05 m) to 9 m. Including

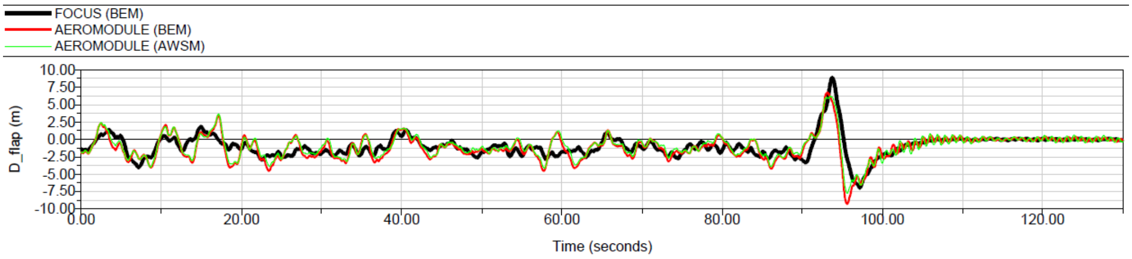

Figure C-8: Case-2888: Average flapwise displacement of blade tips.

the cone and tilt angle the axial distance of blade tip from tower is 11.5 m. As the blades flap maximum to 9 m, this means blade and tower don't collide, hence no damage. Figure C-40 shows the flapwise displacement of blade tips from 90th to 98th second. The ART wind turbine rotor is not misaligned, hence the yaw angle is zero degree.

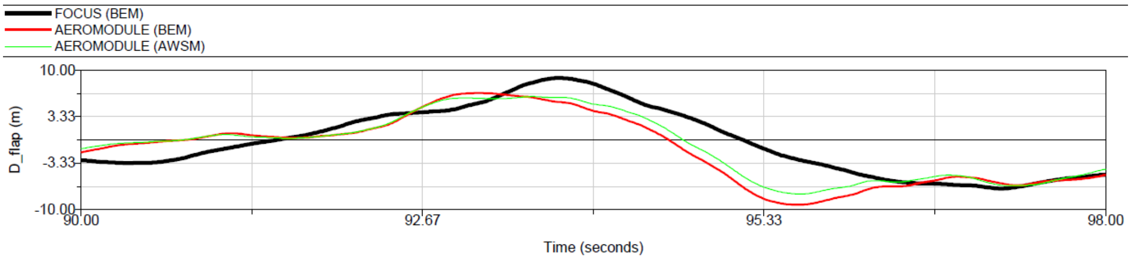

Figure C-9: Case-2888: Average flapwise displacement of blade tips 90th to 98th second.

C.1.1 Aerodynamic aspects

Blades of the ART wind turbine are flexible in this case and thus it takes time for AEROMODULE(BEM) and AEROMODULE(AWSM) to stabilize after pitch controller failure, because SIMPACK needs time to stabilize the vibration in flexible bodies. Figure C-10 shows the aerodynamic angle of attack at 0.81R blade stations. At 0.81R blade station, all the three modules show good match, but after pitch controller failure at 90th second difference among them starts increasing though same controller is used. The difference between AEROMODULE modules and FOCUS(BEM) is because of the AEROMODULE-SIMPACK controller interface which FOCUS(BEM) does not

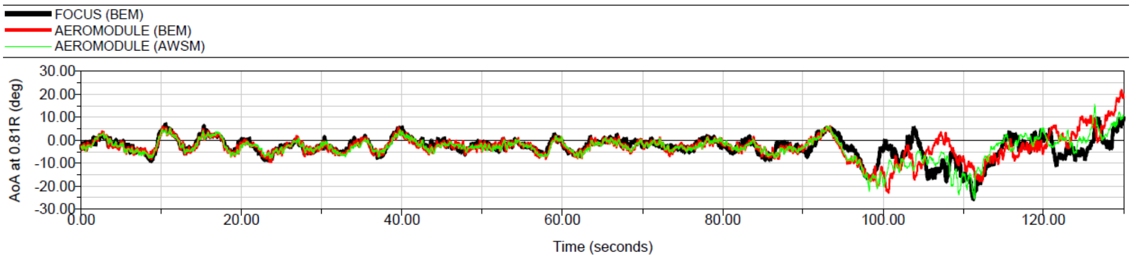

Figure C-10: Case-2888: Aerodynamic angle of attack at 0.81R blade station.

have. Pitch controller failure leads to change in pitch angle slope which leads to dynamic inflow effects. Though dynamic inflow model is same in both the BEM modules still differences are there because of compatibility issues between AEROMODULE-SIMPACK controller interface. When dynamic inflow occur the trailing wake changes and thus takes time to stabilize and causes induction on rotor, due to this AEROMODULE(AWSM) is different from both the BEM modules. α becomes negative for all modules after pitch controller failure because of high pitch angle of 20 degrees. When the pitch angle crosses 40 degrees, FOCUS(BEM) shows completely a different trend, whereas AEROMODULE(BEM) and AEROMODULE(AWSM) are still close to each other and almost follow the same trend.

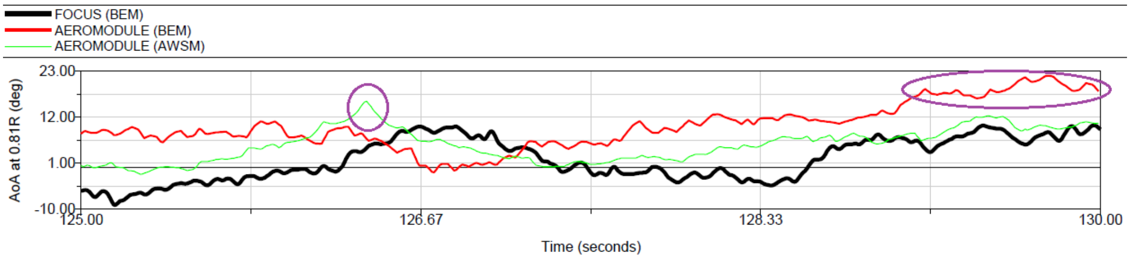

Figure C-11: Case-2888: Aerodynamic angle of attack at 0.81R blade station from 125th to 130th second.

Figure C-11 shows the aerodynamic angle of attack at 0.81R blade stations from 125th to 130th second. AEROMODULE(BEM) and AEROMODULE(AWSM) exceed α above 14 degrees and this suggests under such conditions the airfoil at 0.81R blade station is in stall region. FOCUS(BEM) for the 0.81R blade station does not reach stall at all from 125th to 130th second. When the pitch angle reaches 90 degrees and becomes constant, α increase positively for all modules because of increase in wind speed.

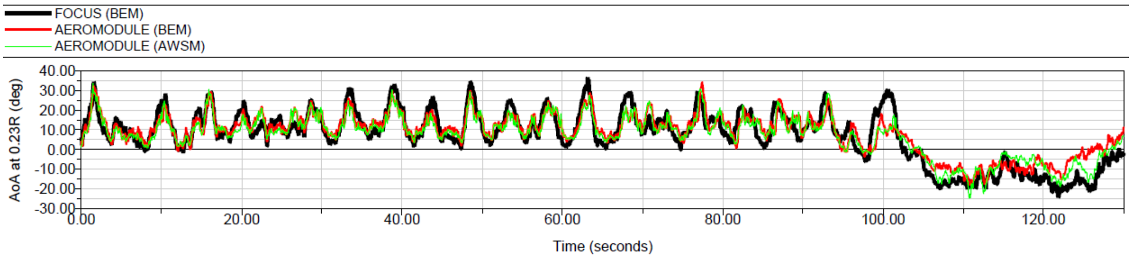

Figure C-12: Case-2888: Aerodynamic angle of attack at 0.23R blade station.

Figure C-12 shows the aerodynamic angle of attack at 0.23R blade stations. At 0.23R blade station, all the modules follow the similar trend before the pitch controller failure, but after pitch controller failure the difference among them starts increasing. Before the pitch controller failure all the modules show many peaks and this is because as this airfoil is near the root and thus has large thickness as compared to airfoils near tip. Due to large thickness, it becomes easier for the flow to separate and thus the airfoil at 0.23R reaches stall again and again, which is evident from the repetitive peaks. Figure C-13 shows the aerodynamic angle of attack at 0.23R blade stations from 42nd to 45th second, it can be seen that FOCUS(BEM) has a higher peak than both the modules of AEROMODULE. AEROMODULE(BEM) has the same trend as FOCUS(BEM) but with a certain phase difference, and the phase difference is because, AEROMODULE-SIMPACK couple takes time to stabilize. Purple circle in the figure C-13 shows the time interval in which 0.23R blade station is stalled for all the modules. After dynamic

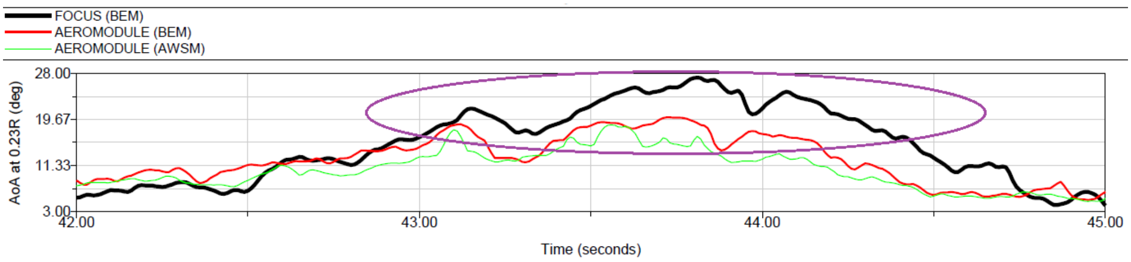

Figure C-13: Case-2888: Aerodynamic angle of attack at 0.23R blade station from 42nd to 45th second.

inflow at 90th second, still all the modules shows a close match but when the pitch angle reaches 40 degrees, difference between all modules increases, though both AEROMODULE modules are close and have almost the same trend. This difference is because of compatibility issues between AEROMODULE-SIMPACK couple controller interface. When the pitch angle reaches 90 degrees and becomes constant, then α increases for all modules because of increase in wind speed.

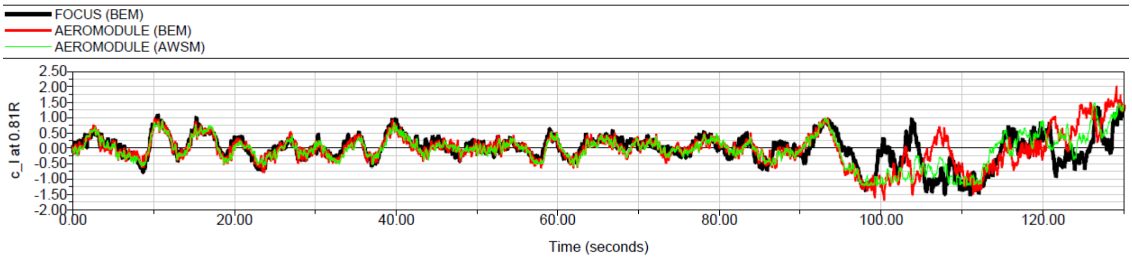

Figure C-14: Case-2888: Lift coefficient c_l at 0.81R blade station.

Figure C-14 shows the lift coefficient c_l at 0.81R blade stations. At 0.81R blade station, lift coefficient c_l follows the same trend as α. All the modules behave in the same way as they did for α because α lies in the slope region of c_l, α curve. Whenever α crosses -3 degrees, c_l reaches zero because this is the zero lift angle of attack for the airfoil at this blade station. Beyond -3 degrees of α, c_l also becomes negative as it lies in the linear slope region. When dynamic inflow occurs at 93rd second both all the modules are close to each other. Figures C-15 and C-16 show α and c_l respectively at 0.81R from 95th to 105th second. Once the supervisory controller takes the charge at 93rd second and pitch angle increases to 40 degrees the difference between all modules increases, c_l follows the trend of α. Whenever α crosses -18 degrees, airfoil at 0.81R is in stall and thus c_l increases. For FOCUS(BEM) α doesn't reach below -18 degrees while both AEROMODULE modules do and this can be seen from 98th to 101st second. As there is no dynamic stall model in AEROMODULE(AWSM) therefore it shows flat c_l whenever α is below -18 degrees while AEROMODULE(BEM) shows c_l lower than minimum 2D value because of dynamic stall model. Whenever dynamic stall occurs stall delay happens and the flow remains attached to airfoil.

When the pitch angle becomes constant at 90 degrees, α increases because of increase in wind speed, which subsequently increases c_l, this happens for all the modules. c_l

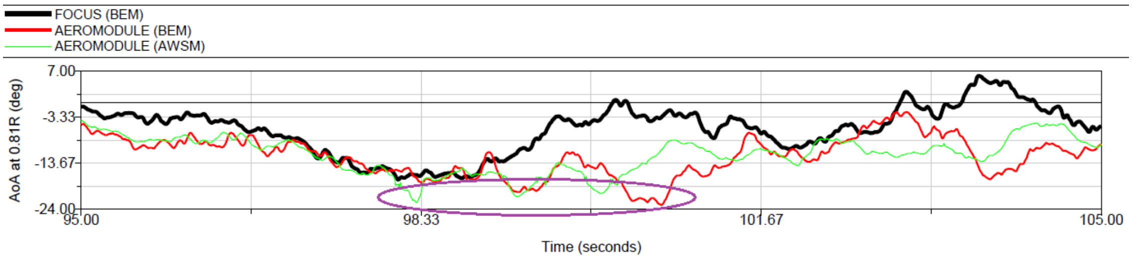

Figure C-15: Case-2888: Aerodynamic angle of attack at 0.81R blade station from 95th to 105th second.

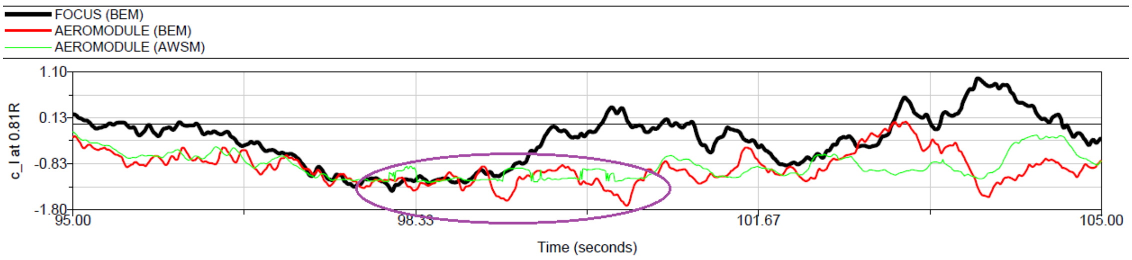

Figure C-16: Case-2888: Lift coefficient c_l at 0.81R blade station from 95th to 105th second.

follows the same trend as α in the figure C-11.

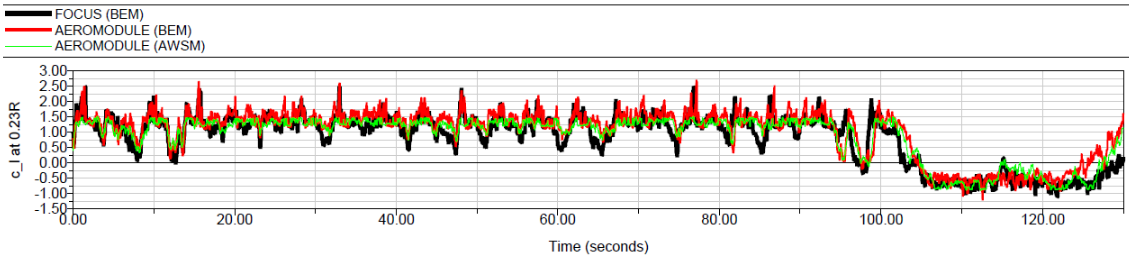

Figure C-17: Case-2888: Lift coefficient c_l at 0.23R blade station.

Figure C-17 shows the lift coefficient c_l at 0.23R blade stations. At 0.23R blade station, all the modules are close to each other. For this blade station the stall α is 12.5 degrees. Before pitch controller failure, there is lot of rising and falling peaks for α, c_l of both the BEM modules follow the trend of their respective α peaks, but AERODOMULE(AWSM) doesn't. This is because whenever α crosses 12.5 degrees, the blade station at 0.23R is in stall and thus c_l should decrease, but it increases because of dynamic stall, AEROMODULE(AWSM) doesn't predicts this because of no dynamic stall model in it whereas both the BEM models does. In both the BEM modules stall delay occurs and thus c_l increases beyond the maximum value. Figures C-13 and C-18 gives good insight about this. Negative stall α for 0.23R blade station is 15 degrees, whenever all the modules cross this angle, c_l is no more in the linear slope region and thus stall occurs which leads to decrease in negative value of c_l i.e. increase in c_l.

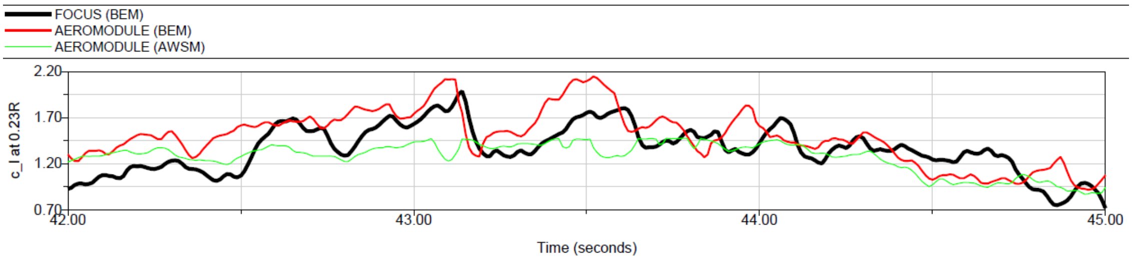

Figure C-18: Case-2888: Lift coefficient c_l at 0.23R blade station from 42nd to 45th second.

Figure C-19 shows the axial induced velocity at 0.81R blade station. AEROMODULE(AWSM) shows a lot of fluctuations for u_{ind}, because it is defined in inertial reference system and even after converting from inertial to rotating reference system using rotation matrix [4] there are fluctuations. The trend of mean value of u_{ind} for all the modules is similar before pitch controller failure. After pitch controller failure, difference between all the modules increases because of different α.

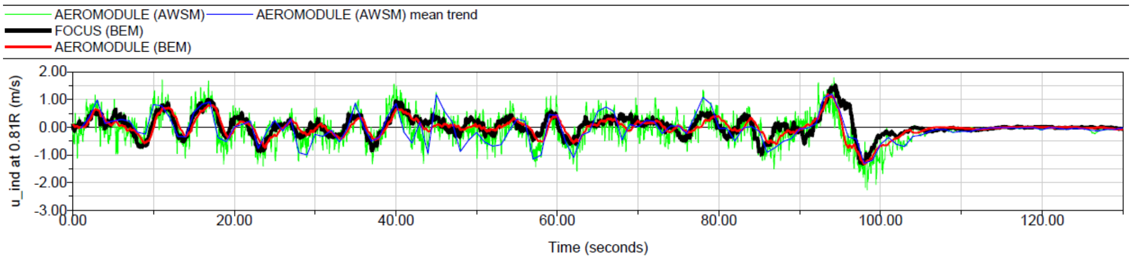

Figure C-19: Case-2888: Axial induced velocity at 0.81R blade station.

When the supervisory controller takes charge at the 93rd second, both AEROMODULE modules have similar trend for the mean value and they slightly differ from FOCUS(BEM) because of different α, this can be seen in figures C-20 and C-21. When the pitch angle becomes constant at 90 degrees and there is no more dynamic inflow then all the modules show similar trend and are close to each other.

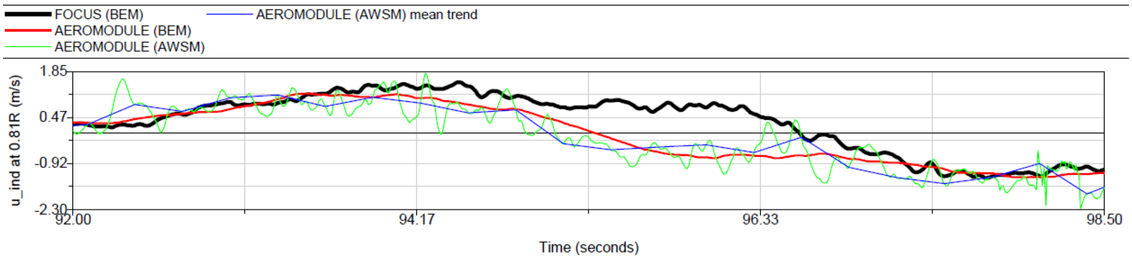

Figure C-20: Case-2888: Axial induced velocity at 0.81R blade station from 92nd to 98.5th second.

Figure C-22 shows the axial induced velocity at 0.23R blade station. Same as 0.81R blade station, at 0.23R blade station also AEROMODULE(AWSM) shows a lot of fluctuations because of problem in converting from inertial to rotating reference system. Still mean value of u_{ind} for all modules is close. From the point of pitch controller failure till 98th second lot of peaks can be seen in FOCUS(BEM) and AEROMODULE(AWSM) mean trend curves, while AEROMODULE(BEM) doesn't show this, fig-

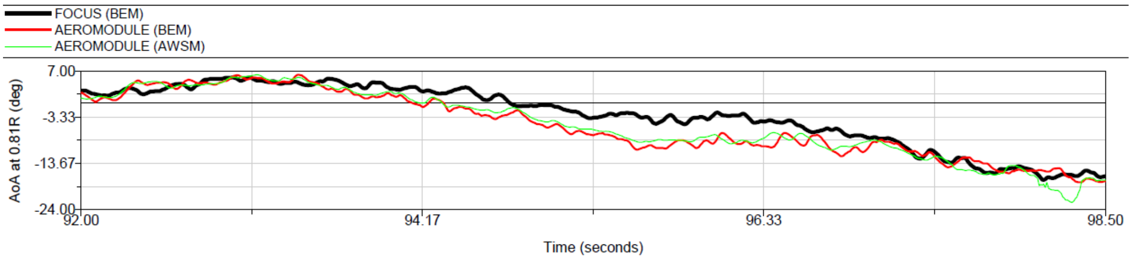

Figure C-21: Case-2888: Aerodynamic angle of attack at 0.81R blade station from 92nd to 98.5th second.

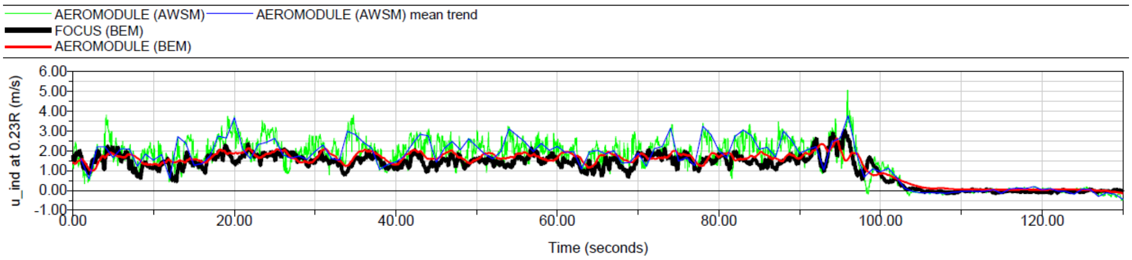

Figure C-22: Case-2888: Axial induced velocity at 0.23R blade station.

ure C-23 gives more insight about it. From figure C-24, it can be seen at this interval the airfoil is mostly in stall region, AEROMODULE(BEM) does not predict stall correctly here and thus shows a different trend as compared to other two modules. Figure C-25 gives more aerodynamic insight at 96th second, AEROMODULE(BEM) predicts higher c_l as compared to other two modules even when all of them have almost the same α at 0.23R blade station i.e. at 14.76 m of radial length. Due to higher c_l, AEROMODULE(BEM) shows the smallest axial induced velocity, u_{ind}, among all the modules.

Figures C-26 and C-27 shows the normal force distribution at 0.81R and 0.23R blade stations respectively. At 0.81R blade station, normal force distribution N for all the modules are close and follow the same trend before and after the pitch controller failure. After the failure, N doesn't follow the same trend as α and c_l because the inflow angle ϕ becomes very high as the pitch angle is very high. N is dependent upon inflow angle ϕ [28], at high ϕ the contribution of the term $c_l \sin\phi$ reduces and the contribution of term $c_d \cos\phi$ increases. Same explanation is for the airfoil at 0.23R blade station as

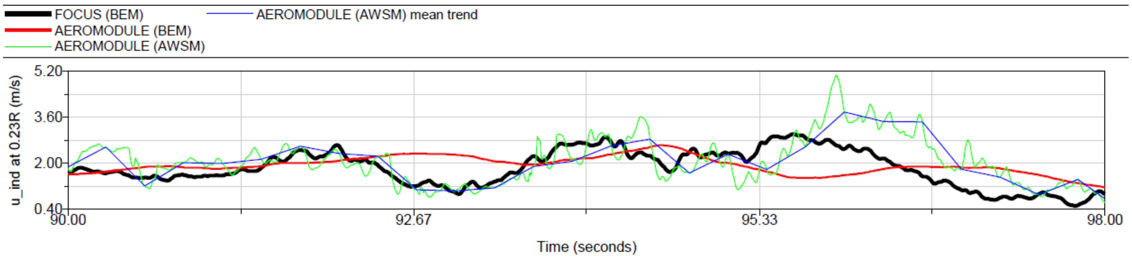

Figure C-23: Case-2888: Axial induced velocity at 0.23R blade station from 90th to 98th second.

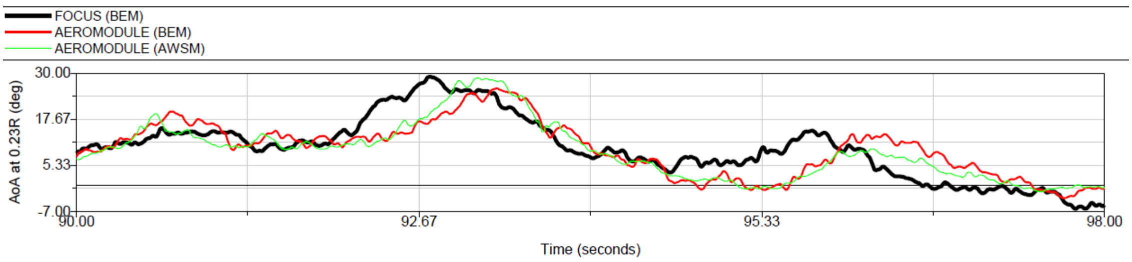

Figure C-24: Case-2888: Aerodynamic angle of attack at 0.23R blade station from 90th to 98th second.

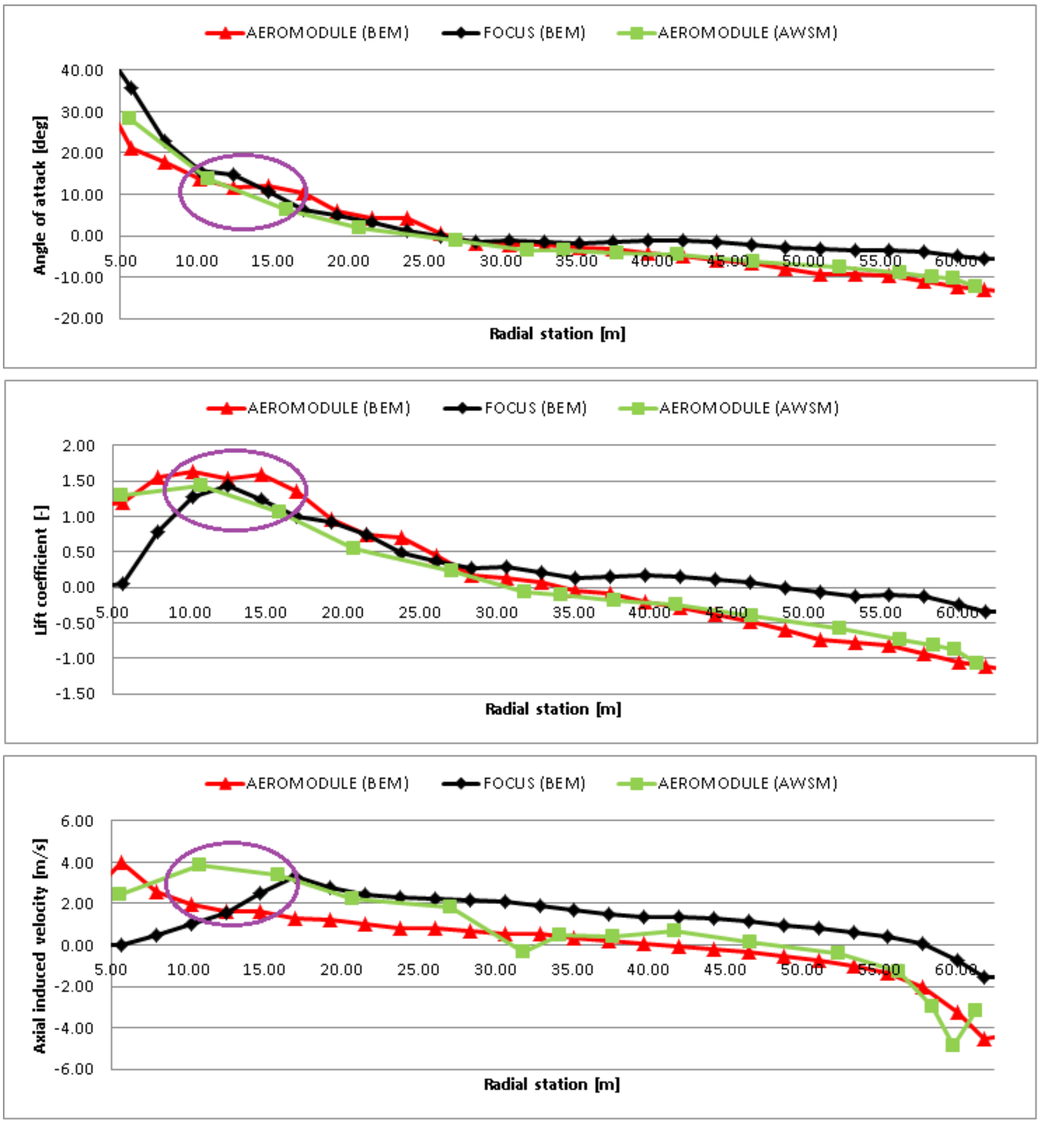

Figure C-25: Case-2888: Aerodynamic analysis at 96th second.

given above. All the modules show close match for N at 0.23R before and after the pitch controller failure. At both 0.23R and 0.81R blade stations, whenever α goes beyond the stall angle, AEROMODULE(AWSM) shows 2D characteristics for c_l and this can be observed in flattening of N for AEROMODULE(AWSM).

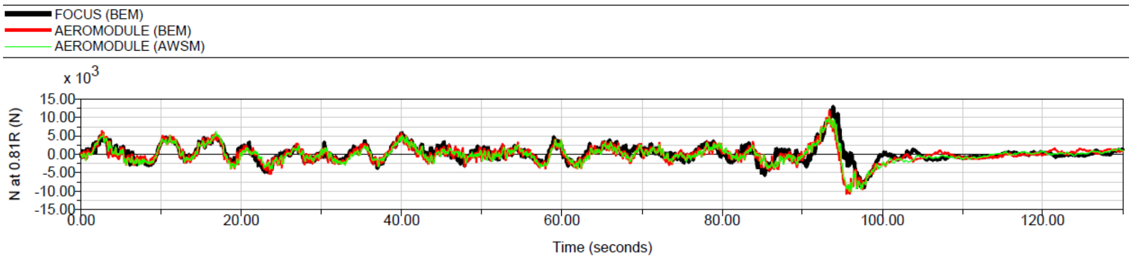

Figure C-26: Case-2888: Normal force distribution at 0.81R blade station.

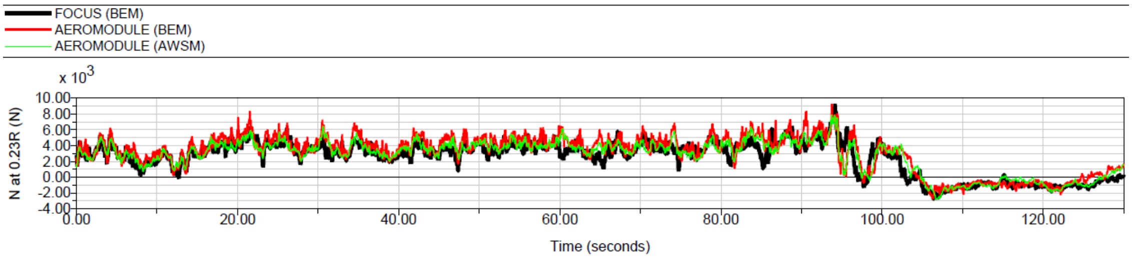

Figure C-27: Case-2888: Normal force distribution at 0.23R blade station.

Figures C-28 and C-29 shows the tangential force distribution at 0.81R and 0.23R blade stations respectively. Tangential force distribution T follows the opposite trend of N because of the inverse relation with c_l and c_d as compared to N. All the modules show close match for T at 0.23R and 0.81R blade stations before and after the pitch controller failure. At both 0.23R and 0.81R blade stations, whenever α goes beyond the stall angle, AEROMODULE(AWSM) shows 2D characteristics for c_l and this can be observed in flattening of T for AEROMODULE(AWSM).

C.1.2 Aerodynamic aspects - Before pitch controller failure

In this section the time series is zoomed from 84.5th to 85.5th second to get more aerodynamic insight. This time interval shows normal operating condition at cut-out

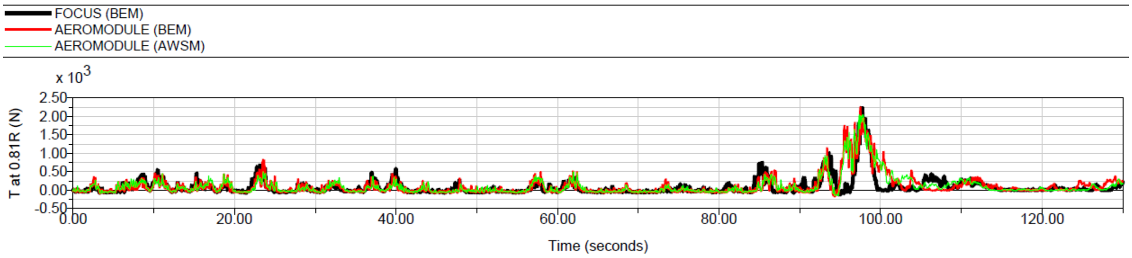

Figure C-28: Case-2888: Tangential force distribution at 0.81R blade station.

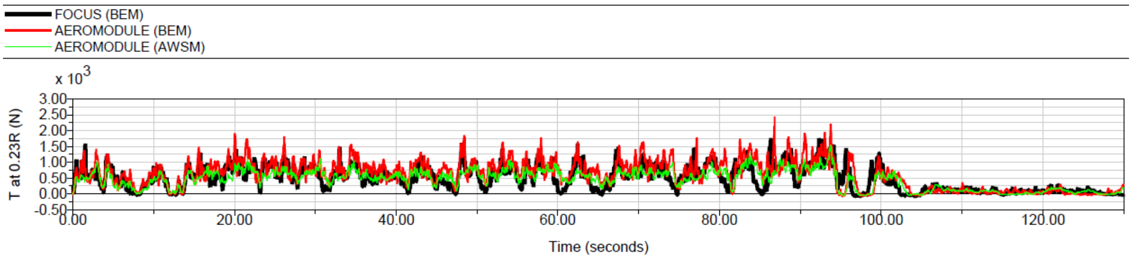

Figure C-29: Case-2888: Tangential force distribution at 0.23R blade station.

wind speed i.e. before the pitch controller failure. From figure C-30, it can be seen that at 0.81R blade station for all the graphs, AEROMODULE(BEM) and AEROMODULE(AWSM) are close to each other while FOCUS(BEM) is slightly deviated. This deviation is because of compatibility issues with AEROMODULE-SIMPACK couple controller interface. For all the modules, α lies in the linear slope region therefore c_l is directly proportional to α. At -3 degrees of α, c_l is zero and this is quite visible in the figure C-30 for all the modules. As N is directly dependent on c_l and cosϕ, ϕ is dependent on α, therefore lower α along with higher c_l will cause N to increase otherwise opposite will happen. As compared to N, T shows an opposite trend because of its dependency on c_l and sinϕ. Due to different controller interface in AEROMODULE-SIMPACK couple and FOCUS(BEM), AEROMODULE modules curve and FOCUS(BEM) curve differ for u_{ind}. The trend of AEROMODULE(AWSM) for u_{ind} follows similarly to it's α trend, but this is not in case of AEROMODULE(BEM) and FOCUS(BEM). This may be because AEROMODULE(AWSM) has wake and wake causes axial induction on each blade station locally, while in both the BEM modules there is no wake.

At 0.23R blade station, α for AEROMODULE(BEM) and AEROMODULE(AWSM) crosses above 12.5 degrees, FOCUS(BEM) does not cross 12.5 degrees of α. 12.5 degrees is the stall angle of attack for 0.23R blade station. As there is no dynamic stall model in AEROMODULE(AWSM), therefore it only shows 2D characteristics for c_l, while AEROMODULE(BEM) shows c_l higher than the maximum 2D value because of dynamic stall model in it. N and T for all the modules show differences because of different c_l and ϕ, but still both AEROMODULE modules are closer to each other. All the modules follow similar trend as α and c_l.

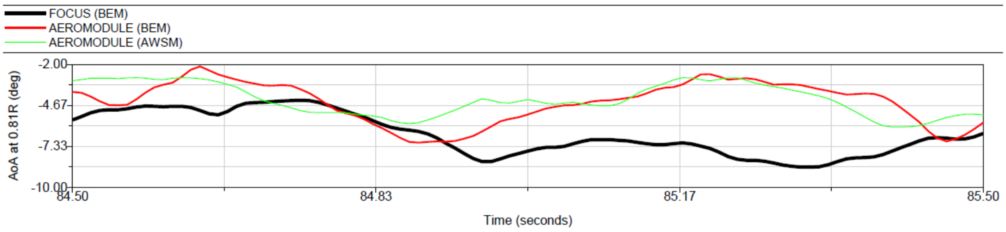

(a)

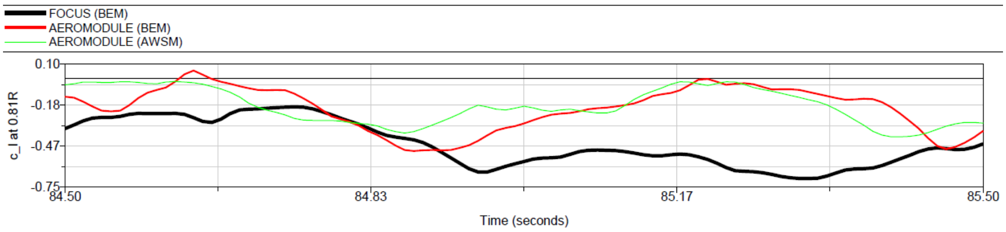

(b)

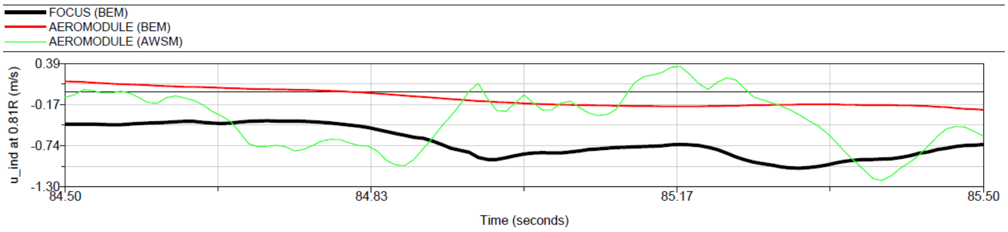

(c)

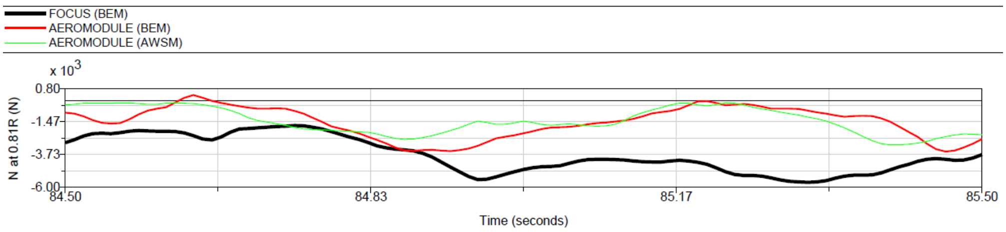

(d)

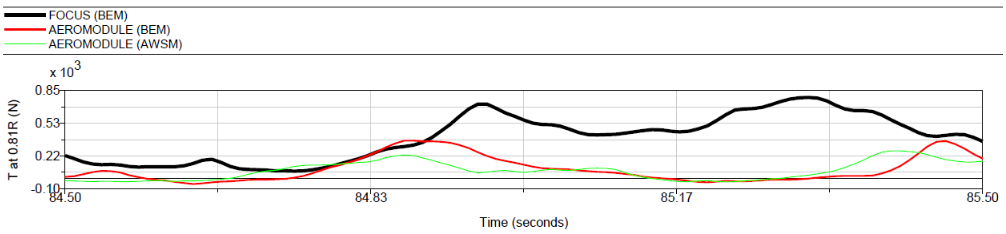

(e)

Figure C-30: Case-2888: Aerodynamic analysis at 0.81R blade station from 84.5th to 85.5th second.

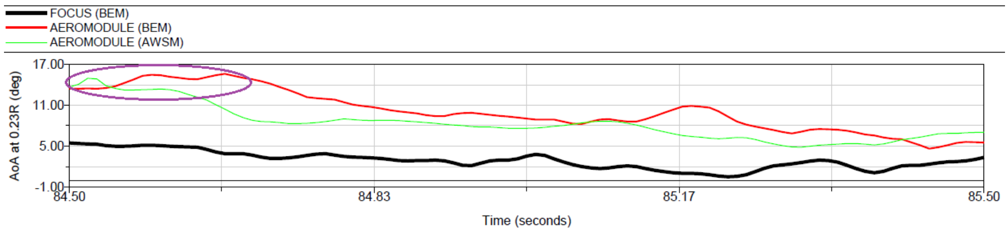

(a)

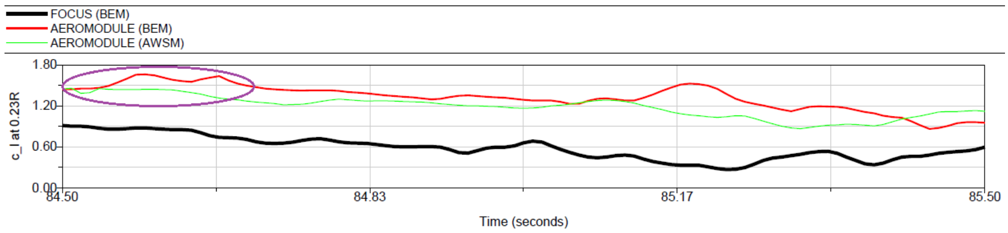

(b)

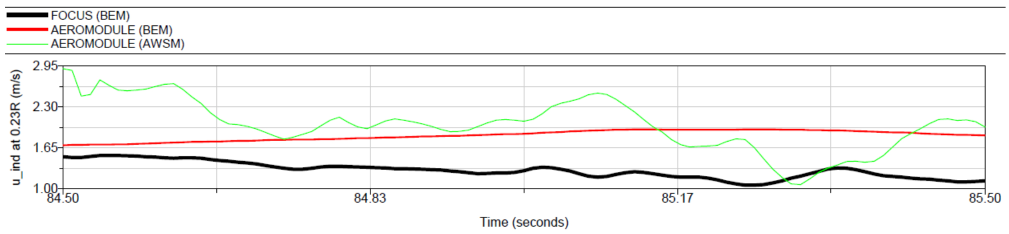

(c)

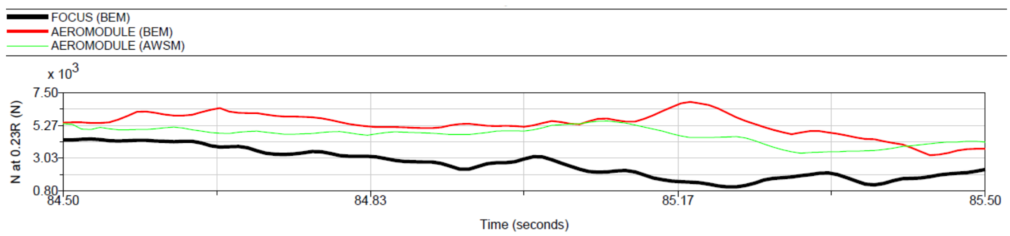

(d)

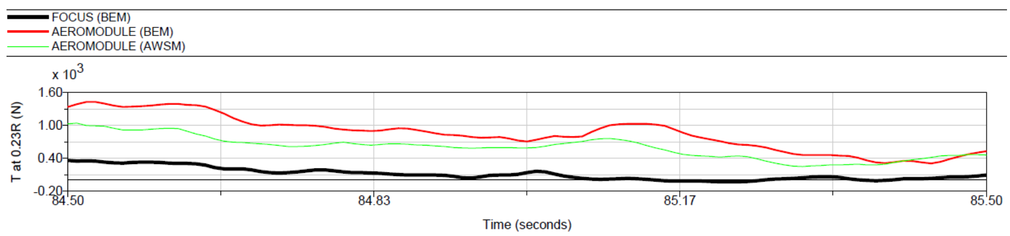

(e)

Figure C-31: Case-2888: Aerodynamic analysis at 0.23R blade station from 84.5th to 85.5th second.

C.1.3 Aerodynamic aspects - During pitch controller failure

In this section the time series is zoomed from 99th to 101st second to get more aerodynamic insight. This time interval is during the pitch controller failure when supervisory controller is in charge and pitch angle is increasing from 40 to 60 degrees.

At 0.81R blade station, negative α at which stall occurs is -18 degrees. From figure C-32, this is evident that FOCUS(BEM) does not reach stall while both AEROMODULE modules reach this is because of the compatibility issues in AEROMODULE-SIMPACK couple controller interface. Because of absence of dynamic stall model in AEROMODULE(AWSM), AEROMODULE(AWSM) shows 2D characteristics and thus c_l flattens out when α goes beyond -18 degrees i.e. the stall angle. AEROMODULE(BEM) shows c_l higher than the minimum 2D characteristics because of dynamic stall model. There are small peaks in AEROMODULE(AWSM) which are not in both the BEM modules, this is may be due to the influence of tip vortex on this blade station and this can be seen near the tip region in figure C-33. FOCUS(BEM) shows higher N than both AEROMODULE modules because of higher c_l and opposite happens for T. Still in all the modules N follows the trend of α and c_l, while T follows the opposite trend of α and c_l. FOCUS(BEM) shows the highest axial induced velocity u_{ind} compared to both AEROMODULE modules because of higher α. u_{ind} for AEROMODULE(AWSM) follows the similar trend as α but not for both the BEM modules, this may be because AEROMODULE(AWSM) has wake and wake causes axial induction on each blade station locally, while in both the BEM modules there is no wake.

Figure C-34 shows the aerodynamic analysis at 0.23R blade station from 99th to 101st second. At 0.23R blade station the positive α for stall is 12.5 degrees, AEROMODULE(AWSM) doesn't reach this angle while both the BEM modules do reach. Both the BEM modules predict stall and thus show decreasing trend for c_l, for increasing α. AEROMODULE(BEM) shows much higher c_l than FOCUS(BEM) and it seems it is over predicting stall here. Small peaks in AEROMODULE(AWSM) are there which are not in both the BEM modules, root vortex may be the cause of this as its influence can be seen in figure C-35 near the root region. Root vortex is accounted in BEM by Prandtl root loss factor. N and T follow the trend of α and c_l for all modules.

u_{ind} for AEROMODULE(AWSM) follow similar trend as α, but not for both the BEM modules and this may be because AEROMODULE(AWSM) has wake and wake causes axial induction on each blade station locally, while in both the BEM modules there is no wake.

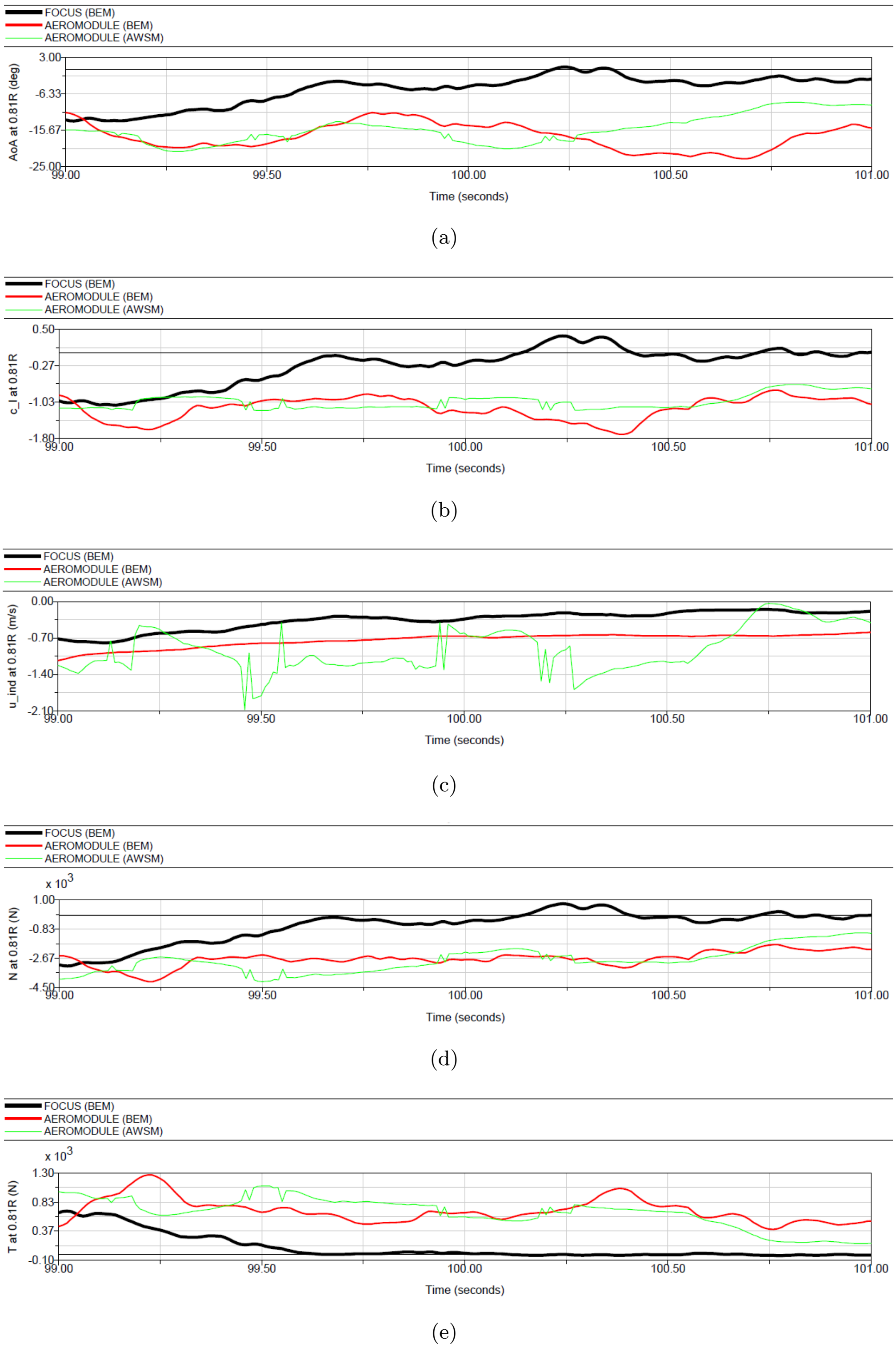

Figure C-32: Case-2888: Aerodynamic analysis at 0.81R blade station from 99th to 101st second.

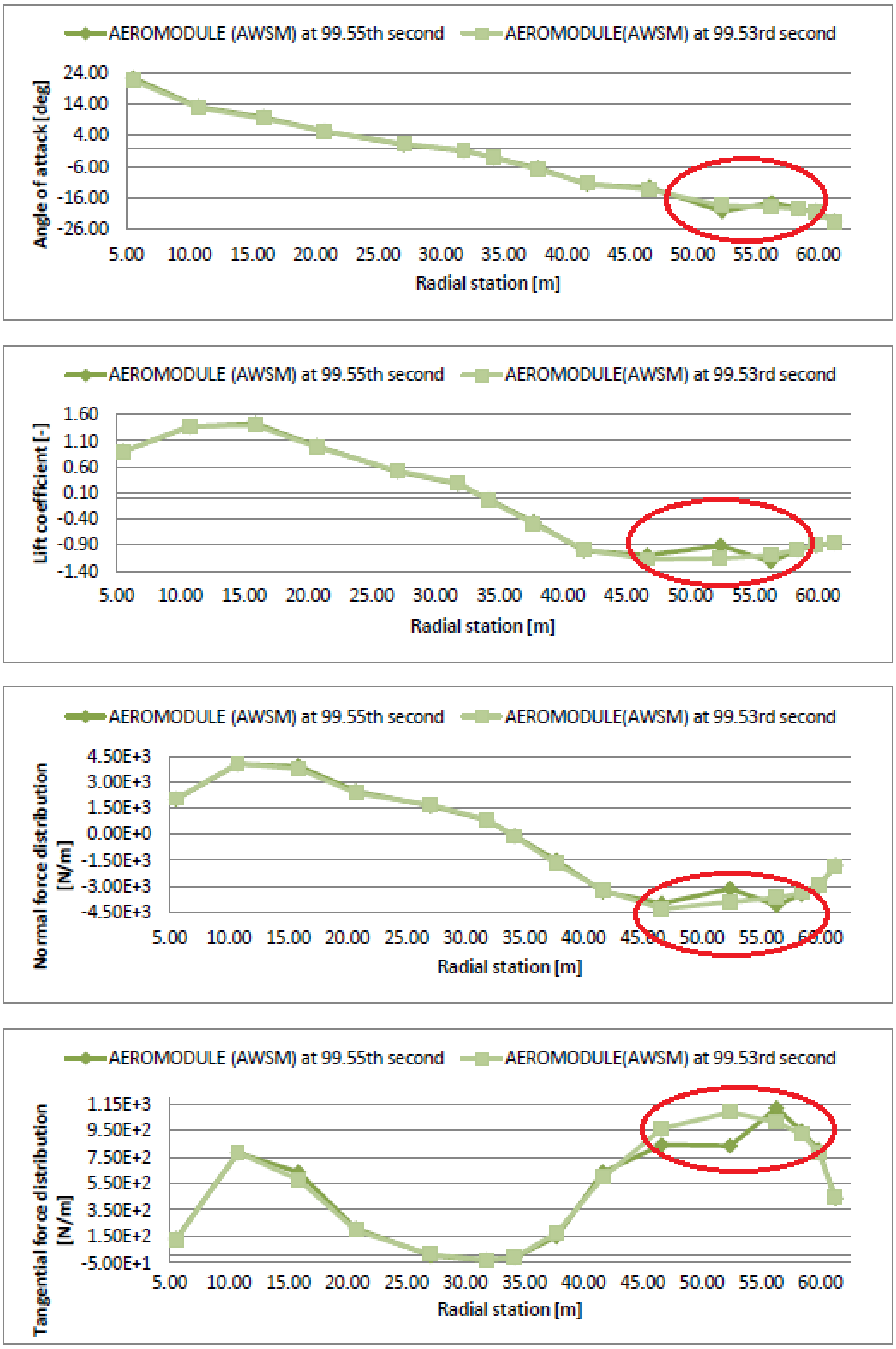

Figure C-33: Case-2888: Effect of tip vortex in AEROMODULE(AWSM).

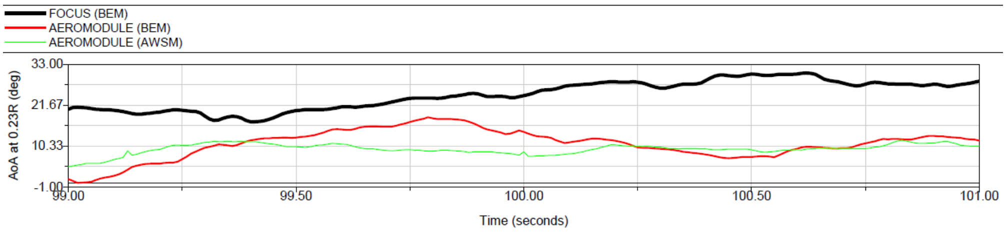

(a)

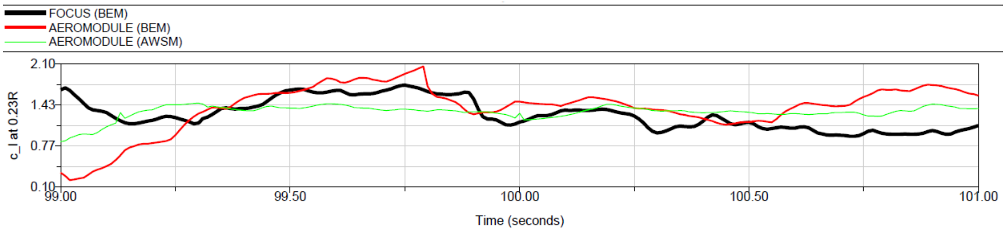

(b)

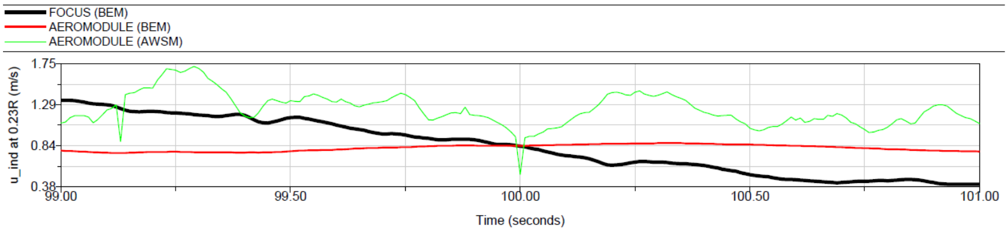

(c)

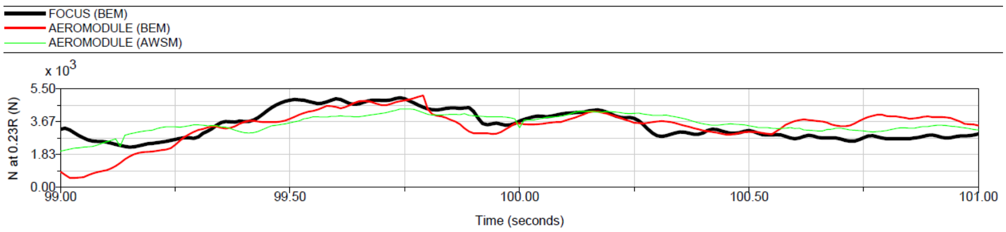

(d)

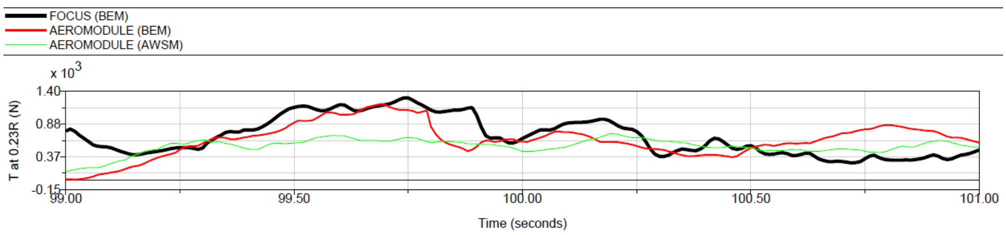

(e)

Figure C-34: Case-2888: Aerodynamic analysis at 0.23R blade station from 99th to 101st second.

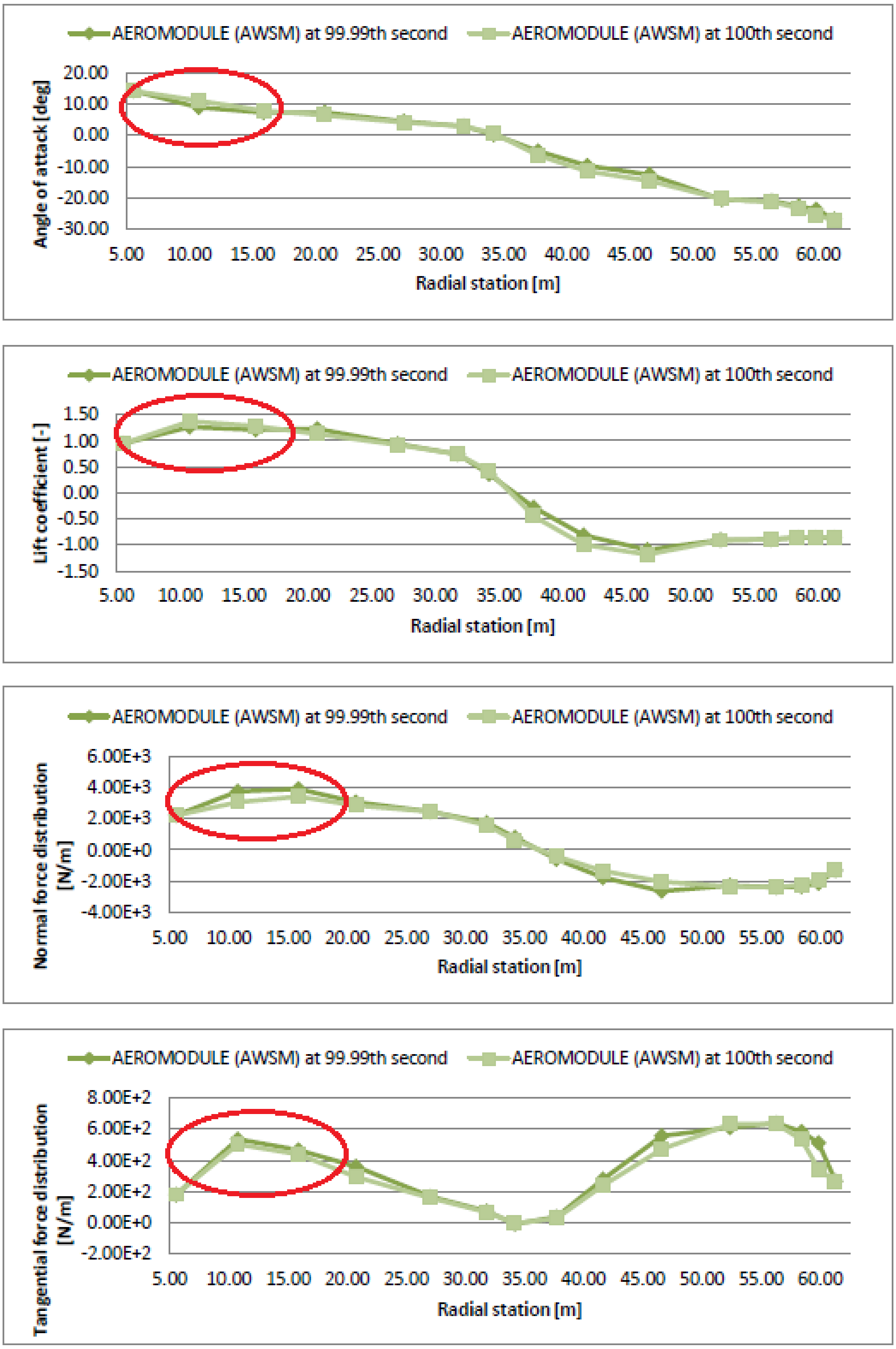

Figure C-35: Case-2888: Effect of root vortex in AEROMODULE(AWSM).

C.1.4 Aerodynamic aspects - After pitch controller failure

In this section the time series is zoomed from 126th to 127th second to get more aerodynamic insight after the pitch controller failure. At this interval blade is completely parallel to wind direction i.e. pitch angle is 90 degrees. In this situation blades are not rotating, therefore spanwise airflow is very small or negligible. In general 2D characteristics of the blade can be seen here.

Figure C-36 shows the aerodynamical analysis at 0.81R blade station from 126th to 127th second. At 0.81R blade station, when α crosses 13 degrees it is stall region. Only AEROMODULE(AWSM) reaches stall, both the BEM modules don't. Due to absence of dynamic stall model c_l flattens out rather increasing with α. Other than the peak in α for AEROMODULE(AWSM), α lies in the linear slope region therefore c_l has the same trend as α. N and T for all the modules also follow the same trend as α and c_l. u_{ind} for FOCUS(BEM) and AEROMODULE(AWSM) show similar trend as their α trend but AEROMODULE(BEM) does not show this.

Figure C-37 shows the aerodynamical analysis at 0.23R blade station from 126th to 127th second. At 0.23R blade station, FOCUS(BEM) reaches stall after a negative α of -15 degrees while both AEROMODULE modules don't cross below this angle. Because of dynamic stall model in FOCUS(BEM) it shows higher c_l than its minimum 2D characteristics value. c_l for other two modules follow the same trend as α, because α for them lies in the linear slope region. N follows the same trend as α and c_l while T follows the opposite. Both N and T are small because of large ϕ and low c_l. u_{ind} follows the opposite trend as α for FOCUS(BEM) and AEROMODULE(AWSM) because of negative α and as the pitch angle is large so ϕ is large.

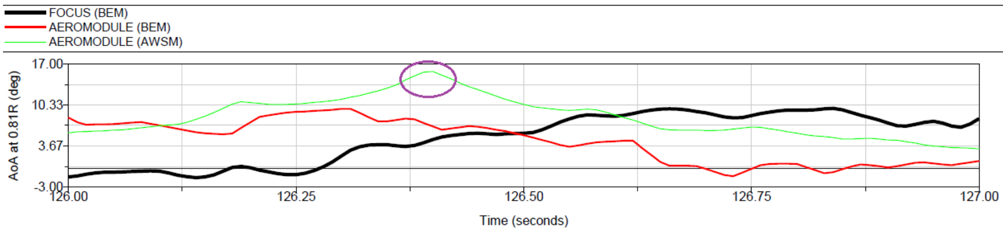

(a)

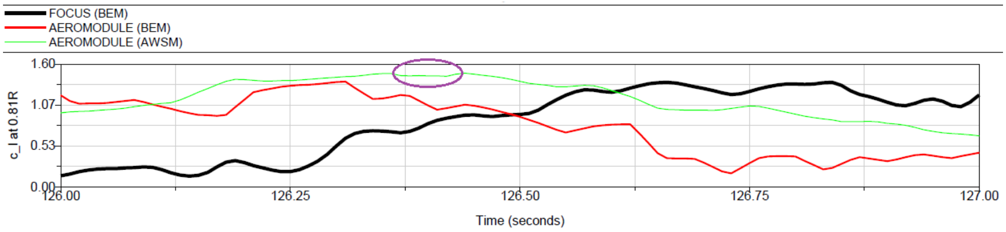

(b)

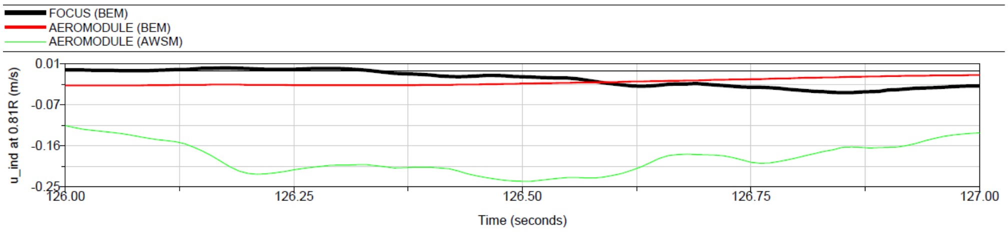

(c)

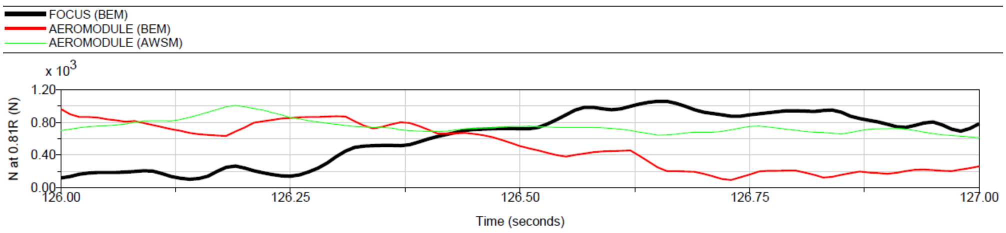

(d)

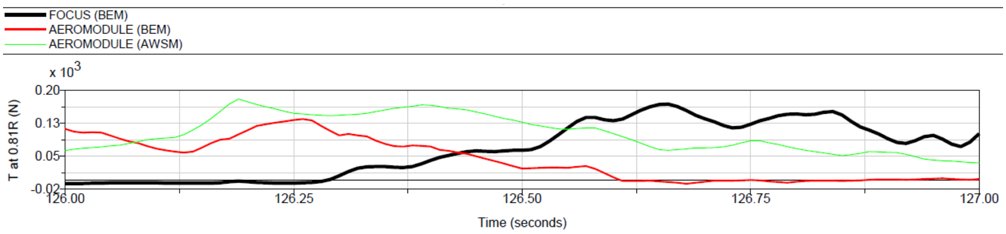

(e)

Figure C-36: Case-2888: Aerodynamic analysis at 0.81R blade station from 126th to 127th second.

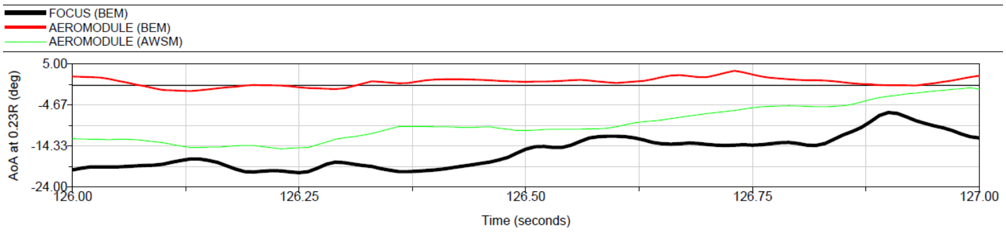

(a)

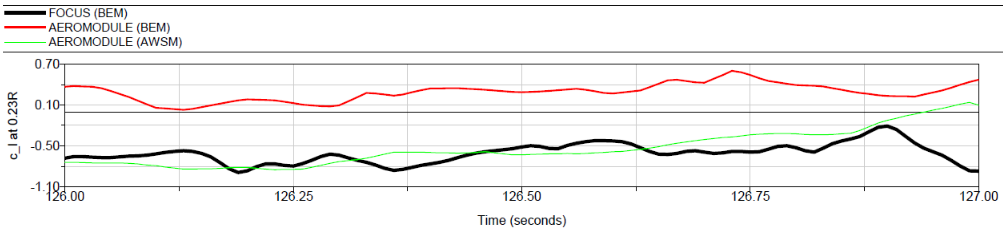

(b)

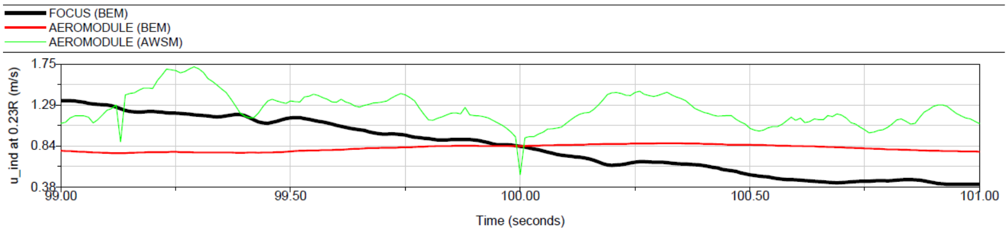

(c)

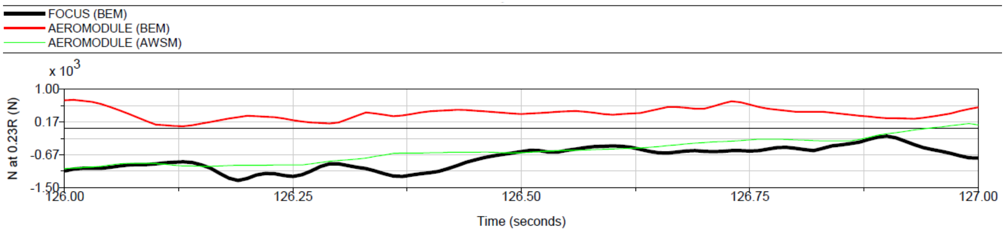

(d)

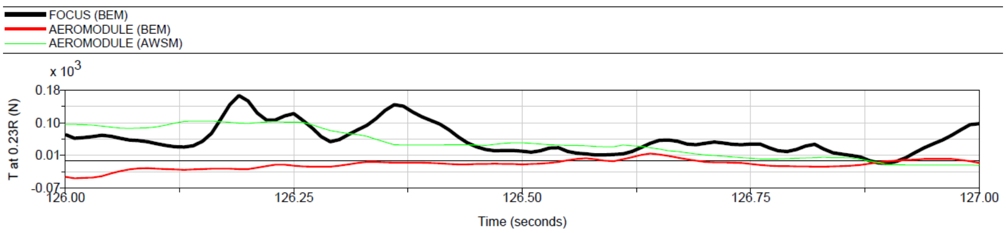

(e)

Figure C-37: Case-2888: Aerodynamic analysis at 0.23R blade station from 126th to 127th second.

C.1.5 Aerodynamic aspects at 93rd second

In this section aerodynamic analysis is done at 93rd second along the complete length of blade. This analysis is done to observe the difference in three modules when the pitch failure takes place. In figure C-38, blade length starts from 5 m and ends at 62.5 m because blade stations before 5 m of length and after 62.5 m of length are not taken in AEROMODULE(AWSM) due to computation problems. It can be seen that all the three modules show a very good match in trend and coincide each other for angle of attack α. Though AEROMODULE(AWSM) shows slightly higher angle of attack α near the root region this may be because of the root vortex. There is close match between AEROMODULE(AWSM) and FOCUS(BEM) for lift coefficient c_l except near root region and this is because of missing station between 5 m and 10 m. AEROMODULE(BEM) shows a completely different curve for c_l from inboard till mid-board region of blade. This suggests that AEROMODULE(BEM) is over predicting stall at all these blade stations. Drop in c_l near 20 m radial distance for AEROMODULE(BEM) suggests that at these blade locations it computes c_l correctly but not at other inboard region, because c_l does not cross the maximum limit. Normal(N) and tangential(T) force distribution along the complete length of the blade for AEROMODULE(AWSM) and FOCUS(BEM) is close. AEROMODULE(BEM) shows a slightly higher N at the mid-board region as compared to other two modules. AEROMODULE(BEM) shows a strange curve for T along the complete length of blade, there is a drop in T at 20 m radial distance because of drop in c_l.

C.1.6 Structural aspects

The failure of pitch controller causes extreme loads on wind turbine parts, below the loads on tower and blades are discussed.

Blade loads

Blade experiences moments in flapwise bending, edgewise bending and torsional moment in the blade root. Figure C-39 shows the flapwise bending moment in the blade root. For the initial 90 seconds, the wind turbine is in normal operating state at cut out wind speed. So the axial wind force, gravity force and centrifugal force contributes the

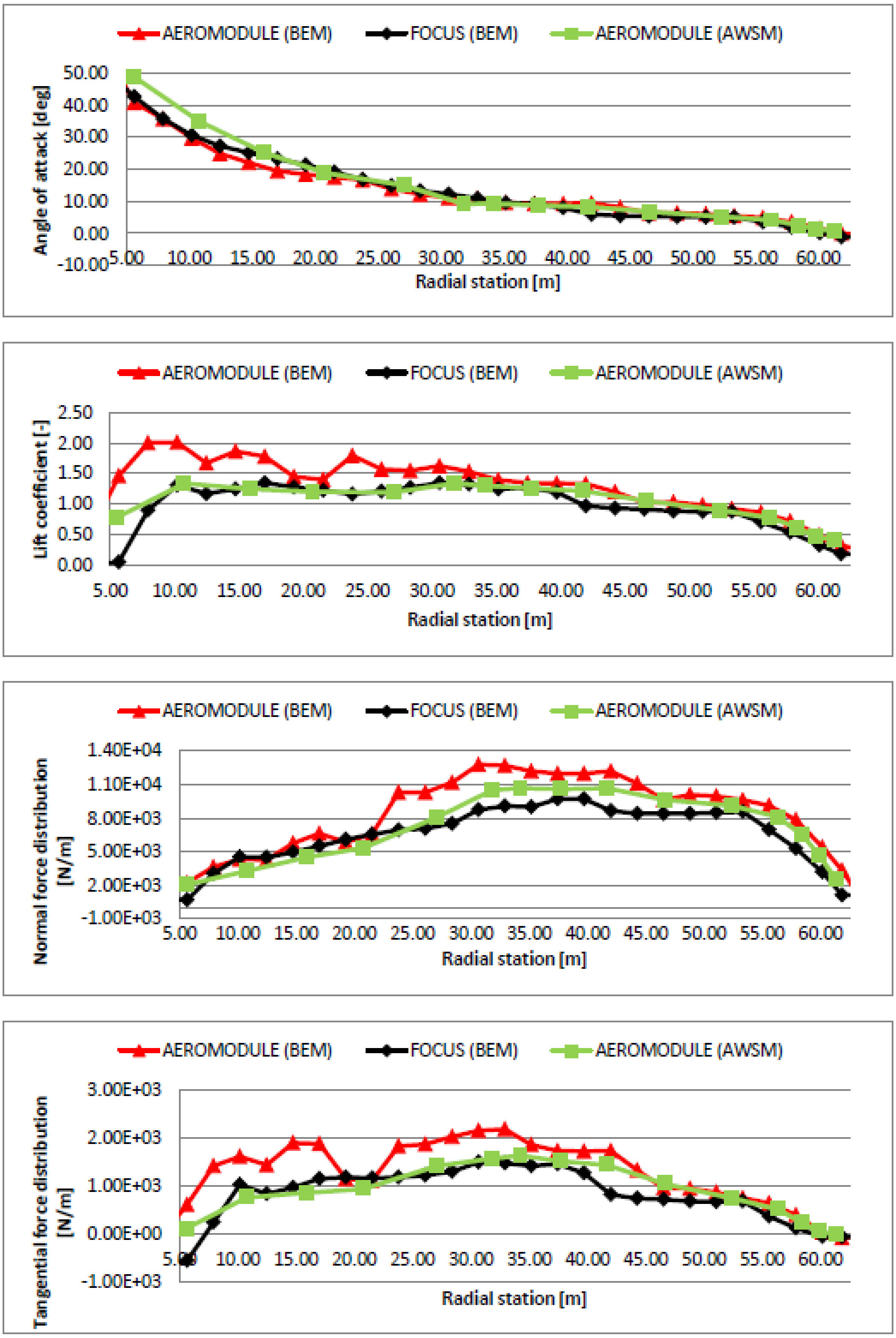

Figure C-38: Case-2888: Aerodynamic analysis at 93rd second.

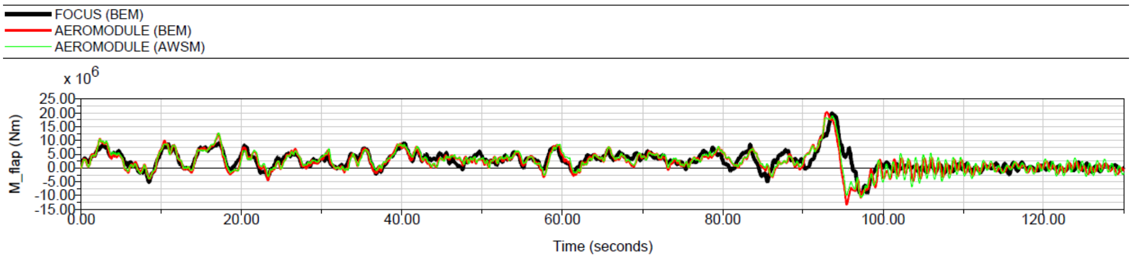

Figure C-39: Case-2888: flapwise bending moment in the blade root.

most to the flapwise bending moment in the blade root, contribution due to gyroscopic force is zero as there is no change in yaw angle. With the advent of pitch controller failure, the flapwise bending moment shoots up and then changes sign due to the inertia of blade. AEROMODULE modules are closer to each other than FOCUS(BEM) and also follow the same trend. Difference between FOCUS and AEROMODULE modules is because of the AEROMODULE-SIMPACK controller interface. Figure C-40 shows the flapwise bending moment in the blade root from 90th to 98th second. All the modules show good match for the flapwise bending moment in the blade root. As the

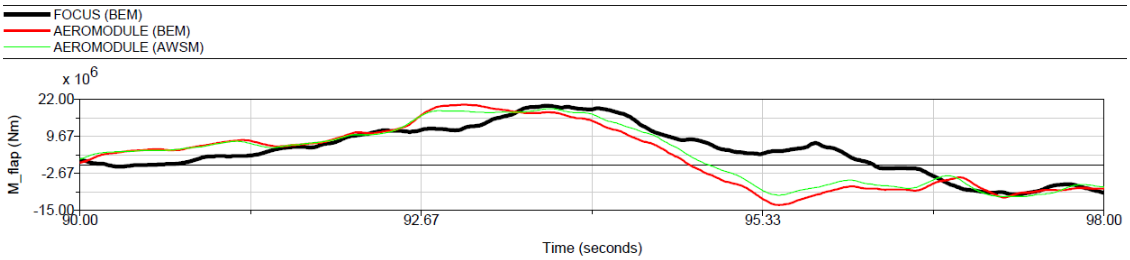

Figure C-40: Case-2888: flapwise bending moment in the blade root from 90th to 98th second.

pitch angle of the blade is increasing therefore the contribution of axial wind force in flapwise bending moment in the blade root decreases. Pitch controller failure causes the rotor speed to decrease, therefore the contribution of centrifugal force in flapwise bending moment in the blade root also decreases. The gravity force component which acts due to tilt and cone angle of rotor is still causing the flapwise bending moment in the blade root. As the pitch angle becomes constant at 90 degrees, the flapwise bending moment fluctuations in the blade root eventually dies, because the contribution due to axial aerodynamic force on rotor becomes negligible. As the rotor speed becomes zero, contribution due to centrifugal force and cyclic gravity force also becomes zero. The fluctuation fades off slowly in flapwise bending moment in the blade root because of small stiffness in flapwise direction of blade. Frequency of fluctuations in flapwise bending moment in blade root before pitch controller failure is 0.2 Hz and this is due to wind shear. After pitch controller failure the frequency of fluctuations in flapwise bending moment in blade root is 0.7 Hz and this is the natural flapwise frequency of the blade. More fluctuations in both AEROMODULE modules are because of compatibility issues in AEROMODULE-SIMPACK interface.

Figure C-41 shows the edgewise bending moment in the blade root. During normal

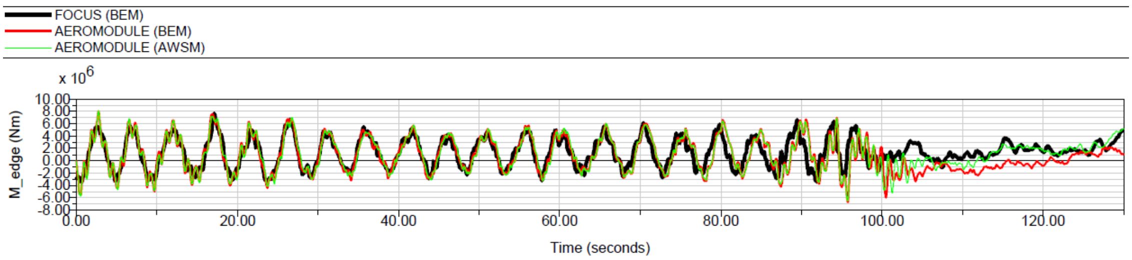

Figure C-41: Case-2888: Edgewise bending moment in the blade root.

operating state (first 90 seconds) edgewise moment in the blade root has almost the constant amplitude fluctuations, this is because of the cyclic nature of gravity force in rotor blades and it can be estimated by the amplitude of the fluctuations. The rotor torque also causes edgewise moment in blade root and its contribution is estimated by the average value of the edgewise moment. Coriolis force due to flapping velocity of blades also contributes to edgewise moment during the normal operating state but its contribution is less. Figure C-42 shows the edgewise moment in the blade root from 100th to 112th second, it can be seen that after pitch controller failure when the pitch angle starts increasing there is a lot of difference between all the modules. Both the BEM model have same dynamic inflow model but due to AEROMODULE-SIMPACK couple controller interface compatibility issues both of them show different trend. AEROMODULE(AWSM) has almost the same trend as AEROMODULE(BEM) but due to different physics involved in computing axial and tangential induction in both of them, they show slightly different mean values.

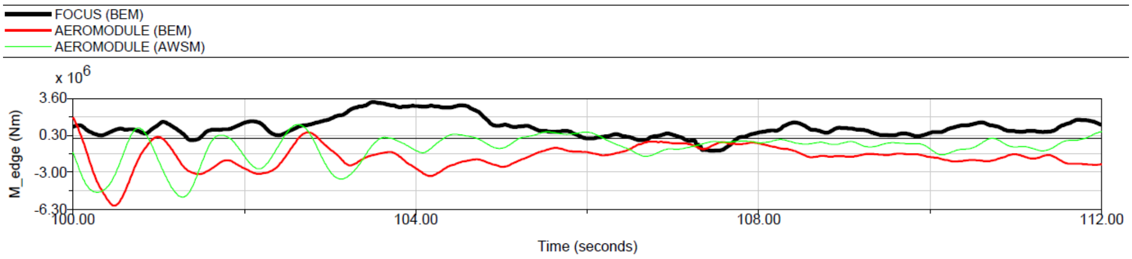

Figure C-42: Case-2888: Edgewise bending moment in the blade root from 100th to 112th second.

After 107th second the pitch angle is 90 degrees which causes the fluctuations to fade off fast in edgewise bending moment in the blade root because of large stiffness in edgewise direction of blade. The positive mean value suggests the contribution of edgewise bending moment is due to a component of gravity force on one blade and the component of gravity force is due presence of tilt and cone angles. Frequency of fluctuations in edgewise bending moment in blade root before pitch controller failure is 0.2 Hz and this is due to cyclic gravity force. After pitch controller failure the frequency of fluctuations in edgewise bending moment in blade root is 1 Hz and this is the natural edgewise frequency of the blade. All the modules show good match for edgewise moment in the blade root before pitch controller failure but after that the difference between them increases.

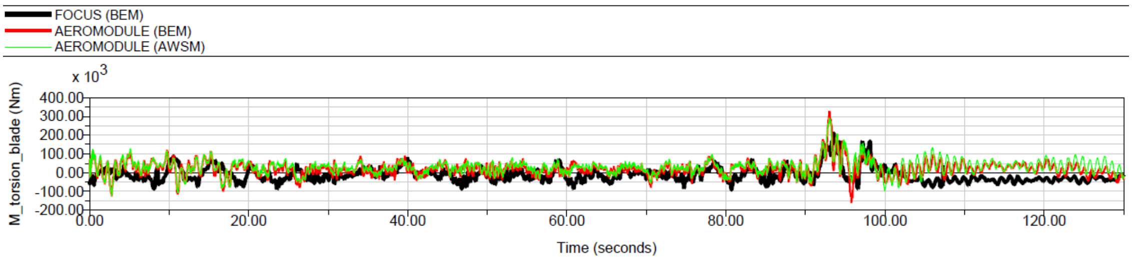

Figure C-43: Case-2888: Torsional moment in the blade root.

Figure C-43 shows the torsional moment in the blade root. Flapwise forces along with lead-lag deflection, edgewise forces along with flapwise deflection are the main factors causing torsion at blade root during for first 90 seconds. Contribution due to pitch mechanism is quite visible after 90 seconds when the pitch controller failure occurs.

The failed pitch controller causes extreme torsional moment in the blade root and this can be seen in figure C-44. Torsional moment in blade root increases first because of

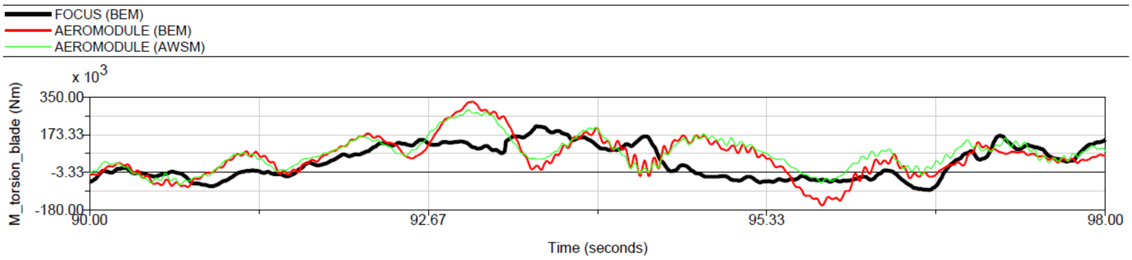

Figure C-44: Case-2888: Torsional moment in the blade root from 90th to 98th second.

increase in thrust force on rotor and after that decreases because of increase in dynamics. Frequency of fluctuations in torsional moment in blade root before pitch controller failure is 0.2 Hz and this is due to gravity force. After pitch controller failure, the frequency of fluctuations in torsional moment in the blade root is 1 Hz and this is the natural edgewise frequency of the blade. Both AEROMODULE modules show good match because of the same controller interface but FOCUS(BEM) shows a slight deviation and this is due to the different controller interface in FOCUS(BEM).

Tower loads

Tower experiences fore-aft and side-ways bending moment at tower base and torsional moment at tower top. Figure C-45 shows the fore-aft bending moment in the tower

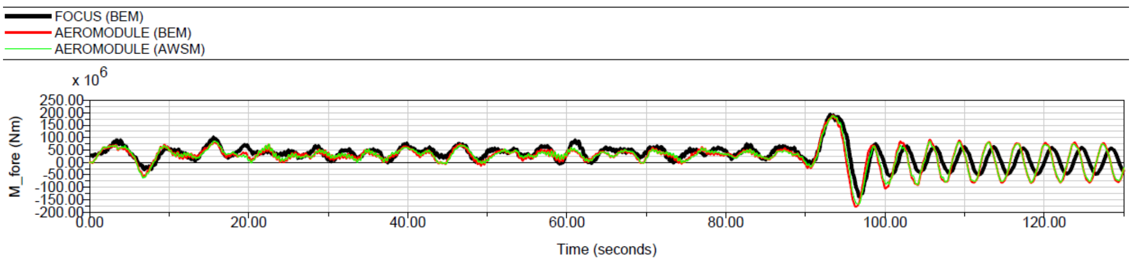

Figure C-45: Case-2888: Fore-aft bending moment in the tower base.

base. Fore-aft bending moment is mainly due to rotor thrust loading. Drag force due to wind shear on tower is small. Tower motions happen due to the tower's dynamic interaction with rotor blades . Due to large fluctuations in axial aerodynamic force on rotor, the tower fore-aft bending moment also fluctuates a lot. As soon as the blades are pitched to its minimum pitch angle, the tower fore-aft moment shoots up and this is because of dynamic interaction. The tower fore-aft moment first decreases and then increases because of the inertia of tower. The tower fore-aft motion does not die out easily because the complete weight of the wind turbine acts on the tower base. Due to this large inertia, the tower shows a cyclic fore and aft motion after the generator is cut off. When the pitch angle of blades starts increasing to 90 degrees, AEROMODULE modules and FOCUS(BEM) show different phase but same trend, this is because SIMPACK needs time to stabilize a flexible body. Figure C-46 shows the fore-aft bending moment in the tower base from 90th to 98th second. Frequency of fluctuations in fore-

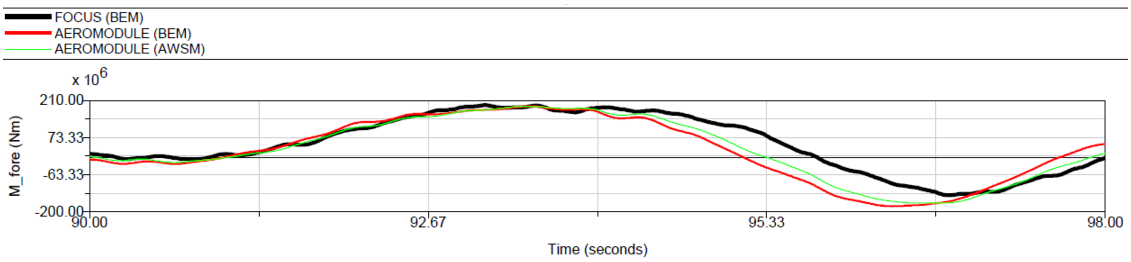

Figure C-46: Case-2888: Fore-aft bending moment in the tower base from 90th to 98th second.

aft bending moment in tower base before and after pitch controller failure is 0.27 Hz and this is due to first natural tower fore-aft frequency. Figure C-47 shows the side-ways

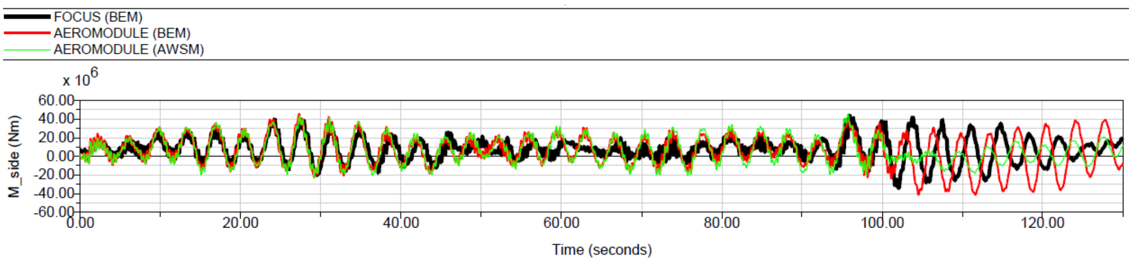

Figure C-47: Case-2888: Side-ways bending moment in the tower base.

bending moment in the tower base. The in-plane loads which cause differential loads on different blades and the longitudinal turbulence which causes torque fluctuations are main contributors of tower side-ways bending moments. The rotor torque that acts on the tower top through gearbox/generator support also causes side-ways tower bending moment at the tower base. After the 90th second, the failure of pitch controller causes side-ways tower bending moment. Due to the large inertia of tower, the tower shows a cyclic side-ways motion after the pitch controller failure and this can be seen in figure C-48. When the generator is cut off there is an exponential decrease in side-ways tower

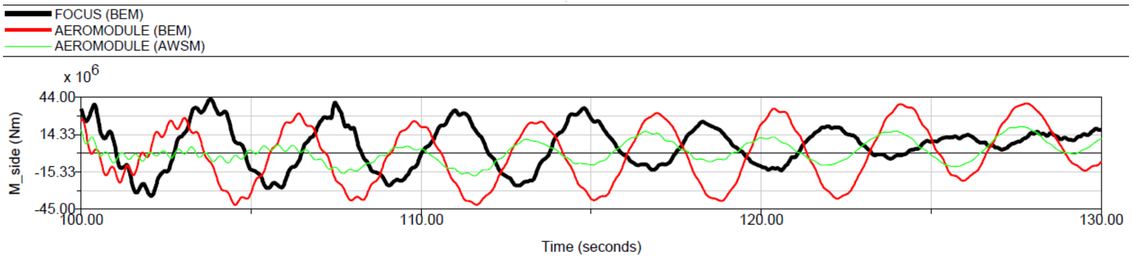

Figure C-48: Case-2888: Side-ways bending moment in the tower base from 100th to 130th second.

bending moment, which suggests that the tower was under damped. Frequency of fluctuations in side-ways bending moment in tower base before and after pitch controller failure is 0.27 Hz and this is due to first natural tower side-ways frequency.

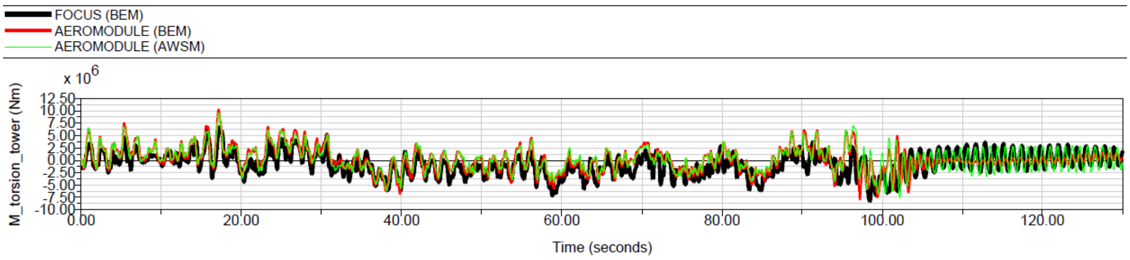

Figure C-49: Case-2888: Torsional moment in the tower top.

Figure C-49 shows the torsional moment in the tower top. Tower also experiences torsional moment, and this moment is relatively smaller than fore-aft and side-ways moments. Torsional moments are caused due to turbulence and changing wind direction. As there is no change in wind direction, so it does not contribute to torsion in tower top. As the rotor is tilted, a component of rotor torque acts on the tower top through gearbox/generator support which causes torsional moment in tower top. In the above figure it can be seen that due to sudden pitch controller failure followed up over speed, the tower shows high fluctuations and this shows the dynamic interaction between blades, controller and tower. The fluctuation eventually dies out with an exponential function, which suggests that the tower is under damped. Frequency of fluctuations in torsional moment in tower top before and after pitch controller failure is 0.9 Hz and this is due to backward whirling mode [27] in blades.

C.2 Load case-3290: Start-up with extreme operating gust (EOG)

This load case belongs to DLC 3.2 according to the IEC standard. Load case 3290 addresses start procedures with occurrence of 1-year extreme operating gust at 25 m/s wind speed at hub with extreme operating gust (EOG) as the external condition. The yaw angle is maintained at 0 degree throughout the simulation. Figure C-50 shows

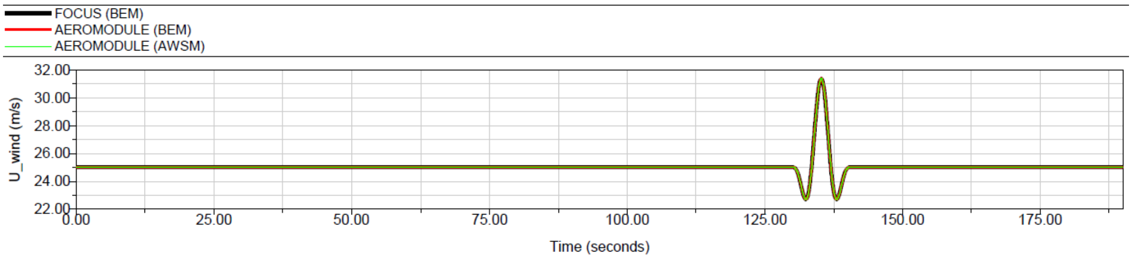

Figure C-50: Case-3290: Wind speed at hub.

the wind speed at hub. Before the gust, the wind speed is at a constant value of 25 m/s i.e. it is above rated wind speed. So the objective of the controller is to maintain designed generator power and reduce the loads. For the first 100 seconds wind turbine does not produce any power as the pitch angle is large and minimum rotor speed has not reached.

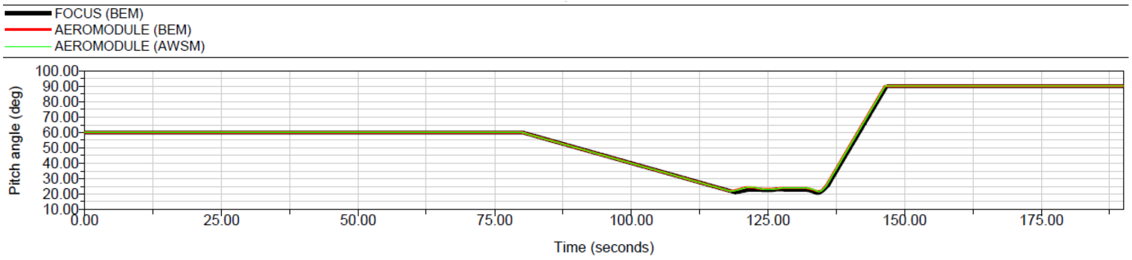

Figure C-51: Case-3290: Pitch angle of one blade.

Start-up starts at 80th second and at 80th second the supervisory controller comes into action and starts reducing the pitch angle and by 118th second the pitch angle becomes 20 degrees. The pitch angle is changed to 20 degrees because of high wind speed of 25 m/s. Decrease in pitch angle causes an increase in rotor speed with an increasing slope and this happens until it reaches the minimum rotor speed which is suitable for power

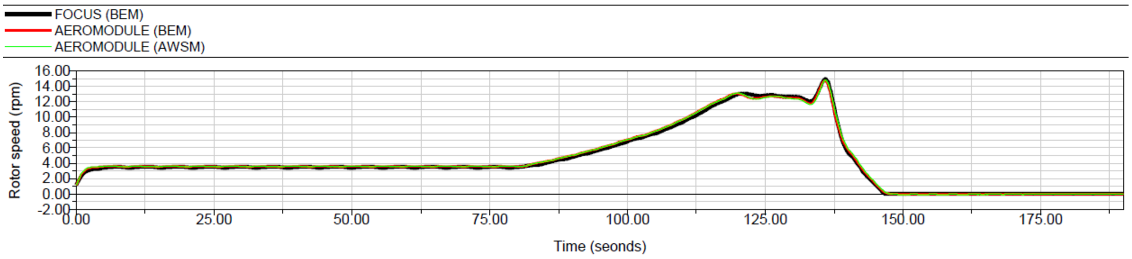

Figure C-52: Case-3290: Rotor speed.

production i.e. 7 rpm. The rotor speed increases because now more wind strikes the blade surface. Figures C-51 and C-52 shows the variation in pitch angle of one blade and rotor speed respectively.

When the rotor speed reaches 7 rpm, the generator torque increases and thus generator starts producing power and the supervisory controller is no more in charge of control operations. This happens till the pitch angle has reached 20 degrees and the generator has reached its rated speed value i.e. till 118th second. From 118th second till 130th second, the rotor speed decreases because the pitch angle increases a bit, increase in rotor speed leads to decrease in generator torque so that the generator power remains constant. Figures C-53 and C-54 shows the generator power and generator torque of the ART wind turbine respectively. From 130th till 141st second an extreme operating

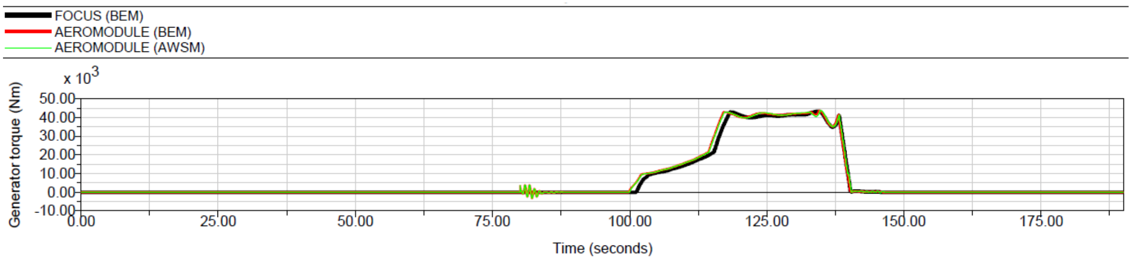

Figure C-53: Case-3290: Generator torque.

gust prevails. First the wind speed decreases and then increases in the gust. When the wind speed decreases suddenly, the pitch angle does not react instantaneously which causes the rotor speed to decrease a bit. The generator power also reduces a bit because the generator torque does not change instantaneously. Increase in wind speed during gust causes the pitch angle to increase, pitch rate is less than the rate of increase of

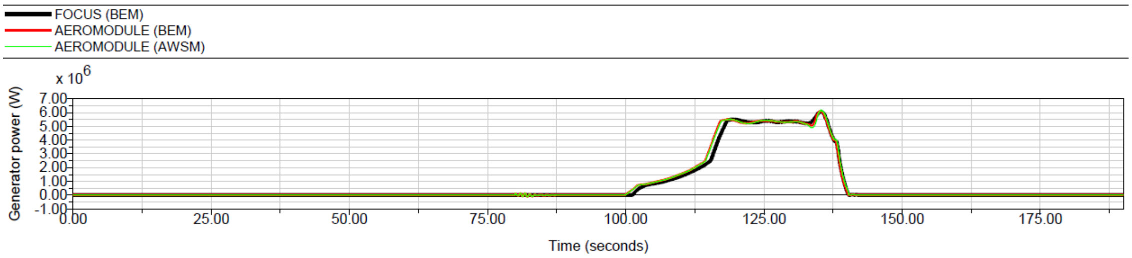

Figure C-54: Case-3290: Generator power.

wind speed, therefore the rotor speed increases until it reaches the over speed value. As soon as the rotor speed reaches the over speed value the supervisory controller comes into action and cuts it off, this causes the rotor speed to decrease. As soon as it reaches minimum value required to generate power i.e. 7 rpm, the generator is cut off and thus the generator power and torque goes to zero immediately. When the gust prevails, there is a peak in rotor speed and a dip in generator torque but still the peak is more than the dip so generator power increases by a factor of 1.2.

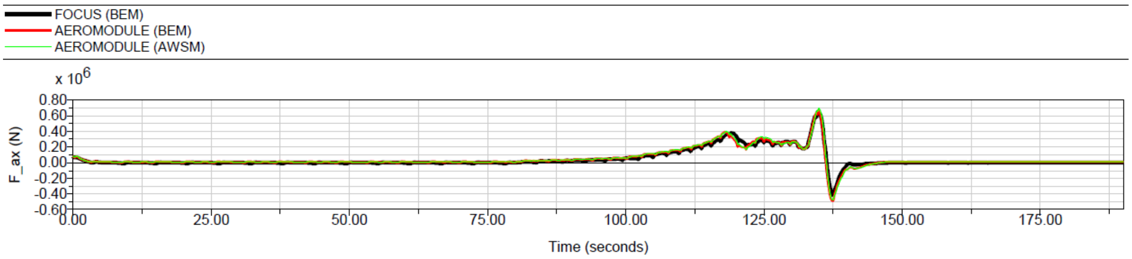

Figure C-55: Case-3290: Axial aerodynamic force on rotor.

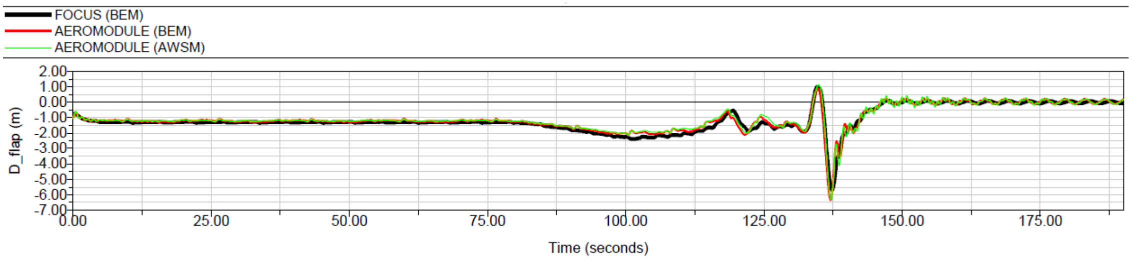

Figure C-56: Case-3290: Average flapwise displacement of blade tips.

Figures C-55 and C-85 show the axial aerodynamic force on rotor and average flapwise displacement of blade tips respectively. With reducing pitch angle the axial aerodynamic force on rotor increases because more area of blade is exposed to wind. Axial aerodynamic force becomes almost constant once the pitch angle reaches a constant value. With the onset of gust, the axial aerodynamic force first shows a dip then a rise, and then it reduces to a negative value and finally increases to zero and becomes constant. Rise in the axial aerodynamic force on rotor after it reached negative value is due to large inertia of the rotor. Average flapwise displacement of blade tips show the same trend as axial aerodynamic force on rotor. Figure C-57 shows the axial aerodynamic force on rotor when the gust prevails from 135th to 137th second, all the modules show same trend and are very close to each other. Figure C-86 shows the average flapwise displacement of blade tips before the gust from 95th to 105th second.

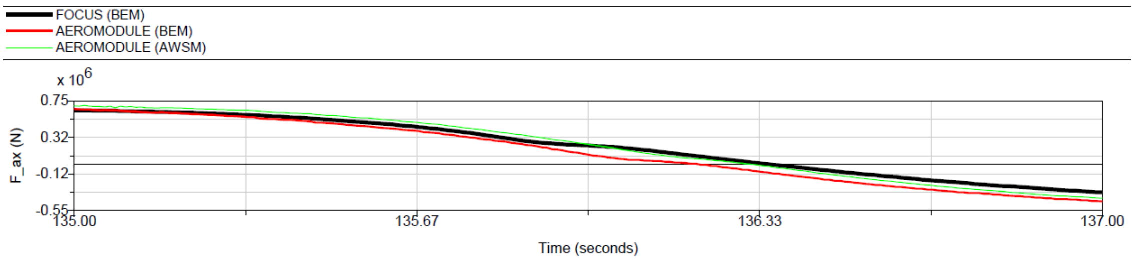

Figure C-57: Case-3290: Axial aerodynamic force on rotor from 135th to 137th second.

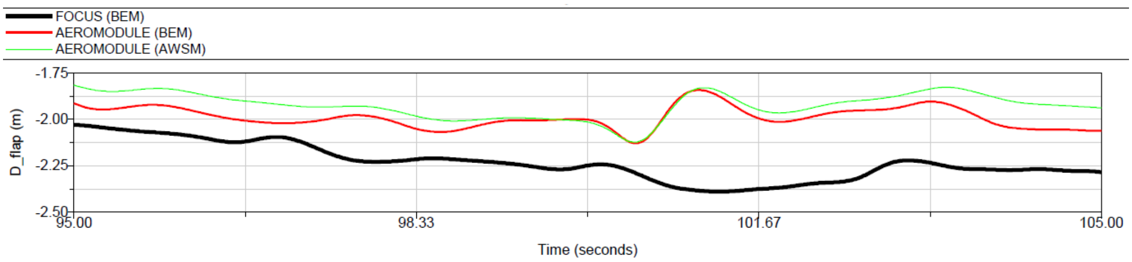

Figure C-58: Case-3290: Average flapwise displacement of blade tips from 95th to 105th second.

This start-up load cases cause extreme loads on wind turbine parts, below the loads on tower and blades are discussed.

C.2.1 Aerodynamic aspects

Blades of the ART wind turbine are flexible in this case and thus it takes time for AEROMODULE(BEM) and AEROMODULE(AWSM) to stabilize when the simulation starts.

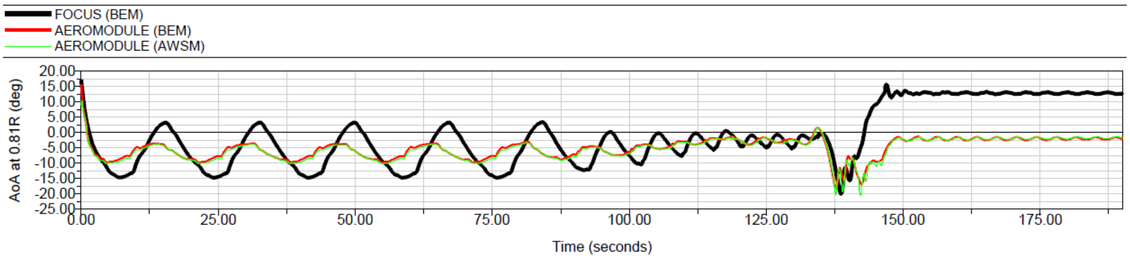

Figure C-59: Case-3290: Aerodynamic angle of attack at 0.81R blade station.

Figure C-59 shows the aerodynamic angle of attack at 0.81R blade stations. At 0.81R blade station, both AEROMODULE modules show same trend but there is phase shift with FOCUS(BEM), this is because in FOCUS(BEM) simulation starts at equilibrium while in SIMPACK it doesn't and thus SIMPACK takes time for the flexible body to stabilize. Both the BEM modules start the simulation with α above 14 degrees i.e. above the stall α. When the rotor is rotating at 3 rpm and the wind speed is 25 m/s, both AEROMODULE modules show a certain trend and this is because of rotor tilt, more explanation is given in report (give reference). FOCUS(BEM) also shows the effect of tilt angle but not clearly and this can be clearly seen in figure C-60. When the gust prevails AEROMODULE modules and FOCUS(BEM) show a

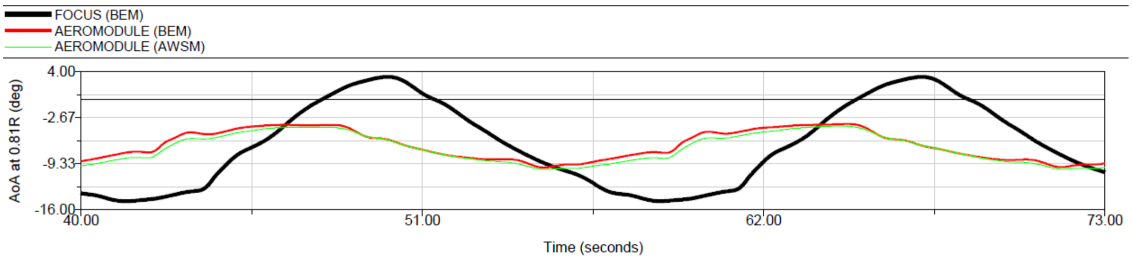

Figure C-60: Case-3290: Aerodynamic angle of attack at 0.81R blade station from 40th to 73rd second.

different trend because of the initial phase difference. When the gust ends at 141st second, FOCUS(BEM) shows a rising trend after the gust ends while AEROMODULE modules show a decreasing trend, because the flexible body in SIMPACK takes time to stabilize. AEROMODULE(AWSM) shows small fluctuations and this is because α is below -18 degrees and this causes stall and this can be seen in figure C-61. Figures

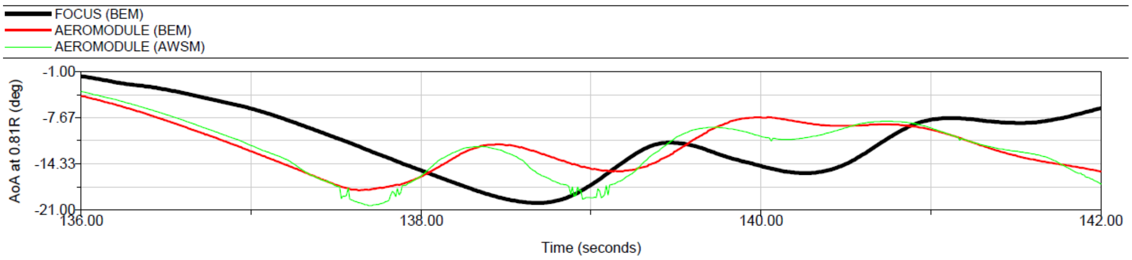

Figure C-61: Case-3290: Aerodynamic angle of attack at 0.81R blade station from 136th to 142nd second.

C-62 and C-63 give the aerodynamic insight about these small fluctuations at 137.52nd and 137.68th seconds respectively. From the figures C-62 and C-63, it can be seen that there is a change in all the aerodynamic parameters near the tip region from 137.52nd to 137.68th second, so it can be said that when stall occurs in AEROMODULE(AWSM) the changes in aerodynamic parameters may be due to tip vortex influence. So the small fluctuations at 0.81R blade station for AEROMODULE(AWSM) may be because of tip vortex influence on this blade station. Both the BEM modules don't show the influence of tip vortex, tip vortex is physically defined in BEM theory by Prandtl tip loss factor, figure gives more insight about this effect.

For all the modules α reaches negative value after pitch controller failure because of high pitch angle of 45 degrees. After the gust ends, the fluctuations in all modules decrease. The difference in mean value between FOCUS(BEM) and AEROMODULE modules is because of flexible model of ART wind turbine considered in AEROMODULE-SIMPACK couple.

Figure C-64 shows the aerodynamic angle of attack at 0.23R blade stations. At 0.23R blade station, both AEROMODULE modules show the same trend but they differ from FOCUS(BEM) trend with a certain phase. Trend in all modules is due to the tilt rotor. All modules reach stall when the gust prevails because α increases above 12.5

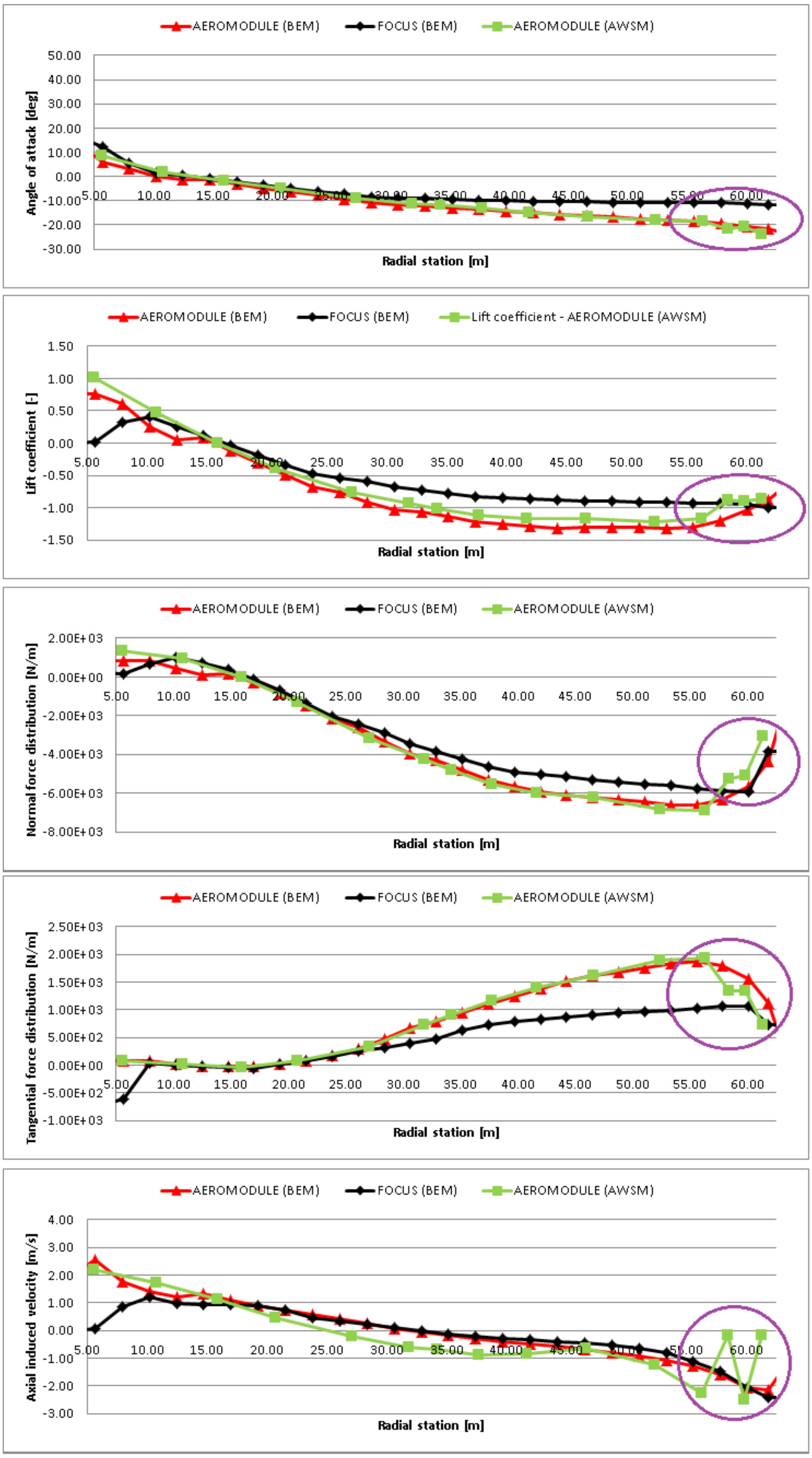

Figure C-62: Case-3290: Aerodynamic analysis at 137.52nd second.

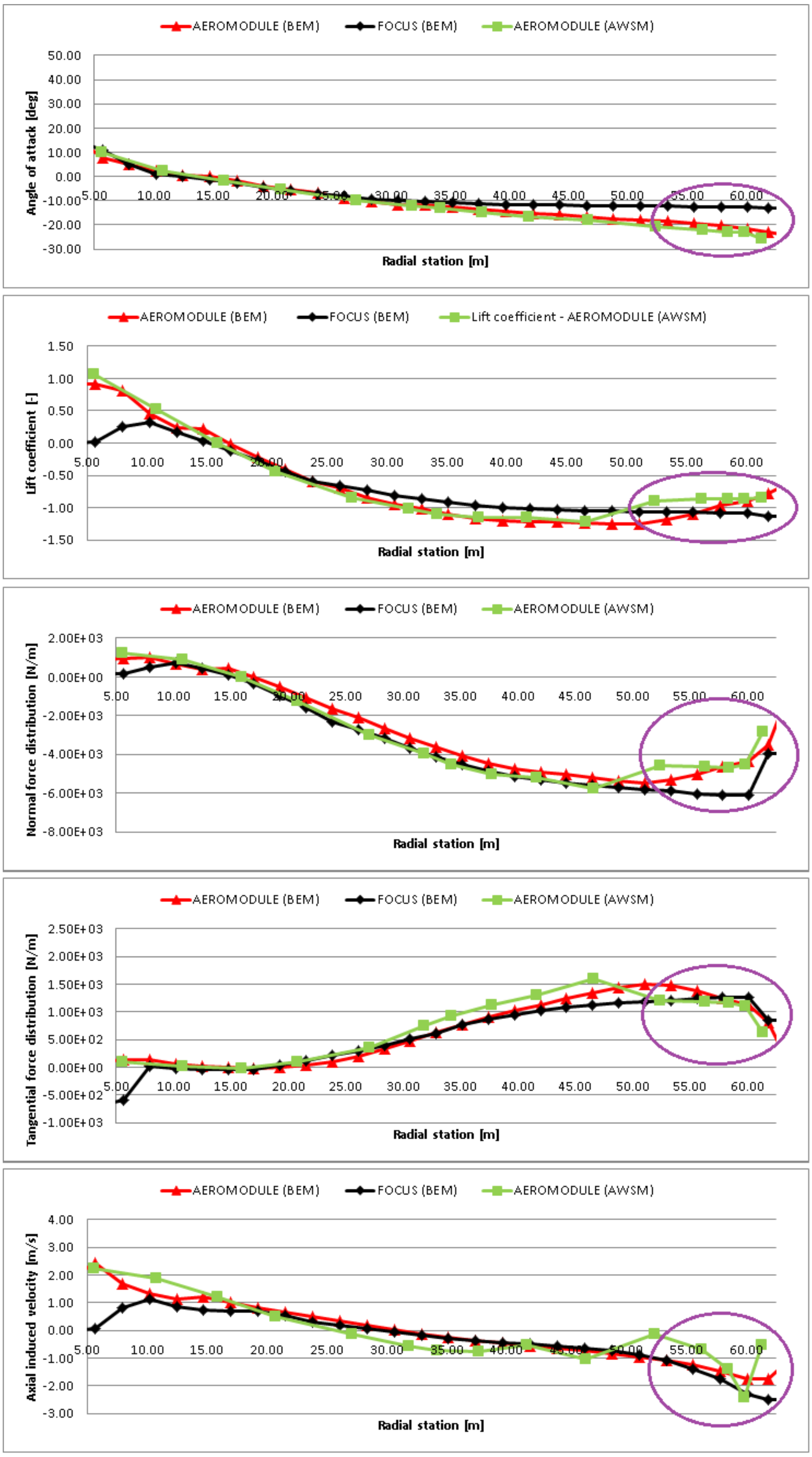

Figure C-63: Case-3290: Aerodynamic analysis at 137.68th second.

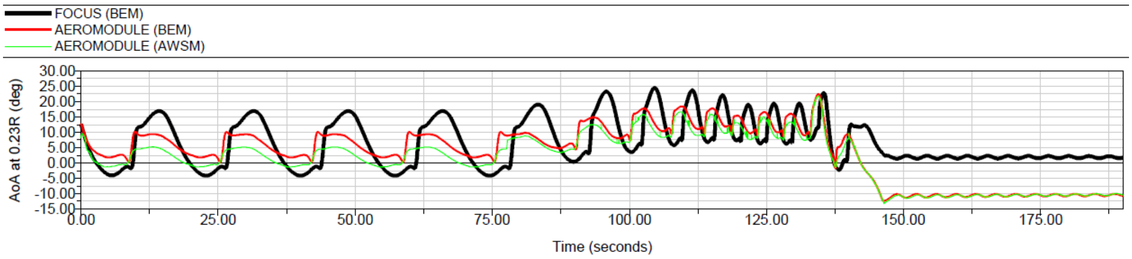

Figure C-64: Case-3290: Aerodynamic angle of attack at 0.23R blade station.

degrees. 12.5 degrees is the positive stall α for 0.23R blade station. After the gust ends at 141st second, AEROMODULE-SIMPACK couple shows a decreasing trend while FOCUS(BEM) doesn't, this is because of flexible ART wind turbine model used in SIMPACK.

Figure C-65 shows the lift coefficient c_l at 0.81R blade stations. At 0.81R blade station,

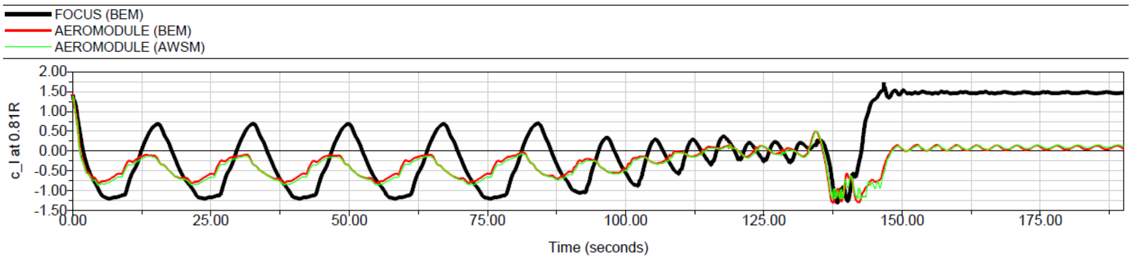

Figure C-65: Case-3290: Lift coefficient c_l at 0.81R blade station.

lift coefficient c_l follows the same trend as α. All the modules behave in the same way as they did for α because α lies in the slope region of c_l, α curve. Whenever α crosses -3 degrees, c_l reaches zero because this is the zero lift angle of attack for the airfoil at this blade station. Beyond -3 degrees of α, c_l becomes negative as it lies in the linear slope region. Whenever α crosses -18 degrees, airfoil at 0.81R is in stall and thus c_l increases. As AEROMODULE(AWSM) doesn't have dynamic stall model therefore it only shows 2D characteristics for c_l, while both the BEM modules show lower c_l than minimum 2D value because of dynamic stall in them. At such high negative α stall delay occurs and thus the flow remains attached to airfoil. Figures C-66 and C-67 show α and c_l respectively at 0.81R from 136th to 142nd second.

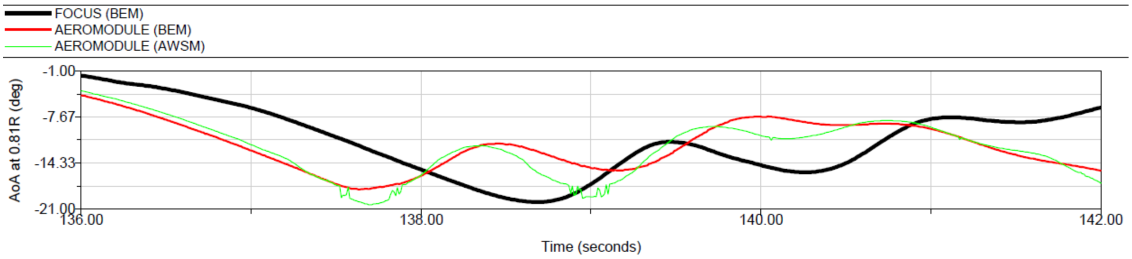

Figure C-66: Case-3290: Aerodynamic angle of attack at 0.81R blade station from 136th to 142nd second.

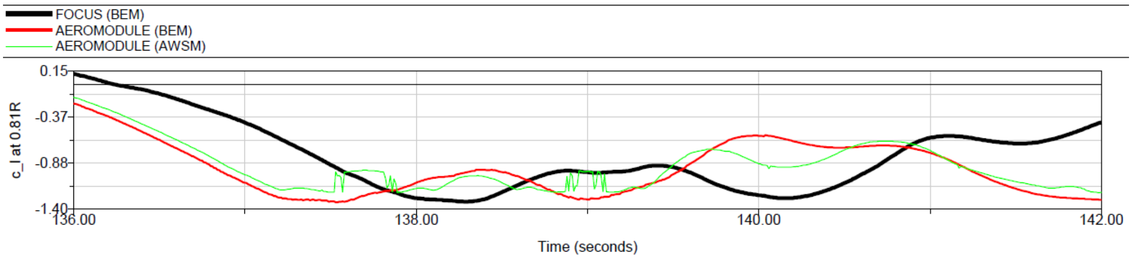

Figure C-67: Case-3290: Lift coefficient c_l at 0.81R blade station from 136th to 142nd second.

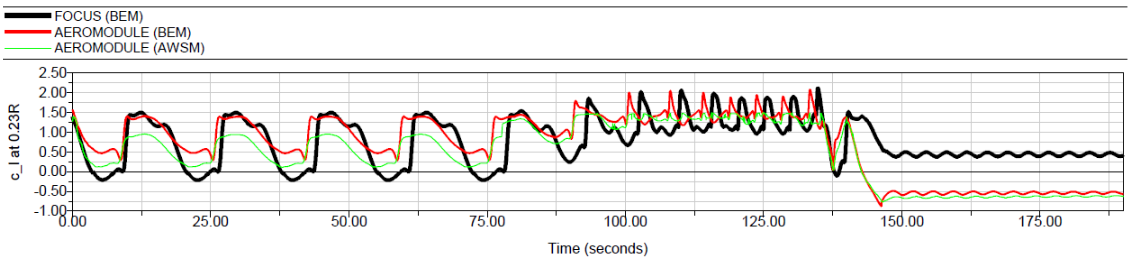

Figure C-68: Case-3290: Lift coefficient c_l at 0.23R blade station.

Figure C-68 shows the lift coefficient c_l at 0.23R blade stations. At 0.23R blade station, c_l follows the same trend as α when α is below 12.5 degrees. Above 12.5 degrees of α stall occurs and thus c_l reduces. When the ART wind turbine starts generating power from 100th second, α at 0.23R blade station crosses above 12.5 degrees and thus stall occurs. All the modules show α above 12.5 degrees, as there is no dynamic stall model in AEROMODULE(AWSM) it does not show c_l above the maximum value while both the BEM modules show higher than maximum c_l value and this can be seen in figures C-69 and C-70.

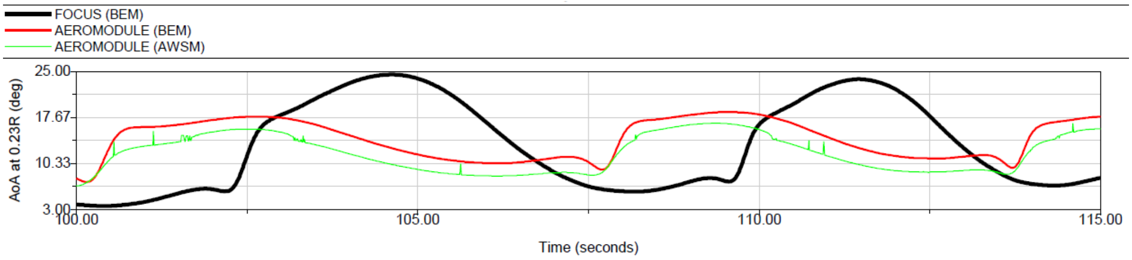

Figure C-69: Case-3290: Aerodynamic angle of attack at 0.23R blade station from 100th to 115th second.

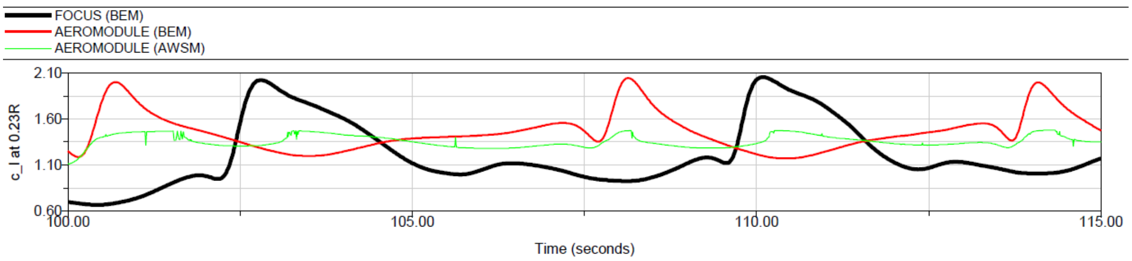

Figure C-70: Case-3290: Lift coefficient c_l at 0.23R blade station from 100th to 115th second.

Figure C-71 shows the axial induced velocity at 0.81R blade station. At 0.81R blade station, AEROMODULE(AWSM) shows a lot of fluctuations for u_{ind}, because u_{ind} for it is defined in inertial reference system and even after converting from inertial to rotating reference system using rotation matrix [4], still there are fluctuations. To make the AEROMODULE(AWSM) curve smooth a mean trend is drawn. u_{ind} for AEROMODULE(BEM) and AEROMODULE(AWSM) have similar mean trend as compared to FOCUS(BEM) before and after gust, though there is difference in phase slightly.

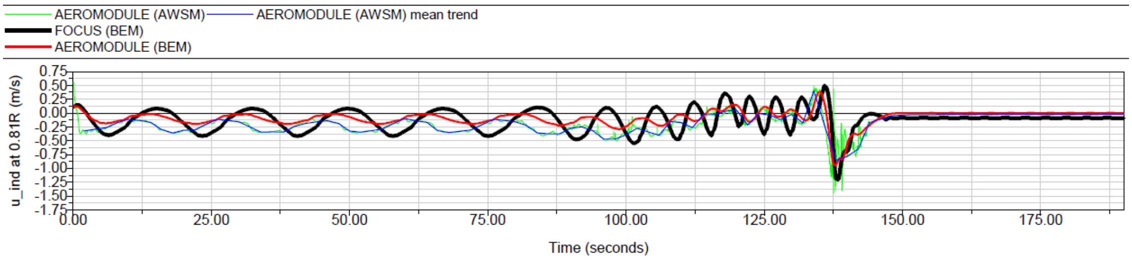

Figure C-71: Case-3290: Axial induced velocity at 0.81R blade station.

Figure C-72 shows the axial induced velocity at 0.81R blade station from 133rd to 145th second, it can be seen that all the modules have almost the similar trends but there is phase difference.

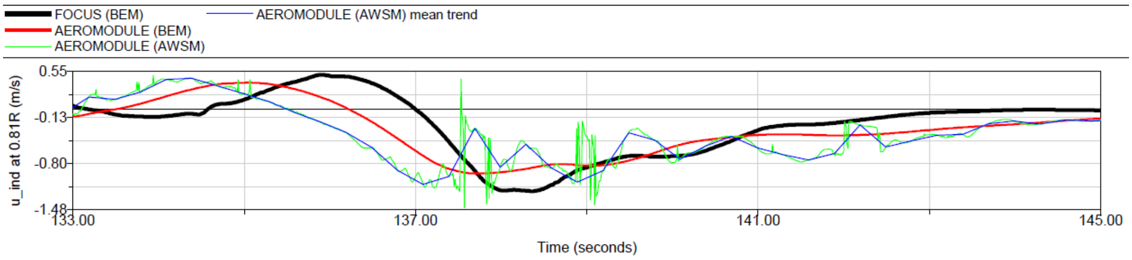

Figure C-72: Case-3290: Axial induced velocity at 0.81R blade station from 133rd to 145th second.

Figure C-73 shows the axial induced velocity at 0.23R blade station. Same as 0.81R blade station, at 0.23R blade station also AEROMODULE(AWSM) show lot of fluctuations because of problem in converting from inertial to rotating reference system. Mean value trend of both the BEM modules are close as compared to AEROMODULE(AWSM).

At 0.81R blade station, normal force distribution N for all the modules are close and follow similar trend before and after the gust. After the gust, N doesn't follow the same trend as α and c_l because the inflow angle ϕ becomes very high as the pitch angle is very high. N is dependent upon inflow angle ϕ [28], at high ϕ the contribution of the term $c_l \sin\phi$ reduces and the contribution of term $c_d \cos\phi$ increases. Figures C-74 and C-75 shows the normal force distribution at 0.81R and 0.23R blade stations

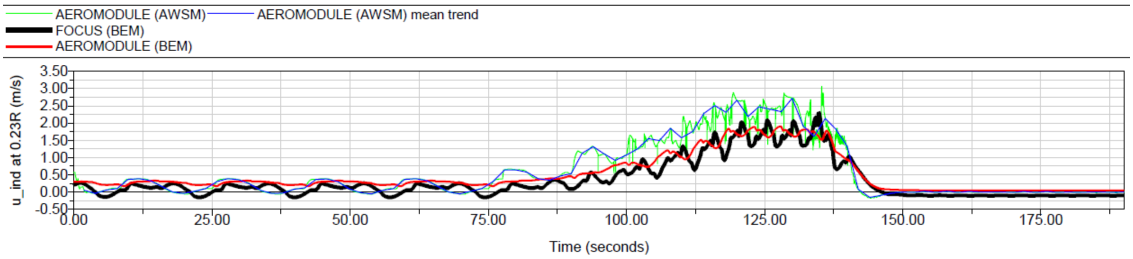

Figure C-73: Case-3290: Axial induced velocity at 0.23R blade station.

respectively. Same explanation is for the airfoil at 0.23R blade station as given above. All the modules show similar for N at 0.23R before and after the gust.

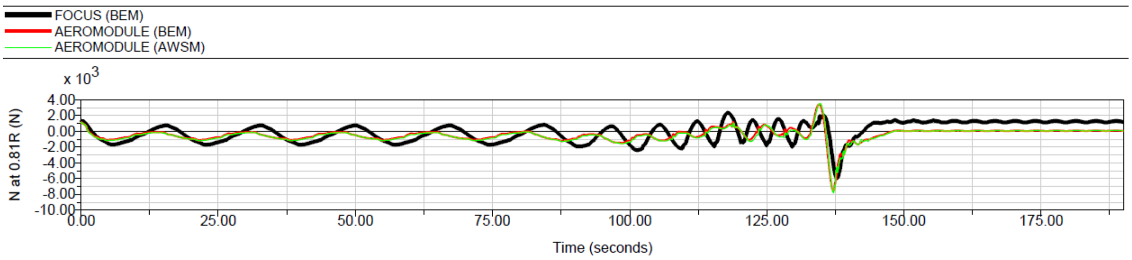

Figure C-74: Case-3290: Normal force distribution at 0.81R blade station.

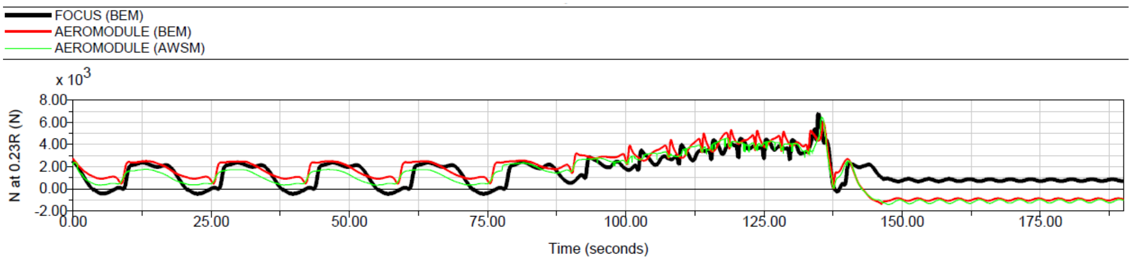

Figure C-75: Case-3290: Normal force distribution at 0.23R blade station.

At 0.81R blade station, tangential force distribution T follows the opposite trend of N because of the inverse relation with c_l and c_d as compared to N. All the modules show close match for T at 0.81R blade stations before and after the gust. At 0.23R blade station T follows the same trend of N because of large positive α at 0.23 blade station. Figures C-76 and C-77 show the tangential force distribution at 0.81R and 0.23R blade stations respectively.

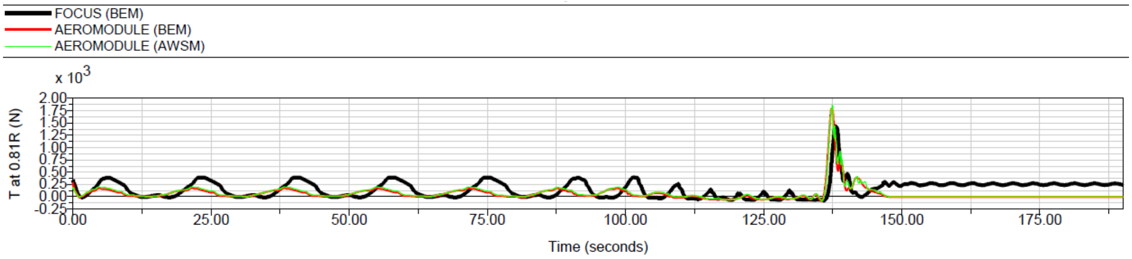

Figure C-76: Case-3290: Tangential force distribution at 0.81R blade station.

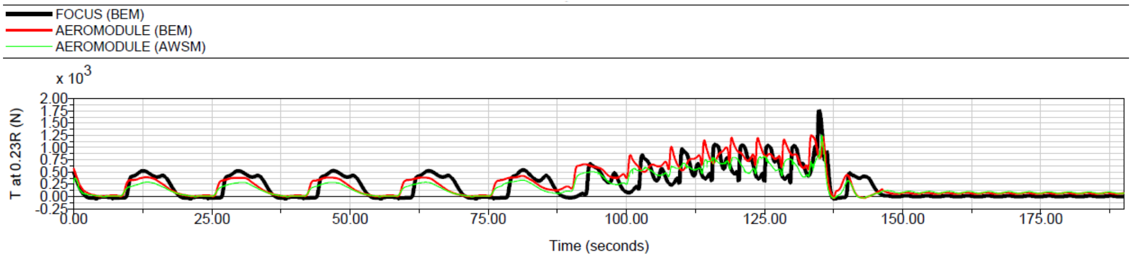

Figure C-77: Case-3290: Tangential force distribution at 0.23R blade station.

C.2.2 Aerodynamic aspects - Before gust prevails

In this section the time series is zoomed from 117th to 118.5th second to get more aerodynamic insight. This time interval shows normal operating condition at cut-out wind speed i.e. before the gust prevails. From figure C-78, it can be seen that at 0.81R blade station, for all the graphs AEROMODULE(BEM) and AEROMODULE(AWSM) are close to each other while FOCUS(BEM) is slightly deviated. This deviation is because of compatibility issues with AEROMODULE-SIMPACK couple controller interface. For all the modules, α lies in the linear slope region therefore c_l is directly proportional to α. At -3 degrees of α, c_l is zero and this is quite visible in the figure C-78 for both AEROMODULE modules. As N is directly dependent on c_l and cosϕ, ϕ is dependent on α, therefore lower α along with higher c_l will cause N to increase otherwise opposite will happen. As compared to N, T shows an opposite trend because of its dependency on c_l and sinϕ. Due to different controller interface in AEROMODULE-SIMPACK couple and FOCUS(BEM), AEROMODULE modules curve and FOCUS(BEM) curve differ for u_{ind}. u_{ind} for all the modules follow the similar trend as their α. There are small peaks in AEROMODULE(AWSM) for u_{ind} and these peaks can also be seen in its α curve. Peaks in AEROMODULE(AWSM) may be due to the influence of tip vortex at this blade station.

At 0.23R blade station, α in both the BEM modules crosses above 12.5 degrees and this can be seen in figure C-79. FOCUS(BEM) shows a decreasing c_l trend because of large α, at large α dynamic stall occurs. AEROMODULE(BEM) shows an increasing trend for c_l because of dynamic stall. At 118.4th second when both the BEM modules have same α, then AEROMODULE(BEM) shows higher c_l than FOCUS(BEM), this suggests that AEROMODULE(BEM) over predicts stall here. N and T for all the modules show differences because of different c_l and ϕ, but still both AEROMODULE modules are closer to each other. u_{ind} for both the BEM modules is close while AEROMODULE(AWSM) shows a higher mean value because of lowest α among all modules.

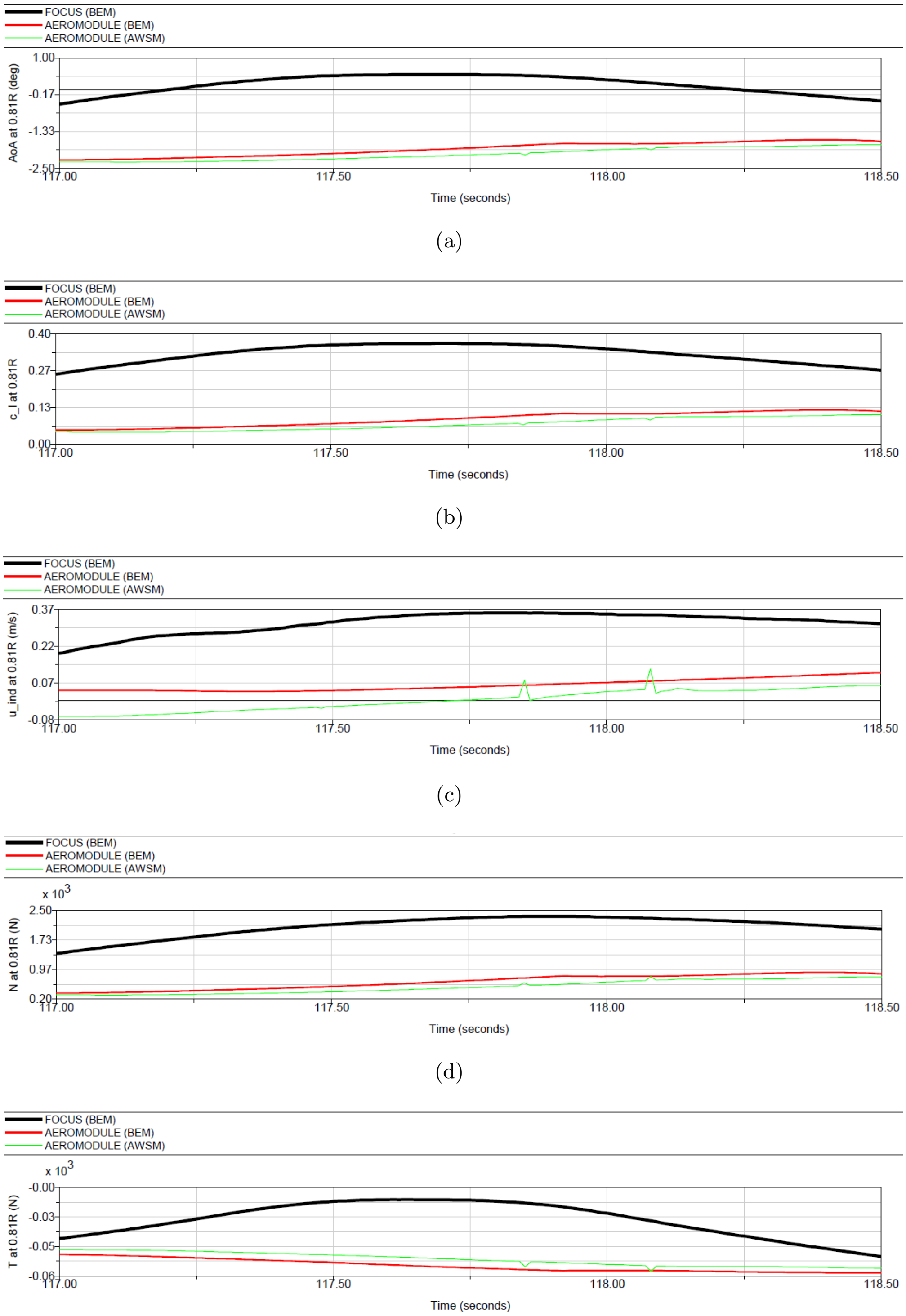

(a)

(b)

(c)

(d)

(e)

Figure C-78: Case-3290: Aerodynamic analysis at 0.81R blade station from 117th to 118.5th.

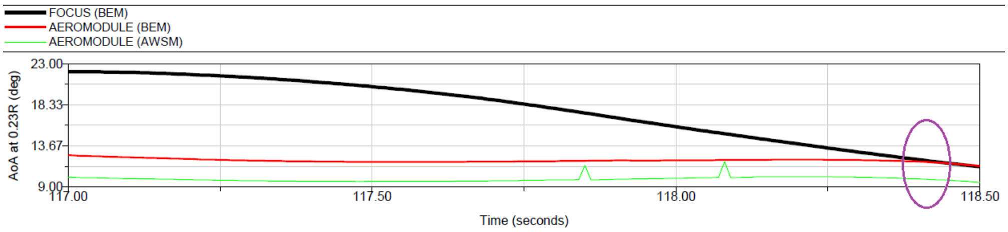

(a)

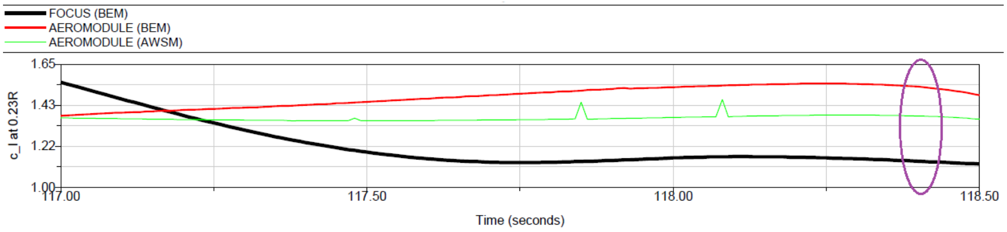

(b)

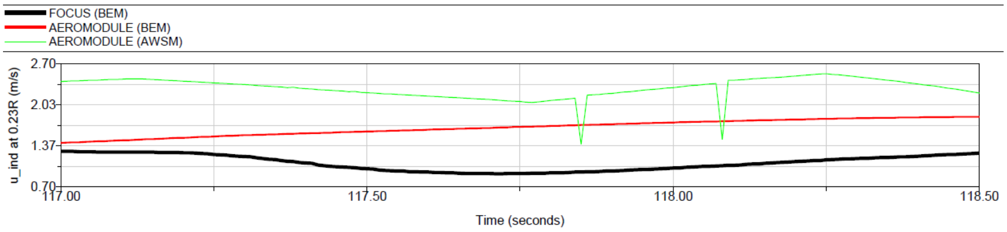

(c)

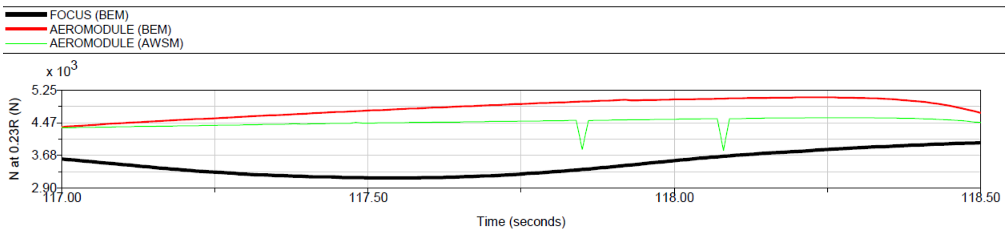

(d)

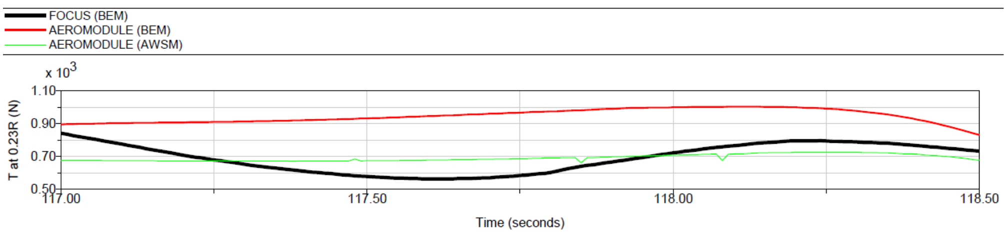

(e)

Figure C-79: Case-3290: Aerodynamic analysis at 0.23R blade station from 117th to 118.5th second.

C.2.3 Aerodynamic aspects - When gust prevails

In this section the time series is zoomed from 137th to 138.5th second to get more aerodynamic insight. This time interval is when gust prevails and pitch angle is increasing from 30 to 40 degrees.

At 0.81R blade station, negative α at which stall occurs is -18 degrees. From figure C-80 this is evident that FOCUS(BEM) and AEROMODULE(AWSM) reach stall. As there is no dynamic stall model therefore AEROMODULE(AWSM) shows 2D c_l characteristics. AEROMODULE(BEM) and AEROMODULE(AWSM) show same trend and are close to each other for α, c_l, N and T, while FOCUS(BEM) has a different trend because of the phase difference between the modules. As most of the time α lies in the linear slope region therefore c_l has same trend as α. In all the modules N follows the trend of α and c_l, while T follows the opposite trend of α and c_l. u_{ind} follow similar trend as α and c_l for all the modules. There are some peaks in AEROMODULE(AWSM) and these peaks occur whenever there is stall.

Figure C-81 shows the aerodynamic analysis at 0.23R blade station from 137th to 138.5th second. At 0.23R blade station, for all the modules α lies in the linear slope region therefore c_l follows the same trend as α. As N and T are also dependent on α and c_l therefore they also follow the same trend as α and c_l. Usually T follows the opposite trend as N but as ϕ is close to 45 degrees therefore T has the same trend as N. u_{ind} for AEROMODULE(AWSM) and FOCUS(BEM) follow similar trend as their α and c_l curves, but AEROMODULE(BEM) doesn't show this. As discussed in other load cases also at 0.23R blade station, AEROMODULE(BEM) does not compute the aerodynamic characteristics properly and thus need more investigation.

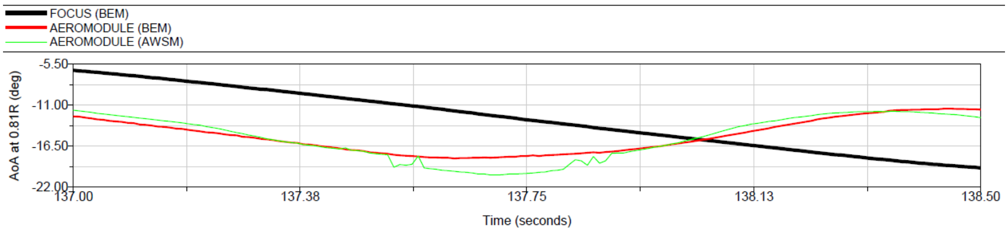

(a)

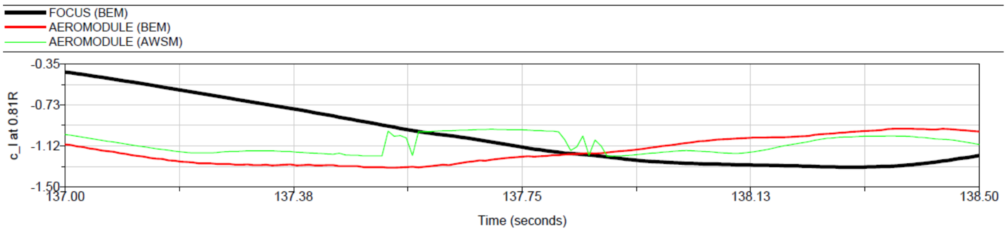

(b)

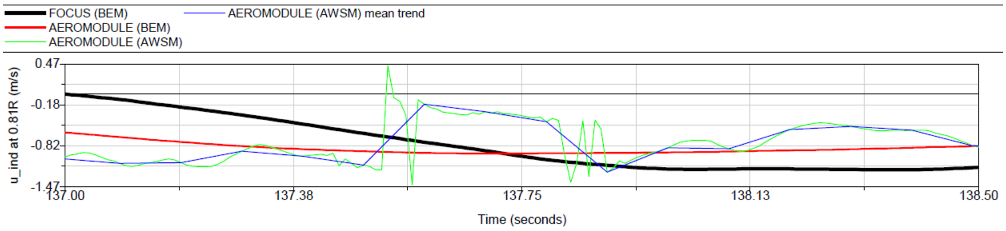

(c)

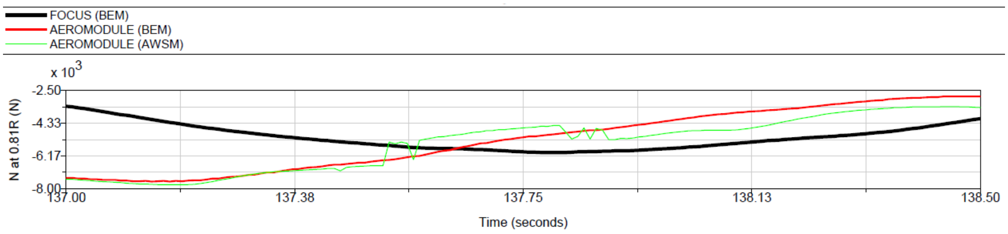

(d)

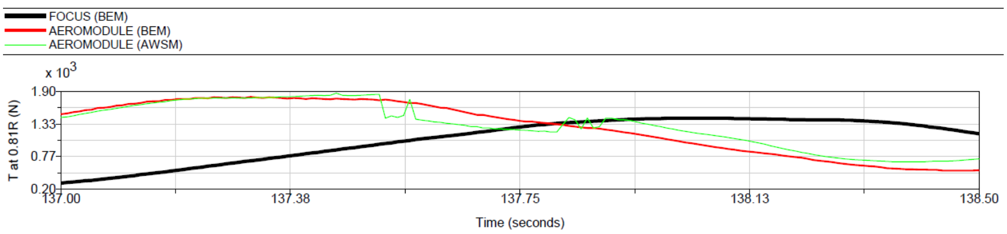

(e)

Figure C-80: Case-3290: Aerodynamic analysis at 0.81R blade station from 137th to 138.5th second.

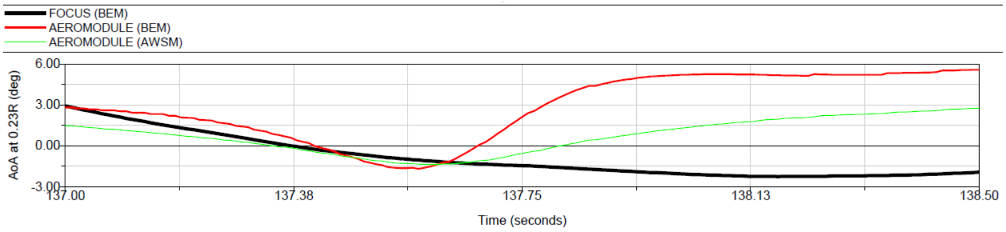

(a)

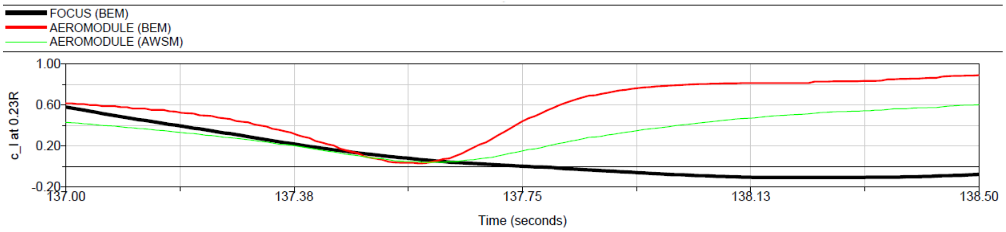

(b)

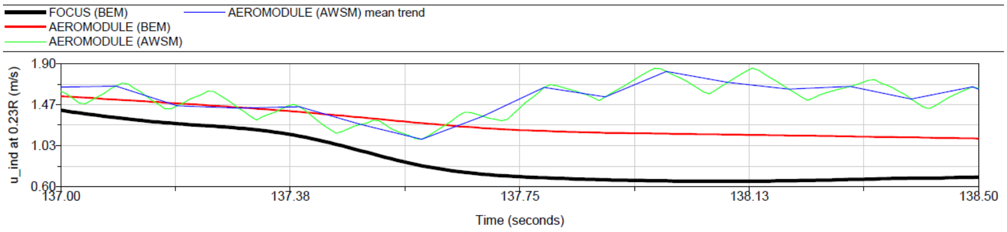

(c)

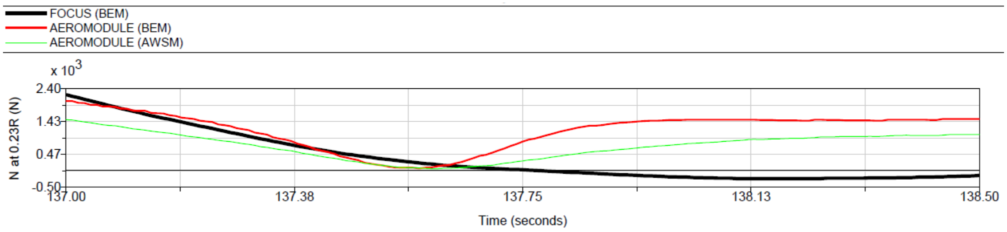

(d)

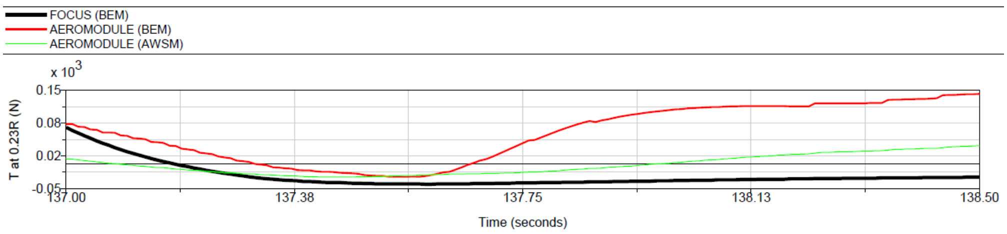

(e)

Figure C-81: Case-3290: Aerodynamic analysis at 0.23R blade station from 137th to 138.5th second.

C.2.4 Aerodynamic aspects - After gust prevails

In this section the time series is zoomed from 149th to 151st second to get more aerodynamic insight after the gust. At this interval blade is completely parallel to wind direction i.e. pitch angle is 90 degrees. In this case blades are not rotating therefore spanwise airflow is very small or negligible. In general 2D characteristics of the blade can be seen here.

Figure C-82 shows the aerodynamic analysis at 0.81R blade station from 149th to 151st second. At 0.81R blade station, for all the modules as α doesn't go above 14 degrees and thus lie in the linear slope region, therefore there is no stall and hence c_l follows the same trend as α. Same can be said for N and T for all the modules. FOCUS(BEM) shows a higher mean value while AEROMODULE modules show a lower mean value because of the initial phase difference between modules. There is not much difference in u_{ind} for all modules, FOCUS(BEM) shows the smallest u_{ind} because of highest α and c_l.

Figure C-83 shows the aerodynamic analysis at 0.23R blade station from 149th to 151st second. At 0.23R blade station, none of the modules reach stall because α lies in the linear slope region and thus c_l follows the same trend as α for all modules. Both N and T are small because of large ϕ and low c_l. N follows the same trend as α and c_l while T follows the opposite. u_{ind} follows the opposite trend as α because it is small and the pitch angle is large so ϕ is large, there is not much difference in u_{ind} for all modules.

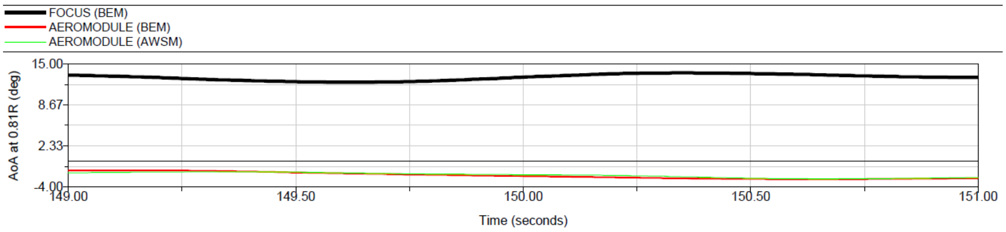

(a)

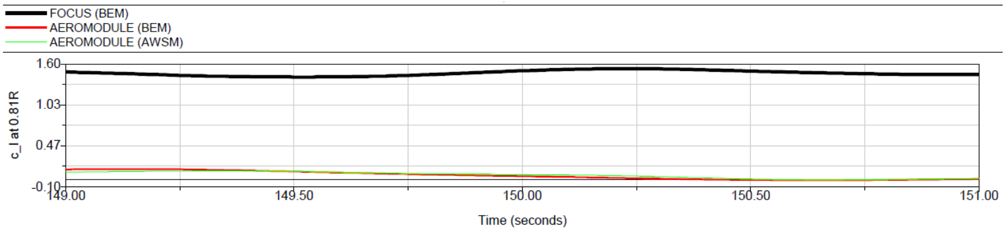

(b)

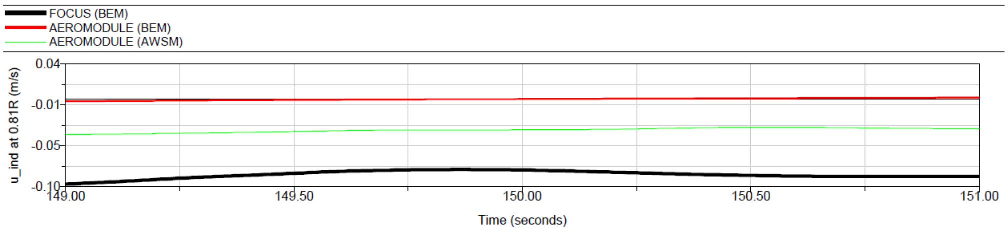

(c)

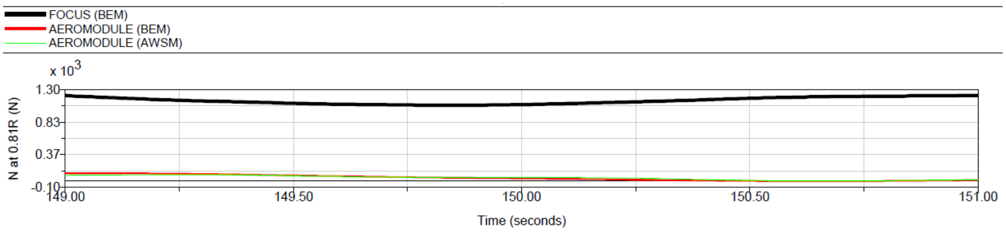

(d)

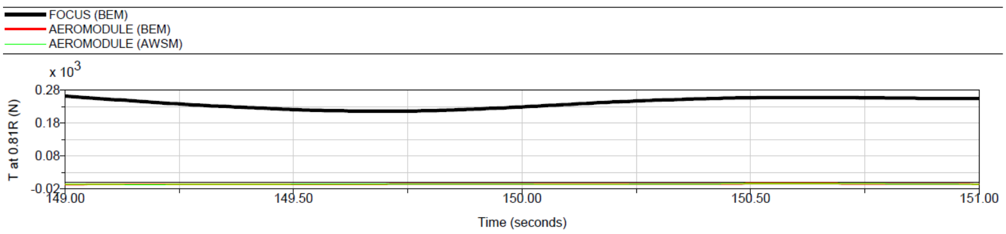

(e)

Figure C-82: Case-3290: Aerodynamic analysis at 0.81R blade station from 149th to 151st second.

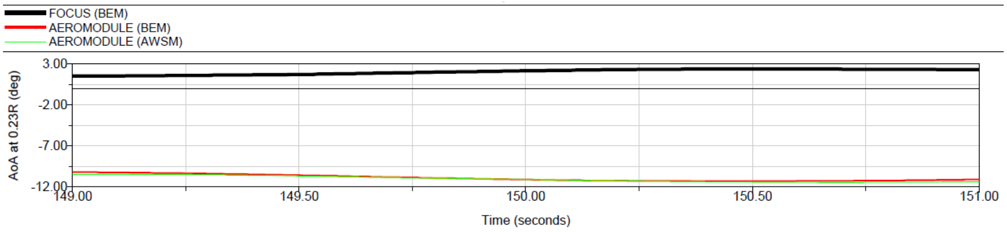

(a)

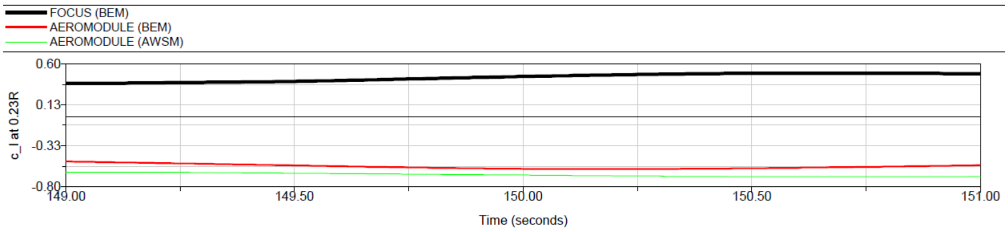

(b)

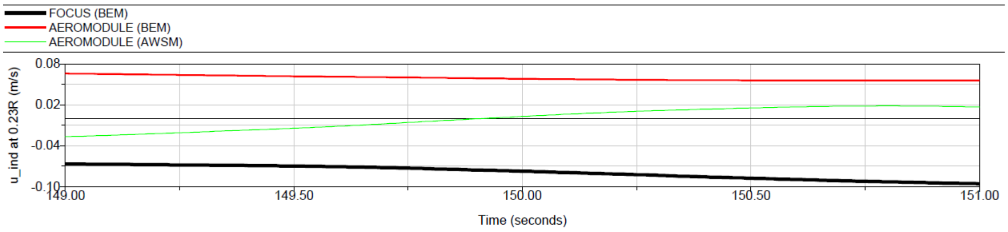

(c)

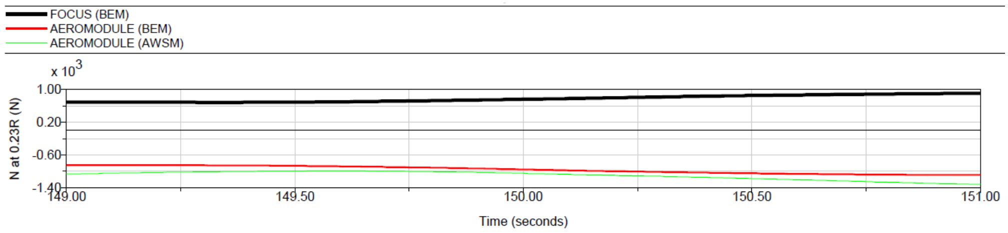

(d)

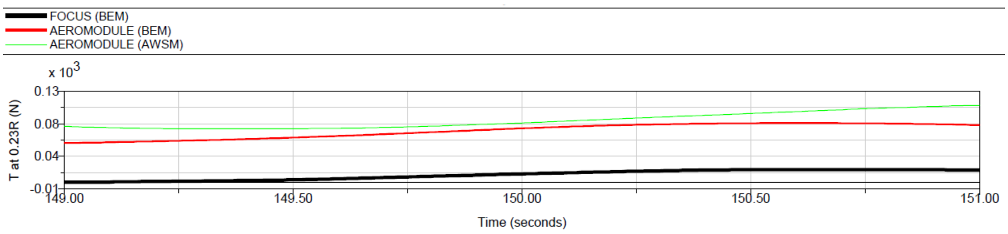

(e)

Figure C-83: Case-3290: Aerodynamic analysis at 0.23R blade station from 149th to 151st second.

C.2.5 Aerodynamic aspects at 139th second

In this section aerodynamic analysis is done at 139th second along the complete length of blade. This analysis is done to observe the difference in three modules when the gust prevails. In figure C-84, blade length starts from 5 m and ends at 62.5 m because blade stations before 5 m of length and after 62.5 m of length are not taken in AEROMODULE(AWSM) due to computation problems. It can be seen that all the three modules show a good match in trend and coincide each other for angle of attack α. Only near the tip region the airfoils are stalled otherwise the rest of the blade length is not in stall. For the lift coefficient curve, AEROMODULE(BEM) shows the same c_l for two consecutive stations near 15 m of blade length, this suggests there is some problem in AEROMODULE(BEM) and thus needs more investigation. Normal force distribution N, follows the same trend as c_l, whereas tangential force distribution follows the opposite trend as c_l. There is close match between AEROMODULE(AWSM) and FOCUS(BEM) for lift coefficient c_l, normal N and tangential T force distribution near tip region and this is because of more station near the tip. Due to less stations near the root section AEROMODULE(AWSM) is deviated from FOCUS(BEM). AEROMODULE(AWSM) shows a good match with AEROMODULE(BEM) from the root till mid-board region.

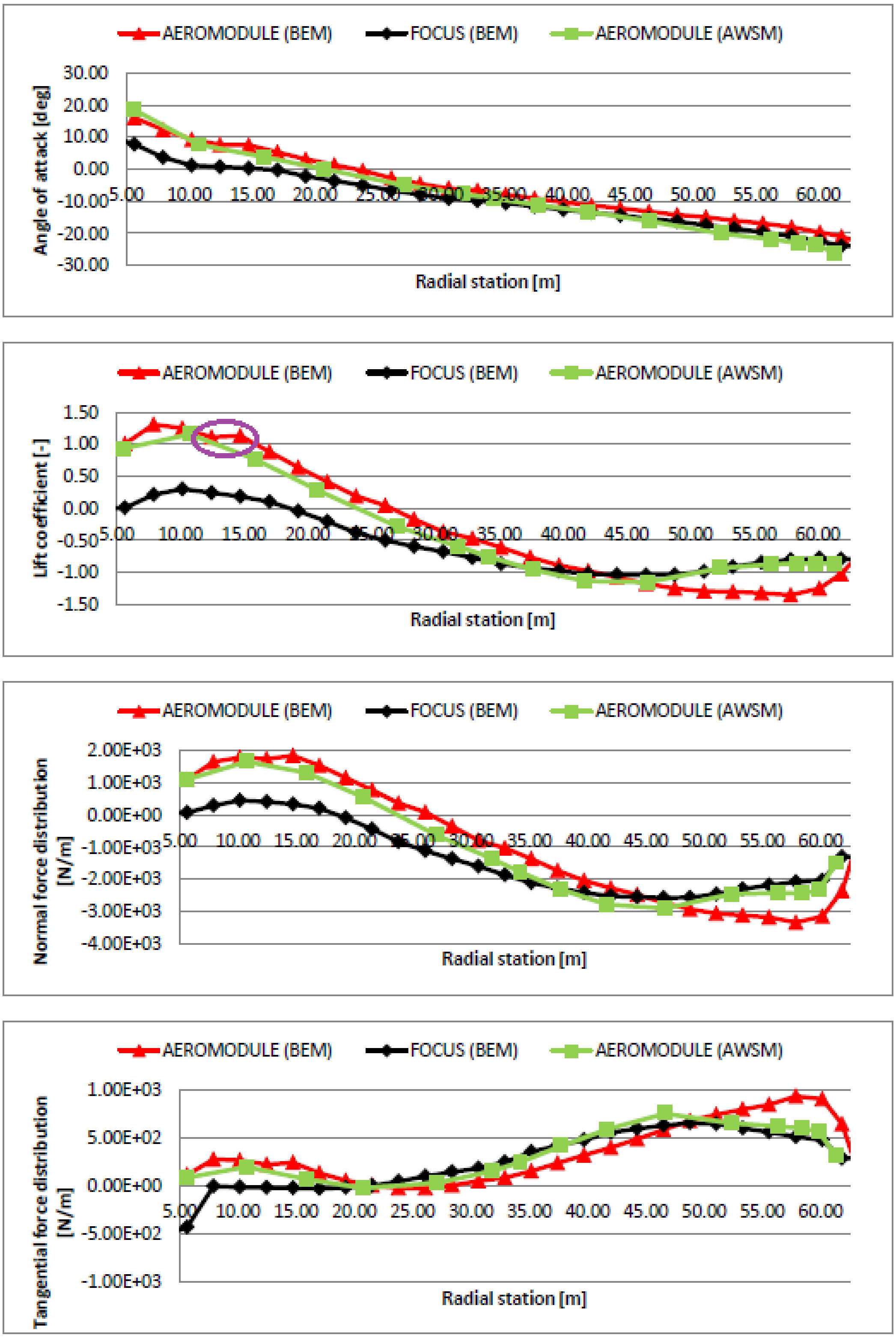

Figure C-84: Case-3290: Aerodynamic analysis at 139th second.

C.2.6 Structural aspects

Start-up with extreme operating gust causes extreme loads on wind turbine parts, below the loads on tower and blades are discussed.

Blade loads

Blade experiences moments in flapwise bending, edgewise bending and torsional moment in the blade root. For the initial 80 seconds the flapwise bending moment is

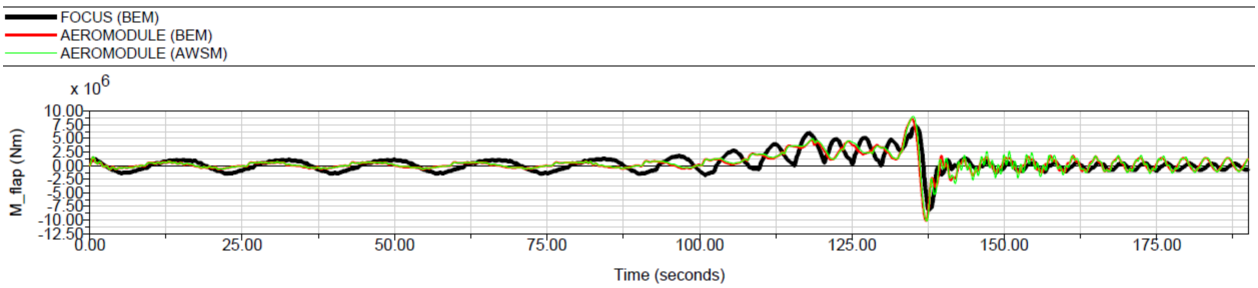

Figure C-85: Case-3290: Flapwise bending moment in the blade root.

due to the axial wind force(wind shear) due to 25 m/s of wind speed. Centrifugal force comes into play when the rotor speed increases and thus it also contributes to flapwise bending moment in the blade root from the 80th second, gravity force which acts on the rotor because of the cone and tilt angle also contributes when rotor speed increases. As the yaw rate is zero, therefore the gyroscopic force is zero and thus its contribution to flapwise bending moment is also zero. As the pitch angle reduces from 60 degrees to 20 degrees from 80th till 118th second, the area of blade exposed to wind increases and thus axial aerodynamic force on rotor increases which causes more flapwise bending moment in the blade root. The contribution of centrifugal force also increases till the rotor speed increases, on decrease in rotor speed the centrifugal force contribution to flapwise bending moment also decreases. With the presence of gust the flapwise bending moment experiences extreme fluctuations and causes extreme loads on blade root. This extreme load is due to gust because the axial wind force and centrifugal wind force increases considerably. When the pitch angle of the blade reaches 90 degrees, the fluctuation fades off slowly in flapwise bending moment in the blade root because of small stiffness in flapwise direction of blade. Figure C-86 shows the flapwise bending moment in the blade root after the gust from 141st to 146th second, it can be seen that AEROMODULE(BEM) and AEROMODULE(AWSM) show large fluctuations as compared to FOCUS(BEM) and this is because of flexible ART model in SIMPACK. AEROMODULE(AWSM) shows more fluctuations than AEROMODULE(BEM) because the gust has just ended and thus dynamic inflow occurs and thus it takes time for the trailing wake to stabilize and cause induction in rotor blades. The

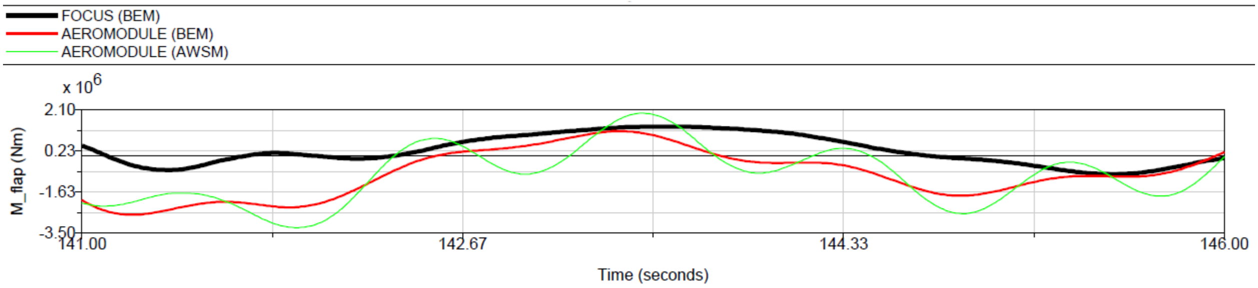

Figure C-86: Case-3290: Flapwise bending moment in the blade root from 141st to 146th second.

mean value of flapwise bending moment after shut down, suggests the contribution of wind shear on one blade. Frequency of fluctuations in flapwise bending moment in blade root before gust is 0.05 Hz and this is due to wind shear. After gust, the frequency of fluctuations is 0.27 Hz and this is due to tower 1st fore-aft frequency. Blade is experiencing tower frequency because of dynamic interactions. Figure C-85 shows the flapwise bending moment in the blade root. Before and after the gust, all the modules have the same trend but different phase and amplitude. Phase is different because SIMPACK takes time to stabilize a flexible body whereas in FOCUS(BEM) simulation starts with equilibrium condition. Difference in amplitude between AEROMODULE modules and FOCUS(BEM) is because of slightly different flapwise frequency taken in FOCUS(BEM) and SIMPACK.

Blade edgewise bending moment at blade root shows cyclic nature before the occurrence of gust. This cyclic nature is due to gravity force. The tangential wind force starts contributing after 100th second because the wind turbine starts producing power only after 100th second. Coriolis force also contributes to the edgewise moment in blade root because of the flapping velocity of the blade. The presence of gust can be clearly

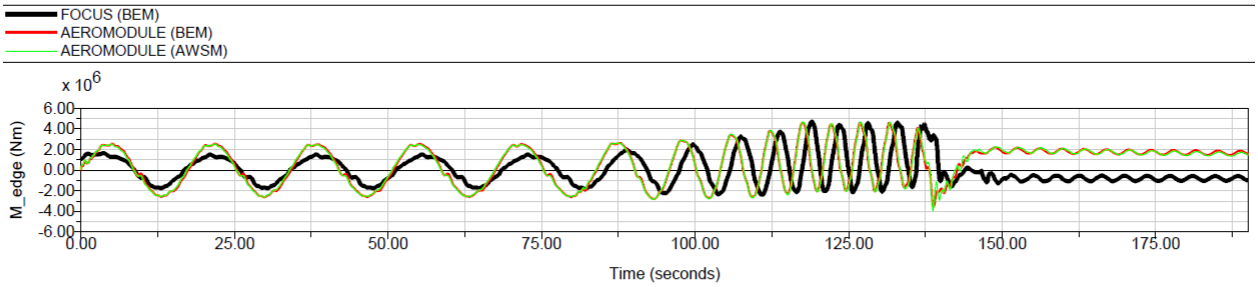

Figure C-87: Case-3290: Edgewise bending moment in the blade root.

seen in the extreme positive peak at 138th second. After the gust ends, the edgewise moment in the blade root eventually dies out because the rotor speed and generator power reduces to zero. When the pitch angle of the blade reaches 90 degrees, the fluctuations fade off fast in edgewise bending moment in the blade root because of large stiffness in edgewise direction of blade. The amplitude of fluctuations in the edgewise bending moment in the blade root after pitch angle has reached 90 degrees is because of gravity force on one blade and the component of gravity force is due to presence of tilt and cone angles. Frequency of fluctuations in edgewise bending moment in blade root before gust is 0.05 Hz and this is due to cyclic gravity force. After gust, the frequency of fluctuations is 0.27 Hz and this is due to tower 1st side-ways frequency. Blade is experiencing tower frequency because of dynamic interactions. Figure C-87 shows the edgewise bending moment in the blade root. AEROMODULE modules show the same trend as FOCUS(BEM) but due to initial phase difference, AEROMODULE modules show a positive mean value of edgewise bending moment while FOCUS shows negative after the gust ends, figure C-88 gives more insight about it.

Figure C-89 shows the torsional moment in the blade root. For the first 80 seconds, as the pitch rate is zero, therefore it does not contribute to blade torsional moment in the blade root. Fluctuations in flapwise and edgewise forces in blade along with lead-lag and flapwise bend respectively in blade causes torsional moment in the blade root. When the pitch angle changes with a pitch rate of 6 degrees/second the pitch mechanism also causes the torsional moment in the blade root and this can be seen in figure C-90. It can be seen that FOCUS(BEM) shows a positive torsional moment during pitch angle change whereas AEROMODULE modules show negative, this is because of

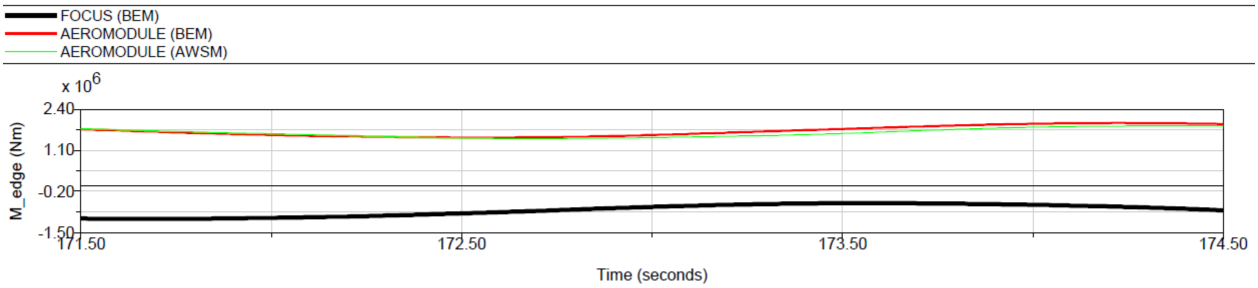

Figure C-88: Case-3290: Edgewise bending moment in the blade root from 171.5th to 174.5th second.

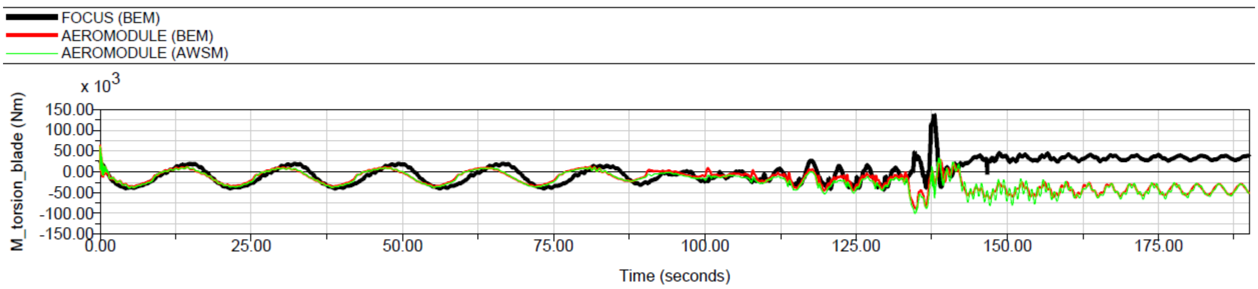

Figure C-89: Case-3290: Torsional moment in the blade root.

initial phase difference between the modules. AEROMODULE(AWSM) shows fluctuations whereas both the BEM modules don't, the frequency of the fluctuations is 13.6 Hz and this is the blade natural torsional frequency. Only AEROMODULE(AWSM) is able to predict this, both the BEM modules doesn't. Peak due to occurrence of gust

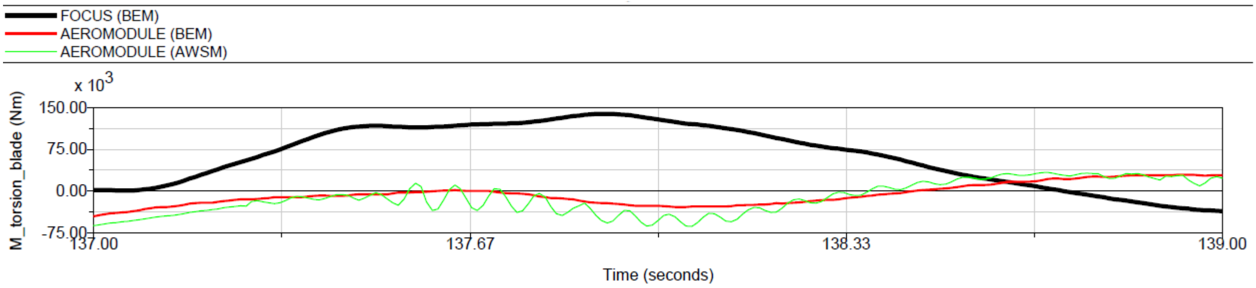

Figure C-90: Case-3290: Torsional moment in the blade root from 137th to 139th second.

can be seen clearly at 138th second and it is accompanied by an increasing pitch angle. After the pitch angle changes to 90 degrees, the decreased flapwise and edgewise force in addition to blade deflection causes fluctuation in torsional moment in the blade root. Frequency of fluctuations in torsional moment in blade root before gust is 0.05 Hz and this is due to gravity force. After gust, the frequency of fluctuations is 0.27 Hz and this is due to tower 1st side-ways frequency. Blade is experiencing tower frequency because of dynamic interactions. Both AEROMODULE modules show a different mean value as compared to FOCUS(BEM) because of different phase when gust prevails.

Tower loads

Tower experiences fore-aft and side-ways bending moment at tower base and torsional moment at tower top. Fore-aft tower bending moment is due to rotor thrust. For the initial 80 seconds, the contribution of this factor is very small but after 80th second its contribution increases and thus the fore-aft tower bending moment increases because the blade is pitched to lower angles. When the gust prevails from 130th to 141st second, extreme fluctuations can be seen and thus the gust leads to extreme loads on tower base. Fore-aft tower moment first shows increases because of increase in rotor thrust and then shows a dip because of dynamics involved in tower. When the gust ends the amplitude of the fluctuations gets damped and decreases exponentially with

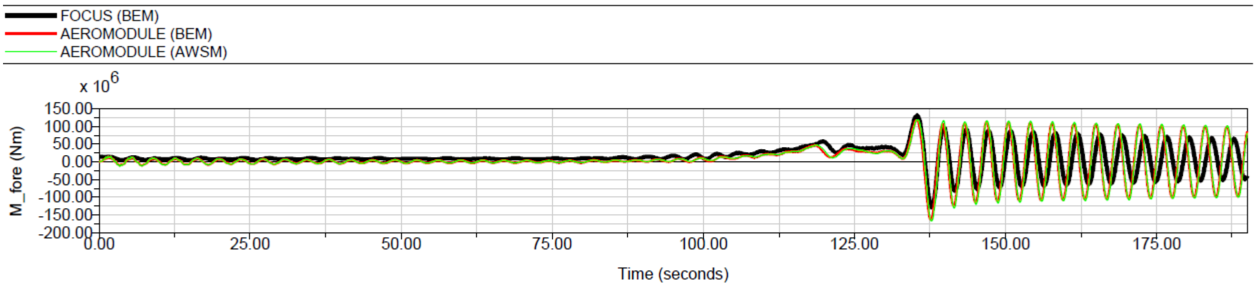

Figure C-91: Case-3290: Fore-aft bending moment in the tower base.

time, like an under damped spring. Exponential decrease suggests that the tower is under damped [24]. Frequency of fluctuations in fore-aft bending moment in tower base before and after gust is 0.27 Hz and this is due to first natural tower fore-aft frequency. Figure C-91 shows the fore-aft bending moment in the tower base. All the modules show good match for the fore-aft bending moment in tower base before the gust, after the gust AEROMODULE modules show higher amplitude fluctuations than FOCUS(BEM), this is because of slightly different tower stiffness and flapwise frequency of blades, and this can be seen in figure C-92.

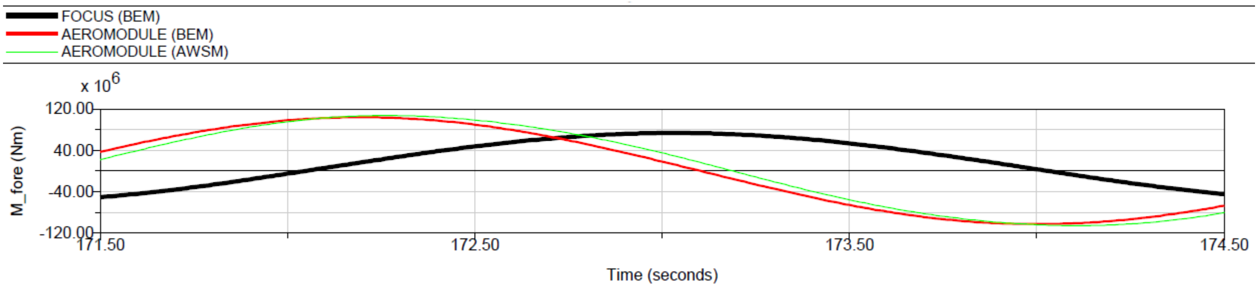

Figure C-92: Case-3290: Fore-aft bending moment in the tower base from 171.5th to 174.5th second.

Figure C-93 shows the side-ways bending moment in the tower base. For the initial 80 seconds it is the differential turbulence in the rotor blades which causes the side-ways bending moment of the tower at tower base. But as soon as the blade pitch angle reduces the amplitude of fluctuations in side-ways bending moment increases as compared to load case-3271, load case-3271 is discussed in report (give reference), because of difference in yaw angle. Difference in yaw angle leads to different inertia of tower and

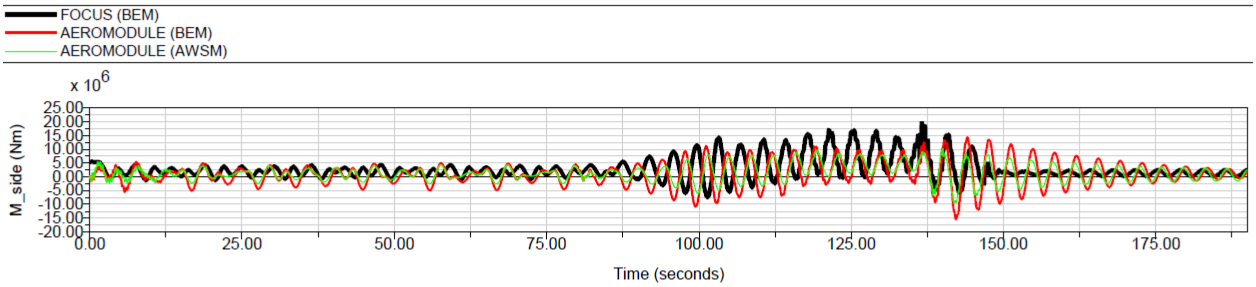

Figure C-93: Case-3290: Side-ways bending moment in the tower base.

rotor in both the cases. Figure C-94 shows the side-ways bending moment from 90th to 102nd second, it can be seen that there is large phase difference between AEROMODULE modules and FOCUS(BEM) and this is because the simulation in FOCUS(BEM) starts with equilibrium but this does not happen in SIMPACK. Phase difference between AEROMODULE(BEM) and AEROMODULE(AWSM) is small. But after the

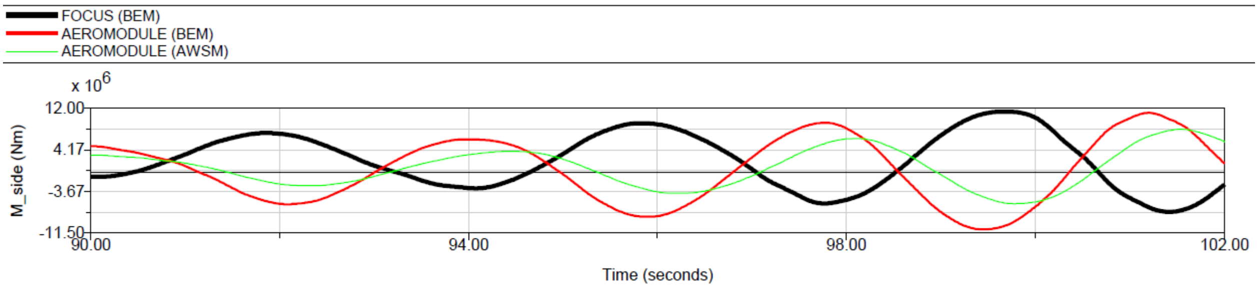

Figure C-94: Case-3290: Side-ways bending moment in the tower base from 90th to 102nd second.

100th second, the wind turbine starts producing power, the rotor torque which acts on the tower top through generator/gearbox support also starts contributing to the side-ways bending moment of the tower along with the edgewise moment of the blade. When the gust comes sudden extreme fluctuation can be seen in the side-ways tower bending moment, this is due to sudden fluctuation in rotor torque. After 138th second the fluctuations decrease with an exponential function, same as is the case with an under damped spring. Frequency of fluctuations in side-ways bending moment in tower base before and after gust is 0.27 Hz and this is due to first natural tower side-ways frequency.

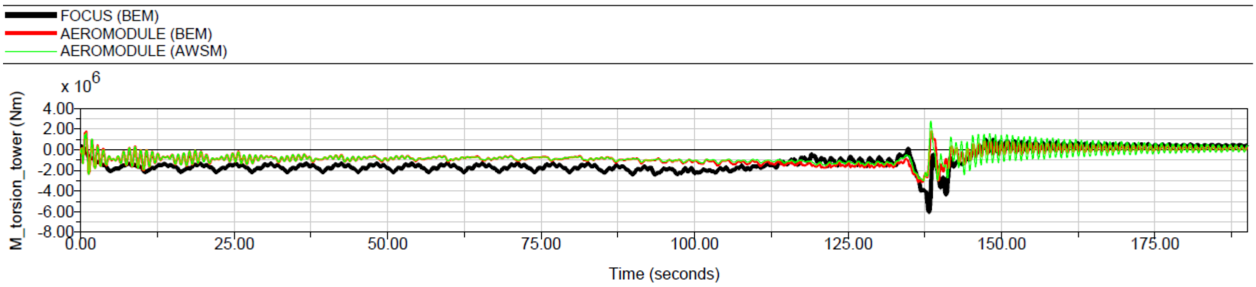

Figure C-95: Case-3290: Torsional moment in the tower top.

Figure C-95 shows the torsional moment in the tower top. Tower also experiences torsional moment, and this moment is relatively smaller than fore-aft and side-ways moments. Torsional moments are caused due to turbulence and changing wind direction. As the rotor is tilted, a component of rotor torque act on the tower top through gearbox/generator support which causes torsional moment in tower top. As the gust comes, its contribution is more than rotor torque and thus causes extreme fluctuation which eventually dies out exponentially like an under damped spring. In figure C-96, it can be seen that due to sudden gust the tower shows high fluctuations and this shows the dynamic interaction between blades, controller and tower. The fluctuation even-

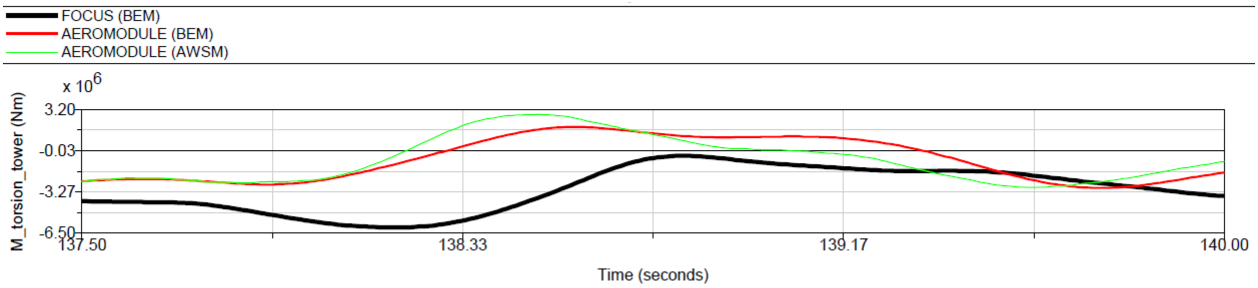

Figure C-96: Case-3290: Torsional moment in the tower top from 137.5th to 140th second.

tually dies out with an exponential function, which suggests that the tower is under damped. Frequency of fluctuations in torsional moment in tower top before and after gust is 0.9 Hz and this is due to backward whirling mode [27] in blades. Both AEROMODULE modules show really good match as compared to FOCUS(BEM) because of slightly different tower stiffness in SIMPACK and FOCUS(BEM).

D ART wind turbine test load case

D.1 Load case-2: Step change in wind speed in flexible wind turbine

Description

A step change in wind is considered from 8 m/s to 11 m/s at 70th second, and the wind is not turbulent. No surface roughness is considered therefore no wind shear. Figure D-1 shows the step wind in load case 2.

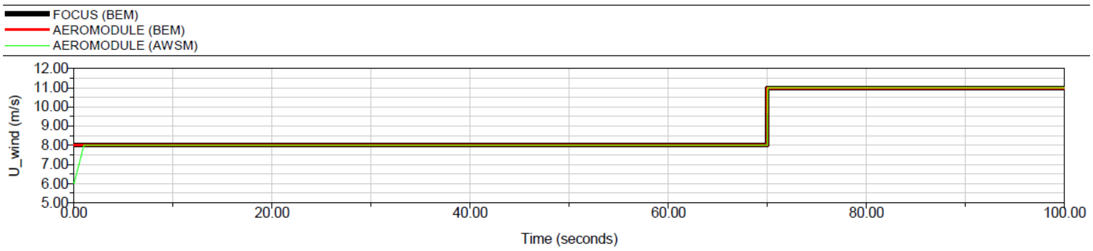

Figure D-1: Case-2: Wind Speed at hub.

The wind turbine rotor is not taken with tilt and cone angle. The rotor of the ART wind turbine is not misaligned i.e. yaw angle is zero. Controller operation is switched off, the pitch angle of all the blades and rotor speed is maintained at a constant value of 0 degree and 12.1 rpm respectively. The generator is maintained at constant generator speed. The ART wind turbine structure is considered flexible i.e. both blades and tower are flexible. As the blades are flexible therefore initial fluctuations in AEROMODULE-SIMPACK couple takes time to reach equilibrium, whereas in FOCUS(BEM), simulation starts with an equillibrium state.

All these parameters are given in all three modules. This case is similar to validation case 1, except a different change in wind speed at 70th second and a different pitch angle. In this load case only differences will be discussed as compared to validation case 1. As the pitch angle of blade is 0 degree and the rotor speed is maintained at 12.1 rpm, therefore the generator torque is lower for the first 70 seconds when wind speed is 8 m/s than for the next 30 seconds when the wind speed is 11 m/s. Even though the rated wind speed for the ART wind turbine is 12 m/s, it reaches rated power at 11 m/s because the pitch angle is 0 degree. Figures D-2 and D-3 shows generator torque and generator power respectively. All the modules show close match with each other for generator torque and power.

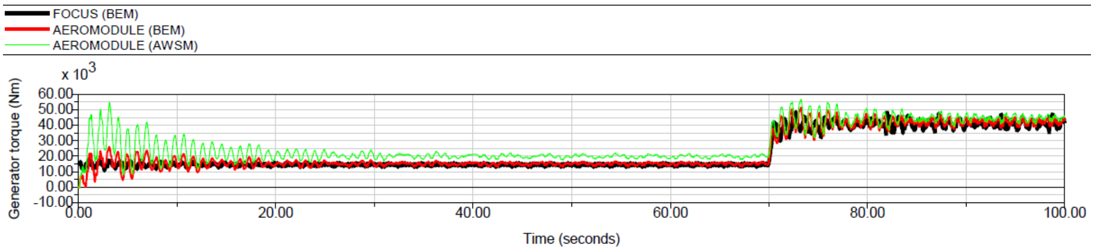

Figure D-2: Case-2: Generator torque.

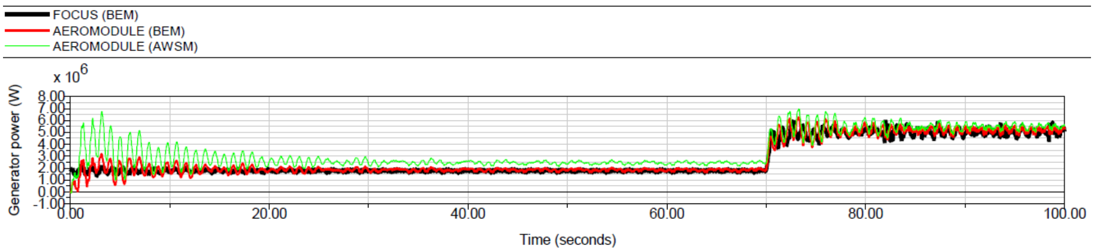

Figure D-3: Case-2: Generator power.

Large fluctuations in generator power and torque around 70th second are because the blades are flexible, the frequency of fluctuations is 1.05 Hz and this is due to natural edgewise frequency of blade. Figure D-4 shows generator power from 70th to 75th second.

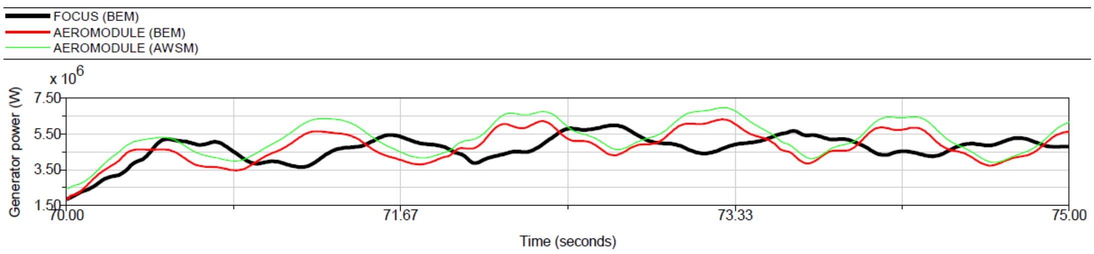

Figure D-4: Case-2: Generator power.

Figures D-5 and D-6 shows axial aerodynamic force on rotor and average flapwise displacement of blade tips respectively. Even though wind speed is low in this case still the axial aerodynamic force on rotor is comparable to case 1 because of small pitch angle of 0 degree. With 0 degree pitch angle more surface area of blade is exposed to wind and thus more wind force on rotor.

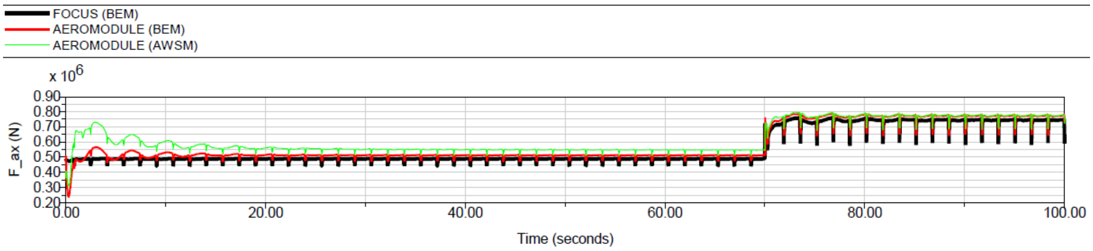

Figure D-5: Case-2: Axial aerodynamic force on rotor.

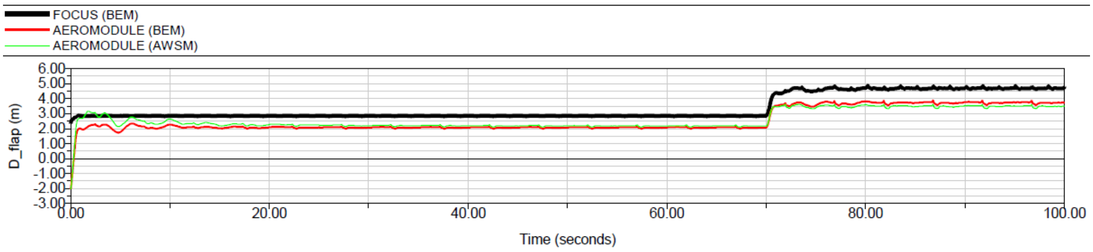

Figure D-6: Case-2: Average flapwise displacement of blade tips.

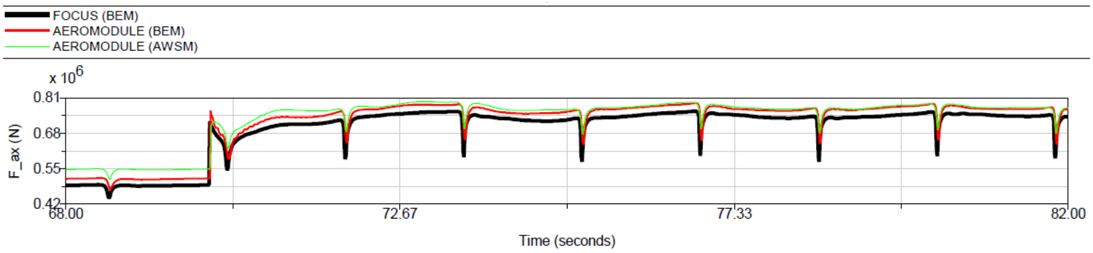

Figure D-7: Case-2: Axial aerodynamic force on rotor.

Figure D-7 shows the axial aerodynamic force on rotor from 68th to 82nd second. At 70th second when the wind speed changes there is fluctuation in axial aerodynamic force on rotor and this is due to flexibility of tower, the frequency of fluctuation is 0.27 Hz and this is tower 1st natural fore-aft frequency. There is a slight difference in axial aerodynamic force between all modules and this can be attributed to differences in α,

c_l and u_{ind} along the blade, these characteristics are discussed in section D.1.1. As the blades are flexible therefore the average flapwise displacement of blades also shows a step change when wind speed changes. AEROMODULE(BEM) and AEROMODULE(AWSM) show a close match but they differ with FOCUS(BEM) with amplitude, this can be attributed due to slightly different flapwise frequency of blades in SIMPACK.

D.1.1 Aerodynamic aspects

As the blades are flexible therefore initial fluctuations in AEROMODULE(BEM) and AEROMODULE(AWSM) take time to reach equilibrium, whereas in FOCUS(BEM), simulation starts with an equilibrium state. Due to different pitch angle and step change in wind, the magnitudes of axial induced velocity, aerodynamic angle of attack, lift coefficient, normal force distribution and tangential force distribution are different as compared to case 1.

Figures D-8 and D-9 show the aerodynamic angle of attack at 0.81R and 0.23R blade stations respectively.

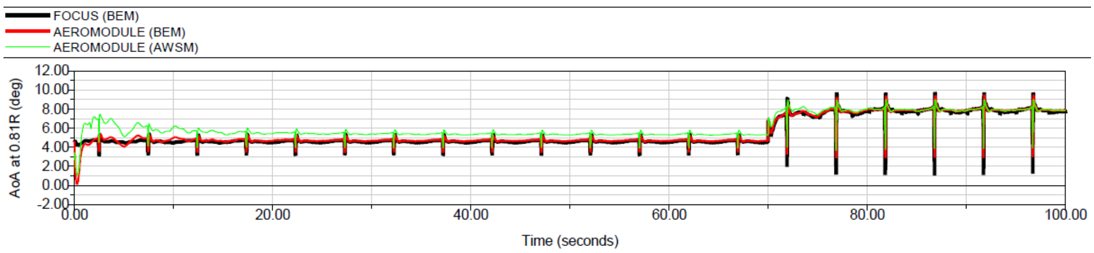

Figure D-8: Case-2: Aerodynamic angle of attack at 0.81R blade station.

Figure D-10 shows the angle of attack (α) at 0.81R from 60th to 80th second. At 0.81R blade station, both the BEM modules show close match whereas AEROMODULE(AWSM) is slightly displaced from them when the wind speed in 12 m/s. After step change in wind speed, all the modules show good match. As the airfoil does not cross 14 degrees of α therefore it is not stalled.

At 0.23R blade station all the modules show close match along the complete time series. After step change in wind, α at 0.23R blade station crosses 12.5 degrees i.e. airfoil

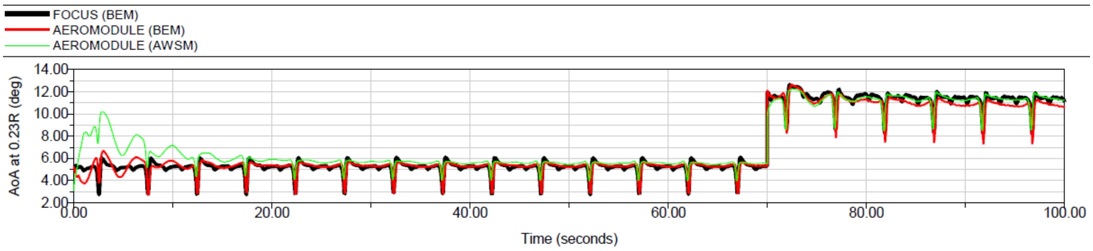

Figure D-9: Case-2: Aerodynamic angle of attack at 0.23R blade station.

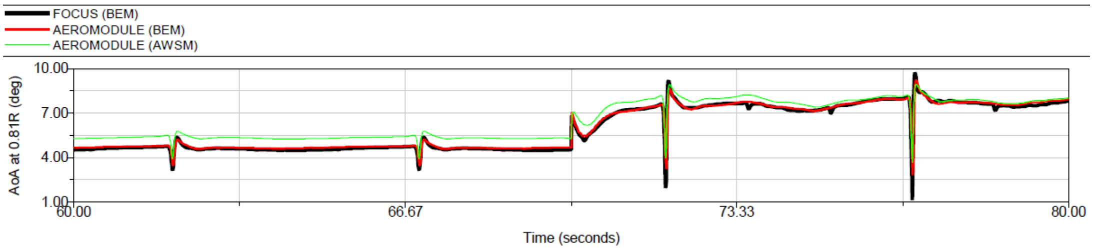

Figure D-10: Case-2: Aerodynamic angle of attack at 0.81R blade station from 60th to 80th second.

reaches stall. As the flow stabilizes α reduces below 12.5 degrees and thus operate in linear slope region. Transition between stall and linear part is shown in figure D-11 from 70th to 90th second. After the flow has stabilized, all the modules show good match.

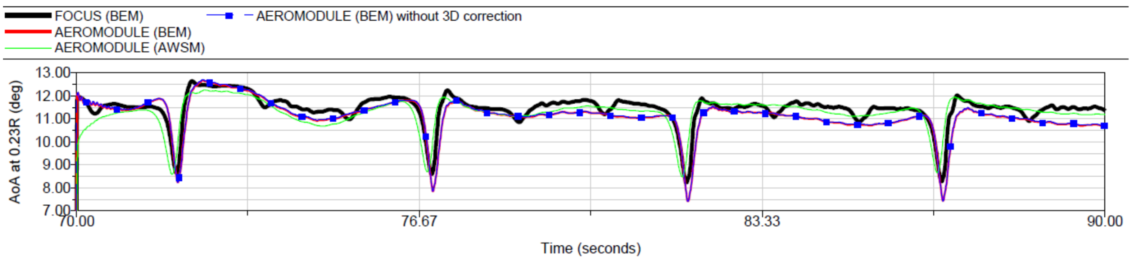

Figure D-11: Case-2: Aerodynamic angle of attack at 0.23R blade station from 70th to 90th second.

Figures D-12 and D-13 shows the lift coefficient c_l at 0.81R and 0.23R blade stations respectively.

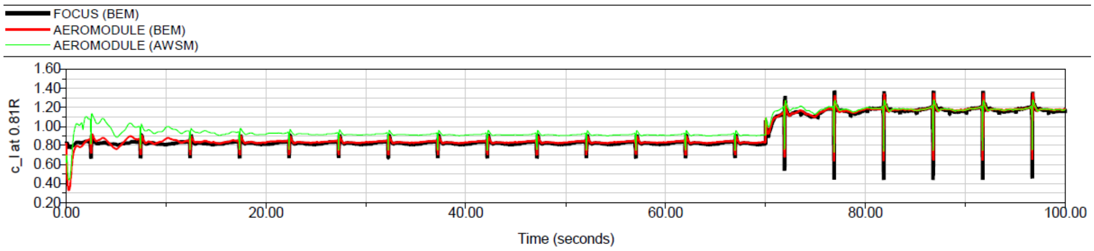

Figure D-12: Case-2: Lift coefficient c_l at 0.81R blade station.

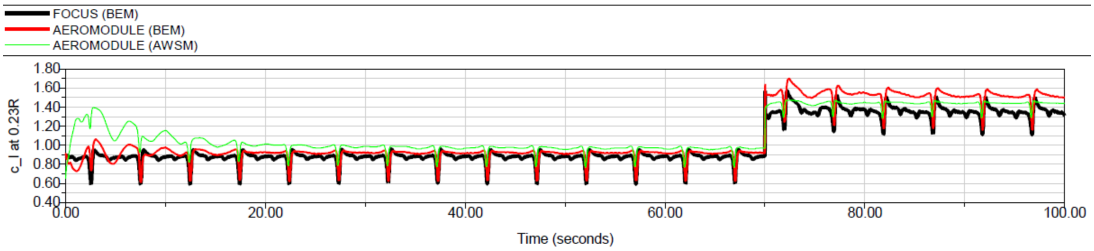

Figure D-13: Case-2: Lift coefficient c_l at 0.23R blade station.

Lift coefficient c_l follows the same trend as the angle of attack α. As both blade stations are below the stall α, therefore c_l is directly proportional to α. When the blade passes the tower, α reduces which subsequently reduces c_l. At 0.81R blade station all the modules show good match for the complete time series. At 0.23R blade station before wind speed step change all the modules show same trend but differ slightly in mean value. After dynamic inflow there is lot of difference in mean value between all the modules, AEROMODULE(BEM) shows c_l above the maximum 2D value of c_l, while FOCUS(BEM) and AEROMODULE(AWSM) does not show, this can be seen in figure D-14. As α does not go above 12.5 degrees therefore there is no stall but still AEROMODULE(BEM) shows c_l above the maximum 2D value which suggests that dynamic stall model in AEROMODULE(BEM) is over predicting stall here and this can also be seen in the α and c_l distributions in figure D-15. The trend of AEROMODULE(BEM) without the 3D correction is same as AEROMODULE(BEM), so this suggests that 3D correction is not cause of highest mean value in c_l for AEROMODULE(BEM). Different trend in c_l for AEROMODULE(BEM) near 15 m of radial distance needs to be investigated further.

Figure D-16 shows the axial induced velocity at 0.81R blade station. At 0.81R blade

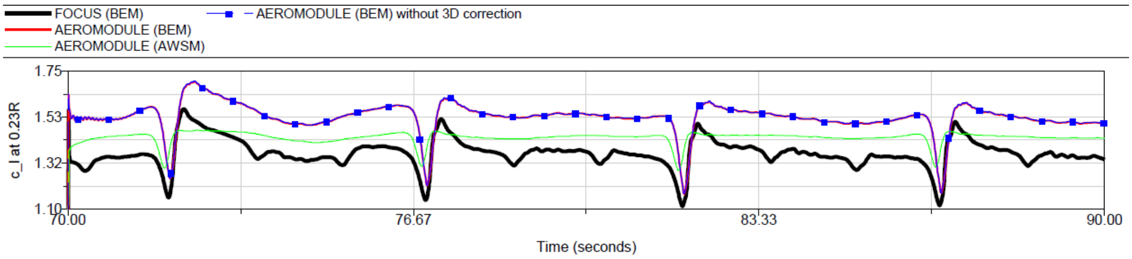

Figure D-14: Case-2: Lift coefficient c_l at 0.23R blade station from 70th to 90th second.

station, both the BEM modules overlap each other but AEROMODULE(AWSM) has lower mean value than them. But the mean value decreases when the wind speed increases. This difference in mean value is because in reality the axial induction is caused by the wake and both the BEM modules do not take into account the wake.

At 0.23R blade station all the modules show a slight difference with each other and this can be seen in figure D-17. Figure D-18 shows the axial induced velocity at 0.23R from 60th to 90th second. AEROMODULE(AWSM) shows a good match with FOCUS(BEM) after the step change in wind speed. Difference in AEROMODULE(AWSM) with both the BEM modules is because of wake induction on rotor. While the difference in both the BEM modules is because AEROMODULE(BEM) over predicts c_l at 0.23R blade station and as u_{ind} is dependent on c_l, therefore u_{ind} is higher for AEROMODULE(BEM) than FOCUS(BEM), this can be seen in figure D-15. AEROMODULE(AWSM) also shows a higher mean value for α and c_l than FOCUS(BBEM) at 0.23R blade station because of less stations taken in AEROMODULE(AWSM) and in AEROMODULE(AWSM) as every blade stations influences each other, so the missing stations has an effect on neighbouring blade stations.

Figures D-19 and D-20 show the normal force distribution at 0.81R and 0.23R blade stations respectively.

At 0.81R blade station all the modules show a good match, except when the wind speed is 8 m/s. AEROMODULE(AWSM) shows slight shift up as compared to both the BEM modules and this is because of higher α and c_l and lower u_{ind}. Figure D-21 shows the normal force distribution at 0.23R blade station from 50th to 90th second. At 0.23R blade station all the modules show similar trend but AEROMODULE(AWSM) shows slight higher mean value as compared to both the BEM modules when the wind

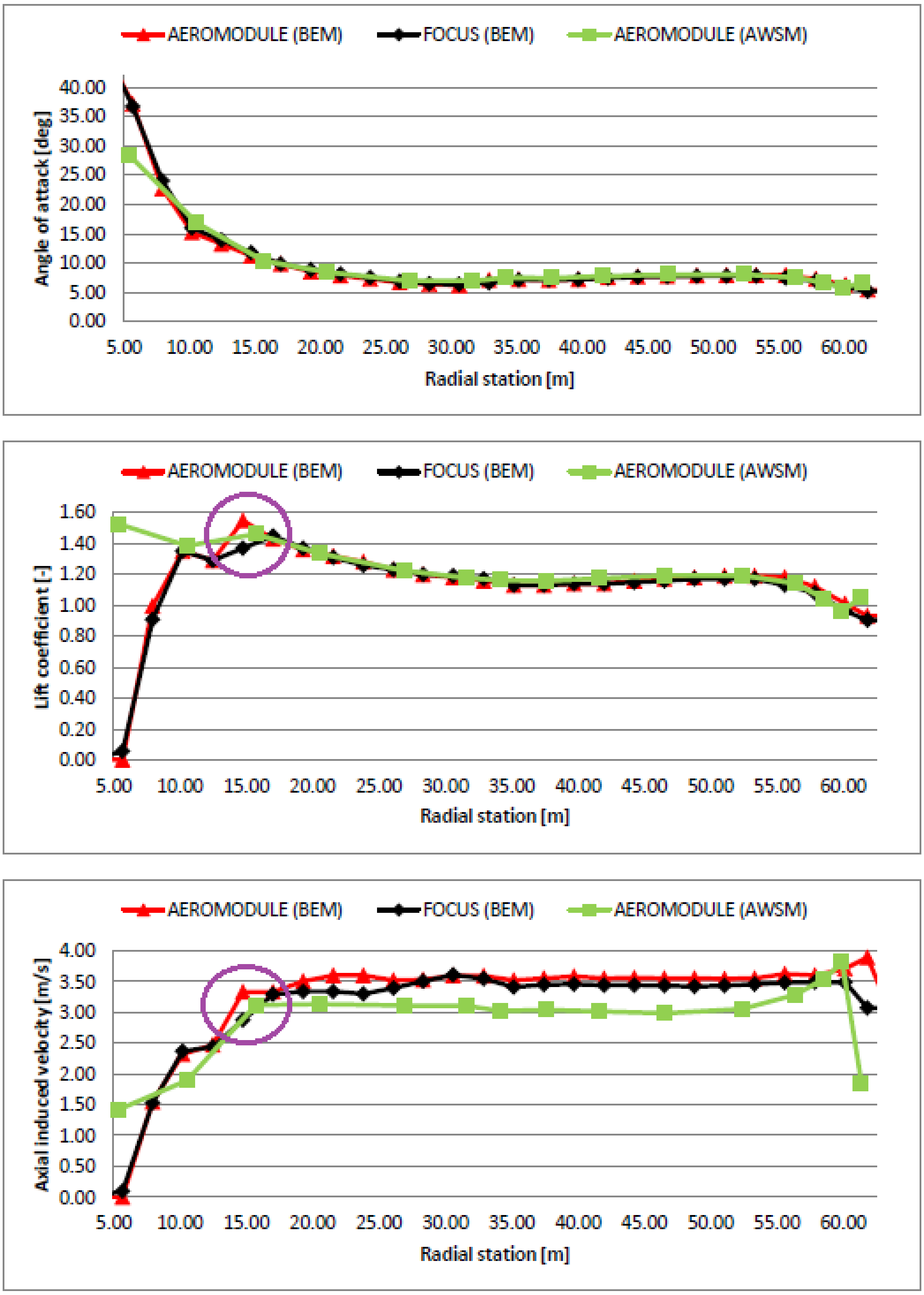

Figure D-15: Case-2: Aerodynamic analysis at 80th second.

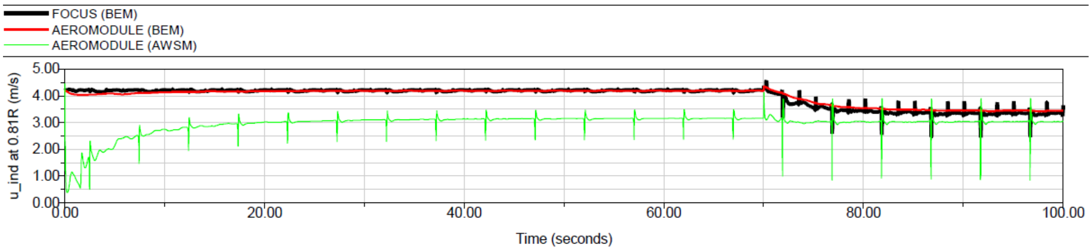

Figure D-16: Case-2: Axial induced velocity at 0.81R blade station.

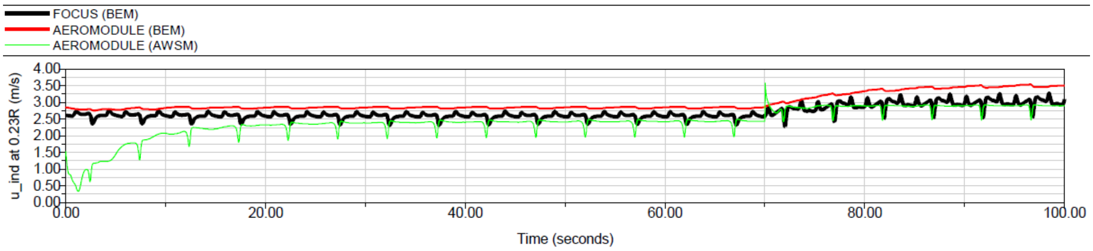

Figure D-17: Case-2: Axial induced velocity at 0.23R blade station.

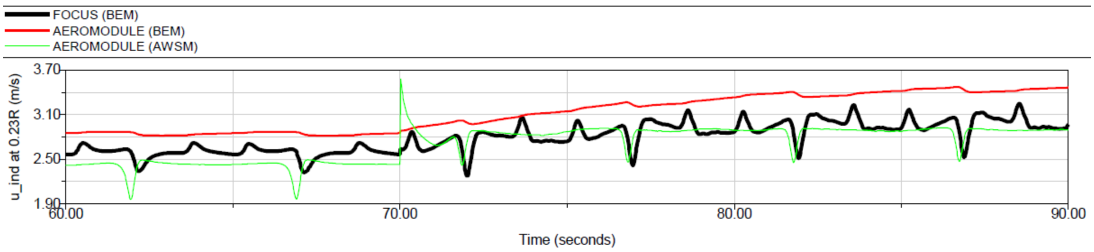

Figure D-18: Case-2: Axial induced velocity at 0.23R blade station from 60th to 90th second.

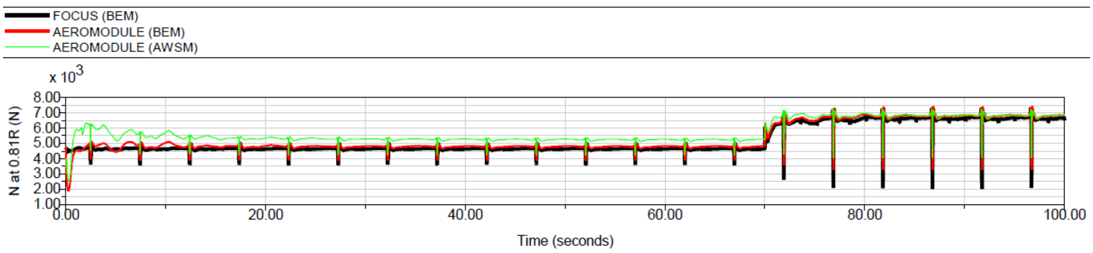

Figure D-19: Case-2: Normal force distribution at 0.81R blade station.

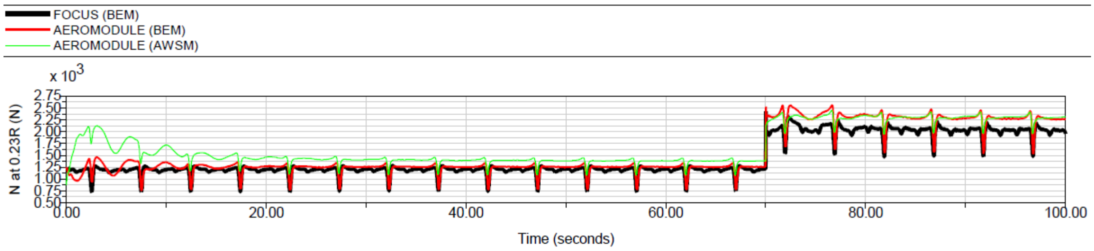

Figure D-20: Case-2: Normal force distribution at 0.23R blade station.

speed is 8 m/s. When the wind speed changes to 11 m/s, AEROMODULE(BEM) and AEROMODULE(AWSM) matches very well, FOCUS(BEM) has a slightly lower mean value. The difference in N for all the modules at 0.23R blade station is because of different α, c_l and u_{ind} in all of them.

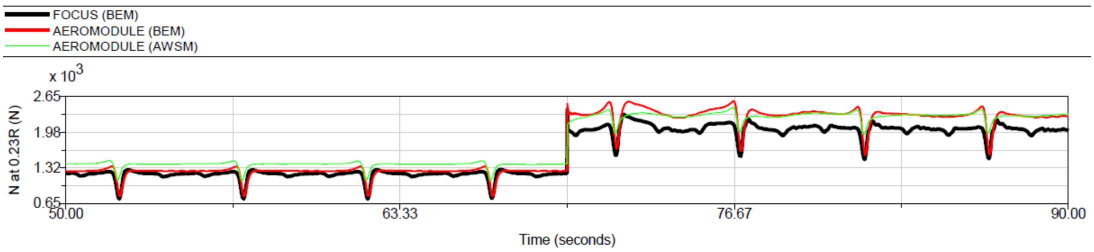

Figure D-21: Case-2: Normal force distribution at 0.23R blade station from 50th to 90th second.

Figures D-22 and D-23 shows the tangential force distribution at 0.81R and 0.23R blade stations respectively. Both at 0.23R and 0.81R blade stations all the modules have a good match, some slight difference are there because of slight difference in α and c_l.

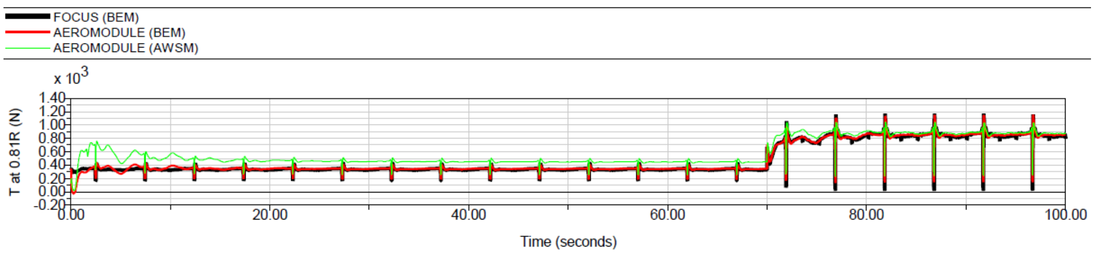

Figure D-22: Case-2: Tangential force distribution at 0.81R blade station.

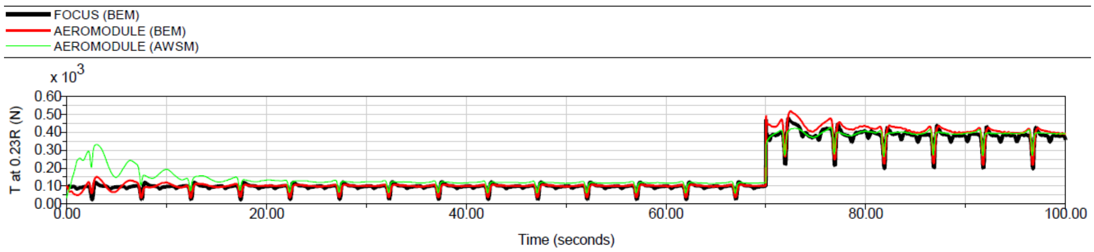

Figure D-23: Case-2: Tangential force distribution at 0.23R blade station.

D.1.2 Aerodynamic aspects - Tower presence before step change in wind

In this section the time series is zoomed to 51.5th to 52.5th second to get more aerodynamic insight. This time interval shows the effect of tower presence in all the modules before the step change in wind speed i.e. the wind speed is at 8 m/s. Tower presence is explained in section 4.1.

Figures D-24 and D-25 give the aerodynamic insight about the phenomenon of tower presence. In these figures, blade length starts from 5 m and ends at 62.5 m because blade stations before 5 m of length and after 62.5 m of length are not taken in AEROMODULE(AWSM) due to computation problems. At 51.96th second, blade is near the tower and at 52.07th second it is in front of tower. There is a good match between all the modules at 51.92nd and 52.06th seconds, all the modules show similar trend because the tower is modelled as a dipole in all the modules. From figures D-24 and D-25, it can be observed that when the blade is in front of tower α distribution along the length of blade reduces because of the induction of tower. Reduction in α distribution leads to decrease in c_l distribution because for all airfoils it is below stall angle, only at 5 m of radial length, α and c_l for AEROMODULE(AWSM) increases slightly. N and T are dependent upon α and c_l, and thus due to reduction in both of them, cause reduction in N and T, this is observed in all modules. Axial induced velocity u_{ind}, for both the BEM modules decrease hardly along the complete length of blade, both of them show only a small decrease at the tip. AEROMODULE(AWSM) shows a significant decrease in u_{ind} as compared to both the BEM modules especially for mid-board and out-board part of blade and the explanation for this is given in section C.2.2. Below the phenomenon of tower presence is explained at 0.23R and 0.81R blade stations.

From figure D-26, it can be seen that at 0.81R blade station, all the three modules almost follow the same trend for α, c_l, N and T, AEROMODULE(BEM) and FOCUS(BEM) show almost the same trend because both of them are based on same theory. As α is not above 14 degrees therefore the airfoil at 0.81R blade station is not stalled and thus c_l follows the same trend as α for all the modules. There is a difference in dip of u_{ind} between AEROMODULE(AWSM) and FOCUS(BEM) and the reason for this is already discussed in section C.2.2. AEROMODULE(BEM) doesn't show the dip and therefore more investigation has to be done in the module. N and T are dependent on α and c_l and this can be seen in the trends of all the modules.

From figure D-27, it can be seen that at 0.23R blade station, both the BEM modules are almost in the same phase but AEROMODULE(AWSM) is slightly deviated. All the modules have similar trend for α, c_l, N and T. As α is below 12.5 degrees therefore the airfoil at 0.23R blade station is not stalled and thus c_l follows the same trend as α for all the modules. As explained in section C.2.2, u_{ind} at 0.23R blade station also have a different phase and dip in AEROMODULE(AWSM) and FOCUS(BEM), AEROMODULE(BEM) doesn't show the dip and this is due to sudden increase in u_{ind} near 15 m of radial length, this can be seen in figures D-24 and D-25. At 0.23R blade station also N and T for all the modules show similar trend as α and c_l.

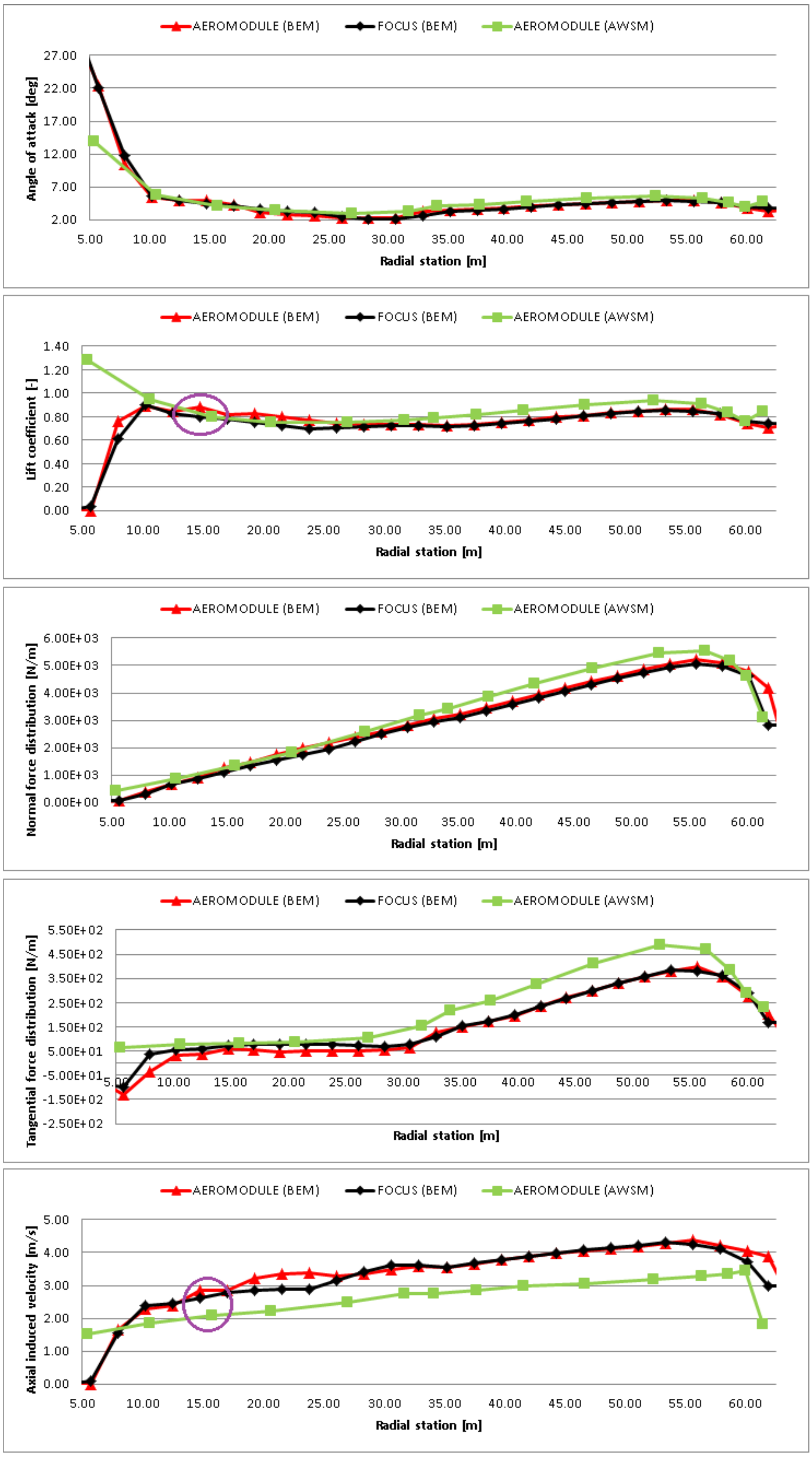

Figure D-24: Case-2: Aerodynamic insight at 51.96th second.

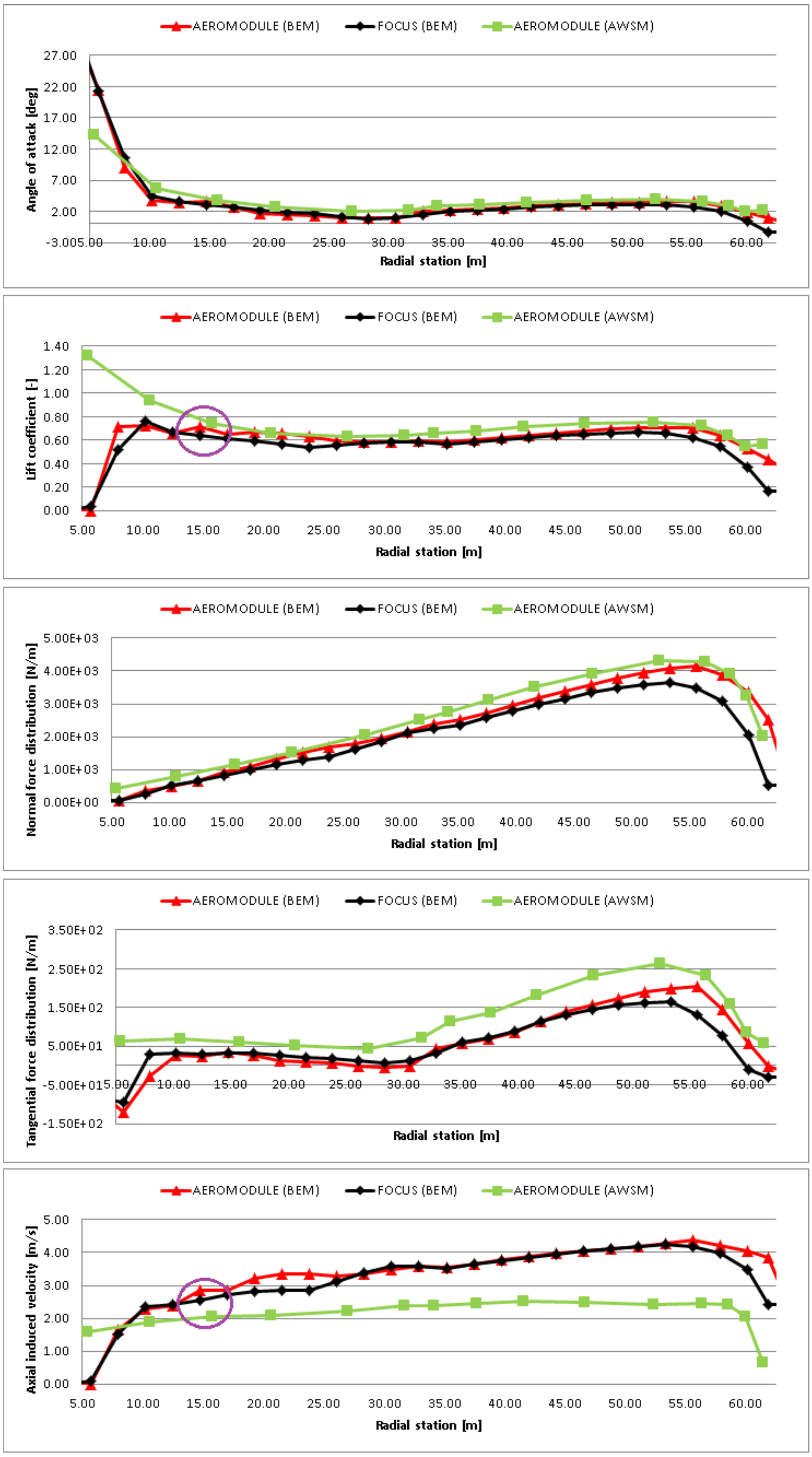

Figure D-25: Case-2: Aerodynamic insight at 52.07th second.

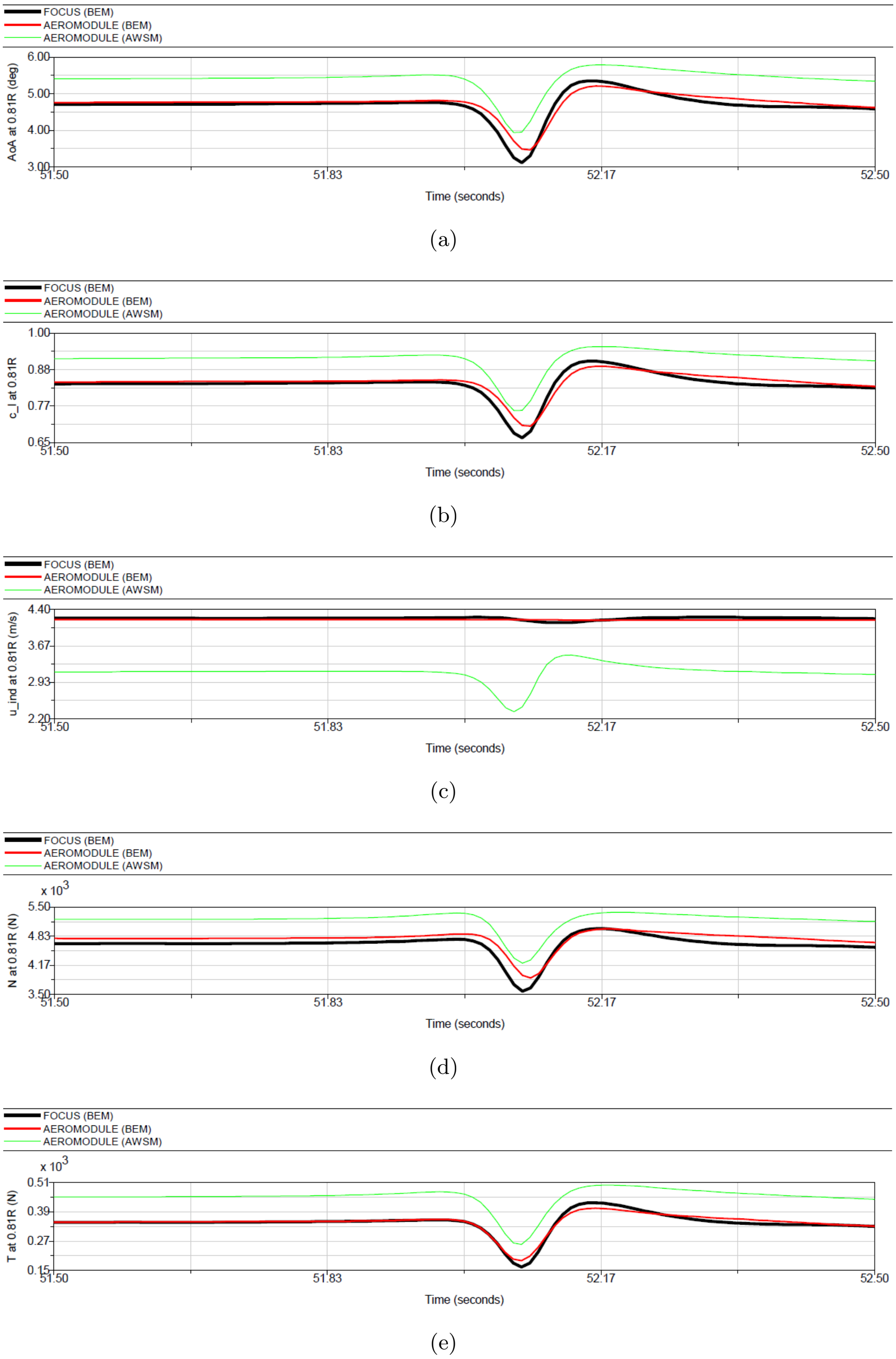

Figure D-26: Case-2: Aerodynamic analysis at 0.81R blade station from 51.5th to 52.5th second.

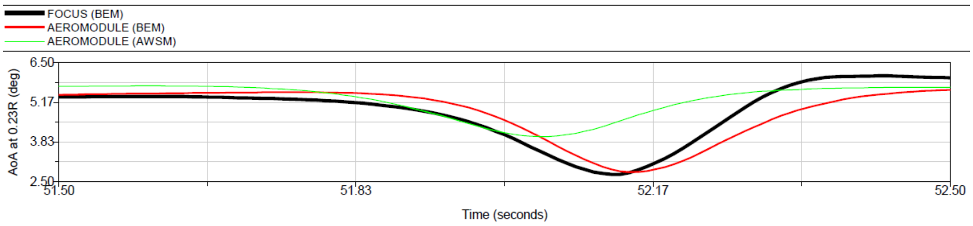

(a)

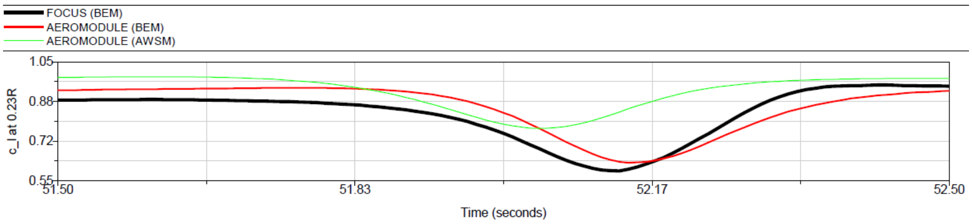

(b)

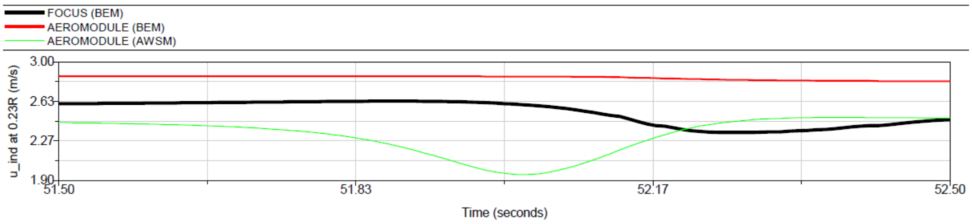

(c)

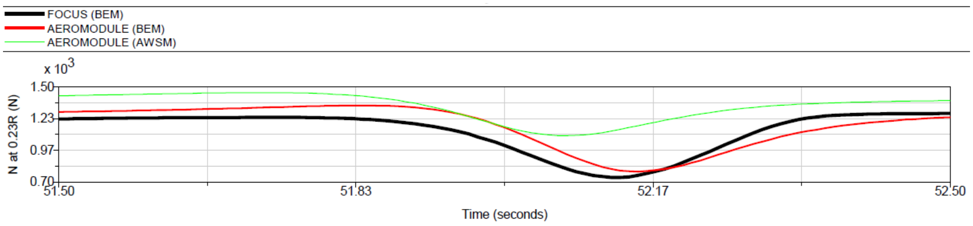

(d)

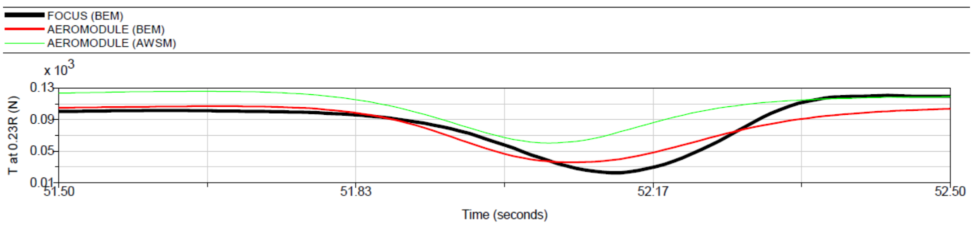

(e)

Figure D-27: Case-2: Aerodynamic analysis at 0.23R blade station from 51.5th to 52.5th second.

D.1.3 Aerodynamic aspects - Dynamic inflow

In this section the time series is zoomed from 69.5th to 70.5th second to get more aerodynamic insight. This time interval shows the dynamic inflow in all the modules when the wind speed changes from 8m/s to 11 m/s at 70th second. In AEROMODULE(AWSM) whenever there is a step change in wind speed, the near wake behind the rotor changes because of changes in bound(shed) and trailing(tip) vortices, this changed near wake causes new induction in the rotor. In BEM, the normal dynamic inflow model is used for step change in wind speed. The time scale of dynamic inflow is directly proportional to D/U, where D is diameter of rotor and U is axial wind speed). Diameter of rotor is 128.4 m and U is 11 m/s, therefore time scale of dynamic inflow is 11.67 seconds. From the figure D-18, it can be seen clearly that the time taken by u_{ind} to become constant when the wind speed changes from 8 m/s to 1 m/s for all the modules is 8.5 seconds and it is in the same order of magnitude as calculated above.

All the modules show the similar trend in figure D-28 at 70th second i.e. before dynamic inflow but when speed changes and dynamic inflow occurs the difference between AEROMODULE(AWSM) and both the BEM modules increase, and this because of different physics involved for computing dynamic inflow. Figure D-29 gives the aerodynamic insight at 70.02th second i.e. during dynamic inflow. In these figures, blade length starts from 5 m and ends at 62.5 m because blade stations before 5 m of length and after 62.5 m of length are not taken in AEROMODULE(AWSM) due to computation problems. It can be observed from the figures D-28 and D-29, that due to increase in wind speed, α increases which leads to increase in c_l in mid-board and out-board region. At in-board region both the BEM modules show large α, which is beyond the stall angle for these airfoils and thus because of dynamic stall it shows very small c_l. Even AEROMODULE(AWSM) shows α above stall angle, but due to absence of dynamic stall model it shows the 2D characteristics of c_l which is higher than both the BEM modules, but decrease in c_l at in-board region, this is because at in-board region airfoils are stalled whereas in the rest of the part of blade it is not stalled. Due to increase in wind speed and c_l, N and T also increase. From axial induced velocity graph it can be seen that in both the BEM modules u_{ind} almost remains the same for the complete length of blade but not near the tip region, but for AEROMODULE(AWSM) it increases significantly for the complete blade length from 70th to 70.02th second. Difference in axial induced velocity for AEROMODULE(AWSM) and both the BEM modules is earlier discussed in section C.2.3. Below effect of dynamic inflow is explained at 0.23R and 0.81R blade stations.

From figure D-30, it can be seen that at 0.81R blade station, all the three modules follow the same trend for α, c_l, N and T, AEROMODULE(BEM) and FOCUS(BEM) show exactly the same trend because both of them use the same principle for the dynamic inflow. AEROMODULE(AWSM) deviates from both the BEM modules because of different physics involved in dynamic inflow. Due to flexibility in blades and tower in this case, all the modules take more time to stabilize the flow after dynamic inflow and also show a dip at 70.25th second which was not there in case-1, section C.2.3. Whenever there is change in wind speed the wake trailing behind the rotor takes time to stabilize. As α at this blade station doesn't go beyond the stall angle, therefore c_l follows the same trend as α. The dynamic inflow peak in AEROMODULE(AWSM) is the smallest for α, c_l, N and T. Exponential decrease in axial induced velocity u_{ind} for AEROMODULE(AWSM) clearly shows how long it takes for the wake to stabilize because the wake causes induction in rotor blade element when dynamic inflow occurs, as there is no wake in both the BEM modules so trend is almost constant after dynamic inflow. On looking at α, c_l, N and T curves it can be said that both the BEM modules show a higher dip than AEROMODULE(AWSM) to compute dynamic inflow when the blades are flexible.
From figure D-31, it can be seen that AEROMODULE(BEM) overlaps with FOCUS(BEM) for α curve but for others there is a deviation at 0.23R blade station. From c_l curve it can be seen that AEROMODULE(BEM) shows a higher mean value than FOCUS(BEM) even having the same α, this is because airfoil at 0.23R blade station is not taking correctly the aerodynamic characteristics. This abrupt behaviour of AEROMODULE(BEM) can also be seen in figures D-28 and D-29. N and T curves for all the modules follow the same trend as there α and c_l curves respectively. Axial induced velocity u_{ind} shows a clear picture of dynamic inflow at 0.23R blade station, peak for AEROMODULE(AWSM) is highest among all modules. Exponential decrease in axial induced velocity u_{ind} for AEROMODULE(AWSM) suggests that the wake is

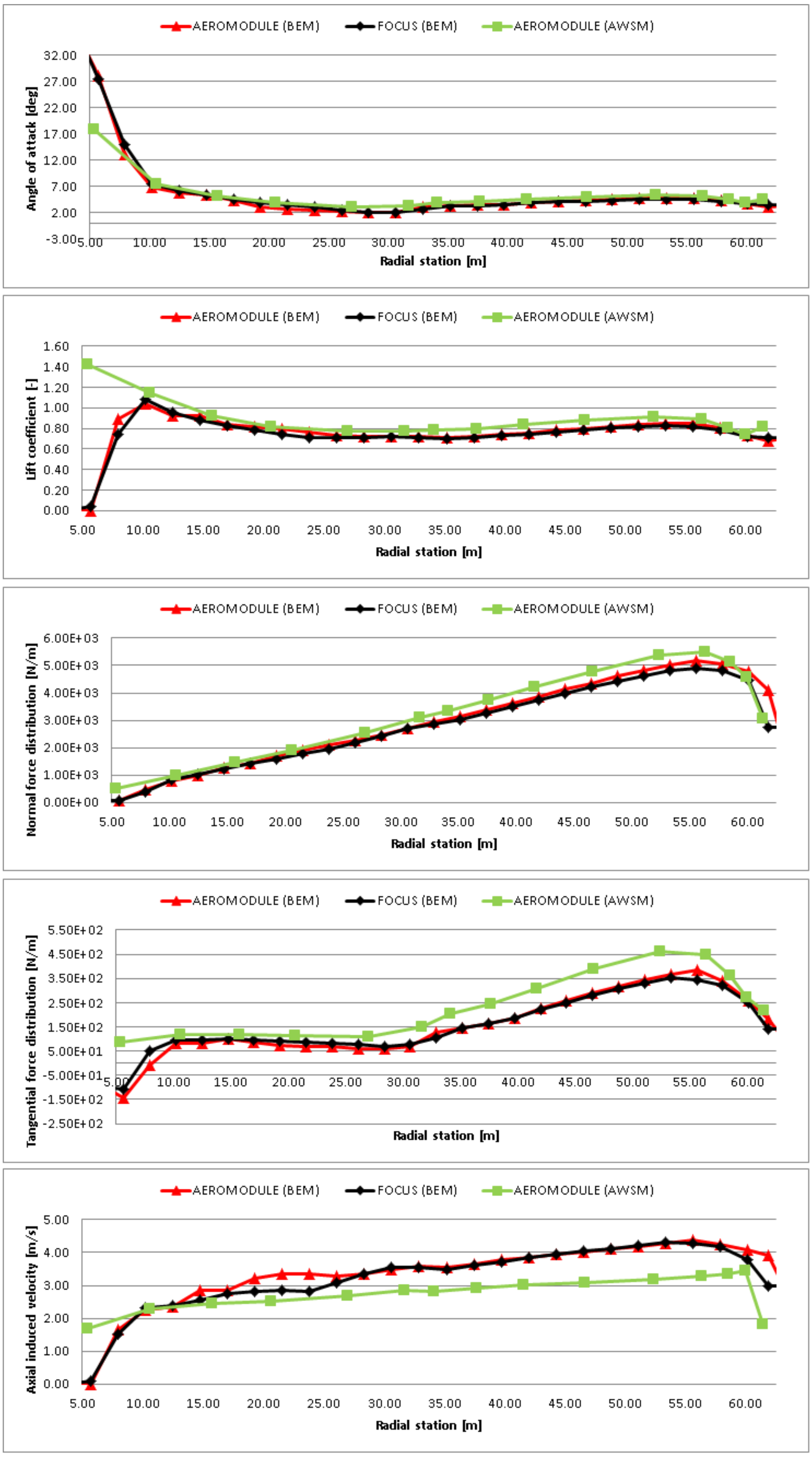

Figure D-28: Case-2: Aerodynamic insight at 70th second.

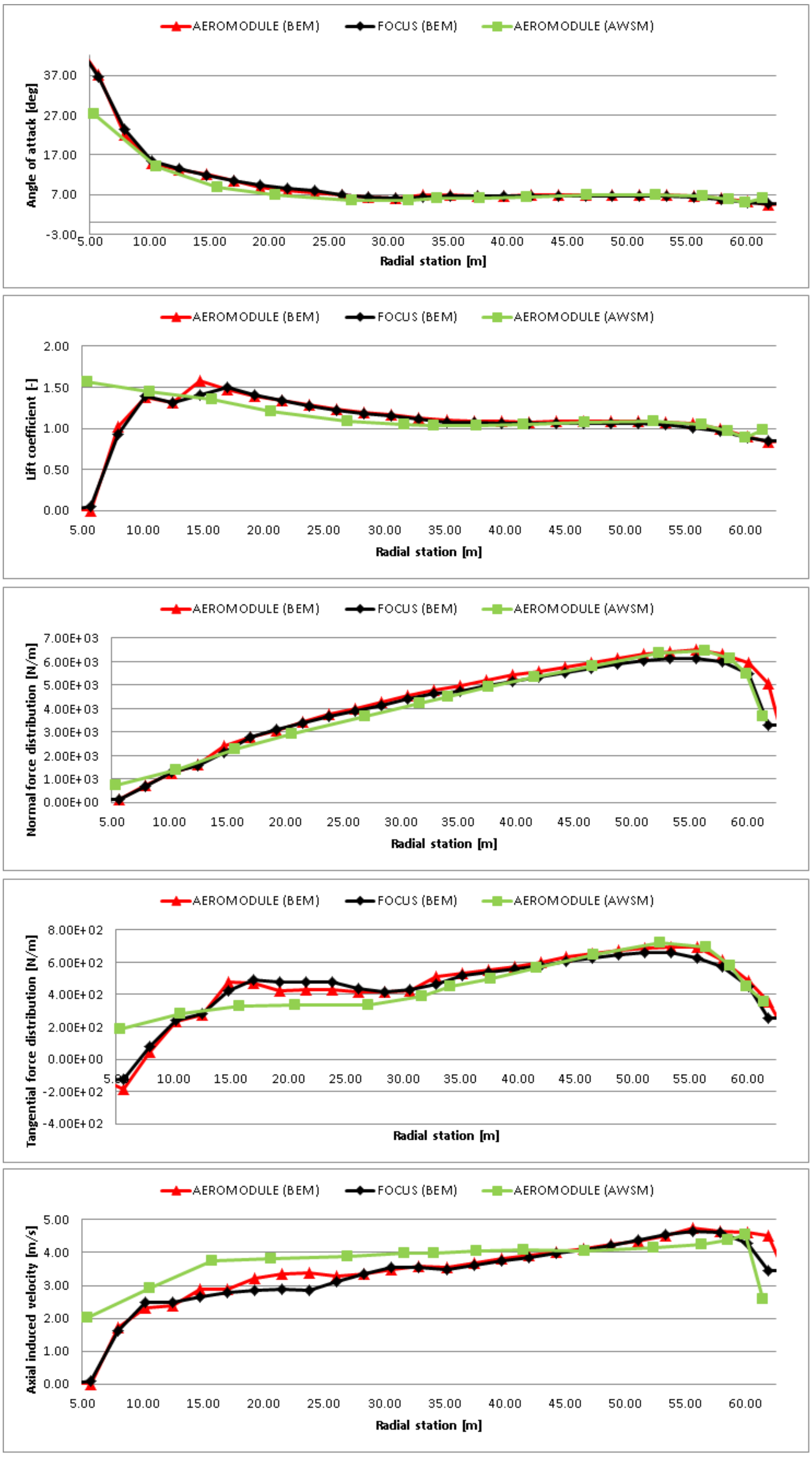

Figure D-29: Case-2: Aerodynamic insight at 70.02th second.

stabilizing, and this cannot be seen in both the BEM modules because of absence of wake.

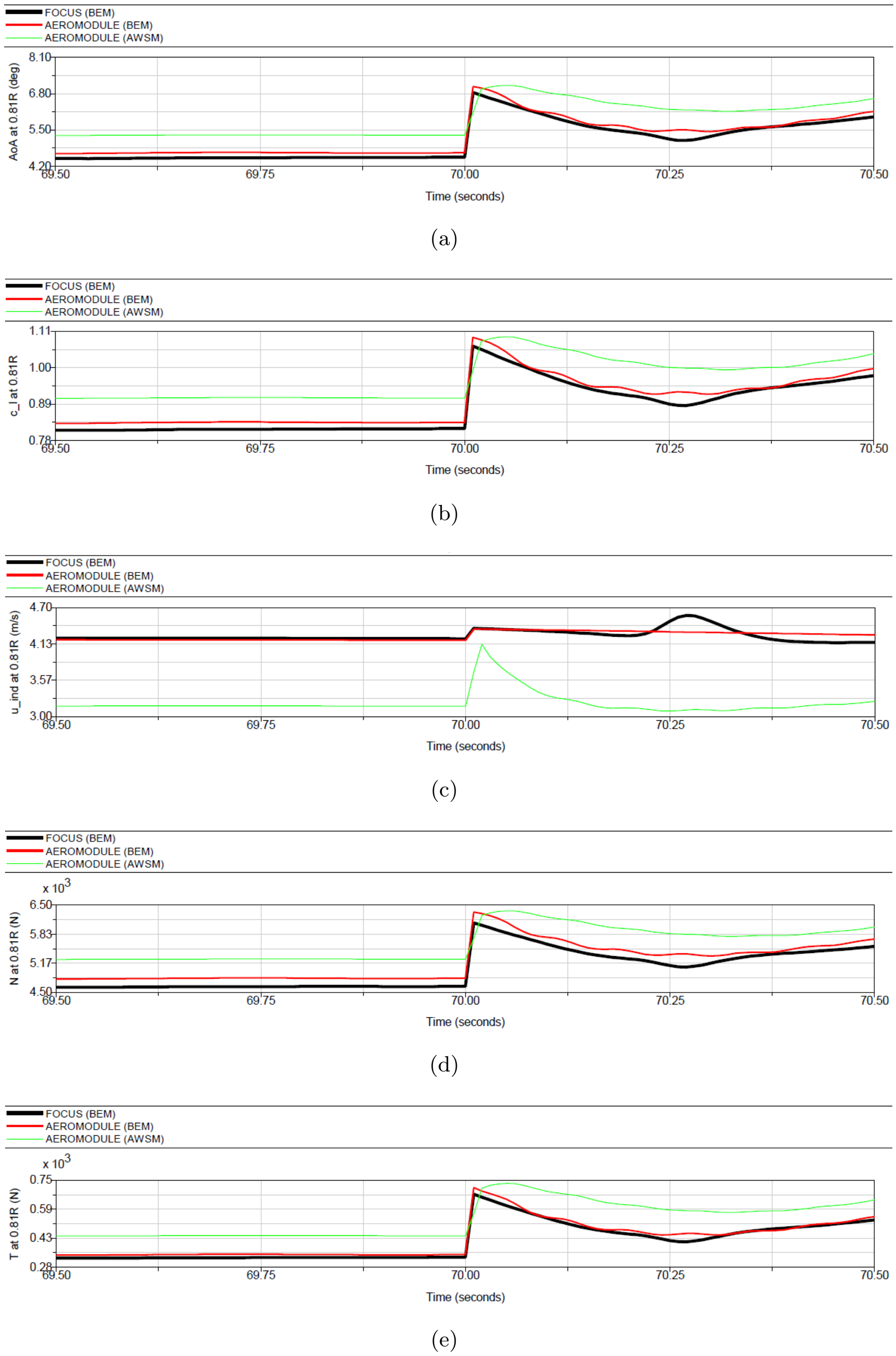

Figure D-30: Case-2: Aerodynamic analysis at 0.81R blade station from 69.5th to 70.5th second.

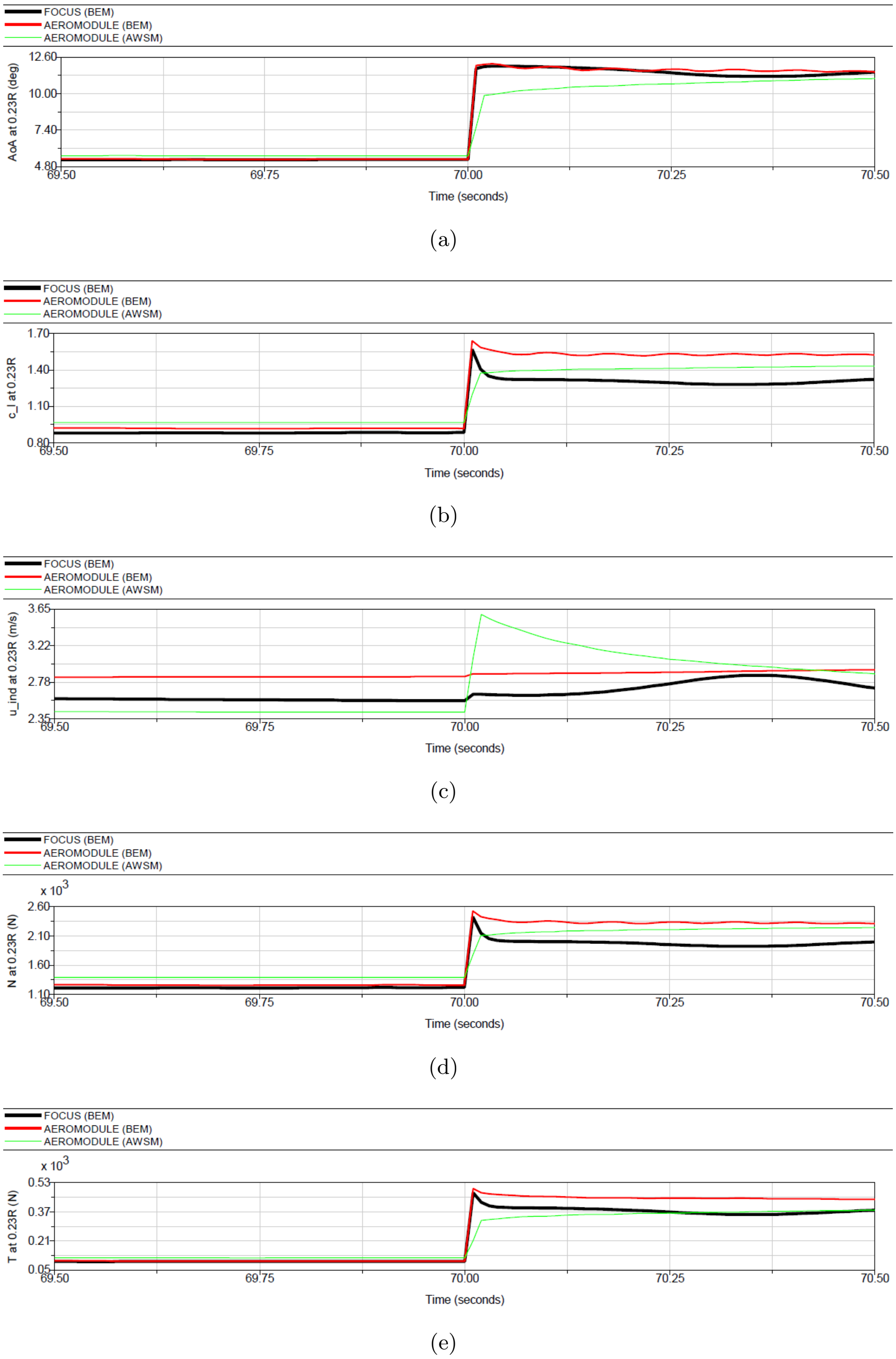

Figure D-31: Case-2: Aerodynamic analysis at 0.23R blade station from 69.5th to 70.5th second.

D.1.4 Aerodynamic aspects - Tower presence after step change in wind

In this section the time series is zoomed from 81.3th to 82.3th second to get more aerodynamic insight. This time interval shows the tower presence in all the modules after the step change in wind speed i.e. the wind speed is at 11 m/s. Tower prsence is explained in section 4.1.

This section is similar to section D.1.4 and also holds the same explanation. In this section only the differences will be mentioned because of change in wind speed. In this section the dips due to tower presence have increased as compared to the former case because of increase in wind speed. From figure D-32, it can be seen that at 0.81R blade station, all the modules show the same trend, though there is phase difference between all the modules. This is because wind turbine blades take some to stabilize after dynamic inflow. Phase difference between AEROMODULE(AWSM) and AEROMODULE(BEM) is because of the wake in AEROMODULE(AWSM). In AEROMODULE(AWSM), rotor wake is modelled and when an airfoil is near the tower, the wake which is shedding from the rotor gets disturbed or changed. As change in wake occurs even before airfoils pass the tower, AEROMODULE(AWSM) shows the phenomenon of tower presence earlier. As in BEM theory there is no wake modelled, thus only when the blade is in front of tower, the induction due to the tower is calculated. Because of these reasons AEROMODULE(AWSM) shows the phenomenon of tower presence earlier than both the BEM modules. Phase difference between both the BEM modules was also there in section when the wind speed was 8 m/s, so the same phase difference is maintained at 11 m/s of wind speed too. From figure D-33, it can be seen that at 0.23R blade station, AEROMODULE(AWSM) shows a small dip than other two modules.

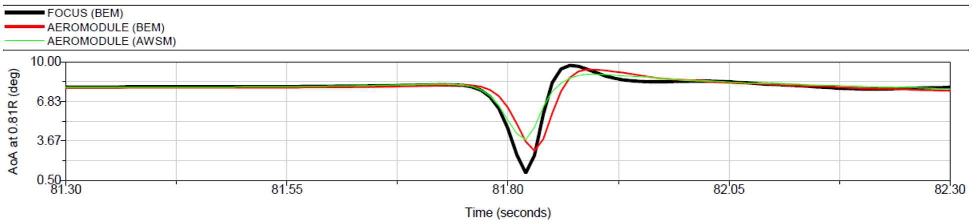

(a)

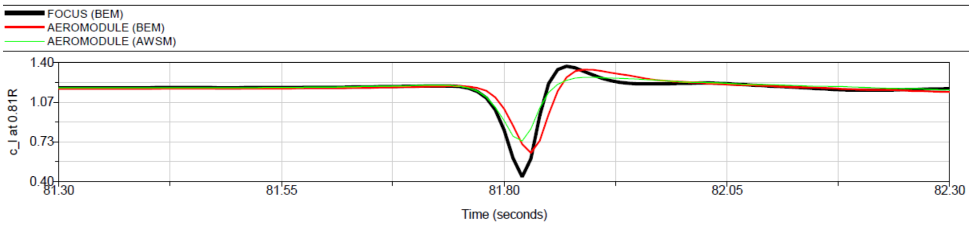

(b)

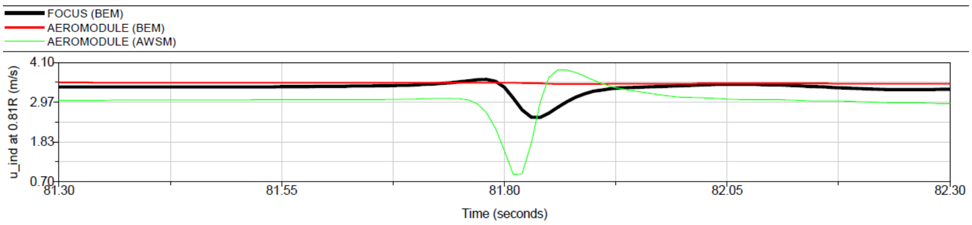

(c)

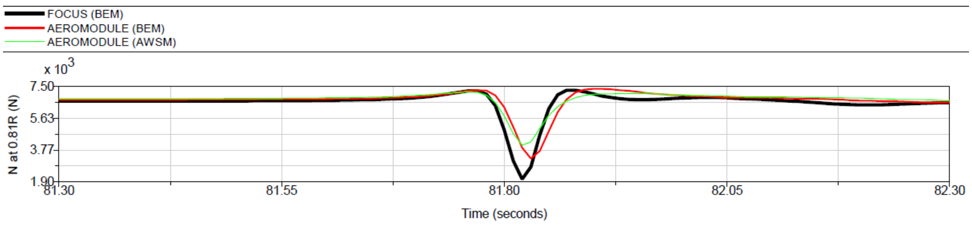

(d)

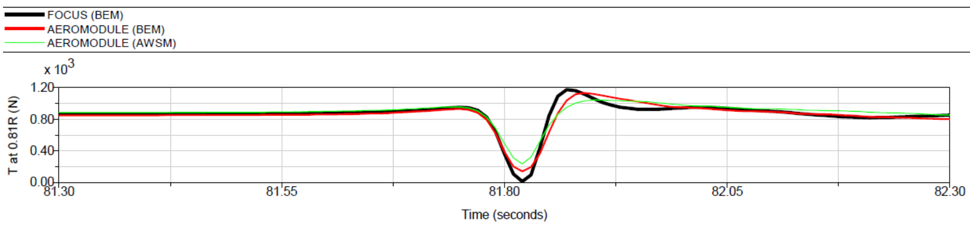

(e)

Figure D-32: Case-2: Aerodynamic analysis at 0.81R blade station from 81.3th to 82.3th second.

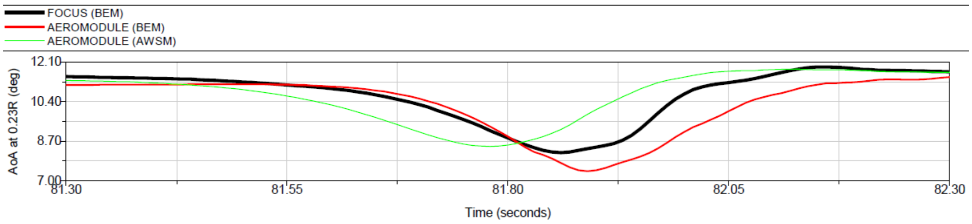

(a)

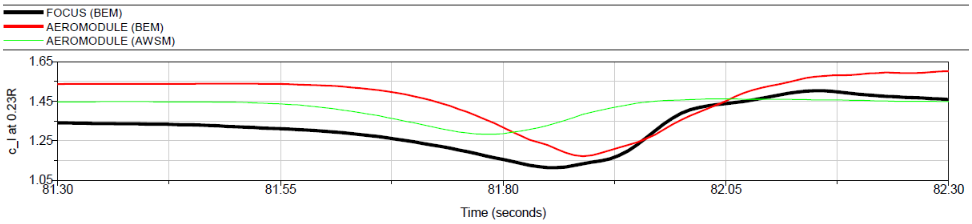

(b)

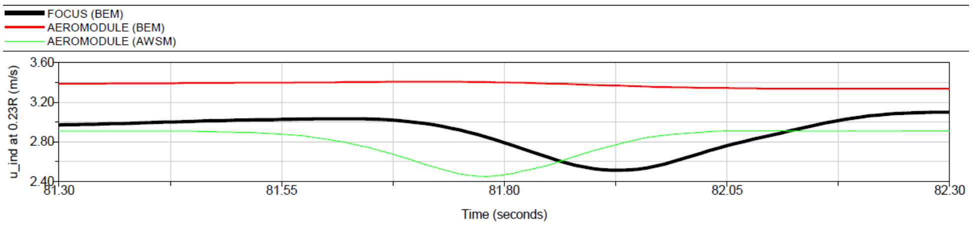

(c)

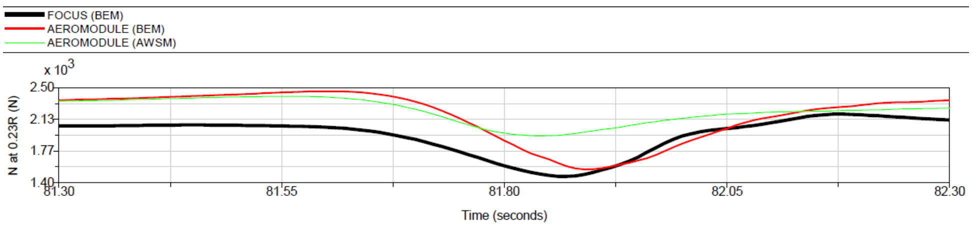

(d)

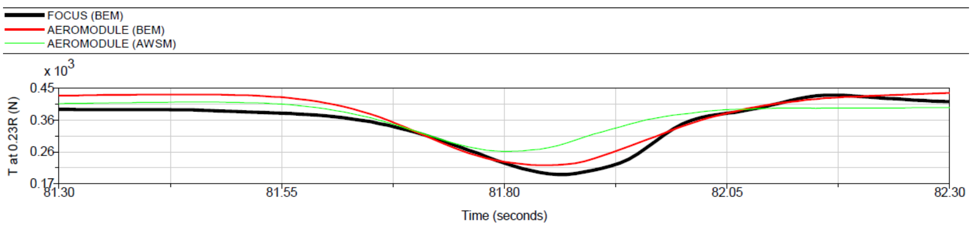

(e)

Figure D-33: Case-2: Aerodynamic analysis at 0.23R blade station from 81.3th to 82.3th second.

D.1.5 Aerodynamic aspects at 100th second

In this section aerodynamic analysis is done at 100th second along the complete length of blade. This analysis is done to observe the difference in three modules when the flow completely stabilizes. From figure D-34, it can be seen that all the three modules show a very good match in trend and coincide with each other for α, c_l, N and T. In these figures blade length starts from 5 m and ends at 62.5 m because blade stations before 5 m of length and after 62.5 m of length are not taken in AEROMODULE(AWSM) due to computation problems. There are small differences in all modules till blade length of 7 m because of different way of computing stall. Angle of attack α at 5 m of blade length is above the stall angle for all the modules, both the BEM modules show very small c_l because of dynamic stall but AEROMODULE(AWSM) shows a higher value as there is no dynamic stall model in it. Due to this difference N and T also show a different trend for AEROMODULE(AWSM) near the root region.

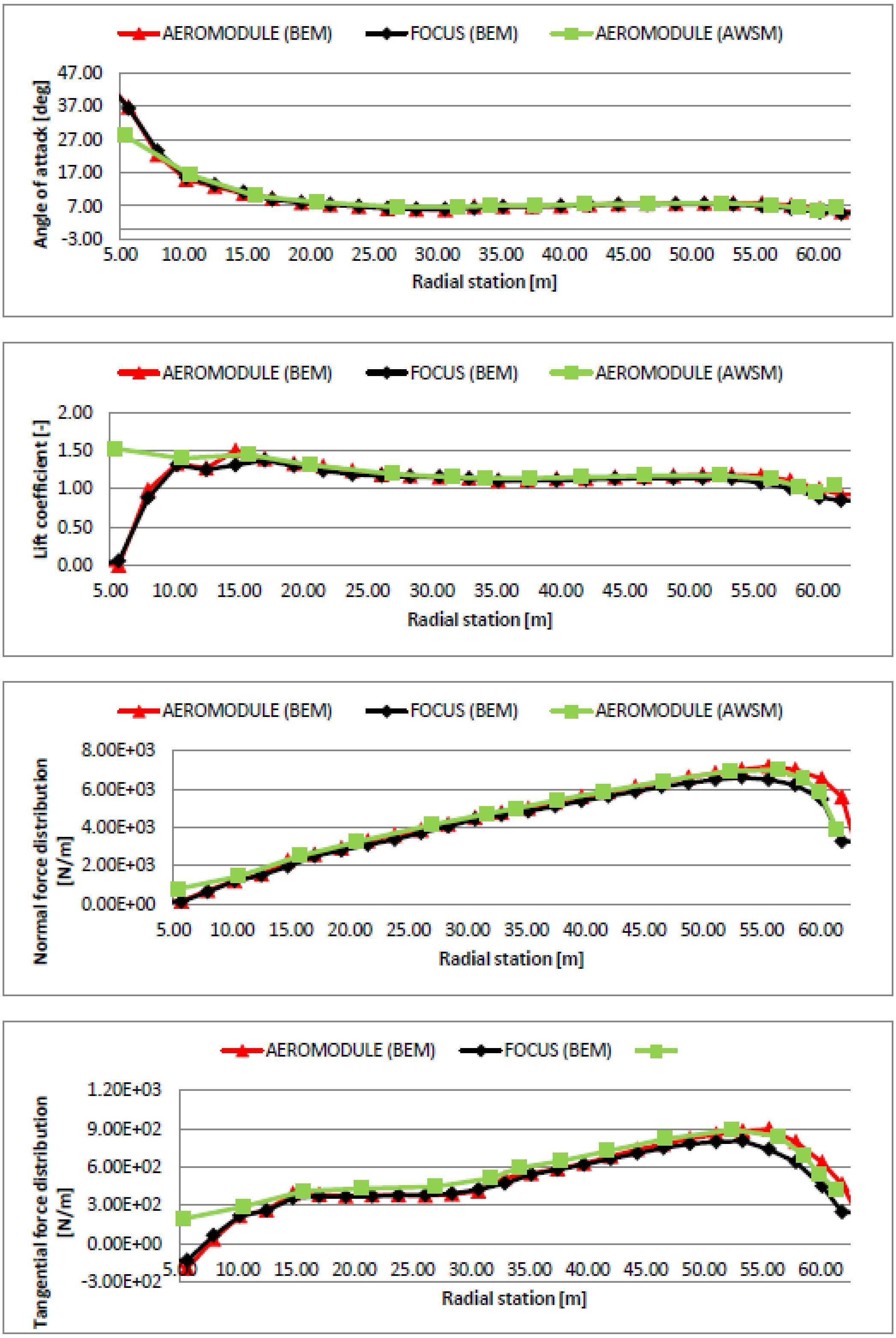

Figure D-34: Case-2: Aerodynamic analysis at 100th second.

D.1.6 Structural aspects

Blade loads

As the blades are flexible, so the blades flap and thus a flap angle is formed therefore the centrifugal force which acts only in radial direction has a component in flapwise direction. Due to no yaw misalignment the yaw rate is zero, so the contribution of gyroscopic forces in flapwise direction of blade is also zero. Contribution due to gravity force is also there because of the flap angle as the blades are flexible. Axial aerodynamic force is the main contributor of flapwise bending moment in the blade root. Large dip in flapwise bending moment is due to blade passing the tower (tower presence). Figure D-35 shows the flapwise bending moments in the blade root. Both AEROMOD-

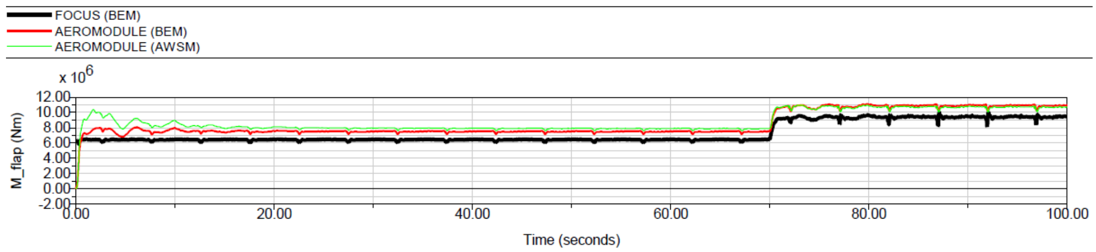

Figure D-35: Case-2: Flapwise bending moment in the blade root.

ULE(BEM) and AEROMODULE(AWSM) have similar pattern but they differ from FOCUS(BEM) because of slightly different flapwise frequency of blade. Figure D-36 shows the flapwise bending moments in the blade root from 91st to 93rd second, and it can be seen that there is phase difference between AEROMODULE modules and FOCUS(BEM).

Sudden increase in wind speed causes the rotor torque to increase which in turn increases the average value of edgewise moment. The amplitude of cyclic edgewise moment shows the contribution of gravity force of one blade. As the blades are flexible so they flap with a certain velocity. Due to this flapping velocity, Coriolis force also causes a small edgewise moment in the blade root. It can be seen that the phenomenon of tower presence is very small in edgewise bending moment in blade root, it only comes into picture when wind speed increases. This is because when the blade passes the tower there is fluctuation in the tangential speed of blades and the fluctuations become

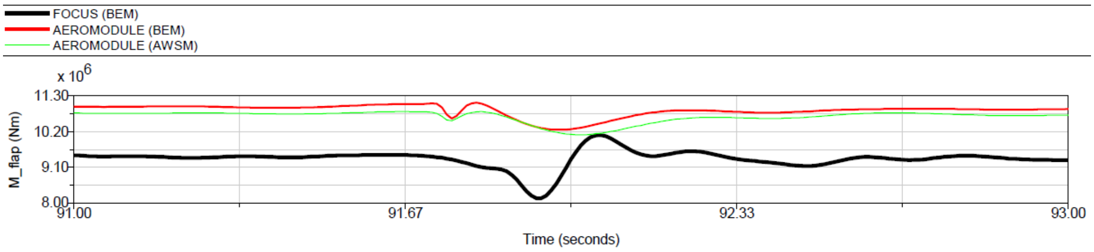

Figure D-36: Case-2: Flapwise bending moment in the blade root from 91st to 93rd second.

more pronounced when wind speed is high. For all the modules there is really a good match. Figure D-37 shows the edgewise bending moment in the blade root.

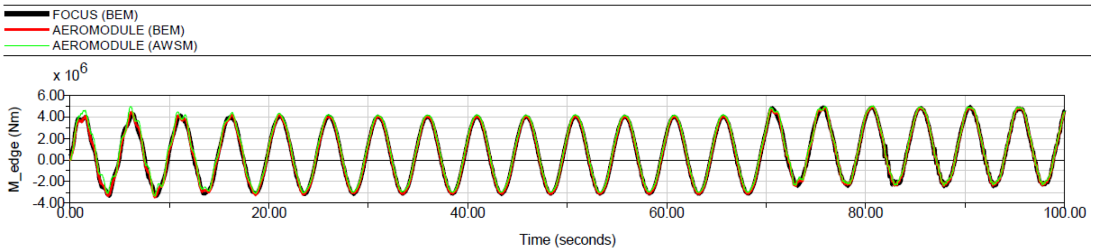

Figure D-37: Case-2: Edgewise bending moment in the blade root.

As there is no pitching action, torsional in blade root due to it is zero. Due to flexibility of blade, blades deform and thus centrifugal force also contributes to torsional moment in the blade root, though its contribution is very small. The offset between aerodynamic axis and elastic axis is very small, therefore the lift force which acts on $c_{1/4}$ point has a very small arm from the $c_{1/4}$ point to the elastic axis, and this also causes very small torsional moment in the blade root. As the blades are flexible therefore the blade lead-lag deflections are there. So the blade flapwise bending moment along with blade lead-lag deflections also cause torsional moment in the blade root. The cyclic fluctuations in edgewise bending moment along with blade flapwise deflection also contributes to torsional moment. As compared to case 1, there is a difference in torsional moment in blade root because the flexible model of ART wind turbine in SIMPACK has different blade torsional stiffness as compared to FOCUS(BEM), therefore both AEROMODULE modules show different amplitude as compared to FOCUS(BEM). Figure D-38 shows the torsional moment in the blade root. There is lot of difference in amplitude

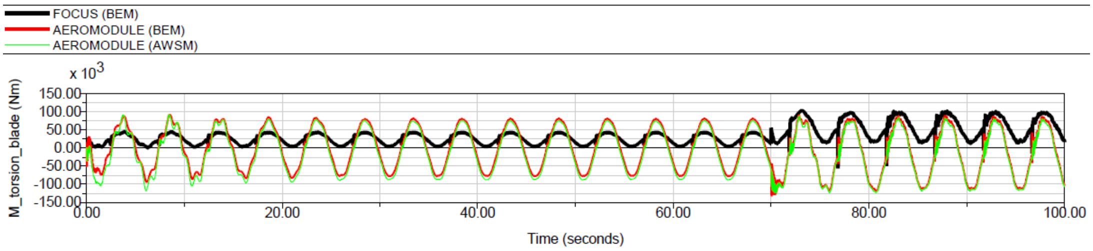

Figure D-38: Case-2: Torsional moment in the blade root.

between AEROMODULE modules and FOCUS(BEM) and on zooming the torsional moment from 91.5th to 95th second, it can be seen that AEROMODULE-SIMPACK couple shows lot of ripples which FOCUS(BEM) is not able to identify. Frequency of these fluctuations is 13 Hz and this is the blade torsion frequency. Figure D-39 shows the torsional moment in the blade root from 91.5th to 95th second.

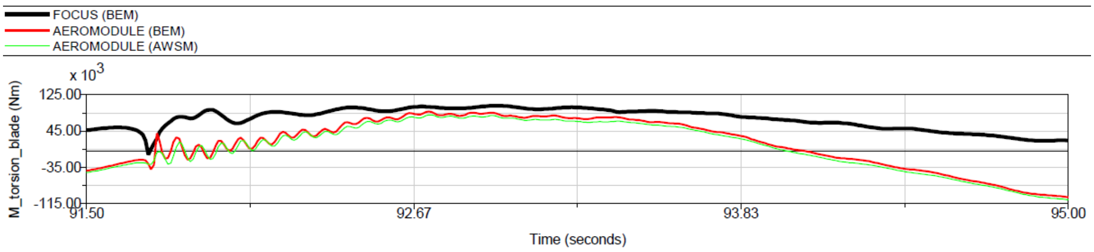

Figure D-39: Case-2: Torsional moment in the blade root from 91.5th to 95th second.

Tower loads

Figure D-40 shows the fore-aft bending moment in the tower base. For all the modules there is really a good match. Fore-aft bending moment in the tower base is constant before step change in wind speed and when each blade passes the tower, the fore-aft bending moment shows a dip and this is due to the phenomenon of tower presence. The constant value is due to constant rotor thrust loading and drag loading due to wind. Tower fore-aft bending moment shows fluctuations after 70th second because of wind

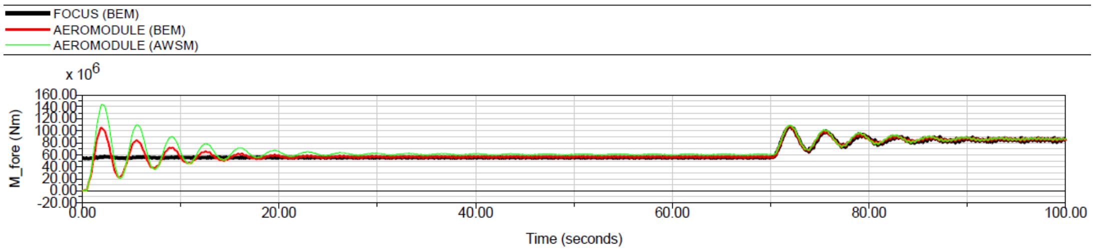

Figure D-40: Case-2: Fore-aft bending moment in the tower base.

speed change. The frequency of fluctuations is 0.27 Hz and this is tower's 1st natural fore-aft frequency. Figure D-41 shows the fore-aft bending moment in the tower base from 69th to 80th second, the effect of dynamic inflow on tower can be seen clearly here.

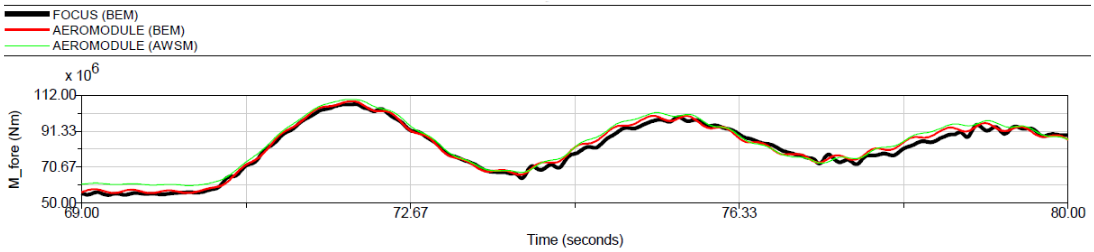

Figure D-41: Case-2: Fore-aft bending moment in the tower base from 69th to 80th second.

Figure D-42 shows the side-ways bending moment in the tower base. Side-ways tower

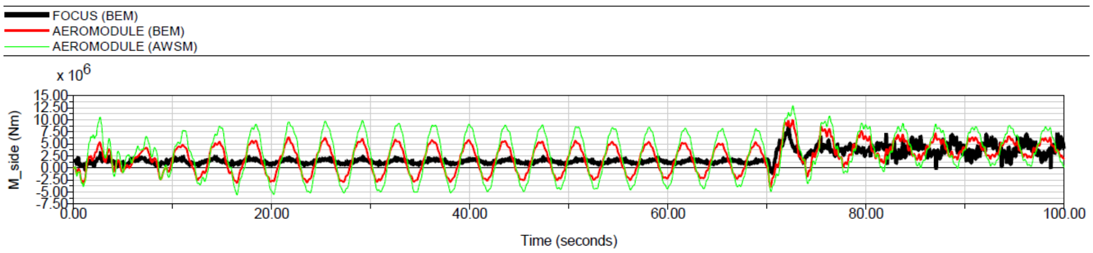

Figure D-42: Case-2: Side-ways bending moment in the tower base.

bending moment is caused due to the edgewise forces in the blade. Rotor torque which acts on the tower top through gearbox/generator support also causes side-ways bending moment. As no turbulence is taken into account in this case, therefore its contribution is zero. Because of no yaw misalignment, gyroscopic force also doesn't cause side-ways bending moment. All these factors discussed are the reason for side-ways bending moment in tower base. Side-ways tower bending moment shows fluctuations because in side-ways direction tower has less damping as compared to fore-aft direction, there is no rotor damping in side-ways direction. There is a lot of discrepancy between all the modules for the fluctuations in side-ways tower bending moment. As the simulation starts in AEROMODULE-SIMPACK couple, it takes time for the tower fluctuations to stabilize and it seems the tower becomes unstable at this point. At large wind speed the amplitude of fluctuations in side-ways bending moment comes closer for all the modules, though there is phase difference. Phase difference is because SIMPACK takes time to stabilize the fluctuations in tower after step change in wind. Figure D-43 shows the side-ways bending moment in the tower base from 61st to 66th second i.e. before step change in wind.

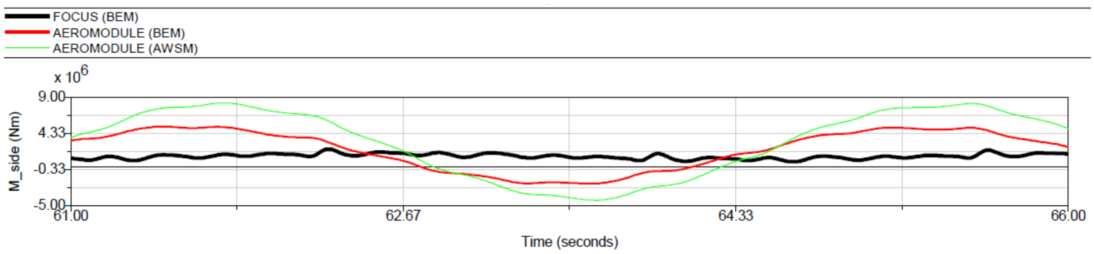

Figure D-43: Case-2: Side-ways bending moment in the tower base from 61st to 66th second.

Figure D-44 shows the torsional moment in the tower top. Torsional moment in the

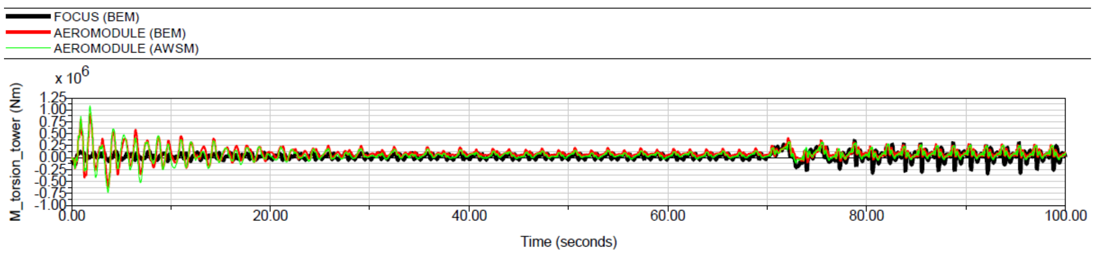

Figure D-44: Case-2: Torsional moment in the tower top.

tower top is due to the rotor torque acting on it through gearbox/generator support when the rotor is tilted. As the yaw drive is working properly therefore its contribution is also zero. Because of zero yaw and tilt angle the mean value of fluctuation of torsional moment is zero. Peaks in torsional moment are due to phenomenon of tower presence. Tower presence causes sudden increase in edgewise bending moment in the blade root, this sudden increase along with flapwise deflection of flexible blade causes increase in torsional moment in the tower top. For first 10 seconds SIMPACK shows large fluctuations for torsional moment in tower top, this is because SIMPACK takes time to stabilize the tower. For all the modules there is really a good match but when the step change in wind speed takes place at the 70th second there is difference in the torsional moment in the tower top for all the three modules.